On the mathematical analysis and the numerical simulation of boiling flow models in nuclear power plants thermal hydraulics

Thi Phuong Kieu Nguyen

NNT : 2016SACLV007

THÈSE DE DOCTORAT
DE
L'UNIVERSITÉ PARIS-SACLAY
PRÉPARÉE À
L'UNIVERSITÉ DE VERSAILLES SAINT-QUENTIN-EN-YVELINES

ECOLE DOCTORALE N° 574
École Doctorale de Mathématique Hadamard
Spécialité de doctorat : Mathématiques appliquées
Par

Mme. Thi Phuong Kieu NGUYEN

Titre de la thèse :
Analyse mathématique et simulation numérique des modèles d'écoulements bouillants pour la thermohydraulique des centrales nucléaires

Titre de la thèse en anglais :
On the mathematical analysis and the numerical simulation of boiling flow models in nuclear power plants thermal hydraulics

Thèse présentée et soutenue à Saclay, le 29 janvier 2016 :

Composition du Jury :

M. HELLUY Philippe	Professeur, IRMA-CNRS	Rapporteur
M. HÉRARD Jean-Marc	Ingénieur Sénior, EDF R&D Châtou	Rapporteur
M. CHALONS Christophe	Professeur, UVSQ	Directeur de thèse
M. NDJINGA Michaël	Ingénieur de Recherche, CEA	Co-Encadrant
M. ALLAIRE Grégoire	Professeur, Ecole Polytechnique	Examinateur
M. SEGUIN Nicolas	Maître de Conférence, Paris 6	Président
M. SÉGRÉ Jacques	Ingénieur Sénior, CEA	Invité

université PARIS-SACLAY | École doctorale de mathématiques Hadamard (EDMH)

Titre : Analyse mathématique et simulation numérique des modèles d'écoulements bouillants pour la thermohydraulique des centrales nucléaires.

Mots clés : écoulement diphasique, phase évanescente, schéma de Roe, écoulement bouillant.

Résumé : Dans la thermohydraulique des réacteurs nucléaires, le fluide de refroidissement est habituellement étudié en utilisant des modèles moyennés d'écoulements diphasiques, dans lesquels le fluide possiblement bouillant est décrit à un niveau macroscopique comme un mélange homogénéisé, et la présence des deux phases est représentée par le taux de vide (fraction volumique de la vapeur) α. Suivant l'approche moyennée, différents modèles d'écoulements diphasiques ont été explorés en fonction de la complexité du régime d'écoulement et de la précision souhaitée. Ces différents modèles sont associés à des hypothèses simplificatrices spécifiques concernant les déséquilibres mécanique et thermique.
Nous nous concentrons dans cette thèse sur le déséquilibre mécanique qui conduit à de nombreuses difficultés mathématiques telles que l'hyperbolicité conditionnelle, les champs caractéristiques non classiques, les points soniques présents même dans le régime subsonique, les produits non conservatifs et les termes source très raides. De nombreuses difficultés numériques sont également inhérentes à ces modèles tels que la positivité du taux de vide $\alpha \in [0, 1]$, et l'absence de régularité des termes sources. Dans les modèles à deux fluides, la transition vers un régime à une seule phase conduit à une phase évanescente dont la vitesse peut devenir singulière et nous avons besoin de caractériser les paramètres liés à cette phase absente.
Afin de mieux comprendre ces modèles d'écoulements diphasiques, nous étudions en détail leur limite incompressible, où les propriétés mathématiques peuvent être étudiées en profondeur. Nous démontrons l'existence et l'unicité de la solution admissible au problème de Riemann dans la limite incompressible du modèle bi-fluide isentropique à six-équations. La solution présente des vitesses non triviales et bien définies pour les deux phases, même dans la limite de la phase évanescente. Pour la simulation numérique, nous avons utilisé des solveurs de Riemann exacts et approchés.
Pour certains modèles compressibles nous proposons une stratégie générale de construction des matrices de Roe et détaillons la construction dans le cas du modèle à deux fluides compressibles en équilibre thermique (modèle à cinq-équations). Nous montrons qu'une correction entropique est nécessaire pour les schémas de type Roe afin de capturer les solutions admissibles dans le cas d'une phase évanescente. L'application d'une correction entropique comme celle de Harten pour le schéma de Roe classique apparaît nécessaire pour obtenir une solution avec $\alpha \in [0, 1]$. La simulation du problème de sédimentation (séparation des phases sous l'effet de la gravité) est réalisée avec succès jusqu'à l'état stationnaire avec des vitesses phasiques bornées malgré l'écoulement à contre-courant et la présence de phases évanescentes. Enfin, nous présentons le test du canal bouillant qui est fondamental dans la simulation du comportement accidentel des cœurs de réacteurs nucléaires. Nous avons réussi à capturer l'état stationnaire admissible malgré la non-régularité sévère du terme source grâce à la stratégie de décentrement du terme source similaire à celle des flux convectifs.

université PARIS-SACLAY | École doctorale de mathématiques Hadamard (EDMH)

Title : On the mathematical analysis and the numerical simulation of boiling flow models in nuclear power plants thermal hydraulics.

Keywords : two-phase flow, vanishing phase, Roe scheme, boiling flow.

Abstract : In the thermal hydraulics of nuclear reactors components, the cooling fluid is usually studied using averaged two-phase flow models, where the boiling fluid is viewed at a macroscopic level as a homogenized mixture, and the presence of the two phases is accounted by the vapor volume fraction ratio α. Following the averaged approach, different two-phase flow models have been explored depending on the complexity of the boiling flow regime and the desired accuracy. These different models are associated with specific simplifying assumptions regarding mechanical and thermal disequilibrium. We focus on this thesis on the mechanical non equilibrium which leads to many mathematical difficulties such as conditional hyperbolicity, characteristic fields with complicate structure and sonic points being common even in the subsonic regime, non conservative products and very stiff source terms. Numerical difficulties are also inherent to these models such as the positivity of the void fraction $\alpha \in [0, 1]$, and the stiffness of the source terms. Also in the case of two-fluid models, the transition toward a single phase regime leads to the vanishing phase singularity where we need to characterize the parameters related to the absent phase.
In order to understand better these two-phase flow models, we study in details their incompressible limit, where the mathematical properties can be thoroughly explored. We prove the existence and uniqueness of the admissible solution to the Riemann problem in the incompressible limit of the two-fluid model. The solution displays non trivial and well-defined velocities for both phases even in the limit of a vanishing phase. For the numerical simulation we used both exact and approximate Riemann solvers.
For some compressible models we propose a general strategy to build Roe matrices and detail the construction in the case of the five equation compressible two-fluid model with a common temperature for the two phases. We show that an entropy fix is necessary for the Roe-type schemes to capture admissible solutions in the case of vanishing phase. Applying the Harten-entropy fix to the classical Roe scheme, appears necessary to obtain a solution with $\alpha \in [0, 1]$. The sedimentation problem is successfully carried out until stationary state with bounded phasic velocities despite counter-current and vanishing phases. Finally, we present the boiling channel test which is fundamental in the simulation of the accidental behavior of nuclear reactor cores. We were able to capture the admissible stationary state despite severe stiffness of the source term thanks to source upwinding strategies.

Remerciements

J'aimerais tout d'abord remercier mon directeur de thèse, Christophe Chalons pour m'avoir guidée, encouragée, conseillée pendant les trois années de ma thèse. Sa gentillesse, sa capacité d'analyse et de synthèse et ses nombreuses connaissances ont répondu à plusieurs de mes questions. Je le remercie pour tous ses conseils mathématiques intéressants qui m'ont aidée à progresser mes études.

J'aimerais remercier mon encadrant au CEA, Michaël Ndjinga. Je le remercie pour m'avoir enseigné non seulement les mathématiques, la physique thermohydraulique mais aussi l'informatique et la vie quotidienne en France. Sa disponibilité, sa patience et ses nombreuses connaissances m'ont appris et trouvé les idées pour avancer dans ma recherche. Je le remercie pour m'avoir écoutée, encouragée, et corrigé mon approche écrit des langues étrangères.

Mes remerciements vont également aux professeurs P. Helluys et J.-M Hérard qui ont accepté d'être mes rapporteurs. Je les remercie pour tous leur conseils et leur suggestions qui m'ont permis d'améliorer cette thèse. Je souhaitais également remercier professeurs Nicolas Seguin et Grégoire Allaire pour avoir pris part au jury.

Je voudrais remercier les laboratoires d'accueil : le Laboratoire de Modélisation et simulation à l'Echelle Composant (LMEC) du CEA-Saclay et le Laboratoire de Mathématiques de Versailles (LMV). Je les remercie pour leur accueil, leur soutien et ses amitiés afin de je peux faciliter mes travail pendant ma thèse. Je remercie tous les membres du LMEC mais également ceux du LMES pour tout leurs suggestions, discussions professionnelles, et également leurs conseils sur la vie quotidienne . Je n'oublie jamais les collègues très sympathiques comme Mark, Mark, Pascal, Arthur, Thibaud, Florient, Anela, Antoine, Olivier, Samuel, A. Mekkas, ... J'étais très heureuse de faire votre connaissance, et de travail de près ou de lois avec vous. J'aimerais on peut toujours tenir au contact même si je suis partie. Je n'oublie pas de remercier Jacques Ségré pour m'avoir aidé à résolve tout les problèmes d'administration relatifs au séjour en France et pour m'avoir aidé à déménager le bureau plusieurs fois.

J'exprime ma gratitude à mes amis et à ma famille qui m'ont soutenue et encouragée. Je voudrais remercier chaleureusement mes amis Minh, Phong, Thao, Lan, Hai, Anh, Chuan, Chien ... je suis heureuse de vous avoir dans ma vie. Je tiens à remercier tout particulièrement toutes les familles qui m'ont accueillie mes quatre années en France, Patrick-Sara, T.Cuong, Mai-Loc, Genièvre, Chantal-Gilles, Chanda-Pascal, Anh-Anh ... . Merci mes parents, ma sœur et mon frère qui m'ont toujours soutenue et encouragé dans mes étude sans oubliée de m'encourager à revenir au Vietnam de temps en temps.

De nombreuse personnes sont encore à remercier, mais je ne peux pas citer toutes ici : vous êtes toujours dans mon coeur.

Table des matières

Synthèse en français de la thèse **13**

General introduction **21**

I Hyperbolic systems of conservation laws and finite volume numerical methods **27**

1 Hyperbolic systems of conservation laws **29**
1.1 General definitions and main theorems . . . 29
1.1.1 The Cauchy and Riemann problems . . . 29
1.1.2 Weak entropy solutions . . . 30
1.1.3 Characteristic fields and simple waves . . . 30
1.1.4 Sonic points . . . 31
1.1.5 Lax and Glimm theorems, Liu criterion . . . 32
1.1.6 The Kruzkov theorem for scalar conservation laws . . . 33
1.2 The case of linear systems . . . 33
1.3 A classical example : the Euler equations . . . 34
1.3.1 Characteristic fields of the 1D Euler system . . . 34
1.3.2 Genuine nonlinearity, linear degeneracy and sonic points . . . 35
1.3.3 Vacuum limit . . . 36
1.3.4 Sonic points of the Euler system . . . 36
1.4 Conclusion . . . 36

2 Introduction to finite volume methods **37**
2.1 Exact Riemann solvers . . . 38
2.2 Approximate Riemann solvers . . . 38
2.2.1 Limitations of approximate Riemann solvers . . . 39
2.2.2 Entropy fix for approximate Riemann solvers . . . 39
2.3 Numerical methods for non-homogeneous systems of conservation laws . . . 41
2.3.1 Source term upwinding for Roe scheme . . . 42
2.3.2 Well-balanced schemes . . . 43

3 Scalar conservation laws **45**
3.1 Structure of the solution . . . 45
3.2 Numerical schemes . . . 46
3.2.1 Godunov scheme . . . 46
3.2.2 Lax-Friedrichs scheme . . . 46
3.2.3 Roe scheme . . . 47
3.2.4 Dubois scheme . . . 47
3.2.5 Harten-type scheme . . . 47
3.3 Some examples for scalar conservation laws . . . 47
3.3.1 Burgers equation $f(u) = \frac{1}{2}u^2$ . . . 47
3.3.2 Flux function $f(u) = u(1-u)^3$ . . . 48
3.3.3 Flux function $f(u) = \sin \pi u$ . . . 48
3.4 Conclusion . . . 49

II Two-phase flow models **51**

4 Two-phase flow models **53**
4.1 Introduction to two-phase flow models . . . 55
4.1.1 Slip model (three-equation model) . . . 55
4.1.2 Drift flux model (four-equation model) . . . 56
4.1.3 Two-fluid model (six-equation model) . . . 58
4.1.4 Five-equation two-fluid model . . . 59
4.1.5 Constitutive equations and equations of state . . . 59
4.2 Quasi-linear form and characteristic fields of boiling flow models . . . 60
4.2.1 Characteristic fields of the slip model . . . 60
4.2.2 Characteristic fields of the drift-flux model . . . 64
4.2.3 Quasi-linear form of the isentropic two-fluid model . . . 67
4.2.4 Quasi-linear form of the five-equation two-fluid model . . . 69
4.3 Difficulties for two phase flow models . . . 74
4.3.1 Complicated characteristic fields . . . 74
4.3.2 Vacuum limit . . . 75
4.3.3 Discontinuous source terms . . . 75
4.3.4 Additional difficulties for the two-fluid models . . . 75

5 The incompressible two-phase flow model **79**
5.1 Introduction . . . 79
5.1.1 The compressible model . . . 80
5.1.2 The incompressible model . . . 80
5.2 Theoretical study . . . 81
5.2.1 Hyperbolicity and characteristic fields . . . 81
5.2.2 Admissible solutions of the Riemann problem . . . 82
5.2.3 Shock and rarefaction waves . . . 82
5.2.4 Solution of the Riemann problem . . . 84
5.2.5 Studying the Cauchy problem . . . 89
5.3 Numerical study . . . 92
5.3.1 Godunov scheme . . . 92
5.3.2 Roe scheme with a Harten type correction . . . 92
5.3.3 Reconstruction scheme . . . 93
5.4 Numerical results . . . 94
5.4.1 The Riemann problem . . . 94
5.4.2 The phase separation under gravity . . . 95
5.4.3 The boiling channel problem . . . 96
5.5 Appendix . . . 97
5.5.1 Appendix : Model derivation . . . 97
5.5.2 Appendix : Vanishing velocity of the sedimentation problem . . . 99
5.5.3 Appendix : Analytical solution of the boiling channel for the incompressible model at the stationary state . . . 101
5.5.4 Appendix : The Roe matrix . . . 102
5.5.5 Appendix : Wave interacting potential for the incompressible model . . . 102
5.5.6 Appendix : The incompressible drift model . . . 104

6 Numerical simulation of the five equations two-fluid model **107**
6.1 Numerical methods . . . 107
6.1.1 Introduction to the computation of the Roe matrix . . . 108
6.1.2 Roe matrix for five-equation model . . . 109
6.1.3 Computation of the sign $\mathrm{sgn}(A)$ and the absolute value $|A|$ of a matrix A . . . 112
6.1.4 Treatment of the non conservative product . . . 113
6.1.5 Treatment of the source term . . . 113
6.1.6 Entropy fix . . . 115
6.1.7 Stiffened gas equation of state . . . 116
6.1.8 Computing the primitive variable from the conservative variables in the five-equation model . . . 116
6.2 Numerical results . . . 117

6.2.1 Water faucet problem . . . 118
6.2.2 Sedimentation . . . 119
6.2.3 Boiling channel . . . 121
6.2.4 Appendix : Numerical simulation of the boiling channel in the case of the drift flux model . . . 123
6.2.5 Appendix : Stationary regime of the boiling channel . . . 124
6.2.6 Appendix : Computing the Roe matrix for the drift flux model . . . 127
6.3 Conclusion . . . 129

7 Package CoreFlows **131**
7.1 Libraries used in CoreFlows . . . 131
7.2 Framework of CoreFlows . . . 132
7.3 Visualization of the CoreFlows . . . 132
7.4 Example of test case code . . . 132
7.4.1 An example of C++ script . . . 133
7.4.2 An example of python script . . . 134

General conclusions and perspectives **137**

Bibliography **139**

Synthèse en français de la thèse

Les écoulements dans les centrales nucléaires

Dans la thermohydraulique des réacteurs nucléaires, l'étude du fluide de refroidissement est extrêmement importante pour l'optimisation de la conception technique, la fiabilité de la distribution de l'électricité ainsi que de la sûreté de la centrale. Dans le cas d'incidents ou d'accidents graves comme une panne de la pompe ou du pressuriseur, même si la réaction en chaîne impliquant la fission nucléaire est arrêtée, le liquide ne peut pas toujours évacuer la chaleur résiduelle générée par la désintégration des produits de fission. En conséquence, celui-ci peut être partiellement ou totalement vaporisé. Si la vapeur générée par l'ébullition du liquide est abondante, la réduction du transfert de chaleur entre les crayons d'uranium et le fluide de refroidissement peut provoquer une surchauffe ces barres. L'augmentation de la température dans le cœur du réacteur peut entraîner des dommages graves et irréversibles telles qu'une fusion partielle ou totale du cœur. L'étude de la dynamique de l'écoulement diphasique dans le cœur du réacteur est donc une tâche très importante. Une vue de la cuve d'un réacteur à eau sous pression (REP) est affichée sur l'image 1. L'eau froide est chauffée en traversant de haut en bas les crayons de combustibles se trouvant dans la cuve.

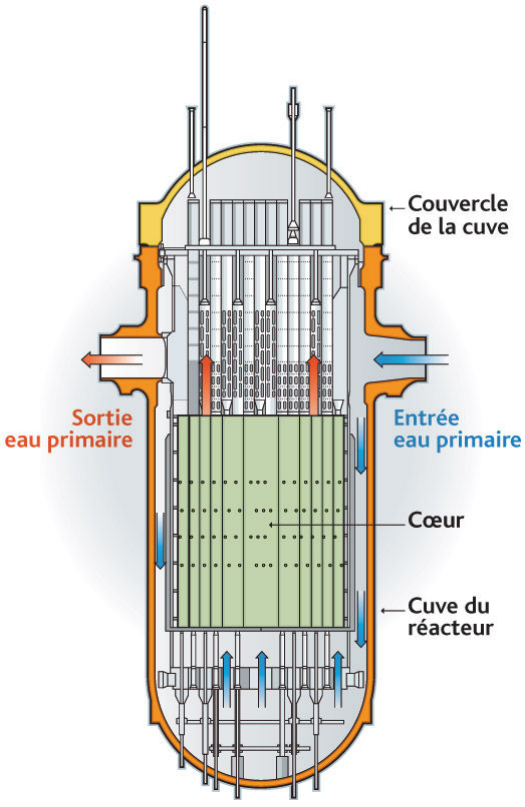

FIGURE 1 – La vue schématique d'une cuve de réacteur à eau pressurisée REP900.

Il y a différentes échelles possibles pour décrire un écoulement diphasique bouillant. Selon l'intérêt spécifique, on peut utiliser une simulation numérique directe pour une description fine de la topologie des inclusions ou des modèles homogénéisés pour la dynamique globale du mélange. Nous sommes ici intéressés par la dynamique globale de la circulation plutôt que de sa structure locale. Par conséquent,

l'écoulement n'est pas considéré ici dans l'échelle microscopique (qui prend en compte les inclusions locales de l'écoulement), et nous allons plutôt l'aborder dans l'échelle macroscopique (avec une hypothèse de continuum ou une prise de moyenne).
Notre objectif ultime est de décrire l'augmentation de la température et l'entrée en ébullition d'un fluide caloporteur dans un canal chauffé représentatif de la dynamique du cœur d'un réacteur nucléaire. En raison de l'ampleur de la cuve ($13\,m \times 5\,m \times 5\,m$) et la complexité des structures locales, seule une estimation macroscopique de la quantité de vapeur générée par l'ébullition est souhaitée et généralement suffisante pour l'analyse de sûreté des centrales nucléaires. L'image (2) affiche un canal bouillant à une échelle où les interfaces entre le liquide et les bulles sont visibles (l'échelle microscopique). Nous allons toutefois décrire l'écoulement à une échelle qui correspond au carré rouge sur la photo. La sortie de nos modèles sera la moyenne locale de la composition du mélange, les vitesses et les températures de chaque phase. Des nombreux auteurs dans la littérature ont modélisé l'échelle macroscopique de

FIGURE 2 – La vue schématique de l'échelle mésoscopique de l'écoulement dans un canal bouillant.

l'écoulement diphasique par deux approches : hypothèse de continuums ou prise de moyenne. Dans la première approche, on considère l'écoulement à deux phases sous la forme d'un mélange où chaque point est supposé être occupé par les deux phases, alors que l'idée principale de la seconde est l'élimination des fluctuations instantanées locales des variables par une opération de moyenne statistique. Les détails de ces deux approches se trouvent dans les livres de Ishii [Ish75 ; IH11] pionnier de la modélisation thermohydraulique à Electricité de France dans les années 1970.
L'application de la méthode de la moyenne, peut se faire par trois approches : l'approche Eulerienne, l'approche Lagrangienne et l'approche statistique de Boltzmann. Parmi celles-ci, la formulation Eulerienne est la plus largement utilisée en raison de son analogie avec la mécanique des fluides monophasiques et les observations expérimentales faites dans un référentiel fixe. Le système obtenu par la moyenne Eulérienne est composé d'équations aux dérivées partielles correspondant aux lois de bilan de masse, de quantité de mouvement et d'énergie du mélange ou de chaque phase. Ces équations sont appelées les équations de champ. On peut distinguer les modèles Eulériens d'écoulements diphasiques par le nombre d'équations de champ et si les déséquilibres mécanique et thermique sont décrits par des équation aux dérivées partielles (EDP) ou des corrélations algébriques. Dans cette thèse, nous nous concentrerons principalement sur les propriétés mathématiques et la simulation numérique des fluides bouillants en déséquilibre mécanique et on supposera l'équilibre thermique entre les phases. Étant donné que le changement de phase s'impose par l'ébullition et pas l'évaporation, le fluide est localement sur la courbe de saturation de liquide-vapeur du diagramme des phases et les températures du liquide et de

la vapeur sont égales à l'échelle microscopique. Cependant, en raison de la description macroscopique moyenne de l'écoulement, il est possible d'avoir la température moyenne de la vapeur supérieure à celle du liquide. Ceci est le cas en particulier dans les réacteurs nucléaires où la vapeur est générée près de la paroi des combustibles chauds et est seulement localement en équilibre thermique avec le liquide environnant. L'équilibre thermique ne peut en toute rigueur pas être satisfait à l'échelle macroscopique en raison du fort gradient de température puisque le liquide au coeur du canal ne bout pas. Nous allons cependant nous concentrer sur l'ébullition saturée où l'hypothèse des phases à saturation s'applique, par opposition à l'ébullition avec liquide sous-refroidi où le liquide est en majorité plus froid que les bulles de gaz. Cette hypothèse permet d'une analyse approfondie du déséquilibre mécanique qui est une question qui soulève de nombreuses difficultés mathématiques et numériques dans la pratique au CEA de Saclay.

Les modèles considérés

Nous sommes surtout intéressés par les écoulements dominés par la convection et les sources tels que le changement de phase, la gravité ou le transfert de chaleur provenant de la fission nucléaire. Pour cette raison, nous allons négliger les effets de conduction thermique et de la viscosité et étudier des systèmes d'EDPs du premier ordre avec termes sources. La théorie des systèmes hyperboliques de lois de conservation sera donc une base importante (partie I). Tous les modèles diphasiques considérés ici (modèle de glissement, modèle à flux à dérive et modèles bifluides) vont afficher deux vitesses caractéristiques rapides correspondant aux ondes acoustiques. Ces champs caractéristiques vraiment non linéaires sont associés à une vitesse du son de mélange qui est plus petite que la vitesse du son de chaque phase (chapitre 4). Les champs caractéristiques associés à la composition du fluide ne sont en général ni vraiment non linéaires, ni linéairement dégénérés et sont particulièrement importantes dans la problématique des phases évanescentes (chapitres 5, 6) et appendix 5.5.6. L'hyperbolicité de ces modèles est conditionnelle à une petite vitesse relative entre phases en comparaison de la vitesse du son du mélange. Ceci est bien le cas dans les centrales nucléaire où les vitesses phasiques ont un ordre de grandeur de quelques mètres par seconde alors que la vitesse du son de mélange a une magnitude de plusieurs centaines de mètres par seconde.

Un modèle bifluide général impliquant des bilans de la masse, de la quantité de mouvement et de l'énergie de chaque phase a été proposé par Ishii comme suit

$$
\begin{aligned}
\frac{\partial \alpha_g \rho_g}{\partial t} + \nabla \cdot (\alpha_g \rho_g \vec{u}_g) &= \Gamma_g, && \text{(1a)}\\
\frac{\partial \alpha_l \rho_l}{\partial t} + \nabla \cdot (\alpha_l \rho_l \vec{u}_l) &= \Gamma_l, && \text{(1b)}\\
\frac{\partial \alpha_g \rho_g \vec{u}_g}{\partial t} + \nabla \cdot (\alpha_g \rho_g \vec{u}_g \otimes \vec{u}_g) + \alpha_g \vec{\nabla} p_g &= \nabla \cdot \left(\alpha_g \left(\bar{\bar{\tau}}_g + \bar{\bar{\tau}}_g^T\right)\right) + \alpha_g \rho_g \vec{g} + \vec{F}_g^w \\
&+ \vec{F}_g^i + \vec{u}^i \Gamma_g + (p_g^i - p_g) \nabla \cdot \alpha_g, && \text{(1c)}\\
\frac{\partial \alpha_l \rho_l \vec{u}_l}{\partial t} + \nabla \cdot (\alpha_l \rho_l \vec{u}_l \otimes \vec{u}_l) + \alpha_l \vec{\nabla} p_l &= \nabla \cdot \left(\alpha_l \left(\bar{\bar{\tau}}_l + \bar{\bar{\tau}}_l^T\right)\right) + \alpha_l \rho_l \vec{g} + \vec{F}_l^w \\
&+ \vec{F}_l^i + \vec{u}^i \Gamma_l + (p_l^i - p_l) \nabla \cdot \alpha_l, && \text{(1d)}\\
\frac{\partial \alpha_g \rho_g E_g}{\partial t} + p_g \frac{\partial \alpha_g}{\partial t} + \nabla \cdot (\alpha_g \rho_g \vec{u}_g H_g) &= \nabla \cdot \left(\alpha_g \left(\bar{\bar{\tau}}_g + \bar{\bar{\tau}}_g^T\right) \cdot \vec{u}_g\right) + \alpha_g \rho_g \vec{g} \cdot \vec{u}_g + Q_g^w + Q_g^i \\
&+ \nabla \cdot (\alpha_g (q_g + q_g^T)) + \vec{F}_g^i \cdot u^i + \Gamma_g H_g^i, && \text{(1e)}\\
\frac{\partial \alpha_l \rho_l E_l}{\partial t} + p_l \frac{\partial \alpha_l}{\partial t} + \nabla \cdot (\alpha_l \rho_l \vec{u}_l H_l) &= \nabla \cdot \left(\alpha_l \left(\bar{\bar{\tau}}_l + \bar{\bar{\tau}}_l^T\right) \cdot \vec{u}_l\right) + \alpha_l \rho_l \vec{g} \cdot \vec{u}_l + Q_l^w + Q_l^i \\
&+ \nabla \cdot (\alpha_l (q_l + q_l^T)) + \vec{F}_l^i \cdot u^i + \Gamma_l H_l^i, && \text{(1f)}
\end{aligned}
$$

où les variables primitives $\alpha_k, \rho_k, u_k, p_k, E_k, H_k = E_k + \frac{p}{\rho_k}$ sont respectivement le taux de présence, la densité, la vitesse, la pression, l'énergie totale et l'enthalpie totale de chaque phase k, l'indice k dénote soit g pour le gaz soit l pour le liquide. La partie droite du système (1a-1f) contient les termes sources suivants

- Les termes transfert interfacial, dénotés par l'indice i :
  - Γ_k^i le changement de phase,
  - F_k^i le frottement interfacial,
  - $\vec{u}^i$ la vitesse interfaciale,
  - Q_k^i le transfert de chaleur interfacial,

— H_k^i l'enthalpie totale interfaciale,
— Les termes d'interaction solide-paroi, dénotés par l'indice w, et dus à la présence des crayons combustibles :
  — $\vec{F}_k^w$ le frottement de la paroi,
  — Q_k^w le transfert de chaleur entre des crayons combustibles et la phase k.
— Les termes diffusifs
  — $\bar{\bar{\tau}}_k$ le tenseur de Reynolds pour la phase k.
  — q_k le flux thermique turbulent de la phase k.
.

Ce modèle est le plus largement utilisé dans des logiciels de la thermohydraulique des réacteurs nucléaires tels que CATHARE (CEA France), Neptune-CFD (EDF-CEA France), RELAP5 (INL USA), CUPID (KAERI Korea du Sud) en raison de sa capacité à décrire des écoulements diphasiques complexes. Dans la pratique, selon les propriétés spécifiques de l'écoulement diphasique, on peut cependant choisir un modèle plus approprié basé sur des hypothèses simplificatrices.

Pour des écoulements co-courant dans un tuyau vertical, les modèles de mélange tels que le modèle de glissement, ou celui à flux de dérive sont également utilisés en génie nucléaire. Dans ces modèle le déséquilibre cinématique est pris en compte par une certaine corrélation sur la vitesse relative $\vec{u}_g - \vec{u}_l = \vec{f}(\alpha, \vec{u}_m, p)$. Le modèle de glissement est basé sur des bilans (masse, quantité du mouvement et énergie) du mélange qui peuvent se mettre sous la forme condensée suivante

$$\begin{aligned}
\frac{\partial \rho_m}{\partial t} + \nabla \cdot (\rho_m \vec{u}_m) &= 0, \\
\frac{\partial}{\partial t}(\rho_m \vec{u}_m) + \nabla \cdot (\rho_m \vec{u}_m \otimes \vec{u}_m + \rho_m c_g (1-c_g) \vec{u}_r \otimes \vec{u}_r + p \cdot \mathrm{Id}) &= \rho_m \vec{g} + \vec{F}^{\mathrm{w}}, \\
\frac{\partial}{\partial t}(\rho_m E_m) + \nabla \cdot (\rho_m \left(\vec{u}_m H_m + c_g (1-c_g)(H_v - H_l)\vec{u}_r\right)) &= \rho_m \vec{g} \cdot \vec{u}_m + \vec{g} \cdot \vec{u}_m + Q^{\mathrm{w}},
\end{aligned}$$

où la masse du mélange est notée $\rho_m = \alpha_g \rho_g + \alpha_l \rho_l$, la vitesse du mélange $u_m = \frac{\alpha_g \rho_g u_g + \alpha_l \rho_l u_l}{\alpha_g \rho_g + \alpha_l \rho_l}$, l'énergie totale du mélange $E_m = \frac{\alpha_g \rho_g E_g + \alpha_l \rho_l E_l}{\alpha_g \rho_g + \alpha_l \rho_l}$ et la vitesse relative est dénotée par $u_r = u_g - u_l$. Le modèle de glissement peut d'obtenir à partir du modèle à deux fluides (1a-1f) en ajoutant les équations des masse, quantité de mouvement et énergie de la vapeur avec celles correspondantes du liquide. Les deux phases sont supposées à saturation. Les taux de présence de chaque phase sont donc calculés par une fermeture supplémentaire $\alpha(p, s^{\mathrm{sat}})$ dans le modèle de glissement.

Dans le modèle à flux de dérive, les deux phases ne sont plus nécessairement à saturation et la composition du mélange est donnée par une EDP supplémentaire portant sur la quantité de vapeur créée par ébullition. Plus précisément, le modèle à flux de dérive comprend les équations de modèle de glissement supplémentées par le bilan de masse de la vapeur comme suit

$$\begin{aligned}
\frac{\partial \alpha_g \rho_g}{\partial t} &+ \nabla \cdot (\alpha_g \rho_g \vec{u}_g) = \Gamma_g, \\
\frac{\partial (\rho_m \vec{u}_m)}{\partial t} &+ \nabla \cdot (\rho_m \vec{u}_m \otimes \vec{u}_m + \rho_m c_g (1-c_g) \vec{u}_r \otimes \vec{u}_r + p \cdot \mathrm{Id}) \\
&= \rho_m \vec{g} + \vec{F}^{\mathrm{w}}, \\
\frac{\partial}{\partial t}(\rho_m E_m) &+ \nabla \cdot \left(\alpha_g \rho_g {H_g}^t \vec{u}_g + \alpha_l \rho_l {H_l}^t \vec{u}_l\right) \\
&= \rho_m \vec{g} \cdot \vec{u}_m + \vec{F}^{\mathrm{w}} \cdot \vec{u}_m + Q^{\mathrm{w}}.
\end{aligned}$$

Généralement, le modèles de glissement et à flux de dérive sont plus simples que ceux à bifluides par rapport à nombre des équations aux dérivées partielles et par rapport aux lois interfaciales. Cependant, pour imposer une vitesse relative entre deux phases il faut faire de nombreuses analyses expérimentales. En outre, la validité de la corrélation de vitesse relative est limitée aux écoulements dont les deux vitesses phasiques sont assez proches.

Tous les trois modèles incluent un déséquilibre mécanique ($\vec{u}_g \neq \vec{u}_l$)) et présentent la difficulté mathématique commune que les champs caractéristiques sont beaucoup plus complexes à analyser que leurs homologues monophasiques. Tout d'abord il n'y a aucune expression simple des champs caractéristiques en raison du fait qu'ils sont issus du spectre de matrices de tailles supérieures à 3 et sans solution

triviale. Deuxièmement, les champs caractéristiques sont généralement ni vraiment non linéaires, ni linéairement dégénérés. Les solutions admissibles admettent ainsi des ondes composites et parfois le nombre d'ondes simples (choc ou détente) est supérieur au nombre d'équations du système de lois de conservation. Enfin, à la différence des écoulements monophasiques, ces modèles diphasiques peuvent faire apparaître des points soniques dans des conditions normales d'écoulement subsonique. Ils nécessitent donc un examen attentif lorsque l'on utilise des schémas non entropiques comme les schémas de type Roe.

Une première difficulté spécifique au modèle bifluides est le problème de la phase évanescente dont la vitesse peut devenir singulière. Par exemple, lorsque le taux de vide α_g approche 0 (liquide pur), la détermination de la par le rapport vitesse du gaz $\vec{u}_g = \frac{\alpha_g \rho_g \vec{u}_g}{\alpha_g \rho_g}$ peut aboutir un singularité. Nous allons étudier spécifiquement la phase évanescente, d'abord à travers une analyse de l'existence d'une solution bornée dans le cas incompressible. Ensuite, nous allons proposer des méthodes numériques de volumes finis à la fois pour les cas incompressible et compressible. Une deuxième difficulté spécifique du modèle bifluide est qu'il est non conservatif en raison des termes $\alpha_k \nabla p$ dans les équations de quantité de mouvement et $p\partial_t \alpha_k$ dans les équations d'énergie. Une attention particulière doit donc être accordée au traitement des produits non conservatifs dans la résolution numérique.

Nous allons valider les méthodes numériques proposées sur plusieurs cas test dans cette thèse. Le premier test est le problème de sédimentation, ce qui représente un problème de disparition de phase avec un état stationnaire discontinu. Le second est le canal bouillant, ce qui représente un problème d'apparition de phase. Le schéma de Roe classique ne parvient pas à simuler ces tests. Nous proposons d'ajouter une correction entropique de type Harten au schéma de Roe dans ces tests. Le schéma ainsi corrigé réussit à simuler le problème de sédimentation jusqu'à l'état stationnaire avec des vitesses bornées et des taux de présence positifs sans artifice particulier. En appliquant le même schéma de Roe avec correction entropique au problème du canal bouillant, la simulation, ne peut pas atteindre un état stationnaire correcte. Les résultats numériques montrent des oscillations parasites en raison des termes sources non-réguliers. Un traitement spécifique des termes source est nécessaire pour faire face à cette difficulté.

Plan de l'ouvrage

Cette thèse est divisée en deux parties principales. La première partie rappelle la théorie des lois de conservation hyperboliques et certaines méthodes numériques classiques. Elle comprend les chapitres suivants.

- Le Chapitre 1 rappelle la théorie générale des lois de conservation hyperboliques se trouvant dans la littérature, on peut citer ici [GR96],[Ser99],[Daf10],[LeF02],[Bou00] par exemple. La première section introduit des définitions classiques pour les lois de conservation, les systèmes hyperboliques et les champs caractéristiques. Nous rappelons les théorèmes d'existence globale et d'unicité de solution entropique de Lax (problème de Riemann) et de Glimm (problème de Cauchy). Le cas linéaire hyperbolique est présenté à la section 1.2 et le système des équations d'Euler, un exemple classique pour les systèmes lois de conservation non-linéaires et hyperboliques, se trouve dans Section 1.3. Finalement, le théorème de Kruzkov sur l'existence globale et l'unicité pour les lois de conservation scalaires est rappelé dans la Section 1.1.6.
- Dans le Chapitre 2, on donne une introduction aux méthodes numériques du type volumes finis qui sont largement répandues dans la mécanique des fluides numérique. Ces méthodes permettent de concevoir des schémas conservatifs et une grande flexibilité dans le choix des maillages. Les solveurs de Riemann exacts et approchés classiques sont introduits. En outre, afin de mieux traiter les termes sources dans les systèmes de lois de conservation et capturer des régimes stationnaires corrects, nous introduisons la méthode de décentrement des termes source décrite dans [BV94] ainsi que le schéma équilibre introduit dans [Bou00].
- Le chapitre 3 est consacré à un cas particulier de lois de conservation, les lois de conservation scalaires, pour lesquelles la théorie de l'existence et l'unicité est complète, voir la Section 1.1.6. Nous visons à apporter quelques exemples d'ondes composites générées par des lois scalaires non convexes et illustrons la difficulté générée par des points soniques avec quelques schémas numériques afin de mieux comprendre la théorie des lois de conservation et les schémas numériques introduits dans les chapitres 1 et 2. Différentes méthodes numériques sont ensuite appliquées pour résoudre les problèmes de Riemann. Nous montrons que le schéma de Roe avec une cor-

rection entropique de type Harten est un bon candidat dans le cas de points soniques et de flux non-convexes.

La contribution principale de cette thèse se trouve dans la deuxième partie, qui est consacrée aux écoulements diphasiques, les modèles et leurs propriétés mathématiques ainsi que des résultats numériques. Elle se compose des chapitres suivants

— Le Chapitre 4 apporte une introduction générale de modèles diphasiques rencontrés en thermohydraulique des réacteurs nucléaires. En raison de la dynamique complexe du mélange, au lieu de faire l'hypothèse d'un équilibre mécanique, les deux vitesses de chaque phase sont soit reliées par une relation algébrique dans les modèles de mélange ou sont traités indépendamment par deux lois de conservation de quantité de mouvement séparées dans les modèles bifluides. Celà introduit de nouvelles difficultés mathématiques et l'on observe que les propriétés de ces modèles diphasiques sont très différente de celles du système des équations d'Euler, qui est largement étudié dans la littérature. Afin de surmonter ces difficultés, nous étudions d'abord la limite incompressible des modèles à flux de dérive.
— Le chapitre 5 continue à étudier la limite incompressible mais pour le modèle à deux fluides. Un tel modèle est un système hyperbolique de 2 lois de conservation. Nous montrons que ce système 1D n'est pas strictement hyperbolique et que les champs caractéristiques ne sont ni vraiment non linéaires, ni linéairement dégénérés. Nous prouvons néanmoins l'existence et l'unicité d'une solution admissible au problème de Riemann. Cette solution reste limitée avec des taux de vide positifs, même lorsque l'une des phases disparaît. La transition entre diphasique et monophasique ne signifie pas l'équilibre mécanique, mais affiche une structure d'onde non classique. Nous proposons ensuite des solveurs de Riemann approchés pour simuler le modèle, en particulier la transition de phase diphasique/monophasique. Les solveurs de Riemann classiques ont été considérés comme le schéma de Godounov, schéma de Roe avec ou sans la correction entropique. Nous proposons également une méthode de reconstruction discontinue inspirée de [DL01 ; Lag04], cette méthode capture bien les discontinuités, tandis que les autres schémas peuvent montrer quelques oscillations parasites dans certains problèmes de Riemann. Enfin, comme une application nous étudions et simulons le problème de la séparation de phase par gravité et le canal bouillant.
  De même, la limite incompressible pour le modèle à flux de dérive est étudiée dans l'annexe 5.5.6. L'analyse de l'équation scalaire résultante fait apparaître des ondes composites dues au fait que les champs caractéristiques ne sont ni vraiment non linéaires, ni linéairement dégénérés.
— Les modèles bifluides compressibles à une pression font l'objet du Chapitre 6. Ces modèles nous intéressent pour une simulation plus réaliste des cas test comme la séparation de phase et le canal bouillant. Cependant, le modèle complet à deux fluides (modèle à six-équation) qui prend en compte les déséquilibres cinématique et thermique fait apparaître de nombreuses difficultés concernant les produits non conservatifs et les relations d'interactions interfaciales. Pour réduire certaines difficultés, on considère d'abord une équilibre thermique. Plus précisément, une seule équation bilan d'énergie du mélange est prise en compte avec deux équations de bilan de masse et deux équations de bilan de quantité de mouvement. Nous qualifierons le système résultant de modèle à cinq équations. Puisque nous ne pouvons pas calculer explicitement le spectre de la matrice jacobienne, on donnera des estimations approchées des valeurs propres. Afin de simuler ce modèle, on utilise un solveur de Riemann du type Roe. Des détails du calcul de la matrice de Roe ainsi que de sa valeur absolue et de son signe inspirés par [Ndj07a] sont rappelés dans ce chapitre. Nous considérons une correction entropique de type Harten au schéma de Roe classique. L'idée principale de cette correction est d'augmenter un peu diffusion numérique afin de permettre que le schéma capture la solution entropique. En effet, cette correction améliore les résultats de simulation dans certains cas tests, où le schéma de Roe classique échoue. Par exemple, le cas test ou il y a une disparation de phase par la séparation de phase due à gravité. La capture de la vitesse des phases évanescentes pose des problèmes avec le schéma de Roe classique. Cependant, on montre que la correction d'entropie ne suffit pas à préserver la régime stationnaire quand des termes source raides sont présents. En s'inspirant du travail de [BV94], nous employons un décentrement du terme source similaire à celui des flux convectifs. En appliquant cette méthode dans le cas test du canal bouillant, on est capable de préserver la solution stationnaire dont la forme est cohérente avec la solution analytique.
— Enfin, le dernier chapitre est consacré à l'introduction de la maquette CoreFlows, avec laquelle ont été obtenus les résultats numériques des écoulements compressible dans cette ouvrage.

Conclusions générales et perspectives

Les travaux de cette thèse se sont consacrés à l'analyse mathématique et la simulation numérique des modèles d'écoulements bouillants dans la thermohydraulique des centrales nucléaires. Les modèles étudiéss ont été le modèle de glissement, le modèle à flux de dérive et les modèles bifluides à une pression. Nous nous sommes tout d'abord demandé si les propriétés mathématiques générales des modèles diphasiques étaient semblables à celles des modèles monophasiques (champs charactéristiques vraiment non linéaires ou linéairement dégénérés, absence de points soniques en régime subsonique...). L'étude a également cherché à savoir s'il existe une solution positive ($\alpha \in [0,1]$) avec des vitesses bornés qui ne sont pas forcément égales quand une phase disparaît dans les modèles à bifluides.

Notre étude sur la limite incompressible des modèles de dérive et à deux fluides montre que les champs caractéristiques de ces systèmes sont différents de ceux des modèles monophasique en raison du fait qu'ils ne sont ni vraiment non linéaires, ni linéairement dégénérés. La solution du problème de Riemann produit des ondes composites et affiche un nombre d'ondes simples qui peut être supérieur au nombre d'équations du système EDP.

Même si les champs caractéristiques sont beaucoup plus complexes à décrire dans le cas des modèles compressibles, nous avons exploré certains cas particuliers (modèle de glissement, modèle à flux de dérive). La conclusion obtenue à nouveau est que les champs caractéristiques ont une structure plus exotique quand un déséquilibre mécanique est pris en compte. Tous les modèles considérés présentent deux ondes acoustiques avec une vitesse du son de mélange qui est plus petite que chaque vitesse du son phasique et qui sont vraiment non linéaire pour les petites vitesses relatives. En outre, l'étude des valeurs propres des modèles à bifluides montre que les points soniques apparaîssent dans des conditions d'écoulement normales, ce qui est complètement différent de l'écoulement monophasique.

En raison de l'existence de points soniques dans les modèles à bifluides, nous proposons d'appliquer le schéma de Roe avec une correction entropique de type Harten dans certains tests classiques. Nous ne cherchons pas à détecter les points soniques et appliquons cette correction sur l'ensemble du domaine. Les résultats numérique du test de sédimentation montrent l'existence de deux vitesses bornées même pour la phase absente et ce sans terme de régularisation (le frottement interphase et la viscosité de chaque phase sont négligés) ou cut-off numérique.

Une partie importante de la thèse est consacrée au problème du canal bouillant. Ce cas de test est difficile non seulement en raison de l'apparition de phase mais aussi les termes sources irrégulièrs. Afin de préserver l'état stationnaire correct, il est essentiel de considérer une discrétisation spéciale de ces termes sources. Le décentrement des termes sources est donc utilisé en plus de la correction entropique de type Harten dans le calcul des flus. L'état stationnaire résultant est finalement bien capturé.

Une limitation de notre étude est que les résultats numériques sont obtenus avec des schémas explicites, soit en utilisant de très petits pas de temps et la capture d'état stationnaire prend beaucoup de temps de calcul, en particulier dans les simulations en 2D et 3D. Le prochain défi sera d'utiliser des schémas implicites afin d'améliorer le temps de calcul.

Les termes sources provenant de la thermohydraulique dépendent du vecteur inconnu et sont généralement irrégulièrs. Etudier l'existence et l'unicité du régime staionaire pour des EDP ayant ce type de terme source discontinu où le théorème de Cauchy-Lipschitz ne s'applique pas est un point fondamental à creuser dans de futures rechercehs.

Au niveau du modèle physique, la prise en compte des termes visqueux et de conduction thermique entraînerait des défis intéressants sur des géométries complexes avec des maillages non structurés ou non conformes. La prise en compte du déséquilibre thermique dans l'analyse mathématique des modèles est également une demande de la communauté de thermohydraulique entrainant la difficulté due au traitement de termes non conservatifs supplémentaires.

General introduction

In the thermal hydraulics of nuclear reactors, the study of the cooling fluid is extremely important owing to the optimization of the engineering design, the reliability of the electricity supply as well as the safety of the plant management. In the case of incidents or severe accidents such as a breakdown of the pump or the pressurize, even if the chain reaction involving Uranium fission is stopped, the liquid may not be able to evacuate the residual heat generated by the decomposition of fission products. As a consequence the liquid may be partially or totally vaporized. If the vapor generated by the boiling of the liquid is abundant, it may reduce the heat transfer between the uranium rods and the cooling fluid yielding an overheating of the rods. The increase in temperature in the reactor core may lead to severe and irreversible damages such as partial or total core meltdown. Studying the dynamics of the boiling two-phase flow in the reactor core is therefore a very important task. A view of the vessel of a pressurized water reactor is displayed on picture 3. The cold water is heated while going upward through the Uranium rods located in the core of the vessel.

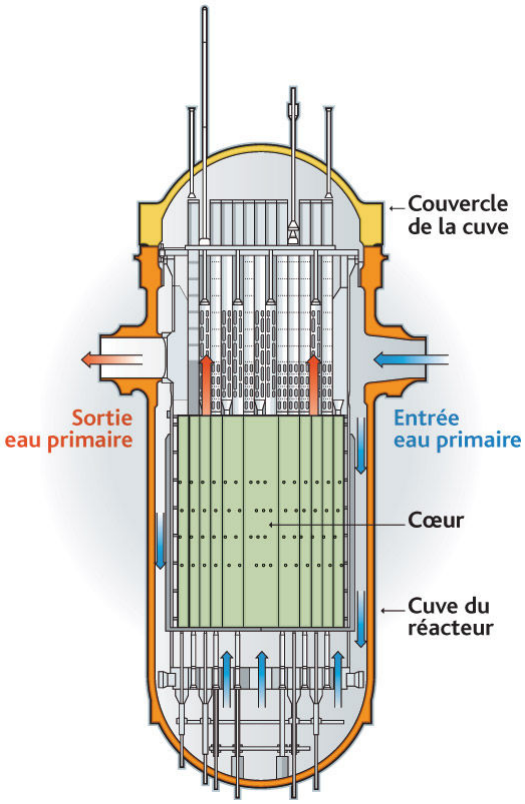

FIGURE 3 – Schematic view of a pressurized water reactor vessel REP900

There are different possible scales to describe a boiling two-phase flow. Depending on the specific interest, one can use a Direct Numerical Simulation for a fine description of the topology of the inclusions, or homogenized models for the global dynamics of the mixture. We are here interested in the global dynamics of the flow rather than its local structure. Therefore the flow is considered neither in the microscopic scale (molecular scale) nor in the meso-scale (which takes into account the local inclusions in of the flow), we will instead address the flow in the macroscopic scale (with continuum

assumption).
Numerous authors in the literature have developed the macroscopic scale of the two-phase flow by two approaches : interacting continua assumption and averaging method. The first approach considers the two-phase flow as a mixture where each point is assumed to be occupied by two phases, whereas the main characteristic of the second one is the elimination of the local instantaneous fluctuations of the variables by a statistical averaging operation. The details of these two approaches are given in the book of Ishii [Ish75 ; IH11] who pioneered thermal hydraulics modeling at Electricité de France in the years 1970s.
Applying the averaging method, one may encounter three main groups : Eulerian, Lagrangian and Boltzmann statistical averages. Among those, the Eulerian formulation is the most widely used due to its similarity with traditional physics and experimental observations. The system obtained by the Eulerian average consists of partial differential equations corresponding to the conservation laws of the governing balance laws of mass, momentum and energy of the two-phase mixture. Such equations are called the field equations.
Our objective is to describe the heat increase of a fluid in a heated channel that is representative of the dynamics encountered in a nuclear reactor core. Due to the scale of the vessel ($13m \times 5m \times 5m$) and complexity of the local structures, only a macroscopic estimate of the amount of steam generated by a boiling flow is desired and usually sufficient for the safety analysis of the power plant. The picture (4) displays a boiling channel at a scale where the interfaces between the liquid and the bubbles are visible (the mesoscale). We will however describe the flow at a scale that corresponds to the red square on the picture. The output of our models will be the local average of the mixture composition, the velocities and temperatures of each phase.

FIGURE 4 – Schematic view of the mesoscopic scale of the flow in a boiling channel

One may distinguish the Eulerian two-phase flow models by the number of field equations and whether the mechanical and thermal disequilibrium is described by PDEs or algebraic correlations. In this thesis we will mainly focus on the mathematical properties and the numerical simulation of boiling flows in mechanical disequilibrium and will mostly assume thermal equilibrium. Since we consider phase change through boiling and not evaporation, the fluid is locally on the liquid-vapor saturation curve of the phase diagram and the liquid and vapor temperatures are equal. However due to the averaged macroscale description of the flow, it is possible to have the average gas temperature higher than the average liquid temperature. This is the case in particular in nuclear reactors where the steam is generated near the hot Uranium wall and is only locally but not globally at thermal equilibrium

with the bulk liquid because of the strong temperature gradient. We will however focus on saturated boiling where the assumption of phases at saturation applies, as opposed to subcooled boiling where the bulk liquid is cooler than the gas bubbles. This assumption a thorough analysis of the mechanical disequilibrium which is an issue that raises many mathematical and numerical difficulties in practice at CEA Saclay.

We are mostly interested by flows dominated by the convection of the fluid and source terms such as phase change, gravity or heat transfer coming from nuclear fission. For this reason we will neglect viscous and thermal conduction effect and consider first order systems of partial differential equation with source terms. The theory of hyperbolic systems of balance laws will therefore be an important basis (part I). All boiling flow models considered here (slip model, drift flux model and two-fluid models) will display two fast characteristic speed corresponding to genuinely nonlinear acoustic waves with a mixture sound speed that is smaller than each phasic sound speed (chapter 4). Also the void waves associated to the fluid composition are in general neither genuinely nonlinear nor linearly degenerate and are addressed specifically through the vanishing phase issue (chapters 5, 6 and appendix 5.5.6). Their hyperbolicity is conditional to small relative velocity compared to the mixture sound speed which is the case in nuclear power plant where the phasic velocities have a magnitude of a few meter per second whereas the mixture sound speed has a magnitude of hundreds of meters per second.

A general two-fluid model was proposed by Ishii from the balance laws governing the evolution of the mass, momentum and energy of each phase as follows

$$\frac{\partial \alpha_g \rho_g}{\partial t} + \nabla \cdot (\alpha_g \rho_g \vec{u}_g) = \Gamma_g, \tag{2a}$$

$$\frac{\partial \alpha_l \rho_l}{\partial t} + \nabla \cdot (\alpha_l \rho_l \vec{u}_l) = \Gamma_l, \tag{2b}$$

$$\begin{aligned} \frac{\partial \alpha_g \rho_g \vec{u}_g}{\partial t} + \nabla \cdot (\alpha_g \rho_g \vec{u}_g \otimes \vec{u}_g) + \alpha_g \vec{\nabla} p_g &= \nabla \cdot \left(\alpha_g \left(\bar{\bar{\tau}}_g + \bar{\bar{\tau}}_g^T\right)\right) + \alpha_g \rho_g \vec{g} + \vec{F}_g^w \\ &+ \vec{F}_g^i + \vec{u}^i \Gamma_g + (p_g^i - p_g) \nabla \cdot \alpha_g, \end{aligned} \tag{2c}$$

$$\begin{aligned} \frac{\partial \alpha_l \rho_l \vec{u}_l}{\partial t} + \nabla \cdot (\alpha_l \rho_l \vec{u}_l \otimes \vec{u}_l) + \alpha_l \vec{\nabla} p_l &= \nabla \cdot \left(\alpha_l \left(\bar{\bar{\tau}}_l + \bar{\bar{\tau}}_l^T\right)\right) + \alpha_l \rho_l \vec{g} + \vec{F}_l^w \\ &+ \vec{F}_l^i + \vec{u}^i \Gamma_l + (p_l^i - p_l) \nabla \cdot \alpha_l, \end{aligned} \tag{2d}$$

$$\begin{aligned} \frac{\partial \alpha_g \rho_g E_g}{\partial t} + p_g \frac{\partial \alpha_g}{\partial t} + \nabla \cdot (\alpha_g \rho_g \vec{u}_g H_g) &= \nabla \cdot \left(\alpha_g \left(\bar{\bar{\tau}}_g + \bar{\bar{\tau}}_g^T\right) \cdot \vec{u}_g\right) + \alpha_g \rho_g \vec{g} \cdot \vec{u}_g + Q_g^w + Q_g^i \\ &+ \nabla \cdot (\alpha_g (q_g + q_g^T)) + \vec{F}_g^i \cdot u^i + \Gamma_g H_g^i, \end{aligned} \tag{2e}$$

$$\begin{aligned} \frac{\partial \alpha_l \rho_l E_l}{\partial t} + p_l \frac{\partial \alpha_l}{\partial t} + \nabla \cdot (\alpha_l \rho_l \vec{u}_l H_l) &= \nabla \cdot \left(\alpha_l \left(\bar{\bar{\tau}}_l + \bar{\bar{\tau}}_l^T\right) \cdot \vec{u}_l\right) + \alpha_l \rho_l \vec{g} \cdot \vec{u}_l + Q_l^w + Q_l^i \\ &+ \nabla \cdot (\alpha_l (q_l + q_l^T)) + \vec{F}_l^i \cdot u^i + \Gamma_l H_l^i, \end{aligned} \tag{2f}$$

where the primitive variables $\alpha_k, \rho_k, u_k, p_k, E_k, H_k = E_k + \frac{p}{\rho_k}$ are respectively the volume fraction, density, velocity, pressure, total energy and total enthalpy of the phase k , subscript k denotes either g for the gas or l for the liquid.

The right hand side of the system (2a-2f) mentions source terms which can be classified as follows

- The interfacial transfer terms, denoted by the superscript i :
  - Γ_k^i the phase change rate,
  - F_k^i the interfacial friction terms,
  - $\vec{u}^i$ the interfacial velocity,
  - Q_k^i the interfacial heat transfer,
  - H_k^i the interfacial total enthalpy.
- The solid- wall interaction terms, denoted by the superscript w, and due to the presence of Uranium rods :
  - $\vec{F}_k^w$ the wall friction force,
  - Q_k^w the wall heat transfer to the phase k.
- The diffusion terms
  - $\bar{\bar{\tau}}_k$, $k = g, l$ are the Reynolds stress for the phase k.
  - q_k the turbulent heat flux of the phase k.

.

This model is the most widely used in nuclear thermal hydraulic software. CATHARE[1], Neptune-

1. Developed by CEA (France)

CFD [2], RELAP5 [3], CUPID [4] are some examples. In practice, depending on the specific properties of the two-phase flow, one may choose a suitable model based on simplifying assumptions.

The mixture models such as the slip model (three-equation model) and drift flux model (four-equation model) are the ones also used in nuclear engineering. The slip model consists of the conservation equations governing the balance laws of mass, momentum and energy of the mixture with the assumption of phases at saturation. More precisely, it is derived from the six-equation two-fluid model (2a-2f) by adding the two phasic equations of mass, momentum and energy. Neglecting diffusion terms we obtain the following system of three balance laws

$$\begin{aligned}
\frac{\partial \rho_m}{\partial t} + \nabla \cdot (\rho_m \vec{u}_m) &= 0, \\
\frac{\partial}{\partial t}(\rho_m \vec{u}_m) + \nabla \cdot (\rho_m \vec{u}_m \otimes \vec{u}_m + \rho_m c_g (1-c_g) \vec{u}_r \otimes \vec{u}_r + p \cdot \mathrm{Id}) &= \rho_m \vec{g} + \vec{F}^{\mathrm{w}}, \\
\frac{\partial}{\partial t}(\rho_m E_m) + \nabla \cdot (\rho_m \left(\vec{u}_m H_m + c_g (1-c_g)(H_v - H_l)\vec{u}_r\right)) &= \rho_m \vec{g} \cdot \vec{u}_m + \vec{g} \cdot \vec{u}_m + Q^{\mathrm{w}}.
\end{aligned}$$

The difference between the slip model and the drift flux model is that the drift flux consists of the two mass balance laws of liquid and vapor and phases are no longer assumed at saturation. It is derived from the six-equation two-fluid model (2a-2f) by adding the two phasic equations of momentum and energy. Neglecting diffusion terms we obtain the following system of four balance laws

$$\begin{aligned}
\frac{\partial \alpha_g \rho_g + \alpha_l \rho_l}{\partial t} &+ \nabla \cdot (\rho_m \vec{u}_m) = 0, \\
\frac{\partial \alpha_g \rho_g}{\partial t} &+ \nabla \cdot (\alpha_g \rho_g \vec{u}_g) = \Gamma_g, \\
\frac{\partial (\rho_m \vec{u}_m)}{\partial t} &+ \nabla \cdot (\rho_m \vec{u}_m \otimes \vec{u}_m + \rho_m c_g (1-c_g) \vec{u}_r \otimes \vec{u}_r + p \cdot \mathrm{Id}) \\
&= \rho_m \vec{g} + \vec{F}^{\mathrm{w}}, \\
\frac{\partial}{\partial t}(\rho_m E_m) &+ \nabla \cdot \left(\alpha_g \rho_g {H_g}^t \vec{u}_g + \alpha_l \rho_l {H_l}^t \vec{u}_l\right) \\
&= \rho_m \vec{g} \cdot \vec{u}_m + \vec{F}^{\mathrm{w}} \cdot \vec{u}_m + Q^{\mathrm{w}}.
\end{aligned}$$

These two models admit mechanical disequilibrium owing to the relative velocity closure law $\vec{u}_r(\rho_m, \vec{u}_m, E_m)$ imposed between the liquid and the vapor velocities. Generally, the slip and drift flux models are simpler than the two-fluid models in the sense of number of partial differential equations and mathematical challenging. However, the relative velocity correlation can be very complicate as it is based on several experimental and analytical studies. Furthermore the validity of the relative velocity closure law limits their applicability to flows where the two velocities are almost equal. This is a serious limitation when for example the phases move in different direction (counter-current flow) and motivates the study of the two-fluid approach which shares many of its properties with the slip and drift models.

All three models include a mechanical disequilibrium and have the common mathematical difficulty that the characteristic fields are much more complicated than their single-phase counterpart. Firstly there is no simple closed expression of the characteristic speeds due to the fact that the exact computation of the spectrum of the Jacobian matrix of the flux functions leads to a very complicated eigenstructure. Secondly the characteristic fields are usually neither genuinely nonlinear nor linearly degenerate. The admissible solutions thus admit composite waves and sometimes the number of simple waves is greater than the number of equations in the system of balance laws. Lastly, at the difference of single phase flows, these two-phase models may give rise to sonic points in normal subsonic flow conditions. It therefore requires a careful consideration whenever one uses non entropic schemes such as the Roe-type scheme. These three models may give very easily rise to sonic points even normal subsonic conditions.
A specific difficulty of two-fluid models is the vanishing phase problem owing to the singularity of the ghost phase velocity. More precisely, when the void fraction α_g approaches to 0 (pure liquid) for example, the velocity computation $\vec{u}_g = \frac{\alpha_g \rho_g \vec{u}_g}{\alpha_g \rho_g}$ yields a singularity. This challenging problem is one of

2. Developed by EDF-CEA (France)
3. Developed by INL(USA)
4. Developed by KAERI (Korea)

the issues in the thermal hydraulics platforms using the two-fluid models. We will investigate specifically the vanishing phase, first through an analysis of the existence of a bounded solution in the incompressible case. Then we will propose finite volume numerical methods for both the incompressible and the compressible two-fluid models. A second difficulty of that is specific to two-fluid model is the fact that it is non conservative. We will have to pay special attention to the treatment of non conservative products.

We will validate the numerical methods proposed on several test cases in this thesis. The first test is the sedimentation problem, which represents a phase disappearance issue with a discontinuous stationary state. The second one is the boiling channel, which represents a phase appearance problem. The classical Roe-scheme fails to simulate these tests. We suggest adding a Harten-type entropy fix to the Roe scheme in the former test, the resulting scheme is successful carried out the simulation until stationary state with bounded velocities and positive void fraction. Using the same method to the later one, the boiling channel, the simulation in fact can not reach a correct stationary state, the numerical results shows spurious oscillation due to the non regular source terms. A careful treatment of the source terms is required to deal with this difficulty.

Structure of the thesis

The thesis is divided in two main parts. The first part recalls the main theory of the hyperbolic conservation laws and some classical numerical methods, it consists of the following chapters.

— Chapter 1, we recall the general theory of the hyperbolic conservation laws which we can find in literature, see [GR96],[Ser99],[Daf10],[LeF02],[Bou00]. The first section recalls some classical definitions of the conservation laws, hyperbolic system, and the characteristic fields. We do not forget to state the Lax theorem for global existence and uniqueness of entropy solution to the Riemann problem and the one of Glimm for the Cauchy problem. The linear hyperbolic system is presented in Section 1.2 and the Euler system, a classical example nonlinear of hyperbolic conservation laws, is found Section 1.3. Finally, the well-known theorem for global existence and uniqueness of scalar conservation laws, Kružkov theorem, is recalled in Section 1.1.6.

— Chapter 2 gives an introduction to numerical methods which are used widely in computational fluid dynamics. They allow the design of conservative schemes and a great flexibility of the mesh structure. The exact and approximate Riemann solvers with some classical schemes are introduced. Moreover, in order to better treat the source terms in the conservation laws system such that the numerical schemes can capture the correct stationary state, we introduce the source upwinding method described in [BV94] as well as the well-balanced scheme in [Bou00].

— The chapter 3 devotes to a particular case of the conservation laws, the scalar conservation laws, for which the theory of existence and uniqueness is complete, see Section 1.1.6. We aim at giving some examples of composite waves generated by non convex scalar laws and illustrate the difficulty generated by sonic points with some numerical schemes in order to better understand the theory of conservation laws and the numerical schemes in Chapter 1 and 2. Different numerical methods are then applied to solve the Riemann problems. We show that the Roe scheme with Harten-type entropy fix is a good candidate in the case of sonic points and non-convex flux.

The main part of the thesis is presented in the second part, which devotes to the two-phase flow models, their mathematical properties and the numerical results. It consists of the following chapters.

— Chapter 4 gives a general introduction of the two-phase flow models used in the nuclear power plant. Due to complex dynamics of the mixture, we do not make the assumption of a mechanical equilibrium, instead the two velocities of each phase are either relaxed by an algebraic relation in the mixture models or are treated independently by two separated momentum conservation laws in the two-fluid models. This leads to new mathematical difficulties and we observe that the properties of two-phase flow model is very different from the single phase one, which is largely studied in the literature. In order to overcome such difficulties, we first study the incompressible limit of the two-phase flow models.

— Chapter 5 continues studying the incompressible limit but for the two-fluid model. Such a model is a 2×2 hyperbolic system of conservation laws. We show that this 1D system is not strictly hyperbolic, that the characteristic speeds can not *a priori* be ordered and that the characteristic fields are neither genuinely nonlinear, nor linearly degenerate. We nevertheless prove the existence and uniqueness of an admissible solution to the Riemann problem. This solution remains bounded with positive volume fractions even when one of the phases vanishes. The multiphase/-single phase transition does not imply mechanical equilibrium but displays a non classical wave

structure. We then propose some approximate Riemann solvers to simulate the model, especially the multiphase/single phase transition. The classical Riemann solvers have been considered such as Godunov scheme, Roe scheme with or without entropy fix. We also propose an in-cell discontinuous reconstruction method which proves to be successful, whereas the other schemes may show some spurious oscillations in some Riemann problem. Finally, as an application we study and simulate the problem of phase separation by gravity and the boiling channel.
Similarly, the incompressible limit for the drift flux model is studied in the Appendix 5.5.6. The analysis shows that the composite waves appears due to the fact that the characteristic fields is neither genuinely nonlinear nor linearly degenerate.

— Chapter 6 concentrates on the compressible two-fluid models, where we mainly study the common temperature five-equation two-fluid model. The quasilinear form is presented. Since we can not explicitly compute the spectrum of the Jacobian matrix, the approximate eigenvalues of the isentropic two-fluid model is instead supposed to be a reference. For the numerical part in this chapter, we present in details the computation of the Roe matrix $\tilde{\mathbf{A}}(U_L, U_R)$. In order to apply the Roe-type scheme, an algorithm for the computation of the absolute matrix $|\tilde{\mathbf{A}}|$ and its sign $\text{sgn}(\tilde{\mathbf{A}})$ in [Ndj07a] is recalled. In addition, the Harten-type entropy fix is suggested to associate with the classical Roe scheme. As for the preservation of the correct stationary state, the source upwinding method is studied and proved efficient. Finally we apply the five-equation two-fluid model to simulate some classical but challenging test cases. The stiffened gas law is used as equation of state for simplicity. The first test case is the water faucet problem, which is a classical one used to validate the numerical methods in two-phase flow. This test is difficult due to the presence of the discontinuous transient state. The center-type schemes are usually not able to simulate this problem whereas the Roe-type schemes or the one using the full eigenvalues shows good results, following [PCC03],[SH13],[EF05], [Ndj07b]. The second test case is a sedimentation problem, i.e. a phase separation by gravity. This test is challenging due firstly to the presence of counter-current flows where the two partial velocities go in different directions, which yields many sonic points ; and secondly to the existence of a nontrivial stationary state displaying vanishing phases and with a discontinuous void fraction profile. This test is classically used to verify numerical methods developed for two-phase flow models, see [Coq+97 ; MEF09 ; SH13] for one pressure two-fluid model, and [ACR12] for the two pressures two-fluid model. In order to obtain a physically relevant solution to the sedimentation test case it is important to use a two-fluid approach since the two phasic velocities are not correlated. Therefore we perform this test using the five-equation two-fluid model. The last numerical test is the boiling channel, which is an important test for the nuclear reactor thermal hydraulics. Numerical results show that source upwinding is important in capturing the correct stationary state.

— The last chapter introduces the package CoreFlows used to simulate the compressible two-phase flow models in this document.

Première partie

Hyperbolic systems of conservation laws and finite volume numerical methods

Chapitre 1

The general theory of hyperbolic systems of conservation laws

This chapter introduces to the general theory of the hyperbolic conservation laws which we can find in literature, see [GR96], [Ser99], [Daf10], [LeF02], [Bou00]. The first section recalls some classical definitions of the conservation laws, hyperbolic system, and the characteristic fields. We do not forget to state the Lax theorem for global existence and uniqueness of entropy solution to the Riemann problem and the one of Glimm to the Cauchy problem. The linear hyperbolic system is presented in Section 1.2 and the Euler system, a classical one of hyperbolic conservation laws, is found in Section 1.3.

1.1 General definitions and main theorems

1.1.1 The Cauchy and Riemann problems

Let Ω an open subset of $\mathbb{R}^p$ and F_j, $1 \leq j \leq d$, d smooth functions from Ω to $\mathbb{R}^p$, let $F = (F_1, \ldots, F_d)$ in $\mathbb{R}^{p\times d}$. The system

$$\frac{\partial}{\partial t}U + \nabla_x \cdot F(U) = 0, \quad x = (x_1, \ldots, x_d) \in \mathbb{R}^d, t \geq 0, \tag{1.1}$$

where $U = (U_1, \ldots, U_p)$ is an unknown vector, is called a *conservative system* or a system of conservation laws. In particular, if $p = 1$, then (1.1) is called a *scalar conservation law*.
Let us denote $A_j(U) = \nabla F_j(U)$ in $\mathbb{R}^{p\times p}$ the Jacobian matrix of F_j. Then, the system (1.1) is said to be *hyperbolic* on Ω if for any $U \in \Omega$, and any $\omega = (\omega_1, \ldots, \omega_d) \in \mathbb{R}^d$, the matrix $A(U, \omega) = \sum_{j=1}^{d} \omega_j A_j(U)$ is diagonalizable in $\mathbb{R}^{p\times p}$. That means this matrix has p real eigenvalues $\lambda_1(U, \omega) \leq \cdots \leq \lambda_p(U, \omega)$ and p linearly independent corresponding eigenvectors. Moreover if all eigenvalues are real and distinct, the system (1.1) is said to be *strictly hyperbolic*.
The following Euler system of gas dynamics

$$\frac{\partial}{\partial t}\rho + \nabla_x \cdot \rho u = 0, \tag{1.2a}$$

$$\frac{\partial}{\partial t}\rho u + \nabla_x \cdot (\rho u \otimes u + p\,\mathbb{I}\mathrm{d}) = 0, \tag{1.2b}$$

$$\frac{\partial}{\partial t}\rho E + \nabla_x \cdot \left(E + \frac{p}{\rho}\right) u = 0, \tag{1.2c}$$

is a classical example of hyperbolic conservation laws systems, where ρ denotes the density, u the velocity vector, p the pressure and E the total energy.

The system (1.1) associated with an initial condition

$$U(x, 0) = U_0(x), \tag{1.3}$$

where $U_0(x) \in \mathcal{L}^\infty_{\mathrm{loc}}\left(\mathbb{R}^d\right)^p$, is called a *Cauchy problem*. In the particular case, where $U_0(x)$ is defined by two constant states U_L and U_R in $\left(\mathbb{R}^d\right)^p$, for instance in one space dimension $d = 1$

$$U_0(x) = \begin{cases} U_L & \text{if } x \leq 0, \\ U_R & \text{if } x > 0, \end{cases} \tag{1.4}$$

then, the Cauchy problem (1.1),(1.3),(1.4) is called a *Riemann problem.*

1.1.2 Weak entropy solutions

The Cauchy problem of (1.1),(1.3) arises in plenty of interesting physics and engineering applications. Solving the Cauchy problem means to find solutions $U \in (\mathbb{R}^d \times [0,+\infty))^p \to \Omega$ satisfying (1.1),(1.3) in some sense. The first sense encountered is *classical sense*, i.e. the solution $U \in \mathcal{C}^1(\mathbb{R}^d \times [0,+\infty))^p \to \Omega$ satisfies (1.1),(1.3), such a solution is called a *strong solution.* However it is well-known that the global classical solution does not always exist for all time $t > 0$ even when the given initial data $U_0(x)$ is smooth, see [LeV92 ; GR96 ; Daf10], therefore one looks for other suitable sense. Among that, a popular one is the so-called distribution sense, and such a solution is called a *weak solution.* For more details, look at the following definition.

Definition 1 *A function $U \in \mathcal{L}^\infty_{loc}(\mathbb{R}^d \times [0,+\infty))^p$ is called a weak solution of the Cauchy problem (1.1),(1.3) if $U(x,t) \in \Omega$ a.e. and the following equation*

$$\int_0^\infty \int_{\mathbb{R}^d} \left\{ U \cdot \frac{\partial \phi}{\partial t} + \sum_{j=1}^{d} F_j(U) \cdot \frac{\partial \phi}{\partial x_j} \right\} dx\,dt = - \int_{\mathbb{R}^d} U_0(x) \cdot \phi(x,0)\,dx, \tag{1.5}$$

holds true $\forall \phi \in \mathcal{C}^\infty_0(\mathbb{R}^d \times [0,+\infty))^p$.

The weak solution of the system (1.1),(1.3) is in general not unique, and there are cases where the weak solution is not physically satisfactory. In order to select a suitable weak solution, one possibility is to use an entropy condition. Let us first define a *pair entropy-entropy flux.*

Definition 2 *Assume that Ω is convex. A convex function $S : \Omega \to \mathbb{R}$ is called a mathematical entropy for (1.1) if there exist d functions $G_j : \Omega \to \mathbb{R}$, called the entropy fluxes, such that the relations*

$$\nabla G_j(U) = \nabla S(U) A_j(U), \quad j = 1, \dots, d \tag{1.6}$$

hold true. Denote $G = (G_1, \dots, G_d)$ in $\mathbb{R}^d$, (S,G) is then called a pair entropy-entropy flux.

Definition 3 *A weak solution $U \in \mathcal{L}^\infty_{loc}(\mathbb{R}^d \times [0,+\infty))^p \to \Omega$ is called an entropy solution to (1.1),(1.3) associated to the pair entropy-entropy flux function (S,G) if the inequality*

$$\frac{\partial S(U)}{\partial t} + \nabla_x \cdot G(U) \leq 0 \tag{1.7}$$

holds true.

In the scalar conservation laws, there exists a variation among entropy conditions. Beside a pair entropy-entropy flux functions theory, there are other selection criteria, Lax condition, Oleinik condition, etc, see [LeV92] for more details. These conditions are equivalent in the case where the flux function is convex (or concave). In the system case, one usually uses a pair entropy-entropy flux function for the gas dynamics system due to the existence of a physical entropy function. In general system, one may use the Lax condition or a more general one, Liu condition. The Lax entropy condition is well-known owing to an important theorem of existence and uniqueness of a Lax entropy weak solution to the Riemann problem, it however requires further properties of the hyperbolic conservation laws. In order to introduce the Lax entropy condition we first define some properties of the characteristic fields which are a generalization of convex function in the scalar case such as genuinely nonlinear and linearly degenerate.

1.1.3 Characteristic fields and simple waves

Consider a strictly hyperbolic conservation system (1.1) in one dimension $d = 1$, the Jacobian matrix $\mathbf{A} = \nabla F(U)$ has p distinct eigenvalues

$$\lambda_1(U) < \lambda_2(U) < \cdots < \lambda_p(U)$$

and p right eigenvectors $\vec{r}_1(U)$, $\vec{r}_2(U)$,..., $\vec{r}_p(U)$ correspondingly.

Definition 4 *We say that the k-th characteristic field is genuinely non-linear (GNL) if*

$$\nabla\lambda_k(U)\cdot\vec{r}_k(U)\neq 0,\quad \forall U\in\Omega, \tag{1.8}$$

and the k-th characteristic field is linearly degenerate (LD) if

$$\nabla\lambda_k(U)\cdot\vec{r}_k(U)= 0,\quad \forall U\in\Omega. \tag{1.9}$$

In the convex scalar case, a solution to the Riemann problem consists of one rarefaction wave or one shock wave (i.e. a contact discontinuity in the linear case). In order to generalize such waves to the system case, we first consider definitions of a Riemann invariant and Rankine-Hugoniot condition.

Definition 5 *A smooth function $\omega:\Omega\to\mathbb{R}$ is called a k-Riemann invariant if it satisfies*

$$\nabla\omega(U)\cdot\vec{r}_k(U)= 0,\quad \forall U\in\Omega. \tag{1.10}$$

Locally around any $U_0\in\Omega$, there exists $(p-1)$ $k-$Riemann invariants whose gradients are linearly independent. An interesting property of the Riemann invariant is that its value remains constant along the trajectories of the vector field $\vec{r}_k$. Let $R_k(U_0)$ be the set of $U\in\Omega$ such that

$$R_k(U_0)=\left\{U\in\Omega:\lambda_k(U)\geq\lambda_k(U_0),\omega_i^k(U)=\omega_i^k(U_0),\forall i=1,\dots,p-1\right\} \tag{1.11}$$

then, if $U\in R_k(U_0)$, we say that U is connected to the right of U_0 by a $k-$*rarefaction wave.*

Definition 6 *The Rankine-Hugoniot set of $U_0\in\Omega$, denoted by $S(U_0)$, is the set of all states $U\in\Omega$ such that there exists $\sigma=\sigma(U_0,U)\in\mathbb{R}$ satisfying*

$$F(U)-F(U_0)=\sigma(U_0,U)(U-U_0). \tag{1.12}$$

We say that the state U_0 connects to a state $U\in S(U_0)$ by a shock wave.

We can now define the Lax entropy condition for the hyperbolic conservation laws.

Definition 7 *The discontinuity between two constant states U_L and U_R and propagating with speed σ satisfying the Rankine-Hugoniot conditions is said to satisfy the Lax entropy conditions if there exists $k\in\{1,\dots,p\}$ such that we have either*

$$\lambda_k(U_R)<\sigma<\lambda_{k+1}(U_R), \tag{1.13}$$
$$\lambda_{k-1}(U_L)<\sigma<\lambda_k(U_L), \tag{1.14}$$

if the k-th characteristic field is genuinely nonlinear; or

$$\lambda_k(U_L)=\sigma=\lambda_k(U_R), \tag{1.15}$$

if the k-th characteristic field is linearly degenerate.

1.1.4 Sonic points

In the one dimensional scalar conservation law, a state $U_0\in\mathbb{R}$ is called a *sonic point* if the eigenvalue $\lambda(U)=\dfrac{\partial F}{\partial U}$ changes sign around U_0 in the sense that

$$\lambda(U_0)=0,\quad \lambda(U_0+\varepsilon)\lambda(U_0-\varepsilon)<0, \tag{1.16}$$

for some ε small enough.
A wave going through the sonic point and corresponding to a rarefaction wave is usually called a transonic rarefaction wave. For example in the Burgers equation $\partial_t u+\frac{1}{2}u^2=0$, the sonic point corresponds to the state where $u=0$ and the transonic rarefaction wave corresponds to the configuration where $u_L<0<u_R$.
Transonic rarefactions are highly nonlinear phenomena because the local behaviour of the solution can not be approximated by a simple linear transport equation. Indeed, a linear transport with speed zero would yield a steady state which not what happens in a transonic rarefaction. Enough care should therefore be put in the linearized numerical methods around sonic points in order to capture possible rarefaction waves.

For systems of conservation laws, the definition of a sonic point is similar to the scalar case where the eigenvalue considered is one of the eigenvalues of the Jacobian matrix. More precisely, assume that λ_k is one of the eigenvalues of the Jacobian matrix of the flux function in a system of conservation laws. A state $U_0 \in \mathbb{R}^p$ is called a *sonic point* corresponding to $k-$field if $\lambda_k(U_0)$ changes sign around U_0 in the sense that

$$\lambda_k(U_0) = 0, \quad \lambda_k(U_0 + \varepsilon)\lambda_k(U_0 - \varepsilon) < 0, \tag{1.17}$$

for some $\varepsilon \in \mathbb{R}^p$ such that $|\varepsilon|$ small enough.
For example in the Euler system (section 1.3), the first eigenvalue $\lambda_1 = u - c_s$ and the third one $\lambda = u + c_s$ corresponds to two genuinely nonlinear fields. Then a sonic point arises when the velocity u reaches the sound speed, i.e. $u = \pm c_s$. This is in fact the origin of the name "sonic point" which has then been generalized to systems of conservation laws.

1.1.5 Lax and Glimm theorems, Liu criterion

We give the theorem of existence and uniqueness of the solution of the Riemann problem, see [GR96].

Theorem 1 *Consider a one dimensional strictly hyperbolic system of conservation laws (1.1), assume that for all $k = 1, \dots, p$ the $k-$th characteristic field is either genuinely non linear or linearly degenerate. Then for all $U_l \in \Omega$ there exists a neighborhood Υ of $U_l \in \Omega$ with the following property : if $U_r \in \Upsilon$, the Riemann problem has a weak solution that consists of at most $(p+1)$ constant states separated by rarefaction waves, admissible shock waves or contact discontinuities. Moreover, such solution is unique.*

For the existence of a general solution to the Cauchy problem, we refer the reader to the theory of the Glimm scheme or a front tracking method, see [Ser99], [Bre00], [LeF02], [Daf10] for example. The existence result to the Cauchy problem is limited to initial data having a small total variation. More precisely, we recall the theorem of Glimm as follows.

Theorem 2 *Considering the Cauchy problem*

$$\frac{\partial U}{\partial t} + \frac{\partial F(U)}{\partial x} = 0, \tag{1.18}$$

$$U(0, x) = U_0(x), \tag{1.19}$$

for a system of conservation laws with a smooth flux F defined in a neighborhood of the origin. Assume that the system is strictly hyperbolic such that all characteristic fields are either genuinely non linear or linearly degenerate and for a sufficiently small $\delta > 0$, the initial data satisfy

$$\|U_0\|_{\mathcal{L}^\infty} < \delta, \quad Tot.Var.\{U_0\} < \delta. \tag{1.20}$$

Then, the Cauchy admits a unique weak entropy solution.

In order to understand better the general theory of hyperbolic systems with genuinely nonlinear or linearly degenerate fields, we will study some important example : linear systems section 1.2, and the Euler system section 1.3.
The theory of conservative systems in cases where the characteristic fields are neither genuinely nonlinear nor linearly degenerate is still limited, except in the scalar case (see the general section 1.1.6 and some particular examples in section 3). The Lax criterion is no longer satisfactory to select a correct weak solution. In this case, one may consider a more general condition, Liu criterion, see [Ser99], as follows.

Definition 8 *Let $(U_L, U_R; \sigma(U_L, U_R))$ be a discontinuity of the conservative system (1.1), it is admissible in the sense of Liu if*

$$\sigma(U_L, U_R) \leq \sigma(U_L, U), \quad \forall U \in \mathcal{S}(U_L) \text{ between } U_L \text{ and } U_R,$$

where $\mathcal{S}(U_L)$ is a shock wave connecting U_L to U_R.

We will need this criterion in Chapter 5, where we study an incompressible two-fluid model due to the presence of the characteristic fields neither genuinely non-linear nor linearly degenerate.

1.1.6 The Kruzkov theorem for scalar conservation laws

Let us now consider a scalar conservation law

$$u_t + \nabla_x \cdot f = 0, \quad x \in \mathbb{R}^d, t > 0, \tag{1.21}$$

where $f = (f_1, \ldots, f_d)$ and $f_i, i = 1, \ldots, d$ are smooth functions from an open set Ω to $\mathbb{R}$. The equation (1.21) is then associated with the initial condition

$$u(x, 0) = u_0(x), \quad x \in \mathbb{R}^d, \tag{1.22}$$

where u_0 is a bounded measurable function on $\mathbb{R}^d$.
The existence of the entropy solution of the Cauchy problem (1.21),(1.22) is stated in the well-known Kružkov theorem as follows.

Theorem 3 *For every bounded measurable function u_0 on $\mathbb{R}$, the Cauchy problem (1.21),(1.22) admits unique entropy weak solution u in $\mathcal{L}^\infty(\Omega) \cap \mathcal{C}([0, T), \mathcal{L}_{loc}(\mathbb{R}))$ such that*

$$\|u\|_{\mathcal{L}^\infty(\Omega)} \leq \|u_0\|_{\mathcal{L}^\infty(\mathbb{R})}. \tag{1.23}$$

1.2 The case of linear systems

A linear system of conservation laws in one dimension is written under the following form

$$\frac{\partial U}{\partial t} + \mathbf{A}\frac{\partial U}{\partial x} = 0, \tag{1.24}$$

where $\mathbf{A}$ is an $p \times p$ real constant matrix. This is a particular case of the system of conservation laws where the flux function is $F(U) = \mathbf{A}U$. We assume that the system (1.24) is strictly hyperbolic, i.e. the matrix $\mathbf{A}$ has p constant distinct eigenvalues in order

$$\lambda_1 < \ldots < \lambda_p. \tag{1.25}$$

In this case, a solution to the Cauchy problem of the system (1.24) with the initial data

$$U(x, 0) = U_0(x) \tag{1.26}$$

can be obtained explicitly, see the following proof.
Due to the strict hyperbolicity, the matrix $\mathbf{A}$ has p linearly independent right eigenvectors $\vec{r}_1, \ldots, \vec{r}_p$ and the same for left eigenvectors $\vec{l}_1, \ldots, \vec{l}_p$ corresponding to the eigenvalues (1.25). Moreover, under a normalization, it is possible to impose that

$$\vec{l}_j \cdot \vec{r}_k = \begin{cases} 1 \text{ if } j = k, \\ 0 \text{ if } j \neq k. \end{cases} \tag{1.27}$$

Then any $U \in \mathbb{R}^p$ is decoupled basing on $(\vec{r}_k)_{k=1,\ldots,p}$ as

$$U = \sum_{k=1}^{p} \left({}^t\vec{l}_k U \right) \vec{r}_k. \tag{1.28}$$

Denote new variables $\alpha_k = {}^t\vec{l}_k U, k = 1, \ldots, p$, then the system (1.24) can be rewritten under a new vector $\alpha = {}^t(\alpha_1, \ldots, \alpha_p)$

$$\frac{\partial \alpha}{\partial t} + \text{diag}(\lambda_1, \ldots, \lambda_p)\frac{\partial \alpha}{\partial x} = 0. \tag{1.29}$$

The new linear system (1.29) consists of p independent transport equations whose speeds are $\lambda_k, k = 1, \ldots, p$ and the corresponding initial data

$$\alpha_{0k}(x) = {}^t\vec{l}_k U_0(x), \quad k = 1, \ldots, p. \tag{1.30}$$

Thank to the solution of linear transport equations, we obtain the solution of the system (1.29) and then the original linear system (1.24) as

$$U(x,t) = \sum_{k=1}^{p} \left(\alpha_{0k}(x-\lambda_k t)\right) \vec{r}_k = \sum_{k=1}^{p} {}^t\vec{l}_k U_0(x-\lambda_k t)\vec{r}_k. \tag{1.31}$$

In addition, if $U_0(x)$ consists in two constant states U_L and U_R as (1.4), then the solution to the Riemann problem of the system (1.24) consists in $(p+1)$ constant states connected by p contact discontinuities as below

$$U(x,t) = \begin{cases} W_0 = U_L & \text{if} \quad x/t \le \lambda_1, \\ W_1 & \text{if} \quad \lambda_1 < x/t \le \lambda_2, \\ \dots \\ W_p = U_R & \text{if} \quad x/t > \lambda_p, \end{cases} \tag{1.32}$$

where $W_j = U_L + \sum_{k=1}^{j} \eta_k \vec{r}_k$, $j = 1, \dots, p-1$ and η_k are defined by

$$U_R - U_L = \sum_{k=1}^{p} \eta_k \vec{r}_k. \tag{1.33}$$

1.3 A classical example : the Euler equations

The Euler system of gas dynamics is made of three balance equations for the mass, momentum and energy of the fluid. Neglecting the source term we otain the following conservative system

$$\frac{\partial}{\partial t}\rho + \nabla_x \cdot \rho\vec{u} = 0, \tag{1.34a}$$

$$\frac{\partial}{\partial t}\rho\vec{u} + \nabla_x \cdot (\rho\vec{u} \otimes \vec{u} + p\,\mathbb{I}\mathrm{d}) = 0, \tag{1.34b}$$

$$\frac{\partial}{\partial t}\rho E + \nabla_x \cdot \left(E + \frac{p}{\rho}\right)\vec{u} = 0, \tag{1.34c}$$

where ρ denotes the density, $\vec{u}$ the velocity vector, p the pressure and $E = e + \frac{1}{2}|\vec{u}|^2$ the total energy.

The Euler system is a classical hyperbolic system of conservation laws well studied in the literature, [GR96 ; Ser99]. In 1D, the Euler system is strictly hyperbolic and the characteristic fields are either genuinely nonlinear or linearly degenerate (see subsection 1.3.1). Thus we can deduce the existence of solutions to the Riemann prolem (Lax theorem) and to the Cauchy problem (Glimm theorem) for small bounded variations initial data. Also the only sonic points are characterised by $|u| = c_s$, where c_s is the sound speed, which implies that subsonic flows do not display sonic points.

1.3.1 Characteristic fields of the 1D Euler system

This section is largely inspired by [GR96]. The vector of conservative variables

$$U = (\rho, \rho u, \rho E) = (U_1, U_2, U_3) \tag{1.35}$$

is very useful in studying shock and rarefaction waves associated to the Euler system and in designing conservative numerical methods. However the variables (ρ, u, s) are sometimes used to derive more easily the eigenvalues and eigenvectors of the Jacobian matrix.

The Jacobian of the one dimensional flux function F

$$\mathbf{A}(U) = \frac{\partial F}{\partial U} = \begin{bmatrix} 0 & 1 & 0 \\ K - u^2 & (2-k)u & k \\ u(K-H) & (H - Ku^2) & (1+k)u \end{bmatrix}, \tag{1.36}$$

where we denoted

$$k = \frac{1}{\rho T}\left(\frac{\partial p}{\partial s}\right)_{|\rho},$$
$$K = c_s^2 + k(u^2 - H),$$

The total enthalpy is defined as

$$H = e + \frac{1}{2}u^2 + \frac{p}{\rho},$$

and the sound speed as

$$c_s = \frac{\partial p}{\partial \rho}_{|s} > 0, \tag{1.37}$$

where the entropy s is defined by its differential $T\partial s = \partial e - \frac{p}{\rho^2}\partial\rho$.

The eigenvalues of the matrix $\mathbf{A}$ are

$$\lambda_1 = u - c_s, \quad \lambda_2 = u, \quad \lambda_3 = u + c_s; \tag{1.38}$$

associated with the following corresponding right eigenvectors

$$\vec{r}_1 = {}^t(1, u - c_s, H - uc_s), \quad \vec{r}_2 = {}^t(1, u, H - \frac{c_s^2}{k}), \quad \vec{r}_3 = {}^t(1, u + c_s, H + uc_s).$$

From equation (1.38) we deduce that the 1D Euler system is strictly hyperbolic with 3 distinct eigenvalues.

1.3.2 Genuine nonlinearity, linear degeneracy and sonic points

In order to study the nonlinear properties of the characteristic field we chose ρ and s as the two independent thermodynamic variables with the equation of state $p = p(\rho, s)$. We choose as in [GR96] the new unknown vector

$$V = (\rho, u, s). \tag{1.39}$$

The mapping $U \to V$ is smooth and one-to-one and the the 1D Euler system is equivalent to

$$\partial_t V + \mathbf{B}(V)\partial_x(V) = 0. \tag{1.40}$$

where

$$\mathbf{B}(V) = \begin{bmatrix} u & \rho & 0 \\ \frac{1}{\rho}\frac{\partial p}{\partial \rho} & u & \frac{1}{\rho}\frac{\partial p}{\partial s} \\ 0 & 0 & u \end{bmatrix}, \tag{1.41}$$

$\mathbf{B}(V)$ has the same eigenvalues as $\mathbf{A}(U)$ given by (1.38). The associated eigenvectors of $\mathbf{B}$ can be chosen as

$$\vec{\tilde{r}}_1 = {}^t(\rho, -c_s, 0), \quad \vec{\tilde{r}}_2 = {}^t(\frac{\partial p}{\partial s}, 0, -c_s^2), \quad \vec{\tilde{r}}_3 = {}^t(\rho, c_s, 0). \tag{1.42}$$

We have

$$\nabla_V \lambda_1 = {}^t(-\frac{\partial c_s}{\partial \rho}, 1, -\frac{\partial c_s}{\partial s}), \quad \nabla_V \lambda_2 = {}^t(0, 1, 0), \quad \nabla_V \lambda_3 = {}^t(\frac{\partial c_s}{\partial \rho}, 1, \frac{\partial c_s}{\partial s}).$$

and

$$\nabla_V \lambda_1(V) \cdot \vec{\tilde{r}}_1 = -(c_s + \frac{\partial c_s}{\partial \rho}), \tag{1.43}$$

$$\nabla_V \lambda_2(V) \cdot \vec{\tilde{r}}_2 = 0, \tag{1.44}$$

$$\nabla_V \lambda_3(V) \cdot \vec{\tilde{r}}_3 = c_s + \frac{\partial c_s}{\partial \rho}. \tag{1.45}$$

From thermodynamics properties, $(\frac{1}{\rho}, s) \to e(\frac{1}{\rho}, s)$ is strictly convex which yields $\frac{\partial p}{\partial \rho}_{|s} > 0$ and $c_s + \frac{\partial c_s}{\partial \rho} > 0$ (see [GR96]).

Hence from (1.43) and (1.45), the first and last field are genuinely non linear whereas from (1.44) the second one is linearly degenerate.

1.3.3 Vacuum limit

Considering a system of fluid dynamics, in the $x-t$ plane, if the density $\rho = 0$, it is called a *vacuum* state. In the Euler system, the presence of the vacuum state implies that the partial differential system is no longer strictly hyperbolic and the resulting characteristic fields are identical. There are many researches made for Euler system, one can find some interesting results about the vacuum state. The most general result for Euler compressible problem was found in [LPS96], where the authors prove the existence of entropy solution for the Cauchy problem of the isentropic Euler system in one dimension associated with a general initial condition, i.e. including the vacuum state. In [Yan06], Yang summarizes the present study of the vacuum state for compressible models including the Euler system. However there is not any general conclusion for the general Euler system (1.34a-1.34c).

1.3.4 Sonic points of the Euler system

Sonic points are defined as values of the unknown U around which the characteristic speed changes sign. In the case of the 1D Euler system, the genuinely nonlinear fields are associated to $\tilde{r}_1$ and $\tilde{r}_3$ and have speed zero if and only if $u = c_s$ or $u = -c_s$. Therefore the sonic points of the Euler system can be characterized by $|u| = c_s$. This sonic points are associated to rapid changes in the wave dynamics of the fluid.

1.4 Conclusion

Through this section, we have been introducing some definitions regarding systems of conservation laws. This part is merely an introduction of a general theory of hyperbolic conservation laws. We studied the specific case of the linear system of conservation laws due to the fact that its beautiful results may be sometime generalized to nonlinear systems and it gives fundamental ideas for many numerical schemes as well. In addition, an important example of the conservative system is the Euler system for gas dynamics was recalled in Section 1.3. The main theorem of the scalar case was presented in Section 1.1.6. Finally, for more examples of the scalar conservation laws, we refer the reader to Chapter 3.

As we mentioned in section 1.1.5 most existence results are restricted to the case of strictly hyperbolic systems with characteristic fields that are either genuinely nonlinear or linearly degenerate in particular to the 1D Euler system. Unfortunately as we will see the hyperbolic systems used for boiling flow models are not strictly hyperbolic and their characteristic fields are neither genuinely nonlinear nor linearly degenerate. Also at the difference of the Euler system, sonic point will be common even for subsonic flows. A special attention will have to be paid in the study and numerical simulation of these solutions.

Chapitre 2

Introduction to finite volume methods (FVM)

This chapter gives an introduction to numerical methods which are used largely in computational fluid dynamics. We mainly focus on the finite volume methods due to their applicability to fluid dynamics and the flexibility of mesh structure. Similarly to other numerical methods for solving partial differential equations, the finite volume methods (FVM) are based on a discretization of the partial differential equations on a finite number of cells. Each cell is considered as a volume and a finite number of cells is called a mesh. An integral of a divergence operator applying to a flux function on a volume becomes an integral of such a function on the surface of the volume due to divergence theorem, i.e. taking the integral of the conservation laws (1.1) on each cell C_j whose volume is denoted by Vol_j yields the following semi-discretization equation

$$\mathrm{Vol}_j \frac{\partial}{\partial t} U_j + \sum_{j_k \in \text{neighbor of } j} S_{jj_k} \mathbf{F}_{\mathrm{i}}(U_j, U_{j_k}) = 0, \tag{2.1}$$

where U_j is an approximation of $U(x,t)$ at the cell j ; S_{jj_k} is an area of the interface between a cell j and its neighbor cell j_k ; $\mathbf{F}_{\mathrm{i}}$ is an interfacial flux in the normal vector $\vec{n}$ direction of the interface S_{jj_k}, see Figure 2. The equation (2.1) implies the flexibility of the mesh structure used in the finite volume method, i.e. structures mesh as well as unstructured mesh are possible.
In order to obtain a full discretization formula of (2.1), one usually considers the upward temporal derivative due to an evolution in time, i.e.

$$\frac{\partial}{\partial t} U_j \approx \frac{U_j^{n+1} - U_j^n}{\Delta t}, \tag{2.2}$$

where U_j^n is an approximation of $U(x,t)$ at cell j and $t = n\Delta t$, Δt is a time step. In the convection part, one might consider either $\mathbf{F}_{\mathrm{i}}(U_j^n, U_{j_k}^n)$ which leads to an *explicit method* or $\mathbf{F}_{\mathrm{i}}(U_j^{n+1}, U_{j_k}^{n+1})$ which

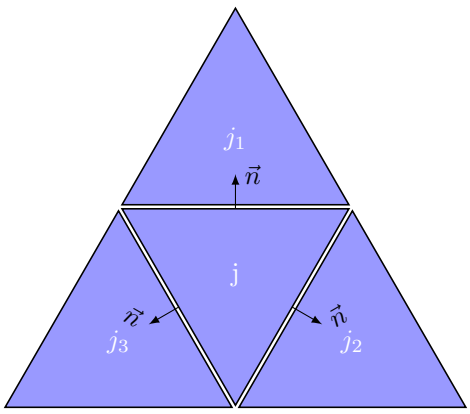

FIGURE 2.1 – The neighbor cells of a cell j.

leads to an *implicit method*. Applying the explicit method, then the numerical solution in the next time step is derived directly from (2.1) and (2.2) as below

$$U_j^{n+1} = U_j^n - \sum_{j_k \in \text{neighbor of } j} S_{jj_k} \mathbf{F}_{\text{i}}(U_j^n, U_{j_k}^n), \tag{2.3}$$

while considering the implicit method requires a resolution of a non-linear system. An important remark is that the stability of the explicit method demands small time steps which satisfy the CFL condition, see [LeV92 ; Bou00]. This drawback may limit the applicability of the explicit method in industrial simulations.

The main step of explicit FVM is the computation of the flux function on the interfaces $\mathbf{F}_i$. Various strategies give rise to numerous different numerical methods. A general solver to compute the interfacial flux of the system (1.1) is solving the Riemann problem for the conservation laws at each interface between a couple of cells. Successfully solving the Riemann problem in some sense will provide a value of the flux function at the interface. Depending on the complexity of the conservation laws and the level of precision required, one may consider either an exact Riemann solver or an approximate Riemann solver. There exist many numerical schemes using these two approaches. Among those, the Godunov scheme is a classical one solving the exact Riemann problem while other schemes, such as the Roe scheme, consider an approximation of the Riemann problem.

2.1 Exact Riemann solvers

The exact Riemann solver is derived by the computation of an exact solution of the Riemann problem at each interface between two cells. The Godunov scheme is derived from the resolution of the one dimensional Riemann problem in the normal vector direction between two neighboring states U_L and U_R

$$\partial_t U + \partial_{x_n} F(U) = 0, \tag{2.4}$$

$$U(x_n, 0) = \begin{cases} U_L \text{ if } x \cdot \vec{n} \leq 0, \\ U_R \text{ if } x \cdot \vec{n} > 0, \end{cases} \tag{2.5}$$

where the left cell L and the right cell R have a common interface with a normal vector $\vec{n}$. Let $U(0,t)$ be the solution of the Riemann problem (2.4,2.5) at $x \cdot \vec{n} = 0$ (in fact, $U(0,t)$ does not depend on time due to the self-similar property). Then the flux value at $U(0,t)$ in the normal direction $\vec{n}$ is considered as the interfacial flux function between U_L, U_R by Godunov, i.e.

$$\mathbf{F}^{\text{G}}(U_L, U_R) = F(U(0)) \cdot \vec{n}. \tag{2.6}$$

More details of the Godunov scheme can be found in [LeV92 ; LeV04].

2.2 Approximate Riemann solvers

There are many different approximate Riemann solvers. Among these, we would like to introduce in details a Roe solver which will be used in the numerical simulation of this document.
Following the work of Roe in [Roe81], given two constant states U_L and U_R, $\tilde{\mathbf{A}}(U_L, U_R)$ denotes a matrix associated to the flux function F in (1.1) and satisfying the following properties

1. $\tilde{\mathbf{A}}_n(U,U) = \mathbf{A}_n(U)$ where $\mathbf{A}_n$ is the Jacobian matrix of the flux function F in the normal direction $\vec{n}$, i.e. $\mathbf{A}_n = \frac{\partial F_n}{\partial U}$ where $F_n = \vec{F} \cdot \vec{n}$.
2. $F_n(U_R) - F_n(U_L) = \tilde{\mathbf{A}}_n(U_L, U_R)(U_R - U_L)$.
3. $\tilde{\mathbf{A}}_n(U_L, U_R)$ is diagonalizable.

The Roe matrix $\tilde{\mathbf{A}}_n(U_L, U_R)$ locally linearizes the gradient of the flux function F in the direction $\vec{n}$ which in turn implies that the conservative system is locally approximated by the following linear system

$$\partial_t U + \tilde{\mathbf{A}}_n(U_L, U_R)\partial_x U = 0. \tag{2.7}$$

As introduced in Section 1.2, the Riemann problem for the linear system (2.7) can be explicitly solved. Following this idea, a Roe scheme is developed.
The *Roe scheme* is a Godunov-type scheme and is based on solving the approximate linear system of the non-linear conservative one. In more detail, the Roe scheme is derived by the resolution of the one dimensional Riemann problem linearized in the normal vector direction

$$\partial_t U + \tilde{\mathbf{A}}_n(U_L, U_R)\partial_{x_n} U = 0, \tag{2.8}$$

$$U(x_n, 0) = \begin{cases} U_L \text{ if } x_n \leq 0, \\ U_R \text{ if } x_n > 0, \end{cases} \tag{2.9}$$

where x_n is an interface between two cells U_L and U_R. The second property of the local Roe matrix $\tilde{\mathbf{A}}_n(U_L, U_R)$ in this case is defined by

$$F_n(U_R) - F_n(U_L) = \tilde{\mathbf{A}}_n(U_L, U_R)(U_R - U_L). \tag{2.10}$$

The numerical Roe flux function at the interface (U_L, U_R) is defined by

$$\mathbf{F}^{\mathrm{R}}(U_L, U_R) = \frac{F_n(U_L) + F_n(U_R)}{2} - \left|\tilde{\mathbf{A}}_n(U_L, U_R)\right| \frac{U_R - U_L}{2} \tag{2.11}$$

where $|\,\mathbf{.}\,|$ of a matrix denotes its absolute matrix, i.e. if $\tilde{\mathbf{A}} = P\Lambda P^{-1}$, where $\Lambda = \mathrm{diag}\{\lambda_1, \ldots, \lambda_p\}$ is a diagonal matrix, then

$$|\tilde{\mathbf{A}}| = P|\Lambda|P^{-1} = P\,\mathrm{diag}\{|\lambda_1|, \ldots, |\lambda_p|\}P^{-1}. \tag{2.12}$$

Furthermore, let us denote

$$\mathrm{sgn}(\tilde{\mathbf{A}}) = P\mathrm{sgn}(\Lambda)P^{-1} = P\mathrm{sgn}\{\mathrm{sgn}(\lambda_1), \ldots, \mathrm{sgn}(\lambda_p)\}P^{-1}. \tag{2.13}$$

be a sign matrix of $\tilde{\mathbf{A}}$. Then, from (2.10) and (2.11), we can rewrite

$$\mathbf{F}^{\mathrm{R}}(U_L, U_R) \quad = \quad \frac{F_n(U_L) + F_n(U_R)}{2} - \left|\tilde{\mathbf{A}}_n(U_L, U_R)\right| \frac{U_R - U_L}{2},$$

The Roe scheme is in general less expensive than the exact solvers and is possibly applicable in the case where it is impossible to compute analytical solutions of the Riemann problem. However the well-known disadvantage of the Roe scheme is that it is not entropy, therefore suitable entropy fix may be applied to overcome this difficulty.

2.2.1 Limitations of approximate Riemann solvers

Approximate Riemann solvers are popular for their easy implementation in computer programs and the reduced computational cost compared to exact Riemann solvers. However due to the fact that they are often based on some sort of linearization or decoupling of the original hyperbolic system they may lack precision or capture non relevant numerical solution in situation where the solution has a very non linear behaviour. This occurs for example around sonic points or at the boundaries of the physical domain states or when the source term is very stiff of fluid dynamics. These difficulties might pose many problems in numerical simulations.

For example, when the fluid velocity reaches to the sound speed in the Euler system, the eigenvalues of the Jacobian may change sign and give rise the sonic points. A more complicated system as one pressure two-fluid model, the sonic points however might appear even the partial velocities are much smaller than the sound speed. Therefore, simulation the two-fluid model needs a careful treatment the sonic points due to the fact that some numerical schemes may fail to capture the transonic rarefaction wave.

2.2.2 Entropy fix for approximate Riemann solvers

Theoretically, weak solutions for a system of initial hyperbolic conservation laws are not unique. In order to select an admissible solution, one uses the entropy condition, recall Section 1.1 and see more in [GR96 ; Bou00 ; Daf10]. Some numerical methods, in particular the approximate Riemann solvers sometimes give inadmissible discontinuities, i.e. do not satisfy the entropy condition. For instance, in case

the admissible solution contains a transonic rarefaction fan, (see definition in Section 1.1.4), the Roe scheme captures instead a shock wave due to its linearization. Therefore, in order to avoid inadmissible discontinuities, one may consider an entropy fix for the classical Roe scheme. There are a variation of entropy fix which we can find in the literature, for instance entropy fix suggested by LeVeque in [LeV92], by Dubois et al in [DM96], [DD05], etc. Among those, the entropy fix suggested by Harten and Hyman [HH83 ; Har83] is one of the most used due to their simplicity and wide applicability in many different systems.

In [Har83], Harten supposed an entropy fix by adding numerical viscosity to the upwind part of the original Roe scheme. More precisely, assume that the numerical flux function of Roe scheme is written by

$$\mathbf{F}^{\mathrm{R}}(U_L, U_R) = \frac{1}{2}\left(F(U_L) + F(U_R)\right) - \frac{1}{2}\sum_{k=1}^{p} |\lambda_k| \alpha_k \vec{r}_k, \tag{2.14}$$

where F is the flux function of the conservation laws, $\vec{r}_k$ are the right eigenvectors of the Roe matrix $\tilde{\mathbf{A}}$ and the coefficients α_k are chosen such that

$$U_R - U_L = \sum_{k=1}^{p} \alpha_k \vec{r}_k.$$

The equation (2.14) is in fact an equivalent expression of (2.11) corresponding to the absolute Roe matrix

$$|\tilde{\mathbf{A}}| = (\vec{r}_1, \ldots, \vec{r}_p)\, \mathrm{diag}\left(|\lambda_1|, \ldots, |\lambda_p|\right) (\vec{r}_1, \ldots, \vec{r}_p)^{-1}\,; \tag{2.15}$$

The numerical flux function with an entropy fix is written

$$\mathbf{F}^{\mathrm{H}}(U_L, U_R) = \frac{1}{2}\left(F(U_L) + F(U_R)\right) - \frac{1}{2}\sum_{k=1}^{p} Q^{\mathrm{H}}(\lambda_k) \alpha_k \vec{r}_k. \tag{2.16}$$

In the case of Harten entropy fix in [Har83],

$$Q^H(\lambda_k) = Q^{\mathrm{Har}}(\lambda_k) = \begin{cases} \dfrac{\lambda_k^2}{4\varepsilon_k} + \varepsilon_k & \text{if} \quad |\lambda_k| \le 2\varepsilon_k, \\ |\lambda_k| & \text{if} \quad |\lambda_k| > 2\varepsilon_k, \end{cases} \tag{2.17}$$

and ε is some chosen positive constant in the interval $(0, 0.5)$. Following (2.17), such an entropy fix is used in the case the propagating velocity is near zero without distinguishing admissible or inadmissible discontinuity, i.e. an amount of numerical viscosity is added even in the case of an admissible shock.

Other entropy fix suggested by Harten and Hyman in [HH83] consider the velocity difference. The numerical flux function of Harten-Hyman (HH) is defined by (2.16) with

$$Q^H(\lambda_k) = Q^{\mathrm{HH1}}(\lambda_k) = \begin{cases} \delta_k & \text{if} \quad |\lambda_k| \le \delta_k, \\ |\lambda_k| & \text{if} \quad |\lambda_k| > \delta_k, \end{cases} \tag{2.18}$$

where

$$\delta_k = \max\{0, \lambda_k - \lambda_k(U_L), \lambda_k(U_R) - \lambda_k\}. \tag{2.19}$$

As an association of the entropy fix (2.17) and (2.18), [HH83] presented another entropy fix, of which the numerical flux function is defined by (2.16) with

$$Q^H(\lambda_k) = Q^{\mathrm{HH2}}(\lambda_k) = \begin{cases} \dfrac{1}{2}\left(\dfrac{\lambda_k^2}{\delta_k} + \delta_k\right) & \text{if} \quad |\lambda_k| \le \delta_k, \\ |\lambda_k| & \text{if} \quad |\lambda_k| > \delta_k, \end{cases} \tag{2.20}$$

We would like to notice that all entropy fix formulas (2.17),(2.18),(2.20) are continuous in terms of λ_k. The numerical simulation of such entropy fix are illustrated in [Har83], [HH83] for Euler system. However we do not intend to go further details of entropy fixes, we will instead present a modified

entropy fix which we will use in the simulation of two-fluid model.

It arises from the fact that entropy fixes found in the literature in general or presented here in particular need a full eigenstructure of the hyperbolic conservation laws, which we do not have in the case of the two-fluid model. The entropy fixes used in (2.17),(2.18),(2.20) consider and modify each characteristic independently while in the two-fluid model the characteristic fields are generally not in order. Apart from two large distinct acoustic waves with opposite sign, the sign of the remaining waves may change in normal flow conditions. Considering the left eigenvalues in comparison with the right ones is therefore not always obvious. That is the reason why we can not apply strictly the entropy fixes presented in [Har83 ; HH83]. We instead suggest a simple entropy fix, the so-called Harten-type entropy fix, defined by (2.16) with

$$Q^H(\lambda_k) = |\lambda_k| + \bar{\delta}, \tag{2.21}$$

where

$$\bar{\delta} = \max_l\{\lambda_k(U_L) - \lambda_k(U_R)\} \text{ and } l \in \{1, .., p\}\backslash\{\text{acoustic waves}\}, \tag{2.22}$$

i.e. we add numerical viscosity for all characteristic fields by the same function $\bar{\delta}$, which takes into account the velocity difference of all waves except the acoustic waves. The numerical flux function with the entropy fix Harten-type is rewritten

$$\mathbf{F}^{\mathrm{H}}(U_L, U_R) = \frac{1}{2}\left(F(U_L) + F(U_R)\right) - \frac{1}{2}(|A(U_L, U_R)| + \bar{\delta}\mathbb{I}\mathrm{d})(U_R - U_L). \tag{2.23}$$

The advantage of this Harten-type entropy fix is that it is simple and easy to implement in any complicated code using the Roe-type scheme. It requires only a computation the eigenvalues of the left state and right state supplementary.

Studying the homogeneous system of conservation laws (without taking into account the source terms) is the cornerstone of studying the more general non homogeneous ones which appear in many applications. In the following section, we will take into account the source terms in the system of conservation laws and introduce some methods to deal with those terms based on the original homogeneous system.

2.3 Numerical methods for non-homogeneous hyperbolic systems of conservation laws

In this section, we introduce to non-homogeneous hyperbolic system of conservation laws, i.e. we take into account the hyperbolic conservation system with non zero source term S as below

$$\frac{\partial}{\partial t}U + \nabla_x \cdot F(U) = S(U, x), \quad x = (x_1, \ldots, x_d) \in \mathbb{R}^d, t \geq 0. \tag{2.24}$$

The source term S is usually a function of the unknown vector U and spacial variable x, $S = S(U, x)$. Due to existence of numerous numerical methods for the numerical treatment of homogeneous hyperbolic systems of conservation laws, a simple approach to solve the non homogeneous system of conservation laws is to adapt those by including a source term in the right hand side as follows

$$\frac{U_j^{n+1} - U_j^n}{\Delta t} + \sum_{j_k \in \text{neighbor of } j} \frac{S_{jj_k}}{V_j}\,\mathbf{F}_{\mathrm{i}}(U_j^n, U_{j_k}^n) \quad = \quad S_j^n, \tag{2.25}$$

where S_j^n is an approximation of

$$S_j = \frac{1}{V_j}\frac{1}{\Delta t}\int_{t^n}^{t^{n+1}}\int_{V_j} S\mathrm{d}x\mathrm{d}t \tag{2.26}$$

and $\mathbf{F}_{\mathrm{i}}$ is some interfacial flux function.
Sometimes both the flux divergence $\nabla_x \cdot F(U)$ and the source term $S(U, x)$ are discretized independently

and in practice, S_j^n is simply considered as the source function at the average value U_j, i.e. $S_j^n = S(U_j^n, x_j)$. The numerical scheme (2.25) is a classical one solving the non homogeneous system of conservation laws. However this approach may generate insabilities in the simulation of the system (2.24), especially for stiff source terms functions S.
We are interested in the capture of the stationary regime of a two phase flow characterised by the stationary equation

$$\nabla_x \cdot F(U) = S. \tag{2.27}$$

In some cases, for example with stiff sources cases, using $S_j^n = S(U_j^n, x_j)$ in (2.26) implies the non stability of the numerical solution at the stationary state. In order to improve the numerical simulation, one suggests either upwinding the source terms or developing well-balanced schemes in the sense that it preserves the stationary state.

2.3.1 Source term upwinding for Roe scheme

We consider locally linearized schemes such as the Roe scheme in this part. the interfacial numerical flux functions of the one dimensional homogeneous system corresponding to (2.24) can be written as

$$\mathbf{F}_{j+1/2} = \frac{F_j + F_{j+1}}{2} - |A^{\text{Roe}}_{j,j+1}|\frac{U_{j+1} - U_j}{2}, \tag{2.28}$$

$$\mathbf{F}_{j-1/2} = \frac{F_j + F_{j-1}}{2} - |A^{\text{Roe}}_{j-1,j}|\frac{U_j - U_{j-1}}{2} \tag{2.29}$$

whare $A^{\text{Roe}}_{j,j+1}$ is an approximation of the Jacobian matrix between the states j and $j+1$.
The most simple and popular approach lies in the work in [BV94], where the upwinding source term S_j is defined as

$$S_j^{\text{up}} = \frac{\mathbb{I}\text{d} - \text{sgn}\left(A^{\text{Roe}}_{j,j+1}\right)}{2}\tilde{S}_{j+1/2} + \frac{\mathbb{I}\text{d} + \text{sgn}\left(A^{\text{Roe}}_{j-1,j}\right)}{2}\tilde{S}_{j-1/2}. \tag{2.30}$$

The Roe scheme with upwinding source can be rewritten as

$$U_j^{n+1} = U_j^n - \frac{\Delta t}{\Delta x}\left(\mathbf{F}_{j+1/2} - \mathbf{F}_{j-1/2} - \Delta x S_j^{\text{up}}\right). \tag{2.31}$$

The numerical result reaches a stationary state when

$$\mathbf{F}_{j+1/2} - \mathbf{F}_{j-1/2} = \Delta x S_j^{\text{up}}. \tag{2.32}$$

In the multidimensional setting, the scheme (2.25) can be rewritten

$$U_j^{n+1} = U_j^n - \frac{\Delta t}{\text{Vol}_j}\sum_{j_k \in \text{neighbor}(j)} s_{jj_k}\left(\mathbf{F}_{\text{i}}(U_j, U_{j_k})\right) + \Delta t S_j^{\text{up}}, \tag{2.33}$$

where

$$S_j^{\text{up}} = \frac{1}{\text{Vol}_j}\sum_{j_k \in \text{neighbor}(j)} \text{Vol}_{jj_k}\left(\frac{\mathbb{I}\text{d} - \text{sgn}\left(A^{\text{Roe}}_{j,j_k}\right)}{2}\tilde{S}_{j,j_k}\right), \tag{2.34}$$

such that

$$\sum_{j_k \in \text{neighbor}(j)} \text{Vol}_{jj_k} = \text{Vol}_j \quad \text{and} \tag{2.35}$$

$\tilde{S}_{j,j_k}$ is some approximation value of the source term S on the interface (j, j_k).

There are evidently other options for the treatment of the source term in the non-homogeneous system. The source function in general is a function of the unknown vector U, therefore instead of considering the centered source term, the authors in [Jin01] suggest studying the source term as a function of U at the interface. In [KPS04], the authors suggests using the so-called upwinding sources at interface, U.S.I method, to solve the non-homogeneous system. Another approach can be found in

[SBA07], where Sahmim et al develop the so-called SRNH (Solver Riemann Non-Homogeneous) scheme which is explicitly defined by

$$\begin{cases} U_{j+1/2} = \frac{1}{2}\left(U_{j+1} + U_j\right) - \frac{1}{2}\mathrm{sgn}(A_{j+1/2})\left(U_{j+1} - U_j\right) + \frac{1}{2}\left|A_{j+1/2}\right|^{-1} S_{i+1/2}, \\ U_j^{n+1} = U_j^n + \frac{\Delta t}{\Delta x}\left(F(U_{j+1/2}) - F(U_{j-1/2})\right) + \frac{\Delta t}{\Delta x} S_i. \end{cases} \tag{2.36}$$

The idea of SRNH scheme is similar to VFRoe scheme, [BGH00], but the interfacial state $U_{j+1/2}$ here takes into account the approximation of the source term. Moreover, in order to verify such a numerical scheme, the authors illustrate it in the shallow water system, Euler equations with gravity and the faucet Ransom simulation. The resulting numerical solutions are quite good at the stationary state. On the other hand, if the system is linear and suppose that $S_{i+1/2} := \mathrm{sgn}(A_{j+1/2})\tilde{S}_{j+1/2}$ and $S_i = \frac{S_{i+1/2}+S_{i-1/2}}{2}$, then the SRNH scheme (2.36) is equivalent to the (2.31).

2.3.2 Well-balanced schemes

Studying the non-homogeneous balance laws system,

$$\frac{\partial}{\partial t}U + \partial_x F(U) = S, \quad x \in \mathbb{R}, t \geq 0, \tag{2.37}$$

the authors in [Bou00] introduced a definition of a well-balanced scheme in the sense that such a scheme guarantees capturing correct stationary state. In fact, this is a non-conservative scheme which is consistent with the original system. More precisely, the well balanced scheme considers a one dimensional discretization of the system (2.37) in the following form

$$U_i^{n+1} - U_i^n + \frac{\Delta t}{\Delta x}\left(F^-_{i+1/2} - F^+_{i-1/2}\right) = 0. \tag{2.38}$$

where $\mathbf{F}^-_{i+1/2} = F_l(U_i, U_{i+1}, Z_i, Z_{i+1})$, $\mathbf{F}^+_{i-1/2} = F_r(U_{i-1}, U_i, Z_{i-1}, Z_i)$ and the source term in this case is supposed to be $S = B(U,Z)Z_x$. Then, the continuous form of a steady state is

$$\partial_x F(U,Z) + B(U,Z)Z_x = 0, \tag{2.39}$$

of which, one may derive a discrete form of the steady state as follows

$$\mathbf{D}\left(U_i, U_{i+1}, Z_i, Z_{i+1}\right) = 0, \tag{2.40}$$

such that (2.40) is consistent with (2.39). Once some discrete steady state (2.40) is selected, they define the well-balanced scheme.

Definition 9 *The scheme is well-balanced relatively to some discrete steady state if one has for this steady state*

$$F_l(U_l, U_r, Z_l, Z_r) = F(U_l, Z_l), \quad F_r(U_l, U_r, Z_l, Z_r) = F(U_r, Z_r). \tag{2.41}$$

The condition (2.41) implies $\mathbf{F}^-_{i+1/2} = \mathbf{F}^+_{i-1/2}$, thus guarantees some discrete steady state. Let us introduce the definition of consistency for a well balanced scheme.

Definition 10 *The scheme is said to be consistent if the numerical fluxes satisfy the consistency with the exact flux, i.e.*

$$F_l(U,U,Z,Z) = F_r(U,U,Z,Z) = F(U,Z) \text{ for any } (U,Z) \in \mathbb{R}^p \times \mathbb{R}^r \tag{2.42}$$

and the asymptotic conservativity/consistency with the source

$$F_r(U_l, U_r, Z_l, Z_r) - F_l(U_l, U_r, Z_l, Z_r) = -B(U,Z)(Z_r - Z_l) + o(Z_r - Z_l) \tag{2.43}$$

as $U_l, U_r \to U$ and $Z_l, Z_r \to Z$.

In [Bou00], the well balanced scheme was well studied with a rigorous demonstration of the consistency and the stability for such a scheme. The authors also apply such a theory of the shallow water system and build the corresponding numerical scheme which guarantees capturing the correct stationary state. For the scalar case, the explicit well-balanced scheme is introduced in the case the flux function F has no critical point. The interfacial flux computed in fact bases on a state U^* which is derived by the discrete steady state of the balance laws. However, the computation of U^* is difficult in the system case due to an expensive calculation as well as possibility of many different state U^*. For example in a two-fluid model, due to the complexity of the flux function and a general source terms are even not regular, it seems impossible to construct a well-balanced scheme following this idea.

Chapitre 3

The Riemann problem for non convex scalar conservation laws

In this chapter, we consider a particular case of the conservation laws, the scalar conservation laws, for which the theory of existence and uniqueness is complete, see Section 1.1.6. We aim at giving some specific examples in the scalar case and illustrate them with some numerical schemes in order to better understand the theory of conservation laws and the numerical schemes in Chapter 1 and 2. The scalar conservation analysis allows us to study profoundly general flux functions. Different numerical methods are then applied to solve the Riemann problems. We show that the Roe scheme with Harten-type entropy fix is a good candidate in the case of sonic points and non-convex flux.

3.1 Structure of the solution

Consider a specific problem of (1.21) and (1.22), the Riemann problem, for which the initial condition is

$$u_0(x) = \begin{cases} u_L & \text{if } x \leq 0, \\ u_R & \text{if } x > 0. \end{cases} \tag{3.1}$$

Assume first that f is a convex function, i.e. $f''(x) \geq 0$. The Riemann problem has a unique entropy solution, which is either a shock or a rarefaction. More precisely,

— If $f'(u_L) \geq f'(u_R)$, then the solution is a shock

$$u(x,t) = \begin{cases} u_L & \text{if } x \leq \sigma, \\ u_R & \text{if } x > \sigma. \end{cases}$$

where $\sigma = \dfrac{f(u_R) - f(u_L)}{u_R - u_L}$.

— If $f'(u_L) < f'(u_R)$, then the solution is a rarefaction

$$u(x,t) = \begin{cases} u_L & \text{if} \quad \dfrac{x}{t} \leq f'(u_L), \\ (f')^{-1}\left(\dfrac{x}{t}\right) & \text{if} \quad f'(u_L) < \dfrac{x}{t} < f'(u_R), \\ u_R & \text{if} \quad \dfrac{x}{t} \geq f'(u_R). \end{cases}$$

However in the general case of a smooth possibly non convex function f, the structure of the entropy solution to the Riemann problem (1.21), (3.1) may be built by using the definition of a convex hull, see [LeV04].

Convex hull curve construction

The entropy solution of the Riemann problem can be determined from the graph of $f(u)$. The convex hull of a set is the smallest convex set containing the original set. If $u_L < u_R$, then construct the convex

hull curve of the set $\{(u, y) : u_L \leq u \leq u_R, y \geq f(u)\}$. If $u_L > u_R$, then construct the convex hull curve of the set $\{(u, y) : u_R \leq u \leq u_L, y \leq f(u)\}$. The resulting curve of this construction may be obtained by straight line segments corresponding to the shock waves and a part coinciding to the curve $f(u)$ corresponding to the rarefaction waves, see Figure 3.1(a), 3.1(b), 3.5(a), 3.5(b) for example.
Before giving some examples of the scalar conservation laws, we would like to introduce some classical numerical schemes, which will be applied in the example tests.

3.2 Numerical schemes

We consider a uniform mesh of the computational domain $[0, 1]$ whose N cells are centered at x_i, $i = 1, \ldots, N$. The space step $\Delta x = x_i - x_{i-1}$ is constant whereas the time step $\Delta t > 0$ must ensure the stability of the explicit schemes, i.e. satisfy the following Courant-Friedrichs-Lewy (CFL) condition :

$$\Delta t \leq \frac{\Delta x}{\max_i\{\lambda^{\max}_{(u_i,u_{i+1})}\}}. \tag{3.2}$$

where $\lambda^{\max}_{(u_i,u_{i+1})} = \max_{u \text{ between } u_L \text{ and } u_R}\{|f'(u)|\}$.
We are going to study different numerical schemes and their ability to solve the Riemann problem for scalar conservation laws where the flux function is either convex or non convex, the different initial conditions which may or may not give rise the sonic points. The scalar conservation laws

$$u_t + f(u)_x = 0$$

whose discretized form is

$$u_i^{n+1} = u_i^n - \frac{\Delta t}{\Delta x}\left(\mathbf{f}^n(u_i, u_{i+1}) - \mathbf{f}^n(u_{i-1}, u_i)\right)$$

where $\mathbf{f}^n(u_i, u_{i+1})$ is the flux function at the interface between u_i^n and u_{i+1}^n.

3.2.1 Godunov scheme

A general Godunov scheme is described in Section 2.1. In the scalar case, the Godunov flux function however may be described in a more explicit and simpler way. We first assume that f is convex, i.e. $f''(u) > 0$ everywhere. The rarefaction arises when $u_L < u_R$. We look for the point u_σ where $f'(u_\sigma) = 0$ and the Godunov flux function at the interface between u_L and u_R is

$$\mathbf{f}^{\mathrm{G}}(u_L, u_R) = \begin{cases} f(u_L) \text{ if } u_L > u_\sigma \text{ and } \sigma > 0, \\ f(u_R) \text{ if } u_R < u_\sigma \text{ and } \sigma < 0, \\ f(u_\sigma) \text{ if } u_L < u_\sigma < u_R, \end{cases} \tag{3.3}$$

where $\sigma = \dfrac{f(u_R) - f(u_L)}{u_R - u_L}$ is the shock speed.
In general, for the nonconvex fluxes, the flux function for Godunov scheme is described by

$$\mathbf{f}^{\mathrm{G}}(u_L, u_R) = \begin{cases} \min\limits_{u_L \leq u \leq u_R} f(u) \text{ if } u_L \leq u_R, \\ \max\limits_{u_R \leq u \leq u_L} f(u) \text{ if } u_L > u_R. \end{cases} \tag{3.4}$$

The description of two formula (3.3), (3.4) are carefully explained in [LeV04].

3.2.2 Lax-Friedrichs scheme

The flux function of the Lax-Friedrichs scheme is described

$$\mathbf{f}^{\mathrm{LF}}(u_L, u_R) = \frac{1}{2}\left(f(u_L) + f(u_R)\right) - \frac{1}{2}\lambda^{\max}_{(u_L,u_R)} \cdot (u_R - u_L), \tag{3.5}$$

where

$$\lambda^{\max}_{(u_L,u_R)} = \max_{u \text{ between } u_L \text{ and } u_R}\{|f'(u)|\}. \tag{3.6}$$

3.2.3 Roe scheme

For the scalar equation, the Roe method simply linearizes the flux function based on two states u_L and u_R as

$$u_t + \sigma_{(u_L,u_R)} u_x = 0,$$

where $\sigma_{(u_L,u_R)} = \dfrac{f(u_R) - f(u_L)}{u_R - u_L}$. Then, the flux function of Roe derives from the upwind scheme is

$$\mathbf{f}^{\mathrm{R}}(u_L, u_R) = \frac{1}{2}\left(f(u_L) + f(u_R)\right) - \frac{1}{2}|\sigma_{(u_L,u_R)}| \cdot (u_R - u_L). \tag{3.7}$$

3.2.4 Dubois scheme

In [DM96], Dubois and Mehlman proposed a correction of the Roe scheme. In the scalar case, this method is simplified by a replacement the flux f by a Hermite polynomial p when the sonic point is detected. The Hermite polynomial p has degree three and satisfies $p(u_L) = f(u_L)$, $p(u_R) = f(u_R)$ and $p'(u_L) = f'(u_L)$, $p'(u_R) = f'(u_R)$. The new flux function $\tilde{f}$ is defined

$$\tilde{f}(u) = \begin{cases} p(u) \text{ if } u \text{ is between } u_L \text{ and } u_R, \\ f(u) \text{ otherwise .} \end{cases} \tag{3.8}$$

If $f'(u_L) < 0 < f'(u_R)$, then the flux function between u_L and u_R

$$\mathbf{f}^{\mathrm{Dub}}(u_L, u_R) = \begin{cases} p(u^{\min}) \text{ if } u_L < u_R, \\ p(u^{\max}) \text{ if } u_L > u_R. \end{cases} \tag{3.9}$$

where $u^{\min}$ and $u^{\max}$ are corresponding to the minimum and the maximum values of the polynomial p on the range between u_L and u_R. Otherwise, $\mathbf{f}^{\mathrm{Dub}}(u_L, u_R)$ is computed by the classical Roe flux, Equation 3.7.

3.2.5 Harten-type scheme

We consider the classical Roe scheme together with a Harten-type entropy fix. The flux function is then described by

$$\mathbf{f}^{\mathrm{Har}} = \frac{1}{2}\left(f(u_L) + f(u_R)\right) - \frac{1}{2}\left(|\sigma_{(u_L,u_R)}| + |\lambda_L - \lambda_R|\right) \cdot (u_R - u_L), \tag{3.10}$$

where $\lambda_L = f'(u_L), \lambda_R = f'(u_R)$.

3.3 Some examples for scalar conservation laws

3.3.1 Burgers equation $f(u) = \dfrac{1}{2}u^2$

The flux function $f(u) = \dfrac{1}{2}u^2$ is convex, the solution is either a single shock or a single rarefaction. In this case, the construction of the convex hull of this flux is very simple. If $u_L < u_R$, then we find that the convex hull curve of the set $\{(u, y) : u_L \le u \le u_R, y \ge f(u)\}$ is the function f itself, see Figure 3.1(a). If $u_L > u_R$, the convex hull curve of the set $\{(u, y) : u_R \le u \le u_L, y \le f(u)\}$ is the straight line segment from $(u_L, f(u_L))$ to $(u_R, f(u_R))$, see Figure 3.1(b).
Looking at numerical results.

- Figure 3.2(a), where $u_L = -1, u_R = 1$, the Roe scheme can not capture the transonic rarefaction while the other schemes do well.
- Figure 3.2(b), where $u_L = 1, u_R = -1$, all described schemes are able to capture the admissible shock wave.

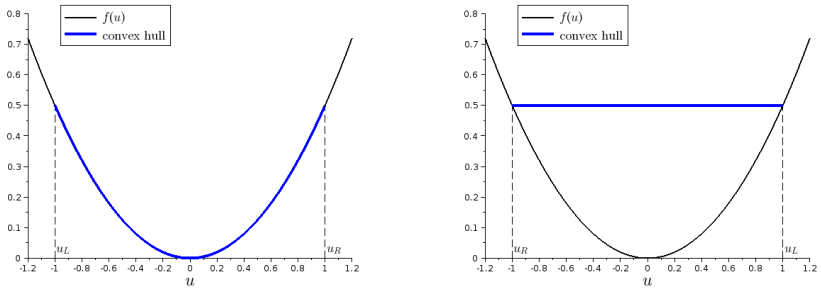

(a) (b)

FIGURE 3.1 – The convex hull curves of the flux function $f(u) = \frac{1}{2}u^2$ corresponding to $u_L = -1$, $u_R = 1$, Figure 3.1(a) and corresponding to $u_L = 1$, $u_R = -1$, Figure 3.1(b).

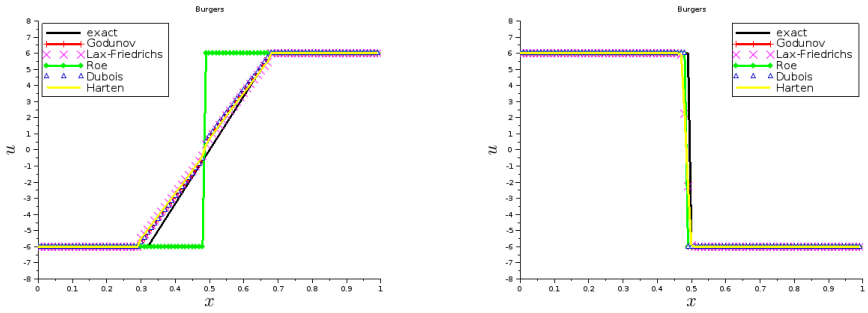

(a) (b)

FIGURE 3.2 – Numerical solution for the Burgers equation corresponding to $u_L = -1$, $u_R = 1$, Figure 3.2(a) ; and corresponding to $u_L = 1$, $u_R = -1$, Figure 3.2(b).

3.3.2 Flux function $f(u) = u(1-u)^3$

The flux function $f(u) = u(1-u)^3$ illustrates the one of the incompressible drift flux model in Appendix 5.5.6, where u stands for the volume fraction which is supposed to be between 0 and 1. The flux f is non-convex on $[0, 1]$ and admits sonic points.
The first Riemann problem is $u_L = 0.1$ and $u_R = 0.9$, the convex hull curve constructed includes a straight line segment starting from u_L and a part of the curve $f(u)$, see Figure 3.3(a). The entropy solution is therefore a composite wave consisting of one shock wave and one rarefaction.
The second Riemann problem is $u_L = 0.9$ and $u_R = 0.1$, the convex hull curve constructed includes a part of the curve $f(u)$ connecting to a straight line segment, see Figure 3.3(b). The entropy solution is therefore a composite wave consisting of one rarefaction wave and one shock wave.
Look at the numerical results.

- Figure 3.4(a), where $u_L = 0.1$ and $u_R = 0.9$, all the numerical schemes captures the entropy solution due to the fact that there is no transonic rarefaction wave.
- Figure 3.4(b), where $u_L = 0.9$ and $u_R = 0.1$, the Roe scheme fails to capture the composite wave which includes a transonic rarefaction wave whereas the entropy fixes of Dubois and Harten-type give rise the admissible solution.

3.3.3 Flux function $f(u) = \sin \pi u$

The flux function $f(u) = \sin \pi u$ is neither convex nor concave in the whole definition domain of u. Our objective is to catch some characteristic properties of the numerical schemes in this case, therefore a suitable value of u_L and u_R is chosen so that $f(u)$ has sonic points but is no longer convex.
The first Riemann problem is $u_L = 0.3$ and $u_R = 2.9$, the convex hull curve constructed includes a straight line segment connecting to curve $f(u)$ then followed by another straight line segment, see

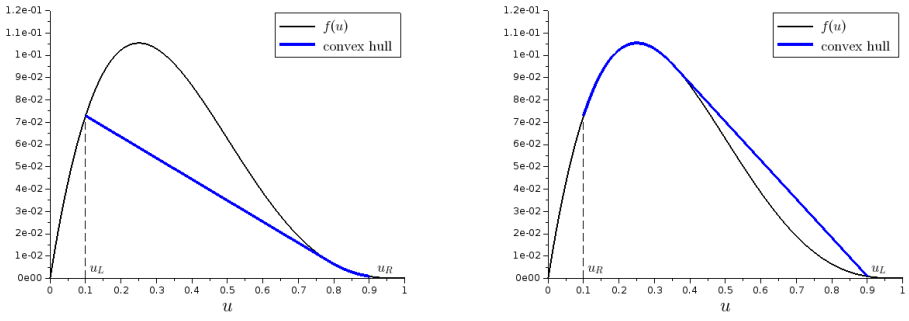

(a) (b)

FIGURE 3.3 – The flux function $f(u) = \sin(\pi u)$. The convex hull curves corresponding to $u_L = 0.1$, $u_R = 0.9$, Figure 3.3(a) and corresponding to $u_L = 0.9$, $u_R = 0.1$, Figure 3.3(b).

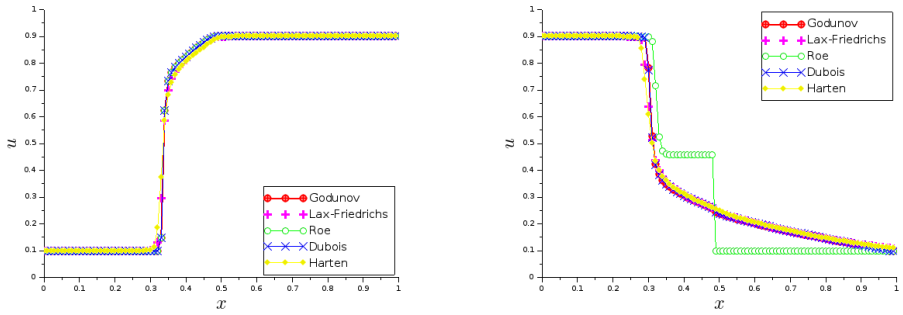

(a) (b)

FIGURE 3.4 – Numerical solutions for the flux function $f(u) = \sin(\pi u)$ at time $t = 0.15$ corresponding to $u_L = 0.1$, $u_R = 0.9$, Figure 3.4(a) and corresponding to $u_L = 0.9$, $u_R = 0.1$, Figure 3.4(b).

Figure 3.5(a). The entropy solution therefore consists of two shock waves and one rarefaction wave.
The second Riemann problem is $u_L = 2.7$ and $u_R = 0.3$, the convex hull curve constructed includes a curve $f(u)$ connecting to a straight line segment then followed by a curve $f(u)$, see Figure 3.5(b). The entropy solution therefore consists of two rarefaction waves and one shock wave.
Look at the numerical results.

- Figure 3.6(a), where $u_L = 0.3$ and $u_R = 2.9$, the Roe scheme and Dubois scheme fail to capture the entropy solution. It is well-known that the linearization consisting in two states u_L and u_R of the Roe method can not capture the transonic rarefaction. Moreover, the Dubois scheme fails in this case due to the fact that it can not detect the sonic points with given values $u_i, i = 1, \ldots, N$. Therefore, the resulting numerical results obtained by the classical Roe scheme and Dubois scheme are the same in this case.
- Figure 3.6(b), where $u_L = 2.7$ and $u_R = 0.3$, i.e. $f'(u_L) < 0 < f'(u_R)$, the Dubois scheme detects well the sonic point and captures the entropy solution.

3.4 Conclusion

It is well-known that the Godunov scheme is entropic and accurate, the resulting numerical solutions of the Godunov scheme is therefore considered as reference for other schemes.
The Lax-Friedrich scheme is a little bit diffusive in the scalar case, although its precision in the system case is not highly appreciated. Through examples, the Lax-Friedrich captures well entropy solutions due to the fact that the eigenvalue defined by (3.6) takes into account all values of u between u_L and u_R.

The classical Roe scheme is not entropic, it is necessary to use an entropy fix to improve the precision

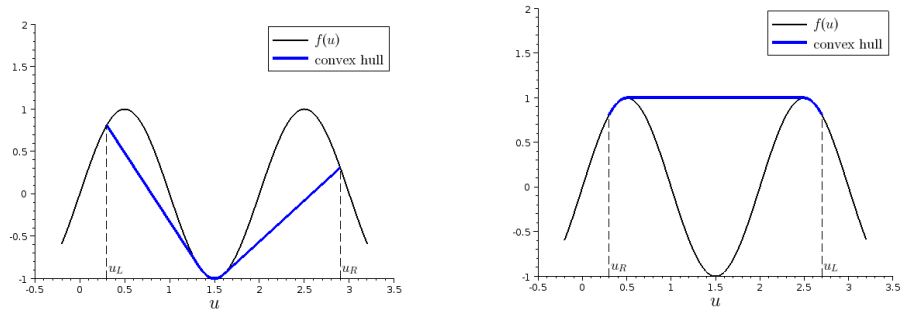

(a) (b)

FIGURE 3.5 – The flux function $f(u) = \sin(\pi u)$. The convex hull curves corresponding to $u_L = 0.3$, $u_R = 2.7$, Figure 3.5(a) and corresonding to $u_L = 2.7$, $u_R = 0.3$, Figure 3.5(b).

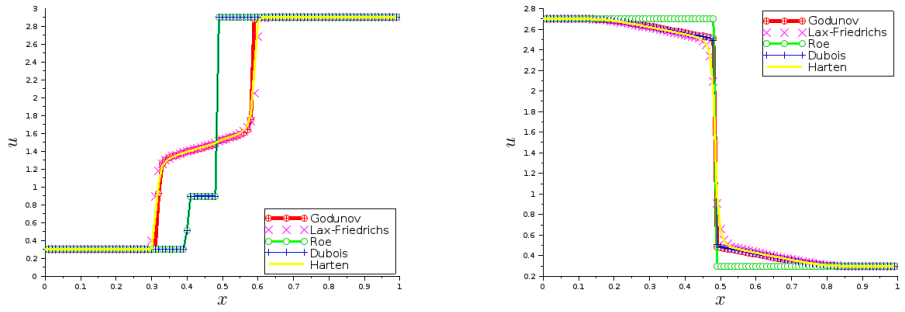

(a) (b)

FIGURE 3.6 – Numerical solutions for the flux function $f(u) = \sin(\pi u)$ at time $t = 0.15$ corresponding to $u_L = 0.3$, $u_R = 2.9$, Figure 3.6(a) and corresponding to $u_L = 2.7$, $u_R = 0.3$, Figure 3.6(b).

of this scheme. The Dubois entropy fix is a good one if it can detect the sonic point (Burgers equation), otherwise it is no longer useful, see Figure 3.6(a). It is therefore risky to use any local entropy fix associated with a prior sonic point detection. However, the Harten-type entropy fix is a little bit more diffusive but it captures the entropy solutions due to the fact that the correction is applied everywhere without detection of the sonic point. In general two-phase flow, the characteristic fields are not GNL (i.e. neither convex nor concave in the scalar equation), it is not easy to know how many sonic points exist between two constant state U_L and U_R, therefore such an entropy fix will be a good candidate.

Deuxième partie

Two-phase flow models

Chapitre 4

Two-phase flow models for boiling flows

Multiphase flows can be found in many different and important industrial applications : power plant system, heat transfer systems, combustion systems, environmental studies, oil industry, etc... One phase in a multiphase flow is a state of the matter which can be liquid, gas, or solid and there is a wide variety of multiphase flows depending on the topology of the inclusions and whether the phases are totally immiscible, whether there are chemical reactions, phase change, strong thermal or mechanical disequilibrium or not. In this thesis we are interested in the two-phase flow encountered in the cooling system of thermal power plants. Because of their good specific heat coefficients, liquid are commonly used but in transient operations of the power plant or in case of a severe accident, the liquid may boil due to a overheating of the liquid. Hence in this document the two-phase flow considered is a liquid-gas flow where the gaseous phase is the steam generated by the liquid boiling.
There are different possible scales to describe a two-phase flow. Depending on the specific interest, one can use a Direct Numerical Simulation for a fine description of the topology of the inclusions, or homogenized models for the global dynamics of the mixture. We are here interested in the global dynamics of the flow rather than its local structure. Therefore the flow is considered neither in the microscopic scale (molecular scale) nor in the meso-scale (which takes into account the local inclusions in of the flow), we will instead address the flow in the macroscopic scale (with continuum assumption).
Numerous authors in the literature have developed the macroscopic scale of the two-phase flow by two approaches : interacting continua assumption and averaging method. The first approach considers the two-phase flow as a mixture where each point is assumed to be occupied by two phases, whereas the main characteristic of the second one is the elimination of the local instantaneous fluctuations of the variables by a statistical averaging operation. The details of these two approaches are given in [IH11]. Applying the averaging method, one may encounter three main groups : Eulerian, Lagrangian and Boltzmann statistical averages. Among those, the Eulerian formulation is the most widely used due to its similarity with traditional physics and experimental observations. The system obtained by the Eulerian average consists of partial differential equations corresponding to the conservation laws of the governing balance laws of mass, momentum and energy of the two-phase mixture. Such equations are called the field equations. One may distinguish the two-phase flow models by the number of field equations and whether the mechanical and thermal disequilibrium is described by PDEs or algebraic correlations. We will introduce here the two-phase flow models used in the simulation of boiling in the cooling system of a nuclear power plant. This boiling usually occurs in the main exchangers of the plant that is the reactor core and the reactor steam generator.

The first one is the *slip model*, usually called a *three-equation model* due to its three conservation laws (mass, momentum, energy) of the mixture of two phases. The set of equations looks like the single phase Euler system but due to the fact that the composition of the mixture is obtained from the thermal equilibrium assumption, the equation of state in this case is not differentiable and the characteristic fields are neither linearly degenerate nor genuinely non linear. However this is the simplest averaged model model for the description of transient boiling flows since thermal equilibrium and saturation are assumed ($T_g = T_l = T^{sat}(p)$), and the two phasic velocity vectors are supposed to be corelated with a slip or drift correlation. In the slip correlation the liquid and vapor velocities are assumed colinear ($\vec{u}_g = s\vec{u}_l$) and the slip ratio s is the corresponding coefficient of proportionality. It is also possible to

use a drift correlation, the relative velocity $\vec{u}_g - \vec{u}_l$ between the gas and liquid phases is given explicitly. The homogeneous equilibrium model (studied in detail section 4.2.1) is a particular case of the slip model where mechanical equilibrium is also assumed and the two phasic velocities are assumed equal (slip ratio equal to one or relative velocity equal to zero). In that case the characteristic fields are linearly degenerate or genuinely non linear. The slip model is used in the software GENEPI [1] to simulate the steam generator of pressurised water reactors. However, the application of such a model to describe the flow dynamics in the regions where the two phasic velocities are not strongly correlated does not yield sufficiently accurate predictions, especially in the 3D dynamics encountered in region where the flow is not directed by Uranium rods in the core or tubes in the steam generator. It is therefore necessary to consider more accurate models.

The second family of models encountered in this thesis, is the *drift flux model*, usually called the *four-equation model* due to the fact that it consists of the three previous balance laws describing the mixture and one conservation laws for the mass vapor. This model is an improvement of the slip model because the assumption that both phases are at saturation is relaxed (only $T_g = T^{sat}(p)$ is assumed in practice) and an algebraic relation between the phasic temperatures or enthalpies can be assumed. This allows the averaged description of a nucleate boiling flow where the bubble nucleate near the hot Uranium wall and then condense in the subcooled surrounding liquid. The phasic velocities are obtained using a drift relation which defines the relative velocity of the liquid and vapor. Similarly to the slip model, this model displays characteristic fields that are neither linearly degenerate nor genuinely non linear. Various drift relations have been proposed for two phase flows in vertical pipes. The main application of the drift flux model is simulating the two-phase flow in vertical vessel. It is used to model the flow in the vessel of nuclear reactor core by thermal hydraulics softwares such as FLOCAL [2] or FLICA4 [3]. This model allows the description of subcooled boiling where the vapor is at saturation but not the bulk liquid, which is an important property in the design of pressurized water reactors.

The third familly of models is the *two-fluid model*, usually called the *six-equation model* due to the fact that it includes three balance equations for each phases. This is the most widely used in nuclear thermal hydraulic packages, CATHARE [4], Neptune-CFD [5], RELAP5 [6], CUPID [7] are some examples. In this family no algebraic correlation is used to describe the mechanical or thermal disequilibria which enables the simulation of a wide variety of flows where such correlation do not exist. The system is however more complex given its larger size and the strong non linearities involved for the determination of each phasic velocities and temperature. This model as the previous has characteristic fields that are neither linearly degenerate neither genuinely nonlinear. Furthermore sonic points are common in this model and a specific emphasis should be put on the design of accurate numerical methods.

In practice, depending on the specific properties of the two-phase flow, one may choose a suitable model due to the fact that each model has its own advantages as well as disadvantages. The slip model is the easiest one to solve numerically and the general model as the two-fluid model however gives rise significant mathematical and numerical difficulties. For more details about limitations of the two-phase flow models, we refer the reader to [KI83] and references therein.

In general, the number of field equations is smaller than the number of unknown variables. In order to completely solve the balance systems, it is necessary that one uses constitutive relations which are supplementary relations corresponding to each model and the *equations of states*. Without specific mention, one of the closure laws used for all models in this document is equal pressure law ($p_g = p_l$) which is fairly accurate given that the pressure in a pressurized water reactor is 155e5 bar and that surface tension $\sigma = 0.0175 N/m$ is generally neglected.

1. Developed by CEA (France)
2. Developed by Forschungszentrum Rossendorf (Germany)
3. Developed by CEA (France)
4. Developed by CEA (France)
5. Developed by EDF-CEA (France)
6. Developed by INL(USA)
7. Developed by KAERI (Korea)

4.1 Introduction to two-phase flow models

4.1.1 Slip model (three-equation model)

The slip model describes the mixture of the two phases of a boiling flow based on the following three fundamental assumptions :

— the vapor is assumed at saturation $T_g = T^{sat}(p)$,
— the liquid is assumed at saturation $T_l = T^{sat}(p)$,
— the two velocities are correlated by a slip relation $\vec{u}_g = s\vec{u}_l$ or a drift relation $\vec{u}_g - \vec{u}_l = \vec{u}_r(\rho_m, \vec{u}_m, h_m)$.

Each phase (vapor or liquid) has its own equation of state $\rho_k = \rho_k(p_k, h_k)$. However, an important consequence of both phases being on the saturation curve is that they share the same pressure $p_g = p_l$ and that the phasic thermodynamic quantities such as the temperatures T_k^{sat}, the entropies s_k^{sat} or enthalpies h_k^{sat} depend only on the pressure and not on the composition of the two phase mixture. Since it is often the easiest parameter to measure in experiments, physicist usually employ the mixture enthalpy h_m to study the phase change and determine the composition of the mixture. The phasic enthalpies $h_k^{sat}(p)$ are threshold values such that the fluid at pressure p is liquid for $h_m < h_l^{sat}(p)$ and gaseous for $h > h_g^{sat}(p)$. Both phases coexist for values of $h_m \in]h_l^{sat}(p), h_v^{sat}(p)[$. From this properties it is possible to determine the composition $\alpha = \alpha(p, h_m)$ of the mixture from the knowledge of p and h_m (see Section 4.1.1).
Neglecting viscosity and thermal conduction effects, the slip model then consists in the following three balance equations of the governing balance of mass, momentum and energy of the mixture

$$\frac{\partial \rho_m}{\partial t} + \nabla \cdot (\rho_m \vec{u}_m) = 0, \tag{4.1a}$$

$$\frac{\partial}{\partial t}(\rho_m \vec{u}_m) + \nabla \cdot (\rho_m \vec{u}_m \otimes \vec{u}_m + \rho_m c_g (1 - c_g) \vec{u}_r \otimes \vec{u}_r + p \cdot \mathrm{Id}) = \rho_m \vec{g} + \vec{F}^{\mathrm{w}}, \tag{4.1b}$$

$$\frac{\partial}{\partial t}(\rho_m E_m) + \nabla \cdot (\rho_m \left(\vec{u}_m H_m + c_g (1 - c_g)(H_v - H_l)\vec{u}_r\right)) = \rho_m \vec{g} \cdot \vec{u}_m + \vec{F}^{\mathrm{w}} \cdot \vec{u}_m + Q^{\mathrm{w}}, \tag{4.1c}$$

where $c_g = \dfrac{\alpha_g \rho_g^{sat}}{\rho_m}$ is the vapor mass concentration, $H_k = E_k + \frac{p}{\rho_k^{sat}}$ is the phasic total enthalpy and $\rho_m, \vec{u}_m, E_m, H_m$ are the density, velocity and total energy and total enthalpy of the mixture, i.e.

$$\rho_m(p, h_m) = \alpha_g(p, h_m)\rho_g(p, h_g^{\mathrm{sat}}(p)) + \alpha_l(p, h_m)\rho_l(p, h_l^{\mathrm{sat}}(p)), \tag{4.2}$$

$$\vec{u}_m = \frac{\alpha_g(p, h_m)\rho_g(p, h_g^{\mathrm{sat}}(p))\vec{u}_g + \alpha_l(p, h_m)\rho_l(p, h_l^{\mathrm{sat}}(p))\vec{u}_l}{\rho_m}, \tag{4.3}$$

$$h_m = \frac{\alpha(p, h_m)_g \rho_g(p, h_g^{\mathrm{sat}}(p)) h_g^{\mathrm{sat}}(p) + \alpha(p, h_m)_l \rho_l(p, h_l^{\mathrm{sat}}(p)) h_l^{\mathrm{sat}}(p)}{\rho_m}, \tag{4.4}$$

$$e_m = \frac{\alpha(p, h_m)_g \rho_g(p, h_g^{\mathrm{sat}}(p)) e_g + \alpha(p, h_m)_l \rho_l(p, h_l^{\mathrm{sat}}(p)) e_l}{\rho_m}, \tag{4.5}$$

$$E_m = e_m + \frac{1}{2}\frac{\alpha_g(p, h_m)\rho_g(p, h_g^{\mathrm{sat}}(p))|\vec{u}_g|^2 + \alpha_l(p, h_m)\rho_l(p, h_l^{\mathrm{sat}}(p))|\vec{u}_l|^2}{\rho_m}, \tag{4.6}$$

$$H_m = E_m + \frac{p}{\rho_m}; \tag{4.7}$$

$\vec{u}_r$ is the relative velocity, $\vec{g}$ is the gravity field vector, Q^{w} is the heat received by the fluid from the nuclear fissions. On the right hand side of (4.1a-4.1c) F^{w} represent wall friction due to the presence of uranium rods, and Q^{w} the heat transferred to the fluid by Uranium rods.
This model can be obtained from the general six-equation model (4.18) by summing respectively the two mass, momentum and energy equation, or from the drift model (4.10a-4.10d) by summing the two mass equations. In particular the slip model does not display any interfacial transfer source term because interfacial mass, momentum and energy transfer term from the the general six-equation model (4.18) cancel each other when summed across the two phases.

The void fraction law $\alpha(p, h_m)$

In the slip model, a single mass equation replaces the two partial mass equation of the six-equation model (4.18). In order to obtain the composition of the mixture one needs to use the fact that both phases are at saturation. α is computed from p and h_m using the relation

$$\rho_m h_m = \alpha_g \rho_g(p, h_g^{\text{sat}}(p)) h_g^{\text{sat}}(p) + \alpha_l \rho_l(p, h_l^{\text{sat}}(p)) h_l^{\text{sat}}(p), \tag{4.8}$$

we obtain

$$\begin{array}{llcl} \text{if} & h_m < h_l^{\text{sat}}(p) & \alpha(p,h_m) & = & 0 \\ \text{if} & h_l^{\text{sat}}(p) < h_m < h_g^{\text{sat}}(p) & \alpha(p,h_m) & = & \dfrac{\rho_m h_m - \rho_l(p, h_l^{\text{sat}}(p)) h_l^{\text{sat}}(p)}{\rho_g(p, h_g^{\text{sat}}(p)) h_g^{\text{sat}}(p) - \rho_l(p, h_l^{\text{sat}}(p)) h_l^{\text{sat}}(p)} \\ \text{if} & h_m > h_g^{\text{sat}}(p) & \alpha(p,h_m) & = & 1. \end{array} \tag{4.9}$$

We see that α is a continuous, piecewise differentiable function of h_m and p. The void fraction α is not differentiable on points (p, h_m) such that $h_m = h_g^{\text{sat}}(p)$ or $h_m = h_l^{\text{sat}}(p)$. The same goes with c_g and c_l, and therefore unless $\vec{u}_r = 0$, the Flux F of the slip model is not $\mathcal{C}^1(U)$. The study of the slip model therefore requires a careful analysis of the single phase ($\alpha_g \alpha_l = 0$) - two phase ($\alpha_g \alpha_l > 0$) and the mechanical equilibrium ($\vec{u}_r = 0$) - mechanical disequilibrium ($\vec{u}_r \neq 0$) transitions.

Estimating the void fraction by the constitutive equation (4.9) has the advantage that we can easily maintain α and c_g in the interval $[0, 1]$. However equation (4.9) relies on the assumption of both phases being at saturation and subcooled boiling ($T_g \neq T_g^{sat}(p)$ or $T_g \neq T_g^{sat}(p)$) is an important physical model that we would like to be able to model. This is an important limitation of the slip model.

4.1.2 Drift flux model (four-equation model)

Since we use a averaged models the assumption of saturation for the averaged thermodynamic quantities is often violated. For example in a nuclear reactor operating in normal conditions, bubble nucleation occur near the very hot Uranium rods and their averaged temperature in a channel is larger than the average liquid temperature in the channel. This comes from the fact that it is only near the Uranium rods that the fluid is at saturation with both phases present and at thermal equilibrium.
In order to be able to describe flows where the phases are not necessarily assumed at saturation, one considers an additional balance PDE governing of vapor to the three-equation model. This yields a four-equation model named the drift flux model, which enables the computation of the fluid composition without requiring phases at saturation.
Similarly to the slip model, the drift flux model contains three conservation equations of the governing balance of mass, momentum and energy of the mixture. However there is an additional balance equation for the evolution of the vapor mass. in adding a conservation equation of gaseous phase. This model admits different velocities between gas and liquid due to the drift relation which usually depends on the flow conditions. Therefore the drift model is based on two fundamental assumptions :

— the vapor is assumed at saturation $T_g = T^{sat}(p)$

— the two velocities are correlated by a slip $\vec{u}_v = s\vec{u}_l$ or a drift relation $\vec{u}_v - \vec{u}_l = \vec{u}_r(\rho, \vec{u}_m, h_m)$

Neglecting viscosity and thermal conduction effects, the drift model then consists in the following four balance equations of the governing balance of total mass, vapor mass, total momentum and total energy of the mixture. The system of four equations is written under a conservation form as follows

$$\frac{\partial \alpha_g \rho_g + \alpha_l \rho_l}{\partial t} + \nabla \cdot (\rho_m \vec{u}_m) = 0, \tag{4.10a}$$

$$\frac{\partial \alpha_g \rho_g}{\partial t} + \nabla \cdot (\alpha_g \rho_g \vec{u}_g) = \Gamma_g, \tag{4.10b}$$

$$\begin{aligned} \frac{\partial (\rho_m \vec{u}_m)}{\partial t} &+ \nabla \cdot (\rho_m \vec{u}_m \otimes \vec{u}_m + \rho_m c_g (1 - c_g) \vec{u}_r \otimes \vec{u}_r + p \cdot \mathrm{Id}) \\ &= \rho_m \vec{g} + \vec{F}^{\mathrm{w}}, \end{aligned} \tag{4.10c}$$

$$\begin{aligned} \frac{\partial}{\partial t}(\rho_m E_m) &+ \nabla \cdot \left(\alpha_g \rho_g {H_g}^t \vec{u}_g + \alpha_l \rho_l {H_l}^t \vec{u}_l \right) \\ &= \rho_m \vec{g} \cdot \vec{u}_m + \vec{F}^{\mathrm{w}} \cdot \vec{u}_m + Q^{\mathrm{w}}. \end{aligned} \tag{4.10d}$$

Γ_g is the steam production rate, $\vec{u}_r$ is the relative velocity, $\vec{g}$ is the gravity field vector, Q^{w} is the heat received by the fluid from the nuclear fissions. In addition, the variable $c_g = \dfrac{\alpha_g \rho_g}{\rho_m}$ denotes the mass concentration of vapour. On the right hand side of (4.10a-4.10d) F^{w} represent wall friction due to the presence of uranium rods, and Q^{w} the heat transferred to the fluid by Uranium rods.

$\rho_k, \vec{u}_k, E_k, e_k$ and $H_k = E_k + \frac{p}{\rho_k}$ are the density, velocity and total energy, internal energy and total enthalpy of each phase. The mixture density, velocity and energies are defined as

$$\rho_m(p, h_m) = \alpha_g \rho_g(p, h_g) + \alpha_l \rho_l(p, h_l), \tag{4.11}$$

$$\vec{u}_m = \frac{\alpha_g \rho_g(p, h_g)\vec{u}_g + \alpha_l \rho_l(p, h_l)\vec{u}_l}{\rho_m}, \tag{4.12}$$

$$h_m = \frac{\alpha_g \rho_g(p, h_g) h_g + \alpha_l \rho_l(p, h_l) h_l}{\rho_m}, \tag{4.13}$$

$$e_m = \frac{\alpha_g \rho_g(p, h_g) e_g + \alpha_l \rho_l(p, h_l) e_l}{\rho_m}, \tag{4.14}$$

$$E_m = e_m + \frac{1}{2}\frac{\alpha_g \rho_g(p, h_g)|\vec{u}_g|^2 + \alpha_l \rho_l(p, h_l)|\vec{u}_l|^2}{\rho_m}; \tag{4.15}$$

This model can be obtained from the general six-equation model (4.18) by summing respectively the two momentum and energy equation. Indded, since $\vec{u}_g = \vec{u}_m + (1 - c_g)\vec{u}_r$ and $\vec{u}_l = \vec{u}_m - c_g \vec{u}_r$ we can derive

$$\alpha_g \rho_g \vec{u}_g \otimes \vec{u}_g + \alpha_l \rho_l \vec{u}_l \otimes \vec{u}_l = \rho_m \vec{u}_m \otimes \vec{u}_m + \rho_m c(1 - c)\vec{u}_r \otimes \vec{u}_r. \tag{4.16}$$

In particular the drift model does not display any interfacial transfer of momentum and energy because interfacial momentum and energy transfer term from the the general six-equation model (4.18) cancel each other when summed across the two phases.

The details of modeling and capability of application of the drift flux model can be found in [Ish75 ; IH11] whereas its mathematical analysis and numerical methods can be found in [Tou87], [Rom98], [EF07].
Following [IH11], [Tou87] and references therein, an example of closure law for the drift velocity $\vec{u}_r$ is a function of the terminal velocity v_∞ of a particle in an infinite medium and the void fraction α. Eliminating the concentration gradient (which is less important), we can suppose the following form of the drift velocity

$$v_{dj} = (1 - \alpha)(u_g - u_l) = (1 - \alpha)^k v_\infty. \tag{4.17}$$

In [Tou87], Toumi gives a rigorous study of the characteristic fields of the drift flux model corresponding to a variation of value k in the equation (4.17). He then demonstrates explicitly the structure of the solution to the Riemann problem in some cases. Especially, due to the existence of non GNL characteristic fields, it gives rise to composite waves in some flow conditions.

The main advantage of the four equations model is that while allowing some mechanical and thermal non-equilibrium, its formulation is conservative which eliminates some mathematical difficulties appearing in the general two-fluid model. Moreover the equation governing the balance of vapor implies a direct computation of the void fraction from the PDE system, it then eliminates the disadvantage of the slip model whose void fraction formula assumes both phases are at saturation and yields a non regular flux function.

Nevertheless, the drift flux model as well as the slip model assume a strong coupling between two velocities due to due to friction between the phases. They are therefore not good models for the flow whose phasic dynamics are strongly different such as counter-current flow. We then need a more general one which allows to model the flow in general conditions. The development of the two-fluid models responds this requirement.

4.1.3 Two-fluid model (six-equation model)

The two-fluid model is obtained by writing the balance of mass, momentum and energy of each phase separately : separately.

$$\frac{\partial \alpha_g \rho_g}{\partial t} + \nabla \cdot (\alpha_g \rho_g \vec{u}_g) = \Gamma_g, \tag{4.18a}$$

$$\frac{\partial \alpha_l \rho_l}{\partial t} + \nabla \cdot (\alpha_l \rho_l \vec{u}_l) = \Gamma_l, \tag{4.18b}$$

$$\begin{aligned} \frac{\partial \alpha_g \rho_g \vec{u}_g}{\partial t} + \nabla \cdot (\alpha_g \rho_g \vec{u}_g \otimes \vec{u}_g) + \alpha_g \vec{\nabla} p_g &= \alpha_g \rho_g \vec{g} + \vec{u}^i \Gamma_g + \vec{F}_g^w \\ &+ (p_g^i - p_g) \nabla \cdot \alpha_g, \end{aligned} \tag{4.18c}$$

$$\begin{aligned} \frac{\partial \alpha_l \rho_l \vec{u}_l}{\partial t} + \nabla \cdot (\alpha_l \rho_l \vec{u}_l \otimes \vec{u}_l) + \alpha_l \vec{\nabla} p_l &= \alpha_l \rho_l \vec{g} + \vec{u}^i \Gamma_l + \vec{F}_l^w \\ &+ (p_l^i - p_l) \nabla \cdot \alpha_l, \end{aligned} \tag{4.18d}$$

$$\begin{aligned} \frac{\partial \alpha_g \rho_g E_g}{\partial t} + p_g \frac{\partial \alpha_g}{\partial t} + \nabla \cdot (\alpha_g \rho_g \vec{u}_g H_g) &= \alpha_g \rho_g \vec{g} \cdot \vec{u}_g + Q_g^i + Q_g^w \\ &+ \vec{F}_g^i \cdot u^i + \Gamma_g H_g^i, \end{aligned} \tag{4.18e}$$

$$\begin{aligned} \frac{\partial \alpha_l \rho_l E_l}{\partial t} + p_l \frac{\partial \alpha_l}{\partial t} + \nabla \cdot (\alpha_l \rho_l \vec{u}_l H_l) &= \alpha_l \rho_l \vec{g} \cdot \vec{u}_l + Q_l^i + Q_l^w \\ &+ \vec{F}_l^i \cdot u^i + \Gamma_l H_l^i, \end{aligned} \tag{4.18f}$$

where the primitive variables $\alpha_k, \rho_k, u_k, p_k, E_k, H_k = E_g + \frac{p_k}{\rho_k}$ are respectively the volume fraction, density, velocity, pressure, total energy and total enthalpy of the phase k, subscript k denotes either g or l. The right hand side of the system (4.18a-4.18f) mentions the source terms which are classified as follows

- The interfacial interaction transfers include :
  - Γ_k the interfacial mass transfer terms,
  - $\vec{u}^i$ the interfacial velocity,
  - Q_k^i the interfacial heat transfer,
  - H_k^i the interfacial total enthalpy transfer,
- Q_k^w the wall heat transfer to k phase, $\vec{F}_k^w$ the wall friction.
- $\vec{g}$ is the gravity.

The energy equations in the system (4.18) are written using the total energy variables (E_k). It is however possible to be replaced by other variables, such as the internal energy (e_k), or enthalpy (h_k), total enthalpy (H_k) or entropy (s_k). We would like to present here the energy equations using the entropy variable, that will give a simple presentation to the energy equation. The entropy variables (s_k) satisfies the relation

$$T_k \mathrm{d}s_k = \mathrm{d}e_k - \frac{p_k}{\rho_k^2} \mathrm{d}\rho_k, \tag{4.19}$$

where T_k denotes the temperature. The equations (4.18e),(4.18f) can be rewritten as the following equation

$$\frac{\partial \alpha_k \rho_k s_k}{\partial t} + \nabla \cdot (\alpha_k \rho_k \vec{u}_k s_k) = \tilde{S}_k + \Gamma_k s_k, \quad k = g, l, \tag{4.20}$$

where

$$T_k \tilde{S}_k = \vec{F}_k^i \cdot (\vec{u}_k^i - \vec{u}_k) + \Gamma_g \left(h_k^i - h_k + \frac{\left(\vec{u}_k^i - \vec{u}_k\right)^2}{2} \right) + Q_k^w + Q_k^i. \tag{4.21}$$

It is possible to rewrite the equation (4.20) by using the conservation of mass in (4.18a),(4.18b) as the following equation

$$\frac{\partial s_k}{\partial t} + \vec{u}_k \cdot \nabla s_k = \frac{\tilde{S}_k}{\alpha_k \rho_k}. \tag{4.22}$$

The equation (4.22) is helpful to compute the characteristic wave associated to the energy equations.

4.1.4 Five-equation two-fluid model

A complete six equations two-fluid model gives rise many mathematical difficulties. One may think first that the two-fluid model is not formulated in conservation form not only owing to the non conservative product in momentum equations but also the presence of $p\partial_t\alpha$ in the partial energy equations. The temporal derivative $p\partial_t\alpha$ leads to mathematical difficulty in the sense that the system is neither conservative nor in a quasi-linear form. If one is not interested in the thermal evolution of the flow and would like to focus on the purely mechanical aspects, one may neglect the two equations of energy in the complete six-equation model by considering an isentropic two-fluid model (see Section 4.3.4).
In order to overcome this difficulty and be able to concentrate on the analysis of void waves and stiff source terms for the simulation of heated and boiling flows, we propose to replace the two phasic energy equation by a single mixture energy equation. We obtain a conservative energy equations and the overall system is easy to write in quasilinear form. This motivates us to study a five-equation two-fluid model which consists of two conservation equations of mass, two conservation equations of momentum and one conservation equation of energy as in the following system

$$\frac{\partial \alpha_g\rho_g}{\partial t} + \nabla\cdot(\alpha_g\rho_g\vec{u}_g) = \Gamma_g, \tag{4.23a}$$

$$\frac{\partial \alpha_l\rho_l}{\partial t} + \nabla\cdot(\alpha_l\rho_l\vec{u}_l) = \Gamma_l, \tag{4.23b}$$

$$\begin{aligned}\frac{\partial \alpha_g\rho_g\vec{u}_g}{\partial t} + \nabla\cdot(\alpha_g\rho_g\vec{u}_g\otimes\vec{u}_g) + \alpha_g\vec{\nabla}p &= \alpha_g\rho_g\vec{g} + \vec{F}_g^w + \vec{F}_g^i + \vec{u}^i\Gamma_g \\ &+ (p_g^i - p_g)\nabla\cdot\alpha_g,\end{aligned} \tag{4.23c}$$

$$\begin{aligned}\frac{\partial \alpha_l\rho_l\vec{u}_l}{\partial t} + \nabla\cdot(\alpha_l\rho_l\vec{u}_l\otimes\vec{u}_l) + \alpha_l\vec{\nabla}p &= \alpha_l\rho_l\vec{g} + \vec{F}_l^w + \vec{F}_l^i + \vec{u}^i\Gamma_l \\ &+ (p_l^i - p_l)\nabla\cdot\alpha_l,\end{aligned} \tag{4.23d}$$

$$\frac{\partial E}{\partial t} + \nabla\cdot(\alpha_g\rho_g\vec{u}_gH_g + \alpha_l\rho_l\vec{u}_lH_l) = \vec{g}\cdot(\alpha_g\rho_g\vec{u}_g + \alpha_l\rho_l\vec{u}_l) + Q^w, \tag{4.23e}$$

where the energy equation (4.23e) is formulated by adding two partial energy equations in the six-equation model, the temporal derivative $p\partial_t\alpha$ is hence simplified. The notation E in equation (4.23e) is defined by

$$E = \alpha_g\rho_gE_g + \alpha_l\rho_lE_l. \tag{4.24}$$

The five-equation model is formulated by the six-equation model using the thermal equilibrium assumption. Studying the five-equation model is first suggested in the thesis [Fer10] where the authors' objective is to compare the numerical results using Roe solver between different two-fluid models : isentropic model, five-equation model and six-equation model.

4.1.5 Constitutive equations and equations of state

There are many different models describing the dynamics of the two phase flows. Studying such models requires to solve a system of partial differential equations (PDE). The number of unknown variables is in general greater than the number of equations in system of PDE. Therefore, it is necessary to consider supplementary constitutive equations and equations of state. We here define two classes of variables in the two phase flow which are *primitive variables* and *conservative variables*. The primitive variables in the two phase flow are volume fraction (α_g, α_l), pressure (p_g, p_l), densities (ρ_g, ρ_l), velocity (u_g, u_l), energy for example internal energy (e_g, e_l). It is possible to replace the internal energy variables by other equivalent variables such as total energy, enthalpy or total enthalpy and so on. The number of the conservative variables varies following a specific two-phase flow model and is equal to number of equations PDE. For example, the conservative variables of the two-fluid six-equation model is $(\alpha_g\rho_g, \alpha_l\rho_l, \alpha_g\rho_gu_g, \alpha_l\rho_lu_l, \alpha_g\rho_gE_g, \alpha_l\rho_lE_l)$.

Due to the fact that the number of primitive variables in the two phase flow are greater than the number of partial differential equations of any two phase flow model, it is therefore essential to take into account the supplementary constitutive equations and equations of state. In general, such equations depend on a specific two phase flow model and the flow conditions as well. A common constitutive equations considered in this document are the occupied geometric assumption

$$\alpha_g + \alpha_l = 1, \tag{4.25}$$

and equal pressure

$$p_g = p_l, \tag{4.26}$$

whereas the equations of state considered in thermaldynamics can be rexpressed

$$\rho_k = \rho_k(p, e_k), \tag{4.27}$$

where the subscript k stands for either g or l.
In order to compute the temperature of the fluid from the conservative variable, an extra constitutive law

$$e_k = e_k(T_k, \rho_k) \tag{4.28}$$

is necessary.

The relations (4.25,4.26,4.28) are enough to close the six-equation model while the slip, drift flux and five-equation models require more constitutive equations for $u_g - u_l$ or $T_g - T_l$.

4.2 Quasi-linear form and characteristic fields of boiling flow models

In this section, we will present the two-phase flow models in quasi-linear forms in order to study the eigenstructure of the Jacobian matrices as well as their characteristic fields.

4.2.1 Characteristic fields of the slip model

Neglecting viscosity and thermal conduction, the 1D slip model then consists in the following three balance equations of the governing balance of mass, momentum and energy of the mixture

$$\partial_t \rho_m + \partial_x(\rho_m u_m) = 0, \tag{4.29}$$

$$\partial_t(\rho_m u_m) + \partial_x\left(\rho_m u_m^2 + \rho_m c_g(1-c_g)u_r^2 + p\right) = F, \tag{4.30}$$

$$\partial_t(\rho_m E_m) + \partial_x(\rho_m\left(u_m H_m + c_g(1-c_g)(H_g - H_l)u_r\right) = Q, \tag{4.31}$$

where $c_k = \frac{\alpha_k \rho_k}{\rho_m}$ is the phase k mass concentration, $H_k = E_k + \frac{p}{\rho_k}$ is the phasic total enthalpy and $\rho_m, \vec{u}_m, E_m, H_m$ are the density, velocity and total energy and total enthalpy of the mixture defined by equations (4.2-4.7).

We recall that the phases being assumed at saturation,

— If $h_m < h_l^{\text{sat}}$ (respectively $h_m > h_g^{\text{sat}}$), then $\alpha = 0$ (respectively $\alpha = 1$) and the system reduces to the single phase Euler equations with three characteristic speeds $\lambda_1 = u_m - c_{sl}, \lambda_2 = u_m, \lambda_3 = u_m + c_{sl}$ (respectively $\lambda_1 = u_m - c_{sg}, \lambda_2 = u_m, \lambda_3 = u_m + c_{sg}$). The first and third fields (acoustic waves) are genuinely nonlinear and the second (entropy wave) is linearly degenerate (see section 1.3).

— If $h_l^{\text{sat}} < h_m < h_g^{\text{sat}}$ then the fluid is a mixture of two phases and the composition α can be determined algebraically from the value of h_m or s_m using the assumption of saturation. This implies that composition waves (often called void waves in thermal hydraulics) are carried by the mixture entropy and are therefore associated to the second characteristic wave.

In the latter case $h_l^{\text{sat}} < h_m < h_g^{\text{sat}}$, the characteristic fields of the system (4.29-4.31) are more complicate to determine and depend strongly on the model of drift velocity $u_r(\rho_m, u_m, h_m)$ chosen. If u_r and $c_g c_l$ are small, then the latter case can be seen as a perturbation of the former. For u_r and $c_g c_l$ small enough the first and third fields remain genuinely nonlinear but the second field is unlikely to remain linearly degenerate. We conjecture that in the general case the characteristic fields may be neither linearly degenerate, nor genuinely nonlinear. However, we are going to study them in details in the particular case where the mechanical equilibrium is neglected $u_r = 0$.

The case $u_r = 0$ (homogeneous equilibrium model)

When $u_r = 0$ the system reduces to the following system

$$\partial_t \rho_m + \partial_x(\rho_m u_m) = 0, \tag{4.32}$$

$$\partial_t(\rho_m u_m) + \partial_x\left(\rho_m u_m^2 + p\right) = F, \tag{4.33}$$

$$\partial_t(\rho_m E_m) + \partial_x(\rho_m u_m H_m) = Q, \tag{4.34}$$

which looks like the Euler system but with a particular equation of state due to the presence of two phases with different equations of state.
We will chose the pressure p and the entropy s_k as the two thermodynamics variables in the equation of state $\rho_k = \rho(p, s_k)$. Since the two phases are supposed at saturation, there is an extra thermodynamical law $s_k^{\text{sat}}(p)$ involved in the model, but we will neglect the influence of the pressure on the saturation value of the entropy. This is motivated first by the Antoine equation (an approximation of the Clausius-Clapeyron law) $T^{sat} = \frac{R}{\mathcal{L}} \frac{1}{c - \ln(p)}$ for three constants $R, \mathcal{L}, c$ which shows that T^{sat} evolves slowly as $\frac{1}{\ln(p)}$ (see for example picture 4.1 from [ST]). Secondly we can measure the slope of the curves $s_k^{sat}(p)$ for p around $155 bars$ on picture 4.2 obtained from [ST] and find

$$\begin{aligned} \frac{\partial s_g^{\text{sat}}}{\partial p} &\approx \frac{-10^3}{150\, 10^5} J/(Kg * K * Pa) \approx -6 \cdot 10^{-5} J/(Kg * K * Pa), \\ \frac{\partial s_l^{\text{sat}}}{\partial p} &\approx \frac{10^3}{150 \cdot 10^5} J/(Kg * K * Pa) \approx 6 \cdot 10^{-5} J/(Kg * K * Pa). \end{aligned}$$

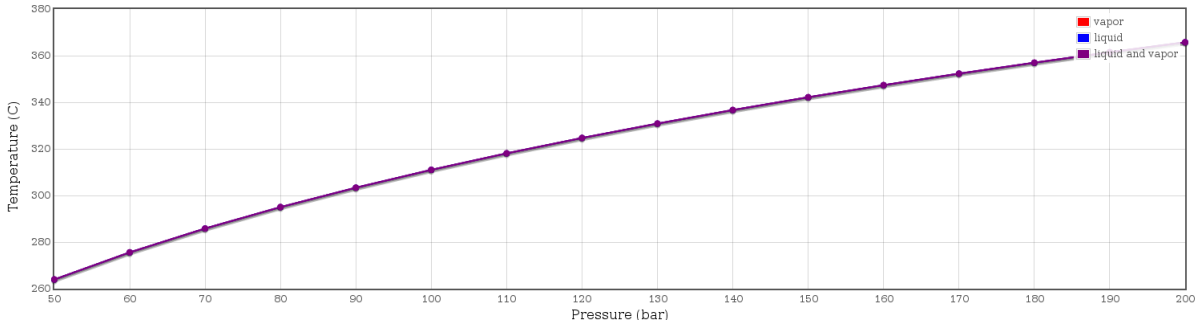

FIGURE 4.1 – Temperature-pressure diagram for water and steam at saturation

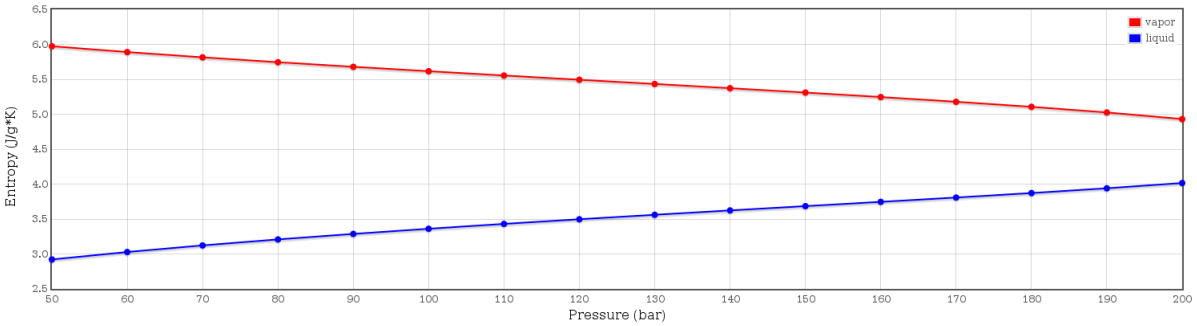

FIGURE 4.2 – Entropy-pressure diagram for water and steam at saturation

In order to obtain easily a quasilinear representation of the system (4.32-4.34) as well as its spectrum of the system we will use in a similar way to section 1.3 the following non conservative variables

$$\rho_m = \alpha_g(p, s_m)\rho_g(p, s_g^{\text{sat}}) + \alpha_l(p, s_m)\rho_l(p, s_l^{\text{sat}}), \tag{4.35}$$

$$\begin{aligned} u_m &= \frac{\alpha_g(p, s_m)\rho_g(p, s_g^{\text{sat}})u_g + \alpha_l(p, s_m)\rho_l(p, s_l^{\text{sat}})u_l}{\rho_m}, \\ s_m &= \frac{\alpha_g(p, s_m)\rho_g(p, s_g^{\text{sat}})s_g^{\text{sat}} + \alpha_l(p, s_m)\rho_l(p, s_l^{\text{sat}})s_l^{\text{sat}}}{\rho_m}, \end{aligned} \tag{4.36}$$

where we made the simplifying assumption that the saturation parameters s_g^{sat} and s_l^{sat} are constants. In that case the density at saturation can be considered a function of the sole pressure p : $\rho_k(p, s_k^{\text{sat}}) = \rho_k^{\text{sat}}(p)$. This simplification of the model does not change much the physical dynamics of the fluid since the saturation entropies do not vary much with pressure and the qualitative behaviour of the two phase flow is preserved with boiling occuring when $s_l^{\text{sat}} < s_m < s_g^{\text{sat}}$. The composition of the fluid can be

deduced from (4.36) as

$$\alpha(p, s_m) = \frac{\rho_m s_m - \rho_l^{\rm sat}(p) s_l^{\rm sat}}{\rho_g^{\rm sat}(p) s_g^{\rm sat} - \rho_l^{\rm sat}(p) s_l^{\rm sat}}. \tag{4.37}$$

From the definition of the mixture density (4.35) and the void fraction formula (4.37) we obtain the relation between ρ_m, s_m and p :

$$\rho_m = \frac{\rho_m s_m - \rho_l^{\rm sat}(p) s_l^{\rm sat}}{\rho_g^{\rm sat}(p) s_g^{\rm sat} - \rho_l^{\rm sat}(p) s_l^{\rm sat}} \rho_g^{\rm sat}(p) + \frac{\rho_g^{\rm sat}(p) s_g^{\rm sat} - \rho_m s_m}{\rho_g^{\rm sat}(p) s_g^{\rm sat} - \rho_l^{\rm sat}(p) s_l^{\rm sat}} \rho_l^{\rm sat}(p),$$

from which we deduce

$$\begin{aligned}
\rho_m &= \frac{s_g^{\rm sat} - s_l^{\rm sat}}{\dfrac{s_g^{\rm sat} - s_m}{\rho_l^{\rm sat}(p)} + \dfrac{s_m - s_l^{\rm sat}}{\rho_g^{\rm sat}(p)}} \\
&= \frac{1}{\dfrac{c_l}{\rho_l^{\rm sat}(p)} + \dfrac{c_g}{\rho_g^{\rm sat}(p)}} \\
\left.\frac{\partial \rho_m}{\partial s_m}\right|_p &= \frac{1}{\dfrac{1}{\rho_g^{\rm sat}(p)} - \dfrac{1}{\rho_l^{\rm sat}(p)}} \\
\left.\frac{\partial \rho_m}{\partial p}\right|_{s_m} &= \frac{s_g^{\rm sat} - s_l^{\rm sat}}{\left(\dfrac{s_g^{\rm sat} - s_m}{\rho_l^{\rm sat}(p)} + \dfrac{s_m - s_l^{\rm sat}}{\rho_g^{\rm sat}(p)}\right)^2} \left(\frac{s_g^{\rm sat} - s_m}{\rho_l^{\rm sat}(p)^2 c_{sl}^2} + \frac{s_m - s_l^{\rm sat}}{\rho_g^{\rm sat}(p)^2 c_{sg}^2}\right) \\
&= \frac{c_l \rho_g^{\rm sat}(p)^2 c_{sg}^2 + c_g \rho_l^{\rm sat}(p)^2 c_{sl}^2}{c_{sg}^2 c_{sl}^2 \left(c_l \rho_g^{\rm sat}(p) + c_g \rho_l^{\rm sat}(p)\right)^2} \\
&= \frac{\dfrac{c_g}{\rho_g^{\rm sat}(p)^2 c_{sg}^2} + \dfrac{c_l}{\rho_l^{\rm sat}(p)^2 c_{sl}^2}}{\left(\dfrac{c_g}{\rho_g^{\rm sat}(p)} + \dfrac{c_l}{\rho_l^{\rm sat}(p)}\right)^2} \\
&= \rho_m^2 \left(\frac{c_g}{\rho_g^{\rm sat}(p)^2 c_{sg}^2} + \frac{c_l}{\rho_l^{\rm sat}(p)^2 c_{sl}^2}\right) \\
&= \rho_m \left(\frac{\alpha_g}{\rho_g^{\rm sat}(p) c_{sg}^2} + \frac{\alpha_l}{\rho_l^{\rm sat}(p) c_{sl}^2}\right),
\end{aligned} \tag{4.38}$$

where we denoted $c_{sk} = \left.\dfrac{\partial \rho_k}{\partial p}\right|_{s_k}$ the sound speed of the phase k, and we used the following characterization of vapor and liquid mass concentration for saturated mixtures

$$c_g = \frac{s_m - s_l^{\rm sat}}{s_g^{\rm sat} - s_l^{\rm sat}}, \tag{4.39}$$

$$c_l = \frac{s_g^{\rm sat} - s_m}{s_g^{\rm sat} - s_l^{\rm sat}}, \tag{4.40}$$

$$\frac{c_g}{\rho_g^{\rm sat}(p)} + \frac{c_l}{\rho_l^{\rm sat}(p)} = \frac{1}{\rho_m}.$$

Using the variables $V = (\rho_m, u_m, s_m)$ the system (4.32-4.34) takes the non conservative form

$$\begin{aligned}
\partial_t \rho_m &+ \rho_m \partial_x u_m + u_m \partial_x \rho_m = 0, \\
\partial_t u_m &+ u_m \partial_x u_m + \frac{1}{\rho_m} \partial_x p = \frac{F}{\rho_m}, \\
\partial_t s_m &+ u_m \partial_x s_m = \frac{Q}{\rho_m}.
\end{aligned}$$

Using the identity

$$\mathrm{d}\rho_m = \left.\frac{\partial \rho_m}{\partial p}\right|_{s_m} \mathrm{d}p + \left.\frac{\partial \rho_m}{\partial s_m}\right|_{p} \mathrm{d}s_m$$

we can set the system into matrix the form

$$\partial_t V + \mathbf{B}_m \partial_x V = S,$$

with $\mathbf{B}_m$ having an expression close to the Euler matrix (1.41)

$$\mathbf{B}_m = \begin{bmatrix} u_m & \rho_m & 0 \\ \dfrac{1}{\rho_m}\left.\dfrac{\partial p}{\partial \rho_m}\right|_{s_m} & u_m & \dfrac{1}{\rho_m}\left.\dfrac{\partial p}{\partial s_m}\right|_{\rho_m} \\ 0 & 0 & u_m \end{bmatrix}.$$

We define the mixture sound speed c_{sm} in a similar way to (1.37) and from (4.38) we deduce

$$c_{sm}^2 = \left.\frac{\partial p}{\partial \rho_m}\right|_{s_m} = \frac{1}{\rho_m\left(\dfrac{\alpha_g}{\rho_g^{\mathrm{sat}}(p)c_{sg}^2} + \dfrac{\alpha_l}{\rho_l^{\mathrm{sat}}(p)c_{sl}^2}\right)} \tag{4.41}$$

$$= \frac{1}{\rho_m^2\left(\dfrac{c_g}{\rho_g^{\mathrm{sat}}(p)^2 c_{sg}^2} + \dfrac{c_l}{\rho_l^{\mathrm{sat}}(p)^2 c_{sl}^2}\right)}. \tag{4.42}$$

We henceforth find the well known result that the mixture Young modulus is the harmonic mean of the phasic Young modulus :

$$\frac{1}{\rho_m c_{sm}^2} = \frac{\alpha_g}{\rho_g^{\mathrm{sat}}(p)c_{sg}^2} + \frac{\alpha_l}{\rho_l^{\mathrm{sat}}(p)c_{sl}^2},$$

and as a well known consequence the sound speed c_{sm} of the mixture is smaller than both c_{sg} and c_{sl}.

The eigenvalues of $\mathbf{B}_m$ are similar to those of the Euler system (1.38)

$$\lambda_1 = u_m - c_{sm} \quad \lambda_2 = u_m \quad \lambda_3 = u_m + c_{sm}. \tag{4.43}$$

and their derivative is

$$\begin{aligned} \nabla_V \lambda_1 &= {}^t\left(-\left.\frac{\partial c_{sm}}{\partial \rho_m}\right|_{s_m}, 1, -\left.\frac{\partial c_{sm}}{\partial s_m}\right|_{\rho_m}\right), \\ \nabla_V \lambda_2 &= {}^t(0,1,0), \\ \nabla_V \lambda_3 &= {}^t\left(\left.\frac{\partial c_{sm}}{\partial \rho_m}\right|_{s_m}, 1, \left.\frac{\partial c_{sm}}{\partial s_m}\right|_{\rho_m}\right). \end{aligned}$$

The eigenvectors of $\mathbf{B}_m$ are similar to those of the Euler system (1.42)

$$\vec{\tilde{r}}_{1m} = {}^t(\rho_m, -c_{sm}, 0), \tag{4.44}$$

$$\vec{\tilde{r}}_{2m} = {}^t\left(\left.\frac{\partial p}{\partial s_m}\right|_{\rho_m}, 0, -c_{sm}^2\right), \tag{4.45}$$

$$\vec{\tilde{r}}_{3m} = {}^t(\rho_m, -c_{sm}, 0), \tag{4.46}$$

and we obtain in a similar way to (1.43-1.45)

$$\nabla_V \lambda_1(V)\cdot \vec{\tilde{r}}_{1m} = -\left(c_{sm} + \rho_m \left.\frac{\partial c_{sm}}{\partial \rho_m}\right|_{s_m}\right), \tag{4.47}$$

$$\nabla_V \lambda_2(V)\cdot \vec{\tilde{r}}_{2m} = 0, \tag{4.48}$$

$$\nabla_V \lambda_3(V)\cdot \vec{\tilde{r}}_{3m} = c_{sm} + \rho_m \left.\frac{\partial c_{sm}}{\partial \rho_m}\right|_{s_m}. \tag{4.49}$$

The second field is therefore linearly degenerate.

In order to prove that the first and third fields are genuinely nonlinear, we need to prove that

$$c_{sm} + \rho_m \left.\frac{\partial c_{sm}}{\partial \rho_m}\right|_{s_m} > 0.$$

or equivalently that

$$c_{sm}^2 + \frac{\rho_m}{2} \left.\frac{\partial c_{sm}^2}{\partial \rho_m}\right|_{s_m} > 0. \tag{4.50}$$

We recall first that in the case of single phase thermodynamics, a consequence of the convexity of the entropy is the following inequality

$$\left.\frac{\partial^2 p}{\partial \rho_k^2}\right|_{s_k} + \frac{2}{\rho_k} \left.\frac{\partial p}{\partial \rho_k}\right|_{s_k} = \frac{2c_{sk}}{\rho_k} \left(\rho_k \left.\frac{\partial c_{sk}}{\partial \rho_k}\right|_{s_k} + c_{sk} \right) > 0. \tag{4.51}$$

We can deduce (4.50) from (4.42) after the following calculations (remember that (4.39) and (4.40) imply $\left.\frac{\partial c_k}{\partial \rho_m}\right|_{s_m} = 0$) :

$$\begin{aligned}
c_{sm}^2 + \frac{\rho_m}{2} \left.\frac{\partial c_{sm}^2}{\partial \rho_m}\right|_{s_m} &= c_{sm}^2 + \frac{\rho_m}{2} \left(\frac{-2}{\rho_m^3 \left(\frac{c_g}{\rho_g^{\rm sat}(p)^2 c_{sg}^2} + \frac{c_l}{\rho_l^{\rm sat}(p)^2 c_{sl}^2} \right)} + \frac{2 \left(\frac{c_g \left.\frac{\partial \rho_g^{\rm sat} c_{sg}}{\partial \rho_m}\right|_{s_m}}{(\rho_g^{\rm sat} c_{sg})^3} + \frac{c_l \left.\frac{\partial \rho_l^{\rm sat} c_{sl}}{\partial \rho_m}\right|_{s_m}}{(\rho_l^{\rm sat} c_{sl})^3} \right)}{\rho_m^2 \left(\frac{c_g}{\rho_g^{\rm sat}(p)^2 c_{sg}^2} + \frac{c_l}{\rho_l^{\rm sat}(p)^2 c_{sl}^2} \right)^2} \right) \\
&= c_{sm}^2 - c_{sm}^2 + \frac{\left(\frac{c_g \left.\frac{\partial \rho_g^{\rm sat} c_{sg}}{\partial \rho_m}\right|_{s_m}}{(\rho_g^{\rm sat} c_{sg})^3} + \frac{c_l \left.\frac{\partial \rho_l^{\rm sat} c_{sl}}{\partial \rho_m}\right|_{s_m}}{(\rho_l^{\rm sat} c_{sl})^3} \right)}{\rho_m \left(\frac{c_g}{\rho_g^{\rm sat}(p)^2 c_{sg}^2} + \frac{c_l}{\rho_l^{\rm sat}(p)^2 c_{sl}^2} \right)^2}
\end{aligned}$$

and we conclude the proof with

$$\begin{aligned}
\left.\frac{\partial \rho_k^{\rm sat} c_{sk}}{\partial \rho_m}\right|_{s_m} &= \left.\frac{\partial p}{\partial \rho_m}\right|_{s_m} \left.\frac{\partial \rho_k^{\rm sat} c_{sk}}{\partial p}\right|_{s_m} \\
&= \left.\frac{\partial p}{\partial \rho_m}\right|_{s_m} \left.\frac{\partial \rho_k}{\partial p}\right|_{s_m} \left.\frac{\partial \rho_k^{\rm sat} c_{sk}}{\partial \rho_k}\right|_{s_m} \\
&= \frac{c_{sm}^2}{c_{sk}^2} \left(\rho_k \left.\frac{\partial c_{sk}}{\partial \rho_k}\right|_{s_k} + c_{sk} \right) > 0.
\end{aligned}$$

4.2.2 Characteristic fields of the drift-flux model

This section is largely inspired by Toumi in [Tou87].
For simplicity and rigorous derivation of the mathematical properties, we consider the one dimensional isentropic drift flux model as follows

$$\frac{\partial \alpha_g \rho_g}{\partial t} + \frac{\partial \alpha_g \rho_g u_g}{\partial x} = \Gamma, \tag{4.52a}$$

$$\frac{\partial \alpha_l \rho_l}{\partial t} + \frac{\partial \alpha_l \rho_l u_l}{\partial x} = -\Gamma, \tag{4.52b}$$

$$\frac{\partial \rho_m u_m}{\partial t} + \frac{\partial \left(\rho_m u_m^2 + \rho_m c_g (1 - c_g) u_r^2 + p \right)}{\partial x} = \rho_m g + F^{\rm w}. \tag{4.52c}$$

The assumption of isentropy simplifies greatly the calculation but we will not be able to characterize the entropy wave associated to the energy equation.

The quasi-linear form of the system (4.52a-4.52c) is

$$\frac{\partial U}{\partial t} + \mathbf{A}\frac{\partial U}{x} = 0, \tag{4.53}$$

where $\mathbf{A}$ is the Jacobian matrix of the flux function and the conservative variables

$$U = {}^t(\alpha_g\rho_g, \alpha_l\rho_l, \rho_m u_m). \tag{4.54}$$

Owning to the isentropic assumption, the equations of state considered are

$$\rho_g = \rho_g(p), \quad \rho_l = \rho_l(p). \tag{4.55}$$

The sound speed of each phase is then given by

$$c_{sg} = \left(\frac{\partial \rho_g}{\partial p}\right)^{-1/2}, \quad c_{sl} = \left(\frac{\partial \rho_l}{\partial p}\right)^{-1/2}. \tag{4.56}$$

The relative velocity is supposed to be a function of the void fraction α and v_∞ such that

$$\Delta u = u_g - u_l = v_\infty(1-\alpha)^{k-1}, \tag{4.57}$$

and the volumetric velocity is defined by

$$u = \alpha_g u_g + \alpha_l u_l. \tag{4.58}$$

The equations (4.57) and (4.58) yield

$$u_g = u + v_\infty(1-\alpha)^k, \tag{4.59}$$
$$u_l = u - v_\infty\alpha(1-\alpha)^{k-1}. \tag{4.60}$$

In order to facilitate the computation of the Jacobian matrix and eigenstructure of the system (4.52a-4.52c), a change of variable is applied. Let us denote

$$V = {}^t(\alpha, p, u). \tag{4.61}$$

The system (4.52a-4.52c) is then rewritten as follows

$$\frac{\partial g(V)}{\partial t} + \frac{\partial \mathrm{fog}(V)}{\partial x} = 0, \tag{4.62}$$

where

$$g(V) = \begin{pmatrix} \alpha\rho_g \\ (1-\alpha)\rho_l \\ \rho_m u + \alpha(1-\alpha)^k(\rho_g - \rho_l)v_\infty \end{pmatrix}, \text{ and}$$

$$\mathrm{fog}(V) = \begin{pmatrix} \alpha\rho_g\left(u + (1-\alpha)^k v_\infty\right) \\ (1-\alpha)\rho_l\left(u - \alpha(1-\alpha)^{k-1}v_\infty\right) \\ \alpha\rho_g\left(u + (1-\alpha)^k v_\infty\right)^2 + (1-\alpha)\rho_l\left(u - \alpha(1-\alpha)^{k-1}v_\infty\right)^2 + p \end{pmatrix}.$$

Let us denote $A_0(V) = \nabla g(V)$, $A_1(V) = \nabla \mathrm{fog}(V)$. More precisely,

$$A_0(V) = \begin{pmatrix} \rho_g & \alpha c_g^{-2} & 0 \\ -\rho_l & (1-\alpha)c_{sl}^{-2} & 0 \\ -\rho_k\nabla u & 0 & \rho_m \end{pmatrix}, \tag{4.63}$$

$$A_1(V) = \begin{pmatrix} \rho_g(u + (1-\alpha-k\alpha)\Delta u) & \alpha c_{sg}^{-2}(u + (1-\alpha)\Delta u) & \alpha\rho_g \\ -\rho_l(u + (1-\alpha-k\alpha)\Delta u) & (1-\alpha)c_{sl}^{-2}(u - \alpha\Delta u) & (1-\alpha)\rho_l \\ A_{3,1} & A_{3,2} & A_{3,3} \end{pmatrix}, \tag{4.64}$$

where

$$A_{3,1} = -\rho_k u\nabla u + \Delta u^2\left(-k\alpha(1-\alpha)\rho_g + (1-k\alpha)\alpha\rho_l\right), \tag{4.65}$$
$$A_{3,2} = 1, \tag{4.66}$$
$$A_{3,3} = \rho_m u + \alpha(1-\alpha)(\rho_g - \rho_l)\Delta u, \tag{4.67}$$

and $\rho_k = k\alpha\rho_g + (1-k\alpha)\rho_l$. Then the Jacobian matrix of the system (4.52a-4.52c) is $\mathbf{A} = A_0^{-1}A_1$ and the eigenvalues are computed by solving the characteristic polynomial

$$\det(A(V) - \lambda A_0(V)) = 0, \tag{4.68}$$

Let us denote the sound speed of the mixture

$$c_m = \left(\rho_m \left(\frac{1-\alpha}{\rho_l c_{sl}^2} + \frac{\alpha}{\rho_g c_{sg}^2}\right)\right)^{-1/2}, \tag{4.69}$$

and define

$$z = \frac{u-\lambda}{c_m}, \quad \varepsilon = \frac{\Delta u}{c_m} = \frac{u_g - u_l}{c_m}. \tag{4.70}$$

The equation (4.68) is then rewritten in the following form

$$\begin{aligned}
&z^3 + \left(\left(1 - \frac{\rho_k}{\rho_m}\right)\mu + 2\gamma + (1-\alpha-k\alpha)\right)\varepsilon z^2 - z + (2\gamma\mu + (1-\alpha-k\alpha)(\gamma + mu))\varepsilon^2 z \\
&+ \left(\frac{\alpha^2(1-\alpha)}{\rho_m}((1-k\alpha)\rho_l - k(1-\alpha)\rho_g)\mu - \alpha(1-\alpha)\frac{\rho_l}{\rho}\frac{\alpha\rho_g c_{sl}^{-2} + (1-\alpha)\rho_l c_{sg}^{-2}}{\alpha\rho_l c_{sg}^{-2} + (1-\alpha)\rho_g c_{sl}^{-2}}\right)\varepsilon^2 z \\
&+ \left(2(1-\alpha-k\alpha)\gamma\mu + \frac{\alpha^2(1-\alpha)}{\rho_m}((1-k\alpha)\rho_l - k(1-\alpha)\rho_g)\frac{\alpha\rho_g c_{sl}^{-2} + (1-\alpha)\rho_l c_{sg}^{-2}}{\alpha\rho_l c_{sg}^{-2} + (1-\alpha)\rho_g c_{sl}^{-2}}\right)\varepsilon^3 \\
&-(1-\alpha-k\alpha)\varepsilon = 0,
\end{aligned}$$

where we denoted

$$\gamma = \frac{1}{2}\alpha(1-\alpha)\frac{\rho_g - \rho_l}{\rho_m}, \tag{4.71}$$

$$\mu = \alpha(1-\alpha)\frac{\rho_l c_{sg}^{-2} - \rho_g c_{sl}^{-2}}{\alpha\rho_l c_{sg}^{-2} + (1-\alpha)\rho_g c_{sl}^{-2}}. \tag{4.72}$$

The equation (4.71) may admit the complex eigenvalues which in turn may lead to the ill-posed problem of the system (4.52a-4.52c). However if the relative velocity is much smaller than the mixture sound speed, i.e.

$$\varepsilon = \frac{u_g - u_l}{c_m} \ll 1, \tag{4.73}$$

then the equation (4.71) admits three real solutions, which are approximated as follows

$$z_1 = -1 - \frac{1}{2}\left(\left(1 - \frac{\rho_k}{\rho_m}\right)\mu + 2\gamma\right)\varepsilon + \mathcal{O}(\varepsilon^2), \tag{4.74a}$$

$$z_2 = -(1-\alpha-k\alpha)\varepsilon + \mathcal{O}(\varepsilon^2), \tag{4.74b}$$

$$z_3 = 1 - \frac{1}{2}\left(\left(1 - \frac{\rho_k}{\rho_m}\right)\mu + 2\gamma\right)\varepsilon + \mathcal{O}(\varepsilon^2). \tag{4.74c}$$

Thus, the equations in (4.70) and (4.74a-4.74c) lead to the following approximate eigenvalues

$$\begin{aligned}
\lambda_{1,3} &= u \mp c_m + \frac{1}{2}\alpha(1-\alpha)^k \frac{\rho_g - \rho_l}{\rho_m}\frac{(2-k)\alpha\rho_l c_{sg}^{-2} + (1-(2-k)\alpha)\rho_g c_{sl}^{-2}}{\alpha\rho_l c_{sg}^{-2} + (1-\alpha)\rho_g c_{sl}^{-2}} v_\infty + \mathcal{O}\left(\frac{v_\infty^2}{c_m}\right), \\
\lambda_2 &= u + (1-\alpha-k\alpha)(1-\alpha)^{k-1} v_\infty + \mathcal{O}\left(\frac{v_\infty^3}{c_m}\right),
\end{aligned}$$

and the corresponding right eigenvalues

$$\begin{aligned}
\vec{r}_{1,3} &= \begin{pmatrix} \alpha(1-\alpha)\dfrac{\rho_g c_{sl}^{-2} - \rho_l c_{sg}^{-2}}{\rho_g \rho_l} - \dfrac{\alpha(1-\alpha)}{\rho_g \rho_l}\left(\dfrac{\rho_m c_m^2}{c_{sg}^2 c_{sl}^2} + (1-\alpha-k\alpha+\beta)(\rho_g c_{sl}^{-2} - \rho_l c_{sg}^{-2})\right)\dfrac{v_\infty}{c_m} \\ 1 + \left(\beta + \alpha(1-\alpha)\dfrac{\rho_g c_{sl}^{-2} - \rho_l c_{sg}^{-2}}{\rho_g \rho_l}\rho_m c_m^2\right)\dfrac{v_\infty}{c_m} \\ \mp \dfrac{1}{\rho_m c_m} \end{pmatrix} \\
&+ \mathcal{O}(v_\infty^2), \\
\vec{r}_2 &= \begin{pmatrix} 1 \\ 0 \\ 0 \end{pmatrix} + \mathcal{O}(v_\infty^2),
\end{aligned}$$

where we defined

$$\beta = \gamma \frac{(2-k)\alpha\rho_l c_{sg}^{-2} + (1-(2-k)\alpha)\rho_g c_{sl}^{-2}}{\alpha\rho_l c_{sg}^{-2} + (1-\alpha)\rho_g c_{sl}^{-2}}. \tag{4.75}$$

Due to the fact that

$$\nabla\lambda_2 \cdot \vec{r}_2(V) = \frac{\partial \lambda_2}{\partial \alpha} = -k(1-\alpha)^{k-2}(2-(k+1)\alpha)v_\infty + \mathcal{O}(v_\infty^2), \tag{4.76}$$

we can conclude that

— if $k \in (0,1]$, the 2-field is genuinely nonlinear (GNL) ;

— if $k > 1$, the 2-field is neither GNL nor linearly degenerate (LD).

On the other hand, if the velocity v_∞ is sufficiently small then the 1-field and 3-field are GNL. Otherwise, $\nabla\lambda_1 \cdot \vec{r}_1$ and $\nabla\lambda_3 \cdot \vec{r}_3$ may change size. Considering $k = 1$, i.e. $u_g - u_l = v_\infty$, Toumi in [Tou87] demonstrates in details the way to construct the admissible solutions when these characteristic fields are not GNL.

4.2.3 Quasi-linear form of the isentropic two-fluid model

Considering a one dimensional homogeneous isentropic model (4.150), the quasi-linear form is formulated as below

$$\partial_t U + \mathbf{A}\partial_x U = 0, \tag{4.77}$$

where the conservative variables

$$U = {}^t\left(\alpha_g\rho_g, \alpha_l\rho_l, \alpha_g\rho_g u_g, \alpha_l\rho_l u_l\right), \tag{4.78}$$

and the Jacobian $\mathbf{A} = \nabla F$. In order to obtain the expression of $\mathbf{A}$, the gradient vectors of the pressure p denoted by ${}^t[p_j]_{j=1,\dots,4}$ and volume fractions α_k denoted by ${}^t[\alpha_{kj}]_{j=1,\dots,4}$ are analyzed whereas the gradient vectors of the remaining terms in the convection part are trivially achieved.
The thermal hydraulic relation in the isentropic one pressure model implies $\rho_g = \rho_g(p)$ and $\rho_l = \rho_l(p)$. Such a relation is useful to compute ${}^t[p_j]_{j=1,\dots,4}$ by first considering the following differentiation

$$\mathrm{d}m_g = \alpha_g \mathrm{d}\rho_g + \rho_g \mathrm{d}\alpha_g, \tag{4.79}$$

$$\mathrm{d}m_l = \alpha_l \mathrm{d}\rho_l + \rho_l \mathrm{d}\alpha_l. \tag{4.80}$$

Multiplying equation (4.79) and equation (4.80) respectively by ρ_l and ρ_g, then adding two deriving equations associating the relation $\mathrm{d}(\alpha_g + \alpha_l) = 1$, we obtain

$$\begin{aligned}
\rho_l \mathrm{d}m_g + \rho_g \mathrm{d}m_l &= \alpha_g\rho_l \mathrm{d}\rho_g + \alpha_l\rho_g \mathrm{d}\rho_l \\
&= \left(\alpha_g\rho_l \frac{\partial \rho_g}{\partial p} + \alpha_l\rho_g \frac{\partial \rho_l}{\partial p}\right)\mathrm{d}p.
\end{aligned} \tag{4.81}$$

Replacing $\mathrm{d}\rho_g = \dfrac{\partial \rho_g}{\partial p}\mathrm{d}p$ and $\mathrm{d}\rho_l = \dfrac{\partial \rho_l}{\partial p}\mathrm{d}p$ deduces

$$\mathrm{d}p = \kappa\rho_l \mathrm{d}m_g + \kappa\rho_g \mathrm{d}m_l, \tag{4.82}$$

where

$$\kappa = \left(\rho_l \alpha_g \frac{\partial \rho_g}{\partial p} + \rho_g \alpha_l \frac{\partial \rho_l}{\partial p} \right)^{-1}. \tag{4.83}$$

Due to the fact that

$$\begin{aligned} \mathrm{d}\rho_k &= \frac{\partial \rho_k}{\partial p} \mathrm{d}p \\ &= \frac{\partial \rho_k}{\partial p} \left(\kappa \rho_l \mathrm{d}m_g + \kappa \rho_g \mathrm{d}m_l \right), \end{aligned} \tag{4.84}$$

$$\tag{4.85}$$

associating with equations (4.79), we can deduce

$$\begin{aligned} \mathrm{d}\alpha_g &= \frac{1}{\rho_g} \mathrm{d}m_g - \frac{\alpha_g}{\rho_g} \frac{\partial \rho_g}{\partial p} \left(\kappa \rho_l \mathrm{d}m_g + \kappa \rho_g \mathrm{d}m_l \right) \\ &= \kappa \alpha_l \frac{\partial \rho_l}{\partial p} \mathrm{d}m_g - \kappa \alpha_g \frac{\partial \rho_g}{\partial p} \mathrm{d}m_l. \end{aligned} \tag{4.86}$$

The Jacobian matrix $\mathbf{A}$ of the one dimensional isentropic two-fluid model is therefore written in the following form

$$\mathbf{A} = \mathbf{A}_c + \mathbf{A}_p, \tag{4.87}$$

such that

$$\mathbf{A}_c = \begin{bmatrix} 0 & 0 & 1 & 0 \\ 0 & 0 & 0 & 1 \\ -u_g^2 & 0 & 2u_g & 0 \\ 0 & -u_l^2 & 0 & 2u_l \end{bmatrix}, \quad \text{and} \tag{4.88}$$

$$\mathbf{A}_p = \begin{bmatrix} 0 & 0 & 0 & 0 \\ 0 & 0 & 0 & 0 \\ \kappa \left(\alpha_g \rho_l + \Delta p \alpha_l \dfrac{\partial \rho_l}{\partial p} \right) & \kappa \left(\alpha_g \rho_g - \Delta p \alpha_g \dfrac{\partial \rho_g}{\partial p} \right) & 0 & 0 \\ \kappa \left(\alpha_l \rho_l - \Delta p \alpha_l \dfrac{\partial \rho_l}{\partial p} \right) & \kappa \left(\alpha_l \rho_g + \Delta p \alpha_g \dfrac{\partial \rho_g}{\partial p} \right) & 0 & 0 \end{bmatrix}. \tag{4.89}$$

Eigenvalues of the isentropic model

The eigenvalues of the matrix $\mathbf{A}$ in (4.87) is the roots of the following characteristic polynomial

$$\begin{aligned} P(\lambda) &= \left(\kappa \left(\alpha_g \rho_l + \Delta p \alpha_l \frac{\partial \rho_l}{\partial p} \right) - (\lambda - u_g)^2 \right) \left(\kappa \left(\alpha_l \rho_g + \Delta p \alpha_g \frac{\partial \rho_g}{\partial p} \right) - (\lambda - u_l)^2 \right) \\ &- \kappa^2 \left(\alpha_g \rho_g - \Delta p \alpha_g \frac{\partial \rho_g}{\partial p} \right) \left(\alpha_l \rho_l - \Delta p \alpha_l \frac{\partial \rho_l}{\partial p} \right). \end{aligned} \tag{4.90}$$

For practical purpose, one usually does not find the exact solution of the fourth degree polynomial. Instead, following the works in [TK96] and [EF03], the authors suggest using a perturbation method to compute approximate eigenvalues. We recall here the results obtained in [EF03].
Denoting the perturbation parameter

$$\varepsilon = \frac{u_g - u_l}{c_{sm}(1+k)}, \tag{4.91}$$

where

$$k = \frac{\alpha_l \rho_g}{\alpha_g \rho_l}, \tag{4.92}$$

and an approximate mixture sound speed, defined by

$$c_{sm} = \sqrt{\frac{\alpha_g \rho_g + \alpha_l \rho_l}{\alpha_g \rho_l \dfrac{\partial \rho_g}{\partial p} + \alpha_l \rho_g \dfrac{\partial \rho_l}{\partial p}}}. \tag{4.93}$$

Following [EF03], the approximate eigenvalues are then presented in the following forms

$$\lambda_{1,4} = \frac{\alpha_g\rho_l u_g + \alpha_l\rho_g u_l}{\alpha_g\rho_l + \alpha_l\rho_g} \mp c_{sm} + c_{sm}\mathcal{O}(\varepsilon^2), \tag{4.94}$$

which corresponds to the pressure waves and

$$\lambda_{2,3} = \frac{\alpha_g\rho_l u_l + \alpha_l\rho_g u_g}{\alpha_g\rho_l + \alpha_l\rho_g} \mp \sqrt{\frac{\Delta p(\alpha_g\rho_l + \alpha_l\rho_g) - \alpha_g\alpha_l\rho_g\rho_l(u_g - u_l)^2}{(\alpha_g\rho_l + \alpha_l\rho_g)^2}} + c_{sm}\mathcal{O}(\varepsilon^3), \tag{4.95}$$

which corresponds to the void waves.
Due to the fact that $\dfrac{1}{1+k}$ with k defined in (4.92) is bounded between 0 and 1, it is possible to consider $\varepsilon = \dfrac{u_g - u_l}{c_{sm}}$ in the above formula.

4.2.4 Quasi-linear form of the five-equation two-fluid model

Considering the homogeneous form of the five-equation two-fluid model (4.23) in one dimensional space associating the interfacial pressure term in the momentum equations as follows

$$\frac{\partial\alpha_g\rho_g}{\partial t} + \frac{\partial\left(\alpha_g\rho_g u_g\right)}{\partial x} = 0, \tag{4.96a}$$

$$\frac{\partial\alpha_l\rho_l}{\partial t} + \frac{\partial\left(\alpha_l\rho_l u_l\right)}{\partial x} = 0, \tag{4.96b}$$

$$\frac{\partial\alpha_g\rho_g u_g}{\partial t} + \frac{\partial\left(\alpha_g\rho_g u_g^2\right)}{\partial x} + \alpha_g\frac{\partial p}{\partial x} + \Delta p\frac{\partial\alpha_g}{\partial x} = 0, \tag{4.96c}$$

$$\frac{\partial\alpha_l\rho_l u_l}{\partial t} + \frac{\partial\left(\alpha_l\rho_l u_l^2\right)}{\partial x} + \alpha_l\frac{\partial p}{\partial x} + \Delta p\frac{\partial\alpha_l}{\partial x} = 0, \tag{4.96d}$$

$$\frac{\partial E}{\partial t} + \frac{\partial\left(\alpha_g\rho_g u_g E_g + \alpha_l\rho_l u_l E_l\right)}{\partial x} + \frac{\partial\left(\alpha_g u_g + \alpha_l u_l\right)p}{\partial x} = 0, \tag{4.96e}$$

where $E = \alpha_g\rho_g E_g + \alpha_l\rho_l E_l$. The corresponding quasi-linear form of the system (4.96a-4.96e) is formulated by

$$\partial_t U + \mathbf{A}\partial_x U = 0, \tag{4.97}$$

where the conservative variables

$$U = {}^t\left(\alpha_g\rho_g, \alpha_l\rho_l, \alpha_g\rho_g u_g, \alpha_l\rho_l u_l, E\right), \tag{4.98}$$

and the Jacobian matrix $\mathbf{A} \in \mathbb{R}^{5\times5}$. Similar to the isentropic model, in order to find the expression of $\mathbf{A}$ for the five-equation model, it is necessary to present the gradient vector of the pressure ${}^t[p_j]_{j=1,\ldots,5}$ and the one of the void fraction ${}^t[\alpha_j]_{j=1,\ldots,5}$.
Considering general thermal hydraulic relations $\rho_g = \rho_g(p, e_g)$ and $\rho_l = \rho_l(p, e_l)$ which imply

$$\mathrm{d}\rho_g = \frac{\partial\rho_g}{\partial p}\mathrm{d}p + \frac{\partial\rho_g}{\partial e_g}\mathrm{d}e_g, \tag{4.99}$$

$$\mathrm{d}\rho_l = \frac{\partial\rho_l}{\partial p}\mathrm{d}p + \frac{\partial\rho_l}{\partial e_l}\mathrm{d}e_l. \tag{4.100}$$

Let us denote

$$a_{1k} = \frac{\partial\rho_k}{\partial p}_{|e_k}, \quad a_{2k} = \frac{\partial\rho_k}{\partial e_k}_{|p}, \quad k = g, l, \tag{4.101}$$

then replacing (4.99) and (4.100) in the following equation

$$\rho_l\mathrm{d}m_g + \rho_g\mathrm{d}m_l = \alpha_g\rho_l\mathrm{d}\rho_g + \alpha_l\rho_g\mathrm{d}\rho_l, \tag{4.102}$$

we obtain

$$\rho_l\mathrm{d}m_g + \rho_g\mathrm{d}m_l = \left(\alpha_g\rho_l a_{1g} + \alpha_l\rho_g a_{1l}\right)\mathrm{d}p + \alpha_g\rho_l a_{2g}\mathrm{d}e_g + \alpha_l\rho_g a_{2l}\mathrm{d}e_l. \tag{4.103}$$

Denoting

$$\kappa = \left(\rho_l \alpha_g a_{1g} + \rho_g \alpha_l a_{1l}\right)^{-1}, \tag{4.104}$$

then

$$\mathrm{d}p = \kappa \left(\rho_l \mathrm{d}m_g + \rho_g \mathrm{d}m_l - \alpha_g \rho_l a_{2g} \mathrm{d}e_g - \alpha_l \rho_g a_{2l} \mathrm{d}e_l\right). \tag{4.105}$$

Replacing (4.105) into (4.99) to obtain

$$\begin{aligned} \mathrm{d}\rho_g &= a_{1g}\kappa \left(\rho_l \mathrm{d}m_g + \rho_g \mathrm{d}m_l - \alpha_g \rho_l a_{2g} \mathrm{d}e_g - \alpha_l \rho_g a_{2l} \mathrm{d}e_l\right) + a_{2g}\mathrm{d}e_g \\ &= \kappa \left(a_{1g}\rho_l \mathrm{d}m_g + a_{1g}\rho_g \mathrm{d}m_l + \alpha_l \rho_g a_{1l} a_{2g} \mathrm{d}e_g - \alpha_l \rho_g a_{1g} a_{2l} \mathrm{d}e_l\right), \end{aligned} \tag{4.106}$$

and similarly,

$$\mathrm{d}\rho_l = \kappa \left(a_{1l}\rho_l \mathrm{d}m_g + a_{1l}\rho_g \mathrm{d}m_l - \alpha_g \rho_l a_{1l} a_{2g} \mathrm{d}e_g + \alpha_g \rho_l a_{1g} a_{2l} \mathrm{d}e_l\right). \tag{4.107}$$

Therefore,

$$\begin{aligned} \mathrm{d}\alpha_g &= \frac{1}{\rho_g}\mathrm{d}m_g - \frac{\alpha_g}{\rho_g}\mathrm{d}\rho_g \\ &= \frac{1}{\rho_g}\mathrm{d}m_g - \frac{\alpha_g}{\rho_g}\left(a_{1g}\kappa \left(\rho_l \mathrm{d}m_g + \rho_g \mathrm{d}m_l - \alpha_g \rho_l a_{2g} \mathrm{d}e_g - \alpha_l \rho_g a_{2l} \mathrm{d}e_l\right) + a_{2g}\mathrm{d}e_g\right) \\ &= \kappa \left(\alpha_l a_{1l} \mathrm{d}m_g - \alpha_g a_{1g} \mathrm{d}m_l - \alpha_g \alpha_l a_{1l} a_{2g} \mathrm{d}e_g + \alpha_g \alpha_l a_{1g} a_{2l} \mathrm{d}e_l\right). \end{aligned} \tag{4.108}$$

Due to (4.105) and (4.108), the remaining work of computing ${}^t[p_j]_{j=1,\dots,5}$ and ${}^t[\alpha_j]_{j=1,\dots,5}$ is to find an expression of $\mathrm{d}e_g$ and $\mathrm{d}e_l$ with respect to the conservative variables (4.98).
The five-equation model considers thermal equilibrium assumption, i.e. the common temperature $T_g = T_l = T$. The thermal equation of state $e_g = e_g(\rho_g, T)$, $e_l = e_l(\rho_l, T)$ implies

$$\mathrm{d}e_g = \frac{\partial e_g}{\partial T}\mathrm{d}T + \frac{\partial e_g}{\partial \rho_g}\mathrm{d}\rho_g, \tag{4.109}$$

$$\mathrm{d}e_l = \frac{\partial e_l}{\partial T}\mathrm{d}T + \frac{\partial e_l}{\partial \rho_l}\mathrm{d}\rho_l. \tag{4.110}$$

Let us denote

$$a_{3k} = \frac{\partial e_k}{\partial T}_{|\rho_k}, \quad a_{4k} = \frac{\partial e_k}{\partial \rho_k}_{|T}, \quad k = g, l. \tag{4.111}$$

Replacing (4.109) and (4.110) into (4.106), then using the relation of $\mathrm{d}\rho_g$ and $\mathrm{d}\rho_l$ in (4.102), we obtain

$$\begin{aligned} \mathrm{d}\rho_g &= \vartheta \rho_l a_{1g}(1 - a_{2l}a_{4l})\mathrm{d}m_g + \vartheta \rho_g a_{1g}(1 - a_{2l}a_{4l})\mathrm{d}m_l \\ &+ \vartheta \alpha_l \rho_g \left(a_{1l}a_{2g}a_{3g} - a_{1g}a_{2l}a_{3l}\right)\mathrm{d}T, \end{aligned} \tag{4.112}$$

where

$$\vartheta = \left(\alpha_g \rho_l a_{1g}(1 - a_{2l}a_{4l}) + \alpha_l \rho_g a_{1l}(1 - a_{2g}a_{4g})\right)^{-1}. \tag{4.113}$$

Similarly to (4.112),

$$\begin{aligned} \mathrm{d}\rho_l &= \vartheta \rho_l a_{1l}(1 - a_{2g}a_{4g})\mathrm{d}m_g + \vartheta \rho_g a_{1l}(1 - a_{2g}a_{4g})\mathrm{d}m_l \\ &+ \vartheta \alpha_g \rho_l \left(a_{1g}a_{2l}a_{3l} - a_{1l}a_{2g}a_{3g}\right)\mathrm{d}T. \end{aligned} \tag{4.114}$$

Recall the last conservative variable

$$E = \alpha_g \rho_g \left(e_g + \frac{u_g^2}{2}\right) + \alpha_l \rho_l \left(e_l + \frac{u_l^2}{2}\right). \tag{4.115}$$

Thus,

$$\mathrm{d}E = e_g \mathrm{d}m_g + e_l \mathrm{d}m_l - \frac{u_g^2}{2}\mathrm{d}m_g - \frac{u_l^2}{2}\mathrm{d}m_l + u_g \mathrm{d}q_g + u_l \mathrm{d}q_l + m_g \mathrm{d}e_g + m_l \mathrm{d}e_l. \tag{4.116}$$

Replacing (4.109) and (4.110) to (4.116),

$$\begin{aligned} \mathrm{d}E &= e_g \mathrm{d}m_g + e_l \mathrm{d}m_l - \frac{u_g^2}{2}\mathrm{d}m_g - \frac{u_l^2}{2}\mathrm{d}m_l + u_g \mathrm{d}q_g + u_l \mathrm{d}q_l \\ &+ m_g a_{4g}\mathrm{d}\rho_g + m_l a_{4l}\mathrm{d}\rho_l + (m_g a_{3g} + m_l a_{3l})\,\mathrm{d}T, \end{aligned} \tag{4.117}$$

which deduces

$$\begin{aligned} \zeta^{-1}\mathrm{d}T &= \mathrm{d}E + \left(\frac{u_g^2}{2} - e_g\right)\mathrm{d}m_g + \left(\frac{u_l^2}{2} - e_l\right)\mathrm{d}m_l \\ &- u_g \mathrm{d}q_g - u_l \mathrm{d}q_l - m_g a_{4g}\mathrm{d}\rho_g - m_l a_{4l}\mathrm{d}\rho_l, \end{aligned} \tag{4.118}$$

where

$$\zeta = (m_g a_{3g} + m_l a_{3l})^{-1}. \tag{4.119}$$

$\mathrm{d}T$ is obtained by replacing $\mathrm{d}\rho_g$ of (4.112) and $\mathrm{d}\rho_l$ of (4.114) into (4.118) as follows

$$\begin{aligned} &\left(\zeta^{-1} + \alpha_g\alpha_l\vartheta\left(a_{1l}a_{2g}a_{3g} - a_{1g}a_{2l}a_{3l}\right)\left(a_{4g}\rho_g^2 - a_{4l}\rho_l^2\right)\right)\mathrm{d}T = \\ &\mathrm{d}E + \left(\frac{u_g^2}{2} - e_g\right)\mathrm{d}m_g + \left(\frac{u_l^2}{2} - e_l\right)\mathrm{d}m_l - u_g\mathrm{d}q_g - u_l\mathrm{d}q_l \\ &-m_g a_{4g}\left(\vartheta\rho_l a_{1g}(1 - a_{2l}a_{4l})\mathrm{d}m_g + \vartheta\rho_g a_{1g}(1 - a_{2l}a_{4l})\mathrm{d}m_l\right) \\ &-m_l a_{4l}\left(\vartheta\rho_l a_{1l}(1 - a_{2g}a_{4g})\mathrm{d}m_g + \vartheta\rho_g a_{1l}(1 - a_{2g}a_{4g})\mathrm{d}m_l\right). \end{aligned} \tag{4.120}$$

Defining

$$\varrho = \left(m_g a_{3g} + m_l a_{3l} + \alpha_g\alpha_l\vartheta\left(a_{1l}a_{2g}a_{3g} - a_{1g}a_{2l}a_{3l}\right)\left(a_{4g}\rho_g^2 - a_{4l}\rho_l^2\right)\right)^{-1}, \tag{4.121}$$

then gradient vector of T is

$${}^t[T_j]_{j=1,\ldots,5} = \varrho\begin{bmatrix} \left(\frac{u_g^2}{2} - e_g\right) - \vartheta\rho_l\left(m_g a_{4g}a_{1g}(1 - a_{2l}a_{4l}) + m_l a_{4l}a_{1l}(1 - a_{2g}a_{4g})\right) \\ \left(\frac{u_l^2}{2} - e_l\right) - \vartheta\rho_g\left(m_l a_{4l}a_{1l}(1 - a_{2g}a_{4g}) + m_g a_{4g}a_{1g}(1 - a_{2l}a_{4l})\right) \\ -u_g \\ -u_l \\ 1 \end{bmatrix} \tag{4.122}$$

Thus, we obtain the following gradient vectors with respect to the conservative variables U

$${}^t[\rho_{gj}]_{j=1,\ldots,5} = \vartheta\alpha_l\rho_g\left(a_{1l}a_{2g}a_{3g} - a_{1g}a_{2l}a_{3l}\right){}^t[T_j]_{j=1,\ldots,5} + \begin{bmatrix} \vartheta\rho_l a_{1g}(1 - a_{2l}a_{4l}) \\ \vartheta\rho_g a_{1g}(1 - a_{2l}a_{4l}) \\ 0 \\ 0 \\ 0 \end{bmatrix}, \tag{4.123}$$

$${}^t[\rho_{lj}]_{j=1,\ldots,5} = \vartheta\alpha_g\rho_l\left(a_{1g}a_{2l}a_{3l} - a_{1l}a_{2g}a_{3g}\right){}^t[T_j]_{j=1,\ldots,5} + \begin{bmatrix} \vartheta\rho_l a_{1l}(1 - a_{2g}a_{4g}) \\ \vartheta\rho_g a_{1l}(1 - a_{2g}a_{4g}) \\ 0 \\ 0 \\ 0 \end{bmatrix}, \tag{4.124}$$

$${}^t[e_g]_{j=1,\ldots,5} = a_{4g}{}^t[\rho_{gj}]_{j=1,\ldots,5} + a_{3g}{}^t[T_j]_{j=1,\ldots,5}, \tag{4.125}$$

$${}^t[e_l]_{j=1,\ldots,5} = a_{4l}{}^t[\rho_{lj}]_{j=1,\ldots,5} + a_{3l}{}^t[T_j]_{j=1,\ldots,5}, \tag{4.126}$$

$$
{}^t[\alpha]_{j=1,\dots,5} = -\kappa\alpha_g\alpha_l a_{1l} a_{2g}\,{}^t[e_{gj}]_{j=1,\dots,5} + \kappa\alpha_g\alpha_l a_{1g} a_{2l}\,{}^t[e_{lj}]_{j=1,\dots,5} + \begin{bmatrix} \kappa\alpha_l a_{1l} \\ -\kappa\alpha_g a_{1g} \\ 0 \\ 0 \\ 0 \end{bmatrix}, \tag{4.127}
$$

$$
{}^t[p]_{j=1,\dots,5} = -\kappa\alpha_g\rho_l a_{2g}\,{}^t[e_{gj}]_{j=1,\dots,5} - \kappa\alpha_l\rho_g a_{2l}\,{}^t[e_{lj}]_{j=1,\dots,5} + \begin{bmatrix} \kappa\rho_l \\ \kappa\rho_g \\ 0 \\ 0 \\ 0 \end{bmatrix}, \tag{4.128}
$$

where a_{1k}, a_{2k} defined by (4.101), a_{3k}, a_{4k} defined by (4.111), κ defined by (4.104), ϑ defined by (4.113), ϱ defined by (4.121).
In order to derive the gradient vector of the flux function, the following differential formula are applied :

$$
\begin{aligned}
\mathrm{d}(\alpha\rho u^2) &= -u^2\mathrm{d}m + 2u\mathrm{d}q, && (4.129)\\
\frac{1}{2}\mathrm{d}(\alpha\rho u^3) &= -u^3\mathrm{d}m + \frac{3}{2}u^2\mathrm{d}q, && (4.130)\\
\mathrm{d}(\alpha\rho u e) &= e\mathrm{d}q + q\mathrm{d}e, && (4.131)\\
\mathrm{d}(\alpha u p) &= \alpha u\mathrm{d}p + pu\mathrm{d}\alpha + \frac{p}{\rho}\left(\mathrm{d}q - u\mathrm{d}m\right). && (4.132)
\end{aligned}
$$

The Jacobian matrix $\mathbf{A}$ of the one dimensional five-equation model is finally written by the following form

$$
\mathbf{A} = \mathbf{A}_c + \mathbf{A}_p, \tag{4.133}
$$

such that

$$
\mathbf{A}_c = \begin{bmatrix} 0 & 0 & 1 & 0 & 0 \\ 0 & 0 & 0 & 1 & 0 \\ -u_g^2 & 0 & 2u_g & 0 & 0 \\ 0 & -u_l^2 & 0 & 2u_l & 0 \\ A_c^E(1) & A_c^E(2) & A_c^E(3) & A_c^E(4) & A_c^E(5) \end{bmatrix},
$$

$$
\mathbf{A}_p = \begin{bmatrix} 0 & 0 & 0 & 0 & 0 \\ 0 & 0 & 0 & 0 & 0 \\ \alpha_g p_1 + \Delta p\alpha_1 & \alpha_g p_2 + \Delta p\alpha_2 & \alpha_g p_3 + \Delta p\alpha_3 & \alpha_g p_4 + \Delta p\alpha_4 & \alpha_g p_5 + \Delta p\alpha_5 \\ \alpha_l p_1 - \Delta p\alpha_1 & \alpha_l p_2 - \Delta p\alpha_2 & \alpha_l p_3 - \Delta p\alpha_3 & \alpha_l p_4 - \Delta p\alpha_4 & \alpha_l p_5 - \Delta p\alpha_5 \\ A_p^E(1) & A_p^E(2) & A_p^E(3) & A_p^E(4) & A_p^E(5) \end{bmatrix},
$$

where

$$
[A_c^E(j)]_{j=1,\dots,5} = \begin{bmatrix} q_g e_{g1} + q_l e_{l1} - u_g^3 \\ q_g e_{g2} + q_l e_{l2} - u_l^3 \\ q_g e_{g3} + q_l e_{l3} + e_g + \frac{3}{2}u_g^2 \\ q_g e_{g4} + q_l e_{l4} + e_l + \frac{3}{2}u_l^2 \\ q_g e_{g5} + q_l e_{l5} \end{bmatrix}, \quad \text{and}
$$

$$
[A_p^E(j)]_{j=1,\dots,5} = \begin{bmatrix} (\alpha_g u_g + \alpha_l u_l)p_1 + p(u_g - u_l)\alpha_1 - \dfrac{u_g p}{\rho_g} \\ (\alpha_g u_g + \alpha_l u_l)p_2 + p(u_g - u_l)\alpha_2 - \dfrac{u_l p}{\rho_l} \\ (\alpha_g u_g + \alpha_l u_l)p_3 + p(u_g - u_l)\alpha_3 + \dfrac{p}{\rho_g} \\ (\alpha_g u_g + \alpha_l u_l)p_4 + p(u_g - u_l)\alpha_4 + \dfrac{p}{\rho_l} \\ (\alpha_g u_g + \alpha_l u_l)p_5 + p(u_g - u_l)\alpha_5 \end{bmatrix}.
$$

The demonstration so far uses general equations of state, the Jacobian matrix is therefore presented in a complicated form. Owing to the interest in the numerical methods, the numerical simulation in this document uses simple equations of state. For example, the following demonstration will use one of the following assumption

$$\mathrm{d}e_k = c_{v,k}\mathrm{d}T, k = g, l, \tag{4.134}$$

i.e. $a_{4k} = 0$ in (4.111), where $c_{v,k}$ is a volume heat capacity constant.

The Jacobian matrix of five-equation model in case where $\mathbf{d}e_k = c_{v,k}\mathbf{d}T$

Using the relation $\mathrm{d}e_k = c_{v,k}\mathrm{d}T$, the equation (4.118) is simplified as follows

$$\mathrm{d}T = \zeta\mathrm{d}E - \zeta(e_g - u_g^2)\mathrm{d}m_g - \zeta(e_l - u_l^2)\mathrm{d}m_l - 2\zeta u_g\mathrm{d}q_g + 2\zeta u_l\mathrm{d}q_l. \tag{4.135}$$

The Jacobian matrix of five-equation model is then derived by (4.133) using the following gradient vectors

$${}^t[T_j]_{j=1,\ldots,5} = \varrho \begin{bmatrix} \frac{u_g^2}{2} - e_g \\ \frac{u_l^2}{2} - e_l \\ -u_g \\ -u_l \\ 1 \end{bmatrix}, \tag{4.136}$$

$${}^t[e_{gj}]_{j=1,\ldots,5} = c_{v,g}\,{}^t[T_j]_{j=1,\ldots,5}, \quad {}^t[e_{lj}]_{j=1,\ldots,5} = c_{v,l}\,{}^t[T_j]_{j=1,\ldots,5}, \tag{4.137}$$

$${}^t[\alpha]_{j=1,\ldots,5} = -\kappa\alpha_g\alpha_l\left(a_{1l}a_{2g}c_{v,g} - a_{1g}a_{2l}c_{v,l}\right){}^t[T_j]_{j=1,\ldots,5} + \begin{bmatrix} \kappa\alpha_l a_{1l} \\ -\kappa\alpha_g a_{1g} \\ 0 \\ 0 \\ 0 \end{bmatrix}, \tag{4.138}$$

$${}^t[p]_{j=1,\ldots,5} = -\kappa(c_{v,g}\alpha_g\rho_l a_{2g} + c_{v,l}\alpha_l\rho_g a_{2l}){}^t[T_j]_{j=1,\ldots,5} + \begin{bmatrix} \kappa\rho_l \\ \kappa\rho_g \\ 0 \\ 0 \\ 0 \end{bmatrix}, \tag{4.139}$$

where $\varrho = c_{v,g}m_g + c_{v,l}m_l$.

Eigenvalues of the five-equation model in case where $\mathbf{d}e_k = c_{v,k}\mathbf{d}T$

Due to the fact that the exact eigenvalues of the Jacobian matrix $\mathbf{A}$ of (4.133) and (4.136), (4.137), (4.138), (4.139) is complicated, we then follow the perturbation approach to compute the approximate eigenvalues.
We recall the notation of the mixture sound speed c_{sm}

$$c_{sm} = \sqrt{\frac{\alpha_g\rho_g + \alpha_l\rho_l}{\alpha_g\rho_l a_{1g} + \alpha_l\rho_g a_{1l}}}, \tag{4.140}$$

and let us denote

$$\varepsilon = \frac{u_g - u_l}{c_{sm}}, \tag{4.141}$$

$$\hat{u} = \frac{u_g + u_l}{2}. \tag{4.142}$$

Equations (4.141) and (4.142) yields

$$u_g = \hat{u} + \frac{\varepsilon c_{sm}}{2}, \quad u_l = \hat{u} - \frac{\varepsilon c_{sm}}{2}. \tag{4.143}$$

Replacing (4.143) into the characteristic polynomial P (which is not presented here due to its complex formula), we then obtain $P(\lambda, \varepsilon)$. Using the software Maple [8], we derive the approximate eigenvalues by the following process.

— Compute $\lambda(\varepsilon = 0)$ by solving the equation $P(\lambda, \varepsilon = 0) = 0$.

— Compute the derivative $\lambda'(\varepsilon = 0)$ thanks to the derivation of the implicit function $P(\lambda, \varepsilon)$, i.e.

$$\lambda'(\varepsilon = 0) = -\left(\frac{\partial P}{\partial \varepsilon}\right)_{|\varepsilon=0} \left(\frac{\partial P}{\partial \lambda}\right)^{-1}_{|\lambda(\varepsilon=0)}. \tag{4.144}$$

— Compute the second derivative $\lambda''(\varepsilon = 0)$ by solving the second derivation of the implicit function $P(\lambda, \varepsilon)$, i.e.

$$\lambda''(\varepsilon = 0) = -\left(\frac{\partial^2 P}{\partial^2 \varepsilon} + 2\frac{\partial^2 P}{\partial \varepsilon \partial \lambda} + \frac{\partial^2 P}{\partial^2 \lambda}\left(\frac{\partial \lambda}{\partial \varepsilon}\right)^2\right)\left(\frac{\partial P}{\partial \lambda}\right)^{-1}. \tag{4.145}$$

However, considering the interfacial pressure leads to very complicated eigenvalues which are not easy to evaluate. We therefore assume that $u_g - u_l = 0$ implies $\Delta p = 0$. Using this assumption, we obtain the following approximate eigenvalues.

$$\lambda_{1,5} = \hat{u} \mp c_{sm}(1 - \gamma) + c_{sm}\mathcal{O}(\varepsilon), \tag{4.146}$$

$$\lambda_{2,3,4} = \hat{u} + \frac{\xi}{c_{sm}}\varepsilon + \mathcal{O}(\varepsilon^3), \tag{4.147}$$

where

$$\xi = \frac{1}{2}\frac{\rho_g\rho_l(\alpha_l\rho_l c_{v,l} - \alpha_g\rho_g c_{v,g}) + p(\alpha_g\rho_l c_{v,g}a_{2,g} - \alpha_l\rho_g c_{v,l}a_{2,l})}{-\rho_g\rho_l(\alpha_l\rho_l c_{v,l} + \alpha_g\rho_g c_{v,g}) + p(\alpha_g\rho_l c_{v,g}a_{2,g} + \alpha_l\rho_g c_{v,l}a_{2,l})}, \tag{4.148}$$

$$\gamma = \frac{p\varrho(\alpha_g\rho_l c_{v,g}a_{2,g} + \alpha_l\rho_g c_{v,l}a_{2,l})}{\rho_g\rho_l}. \tag{4.149}$$

4.3 Difficulties for two phase flow models

Owing to the important application of fluid dynamics, both mathematical theory and numerical methods of gas dynamic Euler system have been studying well in plenty of literature by numerous authors. This system has become a sample one to verify a new numerical approach because of its nonlinear but beautiful mathematical properties such as this system is a system of hyperbolic conservation laws with the two GNL fields and one LD field (in one dimension). With some specific assumption, we can obtain analytical solutions of the Riemann problem of such a system. The theory of single phase flow therefore have been well developed during last century. As a consequence, it is evident that the two-fluid models inherit achievements obtained in the single phase flow including of modeling, mathematical theory and numerical methods. However, the two-phase flow models themselves possess many of specific difficulties due to existence of two phases in the same domain of interest and their interactions as well. In this section we will first discuss some difficulties in general existing in the two phase flow models, then we will go further to the two-fluid model which is the most challenging in the mathematical viewpoint.

4.3.1 Complicated characteristic fields

The analysis of the eigenvalues for the slip model, drift flux model and two-fluid models is approximately made around the mechanical equilibrium, i.e. the eigenvalues are computed as a perturbation of the relative velocity in comparison to the mixture sound speed, ($\varepsilon = \frac{u_g - u_l}{c_{sm}}$). In the zeroth order of ε, these two-phase flow models reproduce the characteristic fields which are similar to the Euler system. However taking into account the proper non-zero relative velocity may lead to complicated eigenstructure. For example in the case of the isentropic drift flux model, the characteristic field corresponding to the void wave is neither GNL nor LD in the case $u_g - u_l = (1-\alpha)^{k-1}v_\infty$ such that $k > 1$. The study of the incompressible two-fluid model in Chapter 5 proves that the characteristic fields are neither GNL nor LD.

8. www.maplesoft.com

4.3.2 Vacuum limit

In the classical system of gas dynamics one can find a problem arising when the vacuum state (i.e. the density $\rho = 0$) appears. In this case the hyperbolicity of the conservation laws breaks down, see [Bou00], [Daf10]. The existence of solutions with $\rho \geq 0$ is not easy. In the two-phase flow models, the vacuum state may appear but it is rarer than another problem, vanishing phase (i.e. one of two phases is absent), which may happen naturally in the flow. The existence of solutions with $\rho_g \geq 0$ and $\rho_l \geq 0$ is not easy.

4.3.3 Discontinuous source terms

In the thermal hydraulics of nuclear reactors all four models (slip model (4.1), drift model (4.10), six equations two-fluid model (4.18) and five equations two-fluid model (4.23)) introduced in section 4.1 display important and stiff source terms $S(U, x)$. The stiffness of these source terms has different origins.

First the heat source Φ is localized on the core of the reactor which yields a discontinuity in space. Moreover the dry-out of the Uranium rod when the temperature reaches a threshold (the critical heat flux) yields a discontinuity of Φ as a function of the temperature. Second the boiling of the fluid is an intrinsically stiff phenomena with a threshold that is the boiling temperature (or enthalpy). For these reasons the simulation of the two phase boiling flow models is challenging both from a mathematical and a numerical point of view.

The source term $S(U, x)$ being discontinuous both in U and x makes it impossible to use Cauchy-lipschitz type of theorems for the existence of solutions even for ODEs. However, there are particular cases where a unique solution may exist (see the pioneering work of Bressan [Bre88]), and we give such an example of stationary solution with such a discontinuity for the stationary drift model in the appendix 6.2.5.

The source term $S(U, x)$ being discontinuous in U makes numerical approximation more difficult in the numerical simulation because of the stiffness of the solution. Most approaches presented in 2.3 to deal with stiff source term assume it is Lipschitz in the variable U. We however used the upwind source approach of [BV94] which gave good results (see section 6.2.3), and formalized its good properties through lemma 2.

4.3.4 Additional difficulties for the two-fluid models

The two-fluid model is more general than the slip model and the drift flux model. However it also displays many mathematical difficulties. A system derived by neglecting the source terms of system (4.18) is in general not hyperbolic, lack of hyperbolicity causes the ill-posedness of the Cauchy problem, [GR96]. Moreover, the presence of the non conservative product $\alpha_k \vec{\nabla} P$ in the momentum equations (4.18c),(4.18d) and $p_k \frac{\partial \alpha_k}{\partial t}$ in the energy equations (4.18e),(4.18f) requires a special attention when applying the theory of system of conservation laws. We will present here the mathematical properties of the two-fluid model. For simplifications, during this part we consider the homogeneous form of system (4.18), i.e. neglect the source term on the right hand side except $\Delta p \nabla \alpha$.

Hyperbolicity and interfacial pressure correction of the two-fluid model

When considering equal pressure law, it is well-known that the original two-fluid model (4.18) is not hyperbolic. So, one did some correction in order to obtain the hyperbolicity. Consideration of the interfacial pressure default and the virtual mass are two of different approaches, the reader is referred to [Stu77 ; Bes90 ; TK96 ; Ami97 ; TKP99 ; Ndj07a] for details. We are here interested in the interfacial pressure correction which is presented in and used in CATHARE, a thermal-hydraulic platform simulating the two-phase flow in the primary loop of nuclear power plants. The hyperbolicity of the two-fluid model does not depend on the energy equations, since their eigenvalues are trivially computed using the entropy variable which is presented in Equation (4.22). Therefore, for simplification but not lack of generality, we only consider the *isentropic* two-fluid model when studying the hyperbolicity of the general two-fluid model. Neglecting source terms, the isentropic two-fluid model in one dimension is

derived from the general two-fluid model without taking into account the energy equations.

$$\frac{\partial \alpha_g \rho_g}{\partial t} + \frac{\partial \alpha_g \rho_g u_g}{\partial x} = 0, \tag{4.150a}$$

$$\frac{\partial \alpha_l \rho_l}{\partial t} + \frac{\partial \alpha_l \rho_l u_l}{\partial x} = 0, \tag{4.150b}$$

$$\frac{\partial \alpha_g \rho_g u_g}{\partial t} + \frac{\alpha_g \rho_g u_g^2}{\partial x} + \alpha_g \frac{\partial p}{\partial x} + \Delta p \frac{\partial \alpha_g}{\partial x} = 0, \tag{4.150c}$$

$$\frac{\partial \alpha_l \rho_l u_l}{\partial t} + \frac{\alpha_l \rho_l u_l^2}{\partial x} + \alpha_l \frac{\partial p}{\partial x} + \Delta p \frac{\partial \alpha_l}{\partial x} = 0. \tag{4.150d}$$

Here we add a new term $\Delta p \frac{\partial a_k}{\partial x}$ in the momentum equations, this new term is called the interfacial pressure correction which will play an important role to get the hyperbolicity of the system (4.150). Denoting the unknown variables $U = (\alpha_g \rho_g, \alpha_g \rho_g u_g, \alpha_l \rho_l, \alpha_l \rho_l u_l)$, the system (4.150) can be rewritten as the quasi-linear form

$$\frac{\partial U}{\partial t} + A(U) \frac{\partial U}{\partial x} = 0, \tag{4.151}$$

where $A(U)$ is the Jacobian matrix of system (4.150). Let us call

$$\gamma^2 = \frac{c_{sg}^2 c_{sl}^2}{\alpha_g \rho_l c_{sl}^2 + \alpha_l \rho_g c_{sg}^2}, \tag{4.152}$$

where c_{sg}, c_{sl} are the sound speeds of gas and liquid respectively. Then, we get

$$A(U) = \begin{pmatrix} 0 & 0 & 1 & 0 \\ 0 & 0 & 0 & 1 \\ \alpha_g \rho_l \gamma^2 - u_g^2 & \alpha_g \rho_g \gamma^2 & 2u_g & 0 \\ \alpha_l \rho_l \gamma^2 & \alpha_l \rho_g \gamma^2 - u_l^2 & 0 & 2u_l \end{pmatrix}. \tag{4.153}$$

Follow the work in [Bes90 ; Stu77], the matrix $A(U)$ has four real eigenvalues, i.e. the system (4.150) is hyperbolic for small relative velocity, if

$$\Delta p \geq \frac{\alpha_g \alpha_l \rho_g \rho_l}{\alpha_g \rho_l + \alpha_l \rho_g} (u_g - u_l)^2. \tag{4.154}$$

Let us call

$$\Delta p_{\text{tangent}} = \delta \frac{\alpha_g \alpha_l \rho_g \rho_l}{\alpha_g \rho_l + \alpha_l \rho_g} (u_g - u_l)^2, \tag{4.155}$$

where $\delta \geq 1$ the interfacial pressure of Bestion type.

In the more general case of the relative velocity, the hyperbolicity of the isentropic system (4.150) have been studied in [Ami97 ; Ndj07a ; Ndj07b ; Ver06]. Following the work in [Ver06], the interfacial pression correction defined by

$$\Delta p_{\text{parabol}} = \frac{\alpha_g \alpha_l \rho_g \rho_l}{\alpha_g \rho_l + \alpha_l \rho_g} (u_g - u_l)^2 + \frac{1}{c_{sg}^2} \left(\rho_g - \frac{\alpha_g \alpha_l \rho_g \rho_l}{\alpha_g \rho_l + \alpha_l \rho_g} \right) (u_g - u_l)^4, \tag{4.156}$$

guarantees the hyperbolicity for the relative velocity up to the sound speed of gas c_{sg}. On the other hand, the author in [Ami97 ; Ndj07b] introduces the interfacial pressure of the following form

$$\Delta p_{\text{linear}} = \rho_g (u_g - u_l)^2, \tag{4.157}$$

that guarantees the hyperbolicity in the region where $|u_g - u_l| \leq c_{sg}$.

The diagrams of the hyperbolic region of (4.155), (4.156) and (4.157) is found in Figure 4.3.4.

Vanishing phase

Considering a two phase flow model (liquid and gas), one of two phases however may be absent due to total boiling or condensation and so on. The absent phase is called *vanishing phase*, or *ghost phase*. Due to the consideration of the mixture momentum, the vanishing phase in the slip and the

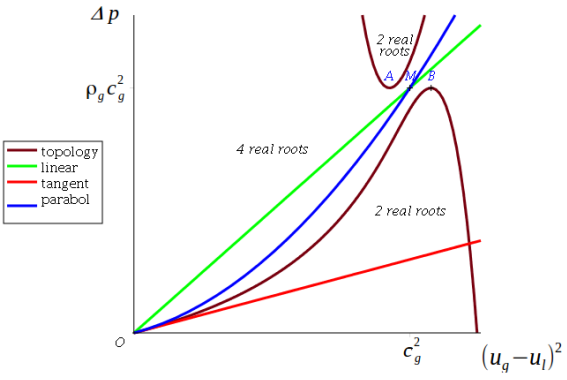

FIGURE 4.3 – Hyperbolic diagram.

drift flux models does not give rise to any particular singularity. It however poses a notable difficulty in the two-fluid model owing to its independent velocities. The singularity arises when one computes the absent phase velocity using the conservative variables $u_k = \dfrac{\alpha_k \rho_k u_k}{\alpha_k \rho_k}$ as $\alpha_k \rho_k \to 0$, where k stands for either liquid (l) or gas (g).

Studying the one dimensional two-fluid model, we are first interested in the mathematical properties of the vanishing phase which is assumed to be *gas*, i.e. $\alpha = \alpha_g = 0$, (mathematically, it will the same if the absent phase is liquid). Let us take into account the isentropic model in (4.150). When $\alpha = 0$, the Jacobian matrix

$$A_{\alpha=0} = \begin{bmatrix} 0 & 0 & 1 & 0 \\ 0 & 0 & 0 & 1 \\ -u_g^2 & 0 & 2u_g & 0 \\ \frac{\rho_l c_{sl}^2}{\rho_g} & c_{sl}^2 - u_l^2 & 0 & 2u_l \end{bmatrix} \tag{4.158}$$

In this case the system (4.150) degenerates, the Jacobian matrix has four eigenvalues

$$u_g, \quad u_g, \quad u_l + c_{sl}, \quad u_l - c_{sl},$$

but only three eigenvectors, the hyperbolicity is therefore broken. A two-phase flow model is in general not natural adapted to model a single phase one, there will be not adequate information for the absent phase. Therefore, the simple way to resolve this problem is to consider it as a single phase flow. However, the difficulty lies on the configuration where there exists an interaction between a single phase region and a two-phase region. More precisely, consider a Riemann problem in one dimension with two limit states such that $\alpha_L \neq \alpha_R$ and $\alpha_L \alpha_R = 0$. In this case, we must consider the flow as a two-phase one due to the present of both liquid and gas. The difficulty is similar to the vacuum in the single phase, see [LS80] for example, where authors try to study the space domain where there exists both fluid and vacuum. The difficulty in the two-fluid model is that it does not have explicit formula for eigenstructure as in the single phase flow. Therefore, studying the vanishing phase in this case becomes really complicated.

We remark that this challenging point is rarely taken into account in the literature. A remarkable one may be found in [Sal12], in which the authors study the Riemann problem where one state is a pure phase and other is a mixture for the Baer-Nunziato model (two pressure two-fluid model). However since we do not give here much information about that model, the interesting reader is referred to [RH84 ; Coq+02] for more details. In general the Baer-Nunziato model has properties that are similar to the Euler system and its eigenstructure can be explicitly calculated. This explains partially why the solutions of the Riemann problems near the single phase are explicitly achieved in [Sal12], where the reader can find all details.

Non conservative product in the two-fluid model

A theory of hyperbolic conservation laws studied in depth in the literature has been introduced in the first part of this document. Such a theory gives a fundamental understanding and main ideas for plenty of

numerical methods to solve a hyperbolic conservation laws system, i.e. find a weak solution in the sense of distribution. However, our system (4.18) possesses non conservative products. A discontinuous solution is thus not well-defined in the distribution sense due to the fact that a product of two distributions in this case is not well-defined. In order to study a hyperbolic non conservation laws, one may consider different approaches. For instance, Aragonaa, Colombeau et al in [ACJ14] used the theory of non linear generalized functions to define a non conservative product. Following this approach, the authors add supplementary physical information into the original system in order to choose a suitable jump formula among infinitely many possible variation of jump conditions. Another approach can be found in [PCC03 ; CP06], where the authors use an advection upwind splitting method in the sense that the non conservative product terms are all considered as the source terms. However such an approach causes some spurious oscillations, see [CP06]. In general, the most popular approach to study non conservative products encountered is the theory of non conservation laws studied by Dal Maso et al in [MLM95], where the authors define a product of two distribution as a Borel measure. Such a definition however depends on a specific path which connects a left state to a right state in the case of non conservative product, whereas a shock wave definitely depends merely on its left state and right state in the conservative one. Defining such an appropriate path requires realistic physical information which is not easy, especially in a complicated two-fluid model. Moreover, once the appropriate path is chosen, different numerical methods may converge to different solutions, see comments in [AK10] and references therein. Therefore, one may prefer to solve the two-fluid model by using a simpler consideration of the non conservative product. For example, in [TK96], the authors rewrite the two-fluid model and choose jump condition based on a particular case where the system has a conservative form. The resulting two-fluid model includes two conservation laws of mass of each phase, one conservation law of mixture of momentum derived by adding the two partial conservation of momentum and one equation of velocity of liquid which is assumed to be incompressible. More precisely, it consists of the following equations

$$\frac{\partial \alpha_g \rho_g}{\partial t} + \frac{\partial \alpha_g \rho_g u_g}{\partial x} = 0, \tag{4.159a}$$

$$\frac{\partial \alpha_l \rho_l}{\partial t} + \frac{\partial \alpha_l \rho_l u_l}{\partial x} = 0, \tag{4.159b}$$

$$\frac{\partial (\alpha_g \rho_g u_g + \alpha_l \rho_l u_l)}{\partial t} + \frac{\partial (\alpha_g \rho_g u_g^2 + \alpha_l \rho_l u_l^2 + p)}{\partial x} = 0, \tag{4.159c}$$

$$\frac{\partial u_l}{\partial t} + \partial \frac{\frac{u_l^2}{2} + \frac{p}{\rho_l}}{\partial x} = 0. \tag{4.159d}$$

Then, they found a formula to locally linearize α_k, denote $\tilde{\alpha}_k$, in the product $\alpha_k \frac{\partial p}{\partial x}$, $k = g, l$, such that the original isentropic model (4.150a-4.150d) (considering $\Delta P = 0$) and the system (4.159a-4.159d) have the same Rankine-Hugoniot relation. According to the work in [TK96],

$$\tilde{\alpha}_l = \frac{2\alpha_l^L \alpha_l^R}{\alpha_l^L + \alpha_l^R}, \quad \tilde{\alpha}_g = 1 - \tilde{\alpha}_l. \tag{4.160}$$

This formula is then applied in the simulation of two-fluid model, [TKP99]. Of course, this is not the unique possible choice. For example, the authors in [EF03 ; DT11] prefer to a local phasic symmetry linearization of α_k in the sense that

$$\tilde{\alpha}(\alpha_k^L, \alpha_k^R) = 1 - \tilde{\alpha}(1 - \alpha_k^L, 1 - \alpha_k^R). \tag{4.161}$$

The arithmetic average formula satisfying (4.161) is thus chosen, i.e.

$$\tilde{\alpha}_k = \frac{\alpha_k^L + \alpha_k^R}{2}, \quad k = g, l. \tag{4.162}$$

On the other hand, in order to treat the non-conservative terms $p\partial_t \alpha_k$ in the partial energy equations, the authors in [TK96] approximate it by a spacial derivative using the incompressible liquid assumption associated with the liquid mass equation, i.e.

$$\partial_t \alpha_l = -\partial_x (\alpha_l u_l). \tag{4.163}$$

Some authors focusing on the numerical methods usually eliminate the product of $p\partial_t \alpha$ in the energy equations, for example [MEF09 ; MFM10].

Chapitre 5

The incompressible two-phase flow model

We propose a 2×2 hyperbolic system of conservation laws to model the dynamics of two incompressible fluids in mechanical disequilibrium. In the theoretical part of the paper we show that this 1D system is not strictly hyperbolic, that the characteristic speeds can not *a priori* be ordered and that the characteristic fields are neither genuinely nonlinear, nor linearly degenerate. We nevertheless prove the existence and uniqueness of an admissible solution to the Riemann problem. This solution remains bounded with positive volume fractions even when one of the phases vanishes. The multiphase/single phase transition does not imply mechanical equilibrium but displays a non classical wave structure.
In the numerical part of the paper we propose some approximate Riemann solvers to simulate the model, especially the multiphase/single phase transition. The classical Riemann solvers have been considered as Godunov scheme, Roe scheme with or without entropy fix. We also propose an in-cell discontinuous reconstruction method which proves to be successful, whereas the other schemes may show some spurious oscillations in some Riemann problem. Finally, as an application we study and simulate the problem of phase separation by gravity.
The numerical results presented in this chapter can be found in [NNC14] whereas the theoretical part was been submitted, see [NNC15b].

For the incompressible drift flux model, a similar approach is also studied. The reader can find detail in Appendix 5.5.6.

5.1 Introduction

The flow regime involved in a nuclear reactor core is purely liquid in normal operating conditions but may become a liquid-gas mixture in incidental conditions or even purely gaseous in case of a serious accident involving a core dewatering. The simulation of the single phase/multiphase transition is numerically challenging and has been a major difficulty in the design of new simulation platforms based on advanced two-fluid models, see for instance [CDK14 ; Jeo+08] and references therein. An important issue is to guarantee the positivity of the volume fraction of each phase. There is an open debate as to whether this positivity is intrinsic to the conservation laws or requires some adequate source terms such as inter-phase friction. The thermal hydraulics platform CATHARE [Bes00] assumes that when a phase disappears, its velocity is equal to the velocity of the other phase. In order to strongly couple the two phase velocities, they use a very high interfacial friction term to deal numerically with these transitions. This chapter intends to prove in the case of incompressible phases that the Riemann problem admits a positive solution without any frictional term and that the two velocities are not necessarily equal (section 5.2), to propose some numerical methods able to deal with vanishing phases (section 5.3) and then presents some numerical results (section 5.4). Allowing phase disappearance with mechanical disequilibrium enables for example the modeling of bubbles ascending in a liquid as a consequence of Archimedes' principle.

5.1.1 The compressible model

We consider a one dimensional isentropic two phase flow involving two fluids with densities $\rho_1 < \rho_2$, pressures P_1 and P_2, volume fractions $\alpha_1 \in [0,1]$, $\alpha_2 = 1-\alpha_1$, and velocities u_1 and u_2. After averaging the mass and momentum balance equations for each phase (see [Ish75 ; SW84 ; DP99]), the two-fluid model consists in the following four equations ($k = 1, 2$)

$$\partial_t \alpha_1\rho_1 + \partial_x(\alpha_1\rho_1 u_1) = \Gamma_1, \tag{5.1a}$$

$$\partial_t \alpha_2\rho_2 + \partial_x(\alpha_2\rho_2 u_2) = \Gamma_2, \tag{5.1b}$$

$$\partial_t(\alpha_1\rho_1 u_1) + \partial_x(\alpha_1\rho_1 u_1^2) + \alpha_1\partial_x P_1 = \alpha_1\rho_1 g + \Gamma_1 u^i, \tag{5.1c}$$

$$\partial_t(\alpha_2\rho_2 u_2) + \partial_x(\alpha_2\rho_2 u_2^2) + \alpha_2\partial_x P_2 = \alpha_2\rho_2 g + \Gamma_2 u^i, \tag{5.1d}$$

where Γ_1, Γ_2 are phase change functions such that $\Gamma_1 + \Gamma_2 = 0$, u^i is the interfacial velocity and g is the gravitational acceleration. Unlike [KSS03 ; Ndj+08 ; Jeo+08 ; CDK14] we do not assume pressure equality $P_1 = P_2$ nor do we introduce an interfacial pressure default term $\triangle p\partial_x\alpha_k$ in the governing equations (5.1c) and (5.1d). Instead we consider a non zero pressure difference of the form $P_1 - P_2 = \frac{\rho_1\rho_2}{2(\rho_1-\rho_2)}(u_1-u_2)^2$ which yields a hyperbolic system, see below. This pressure gap corresponds to a dynamic surface tension model accounting for the fact that velocity shear yields an increase of the micro-scale interfacial curvature via the well known Kelvin-Helmholtz instability (see[Cha81]). Taking into account surface tension, the increase of local curvature results in a pressure difference via the Laplace law $P_1 - P_2 = \gamma\sigma$ which should vanish only when $u_1 = u_2$. The kinetic energy gap $\frac{1}{2}\rho_1 u_1^2 - \frac{1}{2}\rho_2 u_2^2 = \frac{1}{2}\frac{(\rho_1 u_1 - \rho_2 u_2)^2}{\rho_1-\rho_2} - \frac{1}{2}\frac{\rho_1\rho_2(u_1-u_2)^2}{\rho_1-\rho_2}$ is related to the momentum gap $\rho_1 u_1 - \rho_2 u_2$ and to the velocity gap $u_1 - u_2$. In this first study, we make the simple assumption that the pressure gap exactly compensates the contribution of the velocity gap to the kinetic energy gap.
The system (5.1a-5.1d) has four main unknowns : α_1, P_1, u_1, u_2, the other unknowns can be obtained using the equations of state $\rho_k(P_k)$ and the pressure gap law

$$P_1 - P_2 = \frac{\rho_1\rho_2}{2(\rho_1-\rho_2)}(u_1-u_2)^2.$$

Defining the mixture sound wave $c_m = \sqrt{\frac{(\alpha_1\rho_2+\alpha_2\rho_1)c_2^2c_1^2}{\alpha_1\rho_2c_2^2+\alpha_2\rho_1c_1^2}}$, where $c_k = c_k(P_k), k = 1, 2$ are the sound speeds of each phase, following the work in [Ndj07b], the Taylor expansion of the four eigenvalues of the system (5.1a-5.1d) when $u_1 - u_2 \ll c_m$ is

$$\begin{aligned}
\lambda_1 &= \frac{\rho_1 u_1 - \rho_2 u_2}{\rho_1-\rho_2}\left(1 - \frac{\rho_1\rho_2}{(\alpha_1\rho_2+\alpha_2\rho_1)^2}\right) + \mathcal{O}\left(\frac{u_1-u_2}{c_m}\right) \quad \text{void fraction wave,}\\
\lambda_2 &= \frac{\rho_1 u_1 - \rho_2 u_2}{\rho_1-\rho_2} + \mathcal{O}\left(\frac{u_1-u_2}{c_m}\right) \quad \text{void fraction wave,}\\
\lambda_3 &= \frac{\alpha_1\rho_2 u_1 + \alpha_2\rho_1 u_2}{\alpha_1\rho_2+\alpha_2\rho_1} + c_m + \mathcal{O}\left(\frac{u_1-u_2}{c_m}\right) \quad \text{acoustic wave,}\\
\lambda_4 &= \frac{\alpha_1\rho_2 u_1 + \alpha_2\rho_1 u_2}{\alpha_1\rho_2+\alpha_2\rho_1} - c_m + \mathcal{O}\left(\frac{u_1-u_2}{c_m}\right) \quad \text{acoustic wave.}
\end{aligned}$$

Thus for small relative velocities $u_1 - u_2 \ll c_m$, the system (5.1a-5.1d) is hyperbolic with 2 acoustic waves involving the mixture sound speed and two void waves that are specific to the two phase dynamics. Since we are interested in the void wave dynamics and flows at low Mach numbers, we devote more attention to the incompressible limit of the system (5.1a-5.1d).

5.1.2 The incompressible model

In order to study more precisely the volume fraction waves involved in applications where the fluid densities are almost constant, we follow [KSS03] and assume that both phases are incompressible with constant densities ρ_1 and ρ_2.

First remark that summing $\frac{1}{\rho_1}$(5.1a) and $\frac{1}{\rho_2}$(5.1b) yields $\partial_x(\alpha_1 u_1 + \alpha_2 u_2) = \frac{\Gamma_1}{\rho_1} + \frac{\Gamma_2}{\rho_2}$, and therefore the value of $K = \alpha_1 u_1 + \alpha_2 u_2$ may be determined from the boundary conditions. From now on, without of specific mention we assume that K is a constant both in space and time for simplicity.

For simplification, we will assume that $K = 0$, which is true for example if there is a wall boundary condition. If $K \neq 0$ is constant both in time and space, a Galilean change of reference frame $u'_k = u_k - K$ yields a new system with $K' = \alpha_1 u'_1 + \alpha_2 u'_2 = 0$ (see [KSS03]). It is then possible to obtain a close system of two equations by setting

$$\begin{cases} \alpha = \alpha_1, \\ \omega = \rho_1 u_1 - \rho_2 u_2. \end{cases} \tag{5.2}$$

Note that the velocities u_1 and u_2 can be recovered from (5.2) and $K = 0$ as

$$u_1 = \frac{(1-\alpha)\omega}{\alpha(\rho_2 - \rho_1) + \rho_1}, \quad u_2 = \frac{-\alpha\omega}{\alpha(\rho_2 - \rho_1) + \rho_1}. \tag{5.3}$$

The unknown vector $U = {}^t(\alpha, \omega)$ can be described by a conservative system

$$\partial_t U + \partial_x F(U) = S, \tag{5.4}$$

with

$$F(U) = \begin{pmatrix} \frac{\alpha(1-\alpha)\omega}{\alpha(\rho_2-\rho_1)+\rho_1} \\ \\ \frac{\omega^2}{2(\rho_1-\rho_2)} \end{pmatrix}, \quad S = \begin{pmatrix} 0 \\ \\ (\rho_1 - \rho_2)g \end{pmatrix}, \tag{5.5}$$

$$\nabla F(U) = \begin{pmatrix} \frac{\omega}{\rho_1-\rho_2}\left(1 - \frac{\rho_1\rho_2}{(\alpha(\rho_2-\rho_1)+\rho_1)^2}\right) & \frac{\alpha(1-\alpha)}{\alpha(\rho_2-\rho_1)+\rho_1} \\ \\ 0 & \frac{\omega}{\rho_1-\rho_2} \end{pmatrix}. \tag{5.6}$$

The first equation of (5.4) is obtained from $\frac{1}{\rho_1}$(5.1a) and the second of (5.4) comes from the linear combination of equations $\frac{1}{\alpha_1}$(5.1c) $-\frac{1}{\alpha_2}$(5.1d) (see the details in Appendix 5.5.1).

5.2 Theoretical study

5.2.1 Hyperbolicity and characteristic fields

The following theorem is a direct consequence of formula (5.6).

Theorem 4 (Hyperbolicity of system (5.4)) *The jacobian matrix (5.6) of the system (5.4) always admits real eigenvalues*

$$\lambda_1 = \frac{\omega}{\rho_1 - \rho_2}\left(1 - \frac{\rho_1\rho_2}{(\alpha(\rho_2 - \rho_1) + \rho_1)^2}\right), \quad \lambda_2 = \frac{\omega}{\rho_1 - \rho_2}, \tag{5.7}$$

and is diagonalisable provided $(\alpha, \omega) \in \mathcal{H}$ *where*

$$\mathcal{H} = \mathcal{H}_+ \cup \mathcal{H}_- \cup \{(0,\omega), \omega \in \mathbb{R}\} \cup \{(1,\omega), \omega \in \mathbb{R}\},$$
$$\text{and } \mathcal{H}_\pm = \left\{(\alpha,\omega), \omega \in \mathbb{R}^*_\pm, \text{ and } \alpha \in (0,1)\right\}.$$

The states $(\omega = 0, \alpha = 0)$ and $(\omega = 0, \alpha = 1)$ will play an important role in connecting states in $\mathcal{H}_+$ to states in $\mathcal{H}_-$ and will be called **critical states**.

$\mathcal{H}$ is neither an open nor a simply connected subset of $\mathbb{R}^2$, see Figure 5.1. The eigenvectors of ∇F are

$$\vec{r}_1 = {}^t(1, 0), \quad \vec{r}_2 = {}^t\left(\alpha(1-\alpha)(\rho_1 - \rho_2)(\alpha(\rho_2 - \rho_1) + \rho_1), \rho_1\rho_2\omega\right). \tag{5.8}$$

Considering $\rho_1 < \rho_2$, we notice that the two eigenvalues are not a priori ordered since

$$\begin{cases} \lambda_1 < \lambda_2 & \text{if } \omega < 0, \\ \lambda_1 > \lambda_2 & \text{if } \omega > 0. \end{cases} \tag{5.9}$$

Moreover, the signs of $\vec{\nabla}\lambda_1 \cdot \vec{r}_1 = \frac{-2\rho_1\rho_2\omega}{(\alpha(\rho_2-\rho_1)+\rho_1)^3}$ and $\vec{\nabla}\lambda_2 \cdot \vec{r}_2 = \frac{\rho_1\rho_2\omega}{(\rho_1-\rho_2)}$ are not known a priori since

$$\begin{cases} \vec{\nabla}\lambda_k \cdot \vec{r}_k > 0 & \text{if } \omega < 0, \\ \vec{\nabla}\lambda_k \cdot \vec{r}_k < 0 & \text{if } \omega > 0, \end{cases} \tag{5.10}$$

where $k = 1, 2$. Therefore the characteristic fields associated to λ_1 and λ_2 are genuinely nonlinear in each domain $\mathcal{H}_+$ and $\mathcal{H}_-$, but are neither genuinely non linear, nor linearly degenerate in general.

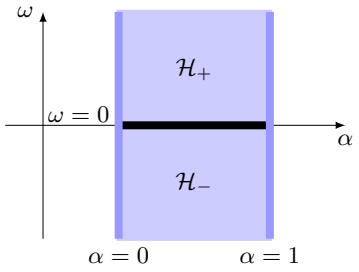

FIGURE 5.1 – Hyperbolic domain $\mathcal{H} = \mathcal{H}_+ \cup \mathcal{H}_- \cup \{(0,\omega), \omega \in \mathbb{R}\} \cup \{(1,\omega), \omega \in \mathbb{R}\}$.

5.2.2 Admissible solutions of the Riemann problem

The fact that the domain $\mathcal{H}$ is not open, that the system is not strictly hyperbolic and that the characteristic fields are neither genuinely nonlinear neither linearly degenerate raises many theoretical as well as numerical difficulties. We cannot use the classical Lax theorem (see [GR96]) to obtain solutions to the Riemann problem but will however build solutions to the Riemann problem having a non classical wave structure for any pair of left and right states data in $\mathcal{H}$.

Definition 5.2.1 (Hugoniot locus and Riemann invariants) *Given a state $U \in \mathcal{H}$, the Hugoniot locus $\mathcal{S}(U)$ associated to (5.16) and U is the set of states that can be connected to U via a shock wave :*

$$\mathcal{S}(U) = \{V \in \mathcal{H}, \quad \exists \sigma(U,V) \in \mathbb{R}, \quad F(U) - F(V) = \sigma(U,V)(U-V)\}.$$

For any $k \in \{1,2\}$, a k-Riemann invariant associated to (5.16) is a function $\mathcal{R}_k$ defined on $\mathcal{H}$ such that

$$\forall U \in \mathcal{H}, \quad \nabla \mathcal{R}_k \cdot \vec{r}_k = 0.$$

and the k-rarefaction wave associated to the Riemann invariant $\mathcal{R}_k$ at a left state U is

$$k\text{-}\mathcal{R}(U) = \{V \in \mathcal{H}, \quad \mathcal{R}_k(V) = \mathcal{R}_k(U), \quad \lambda_k(V) \geq \lambda_k(U)\}.$$

We did not find an entropy to our system and instead of an entropy criterion we use the Liu criterion to define admissible solutions.

Definition 5.2.2 (Admissible solution of the Riemann problem) *An admissible solution to (5.16) is a weak solution that is composed of a finite number of constant states connected by a rarefaction wave or a shock wave, connecting left and right sates U_L and U_R and propagating at a speed σ, that satisfies the Liu criterion :*

$$\sigma(U_L, U_R) \leq \sigma(U_L, U), \quad \forall U \in \mathcal{S}(U_L) \text{ between } U_L \text{ and } U_R.$$

5.2.3 Shock and rarefaction waves

In the theory of 2×2 strictly hyperbolic systems with genuinely nonlinear characteristic fields, each eigenvector family $\vec{r}_k$, $k = 1, 2$ defines at any state U_0 one single shock and one single rarefaction curve, both starting and having tangent vector $\vec{r}_k$ at $U = U_0$. These two curves are defined in an open neighborhood of U_0 and do not necessarily extend to the entire domain, see [LeF02], [GR96] for example.
Our system is neither strictly hyperbolic neither genuinely nonlinear, our hyperbolicity domain is not open. However we prove below that there are two families of shock "curves" (1-shocks and 2-shocks) and rarefaction "curves" (1-rarefactions and 2-rarefactions) and that they extend to the entire domain. The originality in our system is the fact that the shock "curve" associated to a state is not necessarily a connected set. Indeed the 1-shock "curve" associated to the critical states $(\alpha = 0, \omega = 0)$ and $(\alpha = 1, \omega = 0)$ contains only these two states. Moreover the 2-shock family of "curves" can be composed of the two branches of a hyperbola. Furthermore there is no 1-rarefaction associated to the critical state $(\alpha = 0, \omega = 0)$ and there are more than one 2-rarefaction curves passing through the critical state $(\alpha = 1, \omega = 0)$.
We now characterise the shock and rarefaction curves and illustrate them on Figure 5.2. We note that the entropy criterion is not taken into account in the following theorem.

Theorem 5 (Existence of shock curves)
Any state $U_0 = (\alpha_0, \omega_0) \in \mathcal{H} \setminus (\alpha = 1, \omega = 0)$ belongs to two shock curves in $\mathcal{H}$. The state $(\alpha = 1, \omega = 0)$ belong to three shock curves in $\mathcal{H}$.
The equation of the 1-shock family (1-S) of states $(\alpha, \omega_1(\alpha))$ connected to the state $U_0 = (\alpha_0, \omega_0)$ is
- *If $\omega_0 \neq 0, \quad \omega_1(\alpha) = \omega_0$.*
- *If $\omega_0 = 0$, the 1-shock "curve" is composed of the two states $(\alpha = 0, \omega = 0)$ and $(\alpha = 1, \omega = 0)$) since they can be connected by a special shock whose speed is $\sigma = 0$ and we will call it a* **degenerate 1-shock**.

The equation of the 2-shock family (2-S) of states $(\alpha, \omega_2(\alpha))$ connected to the state $U_0 = (\alpha_0, \omega_0)$ is
- *If $\omega_0 \neq 0$ and $\alpha_0 \in (0, 1)$*

$$\omega_2(\alpha) = \frac{\alpha(\rho_2 - \rho_1) + \rho_1}{\alpha_0(\rho_2 - \rho_1) + \rho_1} \times \frac{\alpha_0^2(\rho_2 - \rho_1) + \alpha_0(\rho_1 - 2\rho_2 + \alpha\rho_2 - \alpha\rho_1) + \alpha\rho_1}{\alpha^2(\rho_2 - \rho_1) + \alpha(\rho_1 - 2\rho_2 + \alpha_0\rho_2 - \alpha_0\rho_1) + \alpha_0\rho_1}\omega_0$$

- *If $\omega_0 \neq 0$ and $\alpha_0 = 0$, then either $\alpha = 0$ or $\omega_2 = \frac{(\alpha(\rho_2-\rho_1)+\rho_1)\omega_0}{\alpha(\rho_2-\rho_1)+\rho_1-2\rho_2}$.*
- *If $\omega_0 = 0$ and $\alpha_0 = 0$, then $\alpha = 0$.*
- *If $\omega_0 \neq 0$ and $\alpha_0 = 1$, then either $\alpha = 1$ or $\omega_2 = \frac{-(\alpha(\rho_2-\rho_1)+\rho_1)\omega_0}{-\alpha(\rho_2-\rho_1)+\rho_1}$ if $-\alpha(\rho_2 - \rho_1) + \rho_1 \neq 0$.*
- *If $\omega_0 = 0$ and $\alpha_0 = 1$, then either $\alpha = 1$ or $\alpha = \frac{\rho_1}{\rho_2-\rho_1}$ if $\rho_2 > 2\rho_1$.*

Proof : A state U in $\mathcal{S}(U_0)$ must fulfil the Rankine-Hugoniot condition

$$F(U) - F(U_0) = \sigma(U, U_0)(U - U_0), \tag{5.11}$$

which for the system (5.16) takes the form

$$\begin{cases} \frac{\alpha(1-\alpha)\omega}{\alpha(\rho_2-\rho_1)+\rho_1} - \frac{\alpha_0(1-\alpha_0)\omega_0}{\alpha_0(\rho_2-\rho_1)+\rho_1} = \sigma(U, U_0)(\alpha - \alpha_0), \\ \frac{\omega^2}{2(\rho_1-\rho_2)} - \frac{\omega_0^2}{2(\rho_1-\rho_2)} = \sigma(U, U_0)(\omega - \omega_0). \end{cases} \tag{5.12}$$

- If $\omega = \omega_0$, there always exists $\sigma(U, U_0)$ such that (5.12). This comes from the fact that the second equation is independent from α. The 1-shock family is made of states sharing the same values of ω which is consistent with the expression of the eigenvector $\vec{r}_1$ (equation 5.8).

- If $\omega \neq \omega_0$, the second equation of (5.12) implies $\sigma(U, U_0) = \frac{\omega+\omega_0}{2(\rho_1-\rho_2)}$, which yields in the first equation

$$\begin{aligned} &\frac{\alpha^2(\rho_2 - \rho_1) + \alpha(\rho_1 - 2\rho_2 + \alpha_0\rho_2 - \alpha_0\rho_1) + \alpha_0\rho_1}{\alpha(\rho_2 - \rho_1) + \rho_1}\omega \\ - \quad &\frac{\alpha_0^2(\rho_2 - \rho_1) + \alpha_0(\rho_1 - 2\rho_2 + \alpha\rho_2 - \alpha\rho_1) + \alpha\rho_1}{\alpha_0(\rho_2 - \rho_1) + \rho_1}\omega_0 = 0. \end{aligned} \tag{5.13}$$

- If $\alpha^2(\rho_2 - \rho_1) + \alpha(\rho_1 - 2\rho_2 + \alpha_0\rho_2 - \alpha_0\rho_1) + \alpha_0\rho_1 = 0$, (5.13) implies either $\omega_0 = 0$ or $\alpha = \alpha_0 \in \{0, 1\}$. Since $U_0 \in \mathcal{H}$, $\omega_0 = 0$ implies $\alpha_0 \in \{0, 1\}$. It is clear that $(\alpha_0 = 1, \omega_0 = 0)$ and all states $(\alpha = \frac{\rho_1}{\rho_2-\rho_1}, \omega \in \mathbb{R}^*)$ satisfy the equation (5.13) under the assumption that $\rho_2 > 2\rho_1$.
- If $\omega_0 \neq 0$ and $\alpha^2(\rho_2 - \rho_1) + \alpha(\rho_1 - 2\rho_2 + \alpha_0\rho_2 - \alpha_0\rho_1) + \alpha_0\rho_1 \neq 0$, we obtain an explicit equation of the 2-shock curves as stated in the theorem.

The shape of the shock curves can be seen on Figure 5.2.

□

Theorem 6 (Existence of rarefaction curves)
- *Any state $U_0 = (\alpha_0, \omega_0) \in \mathcal{H} \setminus \{(\alpha = 0, \omega = 0), (\alpha = 1, \omega = 0)\}$ belongs to two rarefaction curves, the 1-rarefaction curve (1-R) is described by the equation $\omega_1(\alpha) = \omega_0$ and the 2-rarefaction curve (2-R) is described by the equation*

$$\omega_2(\alpha) \quad = \quad \omega_0 \frac{\alpha(\rho_2 - \rho_1) + \rho_1}{\alpha_0(\rho_2 - \rho_1) + \rho_1} \left(\frac{\alpha}{\alpha_0}\right)^{\frac{\rho_2}{\rho_1-\rho_2}} \left(\frac{1-\alpha}{1-\alpha_0}\right)^{\frac{-\rho_1}{\rho_1-\rho_2}} \tag{5.14}$$

— *The state* $(\alpha = 0, \omega = 0)$ *belongs to a single rarefaction curve, the 2-rarefaction curve described by* $\alpha = 0$.

— *The state* $(\alpha = 1, \omega = 0)$ *belongs to all 2-rarefaction curves going through* $U_0 = (\alpha_0, \omega_0) \in \mathcal{H} \setminus \{(\alpha = 0, \omega = 0), (\alpha = 1, \omega = 0)\}$ *and described by (5.14). Moreover,* $(\alpha = 1, \omega = 0)$ *also belongs to the 2-rarefaction* $\alpha = 1$.

Proof : From the definition of Riemann invariants, $\mathcal{R}_1$ and $\mathcal{R}_2$ must satisfy

$$\frac{\partial \mathcal{R}_1}{\partial \alpha} = 0; \quad \alpha(1-\alpha)(\rho_1 - \rho_2)(\alpha(\rho_2 - \rho_1) + \rho_1)\frac{\partial \mathcal{R}_2}{\partial \alpha} + \rho_1\rho_2\omega\frac{\partial \mathcal{R}_2}{\partial \omega} = 0.$$

Since $\mathcal{R}_1$ is function of only ω, it is easy to obtain the equation of the 1-rarefaction curves.
Considering the Riemann invariant $\mathcal{R}_2$,

— if $\alpha \in (0, 1)$, we have

$$\frac{\partial \omega}{\partial \alpha} = \frac{\rho_1\rho_2\omega}{\alpha(1-\alpha)(\rho_1 - \rho_2)(\alpha(\rho_2 - \rho_1) + \rho_1)}. \tag{5.15}$$

Solving the linear ordinary differential equation (5.15), we obtain explicitly the equation of the rarefaction curves (5.14) in the theorem.

— if $\alpha \in \{0, 1\}$, then
  — either $\frac{\partial \mathcal{R}_2}{\partial \omega} = 0$, the rarefaction curves are $\alpha(\omega) = 0$ (or $\alpha(\omega) = 1$) corresponding to $\alpha_0 = 0$ (or $\alpha_0 = 1$),
  — or $\omega = 0$. However, only the state $(\alpha = 1, \omega = 0)$ belongs to all $\mathcal{R}_2$ described by (5.14) due to continuing property ($\lim_{\alpha \to 1} \omega_2(\alpha) = 0$, $\lim_{\alpha \to 0} \omega_2(\alpha) = \pm\infty$).

□

The structure of the rarefaction curves is illustrated on Figure 5.2.

5.2.4 Solution of the Riemann problem

We consider the Riemann problem for the conservative system (5.4) in the case $g = 0$ with a piecewise constant initial data :

$$\begin{aligned} &\partial_t U + \partial_x F(U) = 0 \\ &U_0(x) = \begin{cases} U_L(\alpha_L, \omega_L) & \text{if } x \leq 0, \\ U_R(\alpha_R, \omega_R) & \text{if } x > 0, \end{cases} \end{aligned} \tag{5.16}$$

where $U =^t (\alpha, \omega)$, $F(U)$ are defined in (5.5), and $U_L, U_R \in \mathcal{H}$. We start by stating and proving in section 5.2.4 existence and uniqueness of an admissible solution to (5.16) in Theorem 7. We then give in section 5.2.4 four important examples of non classical solutions to the Riemann problem in order to illustrate the proof of Theorem 7 and the unusual behaviour of the system (5.16) as well.

Main result

We intend to prove existence and uniqueness of an admissible solution. Due to the complex structure of the shock curves, there are numerous different cases to be considered. We first describe the structure of admissible solutions in the following lemma.

Lemma 1 *Assume that an admissible solution of the Riemann problem contains two adjacent waves which connect the left state* $U_L = (\alpha_L, \omega_L)$ *to the right state* $U_R = (\alpha_R, \omega_R)$ *through the intermediate state* $U_I = (\alpha_I, \omega_I)$. *Then, these two adjacent waves must be in different family (i.e. one wave from a 1-family and the other from a 2-family) at the exception that a 2-rarefaction may be followed by a 2-rarefaction.*
Moreover, if the two adjacent waves are a 1-wave followed by a 2-wave (resp. a 2-wave followed by a 1-wave), then the intermediate state satisfies $\omega_I = \omega_L \leq 0$ *(resp.* $\omega_I = \omega_R \geq 0$*). Therefore, the value of* ω *satisfies the maximum principle.*

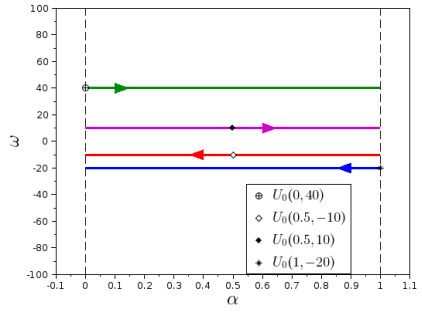

(a) 1-shock curves

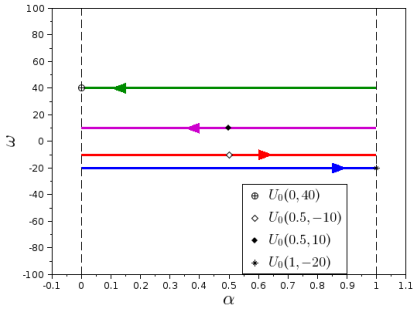

(b) 1-rarefaction curves

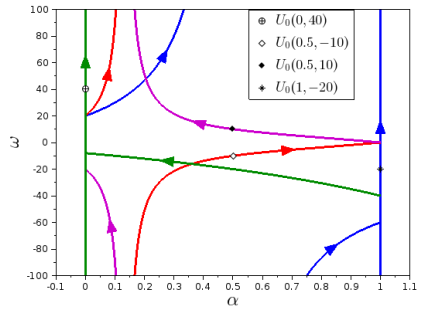

(c) 2-shock curves

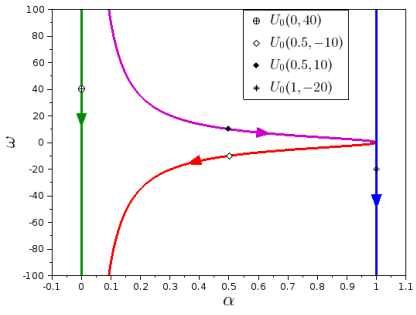

(d) 2-rarefaction curves

FIGURE 5.2 – Shock curves and Rarefaction curves. $U_0 = (0, 40)$: green. $U_0 = (0.5, -10)$: red. $U_0 = (0.5, 10)$: violet. $U_0 = (1, -20)$: blue.

Proof : This lemma is a direct consequence of the characterisation of k-shock curves and k-rarefaction curves (theorems 5 and 6) and of the speed order criterion. Assume first that two adjacent waves are two 1-shock waves connecting the left state $U_L = (\alpha_L, \omega_L)$ to the right state $U_R = (\alpha_R, \omega_R)$ through the intermediate state $U_I = (\alpha_I, \omega_I)$. A consequence of Theorem 5 is that $\omega_L = \omega_R = \omega_I$. From the first equation in (5.12), the speed of the first 1-shock and the second 1-shock is

$$\sigma_{1_1} = \frac{\omega_L}{\rho_1 - \rho_2}\left(1 - \frac{\rho_1\rho_2}{(\alpha_I(\rho_2 - \rho_1) + \rho_1)(\alpha_L(\rho_2 - \rho_1) + \rho_1)}\right), \text{ and} \tag{5.17}$$

$$\sigma_{1_2} = \frac{\omega_R}{\rho_1 - \rho_2}\left(1 - \frac{\rho_1\rho_2}{(\alpha_I(\rho_2 - \rho_1) + \rho_1)(\alpha_R(\rho_2 - \rho_1) + \rho_1)}\right). \tag{5.18}$$

Liu's criterion for both shocks gives $\alpha_R > \alpha_I > \alpha_L$ if $\omega_L = \omega_R = \omega_I > 0$ and $\alpha_R < \alpha_I < \alpha_L$ if $\omega_L = \omega_R = \omega_I < 0$, while the speed order criterion $\sigma_{1_1} < \sigma_{1_2}$ gives $\alpha_R < \alpha_L$ if $\omega_L = \omega_R = \omega_I > 0$ and $\alpha_R > \alpha_L$ if $\omega_L = \omega_R = \omega_I < 0$. Therefore, the admissible solutions of the Riemann problem do not admit two adjacent waves in the same 1-shock family.
The conclusion for the 1-rarefaction family and 2-shock family are completely the same while the conclusion for the 2-rarefaction family is an exception.
Since the two 2-rarefaction curves join at unique point $(\alpha = 1, \omega = 0)$, if two adjacent waves are two 2-rarefaction, then $\omega_L > 0 > \omega_R$. Such two 2-rarefaction satisfy the speed criterion although there exists only an intermediate point $(\alpha = 1, \omega = 0)$ (no intermediate constant state).
As for the second statement of the theorem, assume that the intermediate state $U_I = (\alpha_I, \omega_I)$ connects to the left state (resp. right state) by a 1-wave and connects to the right state (resp. the left state) by a 2-wave, due to the fact that the equation of 1-wave is that ω is constant, see theorem of existence of shock curves Theorem 5 and rarefaction curves Theorem 6, then $\omega_I = \omega_L$ (or $\omega_I = \omega_R$). In order to prove the sign property $\omega_I = \omega_L < 0$ in the case of a 1-wave followed by a 2-wave, let us notice that for the solution to be admissible, the speed of propagation of the 1-wave must be smaller than the one of the 2-wave. (5.9) thus imposes $\omega_I = \omega_L < 0$. Similarly, we also obtain the sign property $\omega_I = \omega_R > 0$ in the case of a 2-wave followed by a 1-wave.

□

Theorem 7 (Existence and uniqueness for the Riemann problem) *For any pair $U_L, U_R \in \mathcal{H}$, the Riemann problem admits a unique admissible solution $U(x,t) \in \mathcal{H}$ which depends continuously on U_L and U_R.*

Proof : Let $U_L = (\alpha_L, \omega_L) \neq U_R = (\alpha_R, \omega_R)$ be in $\mathcal{H}$. Assuming that $\rho_1 < \rho_2$, we find admissible solutions satisfying the initial data (5.16).
Case 1 : $\omega_L = \omega_R$. The solution is a single 1-wave. In particular, if $\omega_L = \omega_R = 0$ and $\alpha_L \neq \alpha_R$, such a 1-wave is the degenerate 1-shock.
Case 2 : $\omega_L > \omega_R$. An admissible solution will contain at least one 2-rarefaction (see Theorem 6 for the existence of the rarefaction curves which are illustrated in Figure 5.2). In detail, we consider two possibilities, $\omega_L\omega_R > 0$ or $\omega_L\omega_R \leq 0$.

- Case 2.1 : $\omega_L\omega_R > 0$. Without loss of generality, we assume that ω_L and ω_R are positive. From (5.9), an admissible solution is a 2-rarefaction followed by a 1-wave. In addition, the 2-rarefaction monotonic curve $\omega_2(\alpha)$ intersects the 1-wave curve, $\omega(\alpha) = \omega_R \neq 0$, at a unique point, see also Figure 5.2. The uniqueness of the admissible solution is thus obtained.
- Case 2.2 : $\omega_L \geq 0 \geq \omega_R$. Due to Lemma 1, the left state must connect to a 2-rarefaction and the right state does the same (otherwise it violates Lemma 1). This property then implies the uniqueness of the admissible solution whose structure depends on the values of α_L and α_R, there are three possibilities
  - If $\alpha_L \neq 0$ and $\alpha_R \neq 0$, the admissible solution is a 2-rarefaction followed by another 2-rarefaction. See Example 5.2.3 and Figures 5.4(a) and 5.4(c). In particular, if $(\alpha_L = 1, \omega_L = 0)$ or $(\alpha_R = 1, \omega_R = 0)$, the solution is a single 2-rarefaction.
  - If $\alpha_L = \alpha_R = 0$, the admissible solution is a single 2-rarefaction due to existence of a 2-rarefaction which goes through $\alpha = 0$, see Theorem 6.
  - If ($\alpha_L = 0$ and $\alpha_R \neq 0$) or ($\alpha_L \neq 0$ and $\alpha_R = 0$), due to Theorem 6 the 2-rarefaction departing from the left state and the one arriving at the right state neither coincide nor intersect. The admissible solution therefore contains more than two waves. The unique solution which satisfies the speed criterion is a 2-rarefaction attached to a degenerate 1-shock and then followed by another 2-rarefaction. See Example 5.2.4 and Figures 5.4(b) and 5.4(d).

Case 3 : $\omega_L < \omega_R$. This case is more technical and the uniqueness of the admissible solution has to be carefully studied. An admissible solution in this case contains a 2-shock, since ω must increase from ω_L to ω_R, see Figure 5.2 for the shock and rarefaction curves.
We introduce a new variable

$$\beta = \alpha(\rho_2 - \rho_1) + \rho_1. \tag{5.19}$$

First of all, we look for admissible solutions whose structure is a 2-shock followed by a 1-wave with U^* as intermediate state. The necessary condition $\omega^* = \omega_R \geq 0$ follows from Lemma 1. In order to select an admissible solution, we introduce the speed order criterion in this specific case, which is

$$\sigma_2 \leq \lambda_1(U^*) \text{ if the solution is a 2-shock followed by a 1-rarefaction,} \tag{5.20}$$

$$\text{or} \quad \sigma_2 < \sigma_1 \quad \text{if the solution is a 2-shock followed by a 1-shock,} \tag{5.21}$$

where $\sigma_2 = \frac{\omega_L+\omega_R}{2(\rho_1-\rho_2)}$, $\sigma_1 = \frac{\omega_R}{\rho_1-\rho_2}\left(1 - \frac{\rho_1\rho_2}{\beta^*\beta_R}\right)$, $U^* = (\alpha^*, \omega_R)$ such that $\alpha^* = \frac{\rho_1-\beta^*}{\rho_1-\rho_2}$. For simplicity, we can rewrite the inequalities (5.20) as $\beta^* \leq \sqrt{\frac{2\rho_1\rho_2\omega_R}{\omega_R-\omega_L}}$ and (5.21) as $\beta^* \leq \frac{2\rho_1\rho_2\omega_R}{\beta_R(\omega_R-\omega_L)}$.
Replacing α by $\frac{\beta-\rho_1}{\rho_2-\rho_1}$ in the 2-shock curve equation in Theorem 5 yields after some calculations that all states (α, ω_R) which are connected to U_L by a 2-shock satisfy the following quadratic equation

$$\beta_L(\omega_L - \omega_R)\beta^2 - (\beta_L(\omega_L - \omega_R)(2(\rho_1 + \rho_2) - \beta_L) - 2\rho_1\rho_2\omega_L)\,\beta - 2\rho_1\rho_2\beta_L\omega_R = 0. \tag{5.22}$$

Let $G(\beta_L, \beta)$ be the left hand side of the equation (5.22), then

$$G(\beta_L, \rho_1) = -\rho_1(\beta_L - \rho_1)\,(\beta_L(\omega_R - \omega_L) + 2\rho_2\omega_L) \text{ and} \tag{5.23}$$

$$G(\beta_L, \rho_2) = \rho_2(\rho_2 - \beta_L)\,(\beta_L(\omega_R - \omega_L) + 2\rho_1\omega_L)\,. \tag{5.24}$$

Recall that $\omega_L < \omega_R$, the concave quadratic function $G(\beta_L, \beta)$ may have no solution or more than one solution. We look for a condition on ω_R such that the equation (5.22) has a non-negative solution $\alpha^* \in [0,1]$, namely $\beta^* \in [\rho_1, \rho_2]$, or equivalently $G(\beta_L, \rho_1)G(\beta_L, \rho_2) \leq 0$ because $G(\beta_L, \rho_1)$ and $G(\beta_L, \rho_2)$ can not be negative at the same time. By considering a variation of α_L, we get different cases.

— Case 3.1 If $\alpha_L \in \{0,1\}$, then $G(\beta_L,\rho_1)G(\beta_L,\rho_2)=0$ and the equation (5.22) may have two solutions with $\beta^* \in [\rho_1,\rho_2]$. Using the speed order criterion, we obtain :
  — Case 3.1.1 If $\alpha_L = 0$, i.e. $\beta_L = \rho_1$ the two potential solutions of (5.22) are $\beta^* = \rho_1$ and $\beta^* = \frac{2\rho_2\omega_R}{\omega_R-\omega_L}$. However $\frac{2\rho_2\omega_R}{\omega_R-\omega_L}$ violates the criteria (5.20) and (5.21). Therefore, only $\beta^* = \rho_1$ is acceptable and the admissible solution is a 2-shock followed by a 1-shock (not a 1-rarefaction) since $\omega_I = \omega_R > 0$ (see 1-shock curves and 1-rarefaction curves on Figure 5.2). Such an admissible solution satisfies the criterion (5.21) if and only if $\beta_R \le \frac{2\rho_2\omega_R}{\omega_R-\omega_L}$.
  — Case 3.1.2 If $\alpha_L = 1$ and $\beta_L \ge \frac{-2\rho_2\omega_L}{\omega_R-\omega_L}$, (which is equivalent to $\omega_R \ge -\omega_L$ and also to $\frac{2\rho_1\omega_R}{\omega_R-\omega_L} \ge \rho_1$), then there exists a unique solution $\beta^* = \min\{\rho_2, \frac{2\rho_1\omega_R}{\omega_R-\omega_L}\}$ satisfying the criteria (5.20) and (5.21).

— Case 3.2 If $\alpha_L \in (0,1)$, or equivalently $\beta_L \in (\rho_1,\rho_2)$, then it is obvious that $G(\beta_L,\rho_1)$ and $G(\beta_L,\rho_2)$ can not be non-positive at the same time, the equation (5.22) therefore has at most one solution $\beta^* \in [\rho_1,\rho_2]$.
The first possibility is $G(\beta_L,\rho_1) \le 0$ and $G(\beta_L,\rho_2) \ge 0$, or equivalently

$$\beta_L \ge \frac{-2\rho_2\omega_L}{\omega_R-\omega_L}, \tag{5.25}$$

i.e. $G(\beta_L,\beta) \ge 0$ implies $\beta \in [\beta^*,+\infty)$.
The second possibility is $G(\beta_L,\rho_1) \ge 0$ and $G(\beta_L,\rho_2) \le 0$, or equivalently

$$\beta_L \le \frac{-2\rho_1\omega_L}{\omega_R-\omega_L}. \tag{5.26}$$

i.e. $G(\beta_L,\beta) \ge 0$ implies $\beta \in (-\infty,\beta^*]$.
As long as the condition (5.25) or (5.26) is satisfied, the speed order criterion (5.20) and (5.21) will help us to select an admissible solution.
  — Case 3.2.1 Assume first that the admissible solution is a 2-shock followed by a 1-rarefaction and use the speed order criterion (5.20). We denote $H(\beta_L) = G\left(\beta_L, \sqrt{\frac{2\rho_1\rho_2\omega_R}{\omega_R-\omega_L}}\right)$ and first prove that $H(\beta_L) > 0$ for all $\beta_L \in (\rho_1,\rho_2)$. Writing $H(\beta_L)$ explicitly,

$$H(\beta_L) = -4\rho_1\rho_2\beta_L\omega_R + (\beta_L(\omega_R-\omega_L)(2(\rho_1+\rho_2)-\beta_L) + 2\rho_1\rho_2\omega_L)\sqrt{\frac{2\rho_1\rho_2\omega_R}{\omega_R-\omega_L}}.$$

Calculating and evaluating $H(\rho_1)$,

$$\begin{aligned} H(\rho_1) &= -4\rho_1^2\rho_2\omega_R + \rho_1\left(\rho_1(\omega_R-\omega_L)+2\rho_2\omega_R\right)\sqrt{\frac{2\rho_1\rho_2\omega_R}{\omega_R-\omega_L}} \\ &\ge -4\rho_1^2\rho_2\omega_R + 2\rho_1\sqrt{2\rho_1\rho_2\omega_R(\omega_R-\omega_L)}\sqrt{\frac{2\rho_1\rho_2\omega_R}{\omega_R-\omega_L}} \\ &= 0. \end{aligned} \tag{5.27}$$

The inequality (5.27) is obtained by the Cauchy's inequality for two non-negative numbers $\rho_1(\omega_R-\omega_L)$ and $2\rho_2\omega_R$. The result $H(\rho_2) \ge 0$ is obtained similarly. Moreover, considering β_L as a variable of the quadratic function $H(\beta_L)$ whose highest order's coefficient is negative and both $H(\rho_1)$ and $H(\rho_2)$ are non-negative, we achieve $H(\beta_L) > 0$ for all $\beta_L \in (\rho_1,\rho_2)$. This result shows that the condition (5.25) satisfies the criterion (5.20) (since $G\left(\beta_L, \sqrt{\frac{2\rho_1\rho_2\omega_R}{\omega_R-\omega_L}}\right) = H(\beta_L)$ and $G(\beta_L,\beta) \ge 0$ implies $\beta \in [\beta^*,+\infty)$, so that $\beta^* \le \sqrt{\frac{2\rho_1\rho_2\omega_R}{\omega_R-\omega_L}}$) while the condition (5.26) is impossible to satisfy (since it implies $\beta^* \ge \sqrt{\frac{2\rho_1\rho_2\omega_R}{\omega_R-\omega_L}}$ because $G(\beta_L,\beta) \ge 0$ implies $\beta \in (-\infty,\beta^*]$ in this case).
  — Case 3.2.2 Assume that the admissible solution is a 2-shock followed by a 1-shock and use the speed order criterion (5.21). If $\frac{2\rho_1\rho_2\omega_R}{\beta_R(\omega_R-\omega_L)} > \rho_2$, the criterion (5.21) is always satisfied. So we will merely consider $\frac{2\rho_1\rho_2\omega_R}{\beta_R(\omega_R-\omega_L)} \le \rho_2$, where we define $M(\beta_L) = G\left(\beta_L, \frac{2\omega_R\rho_1\rho_2}{\beta_R(\omega_R-\omega_L)}\right)$. Rewrite $M(\beta_L)$ as the following

$$M(\beta_L) = \frac{2\rho_1\rho_2\omega_R}{\beta_R^2(\omega_R-\omega_L)}\left((\beta_R\omega_L-\beta_L\omega_R)+\beta_L\beta_R(\omega_R-\omega_L)(2\rho_1+2\rho_2-\beta_L-\beta_R)\right).$$

We compute

$$M(\rho_1) = \frac{2\rho_1\rho_2\omega_R}{\beta_R}(\rho_1-\beta_R)\left(\rho_1-\frac{2\rho_1\rho_2\omega_R}{\beta_R(\omega_R-\omega_L)}\right),$$
$$M(\rho_2) = \frac{2\rho_1\rho_2\omega_R}{\beta_R}(\rho_2-\beta_R)\left(\rho_2-\frac{2\rho_1\rho_2\omega_R}{\beta_R(\omega_R-\omega_L)}\right).$$

The condition (5.25) implies $M(\rho_1)\geq 0$ and $M(\rho_2)\geq 0$, and then obviously $M(\beta_L)>0$, $\forall\beta_L\in(\rho_1,\rho_2)$ (since the second order polynomial $\beta_L\to M(\beta_L)$ is concave), this result satisfies the criterion (5.21).
On the other hand, the condition (5.26) violates the criterion (5.21) as long as we assume the solution has more than one wave. By the continuity, this solution is not admitted.

We summarize the structure of the admissible solution according to the initial data.
— If $\alpha_L\in(0,1]$ and $\beta_L\geq\frac{-2\rho_2\omega_L}{\omega_R-\omega_L}$, the solution is a 2-shock followed by a 1-wave.

— If $\alpha_L=0$ and $\beta_R\leq\frac{2\rho_2\omega_R}{\omega_R-\omega_L}$, the solution is a 2-shock followed by a 1-shock ($\alpha^*=0$).
Similarly, we obtain the following results
— If $\alpha_R\in(0,1]$ and $\beta_R\geq\frac{2\rho_2\omega_R}{\omega_R-\omega_L}$, the solution is a 1-wave followed by a 2-shock.

— If $\alpha_R=0$ and $\beta_L\leq\frac{-2\rho_2\omega_L}{\omega_R-\omega_L}$, the solution is a 1-shock followed by a 2-shock ($\alpha^*=0$).
Before continuing the proof, we can conclude that if $\alpha_L\neq 0$ and $\alpha_R\neq 0$, the solution consisting of a 2-shock (resp. 1-wave) followed by a 1-wave (resp. a 2-shock) is admissible if $\beta_L\geq\frac{-2\rho_2\omega_L}{\omega_R-\omega_L}$ (resp. $\beta_R\geq\frac{2\rho_2\omega_R}{\omega_R-\omega_L}$).
The rest of our proof considers the initial data which are not studied above, i.e. $\alpha_L\alpha_R\neq 0$ and $\beta_L<\frac{-2\rho_2\omega_L}{\omega_R-\omega_L}$ and $\beta_R<\frac{2\rho_2\omega_R}{\omega_R-\omega_L}$. According to Lemma 1, an admissible solution must be a 1-wave followed by a 2-shock connected to another 1-wave. Let us denote the two intermediate states ordered from the left to the right by $U^*(\alpha^*,\omega_L)$ and $U^{**}(\alpha^{**},\omega_R)$.
— If $\alpha^*\neq 0$ and $\alpha^{**}\neq 0$, due to the previous results a 1-wave followed by a 2-shock is admissible if $\beta^{**}\geq\frac{2\rho_2\omega_R}{\omega_R-\omega_L}$ and this 2-shock followed by another 1-wave is admissible if $\beta^*\geq\frac{-2\rho_2\omega_L}{\omega_R-\omega_L}$. Both $\beta^{**}\geq\frac{2\rho_2\omega_R}{\omega_R-\omega_L}$ and $\beta^*\geq\frac{-2\rho_2\omega_L}{\omega_R-\omega_L}$ are satisfied if and only if $\omega_L=-\omega_R$ and $\beta^*=\beta^{**}=\rho_2$, this condition however violates the speed order criterion.
— If ($\alpha^*\neq 0$ and $\alpha^{**}=0$) or ($\alpha^*=0$ and $\alpha^{**}\neq 0$), Theorem 5 shows that it is impossible.
— $\alpha^*=\alpha^{**}=0$ is admissible, this solution satisfies all criteria of speed order. See Figure 5.3(b) for the construction of such an admissible solution. An example is performed in Example 5.2.5, see Figure 5.5(a) and 5.5(c).

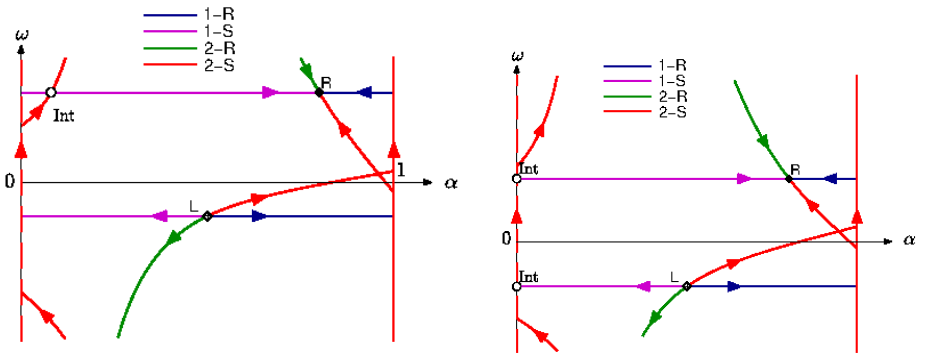

(a) (b)

FIGURE 5.3 – The admissible solution 2-shock 1-shock Figure 5.3(a), 1-shock 2-shock 1-shock Figure 5.3(b).

□

We would like to remark that an admissible solution of a Riemann problem may admit a 2-shock wave which connects a left state which is on a branch of a hyperbola to a right state located on the

other branch, see Figure 5.3(a). In the following section, this 2-shock will be called a **non classical shock wave**. It turns out that such a non classical shock wave is not easily captured by some classical numerical methods.

Key examples and important comments

The first three Riemann problems (Example 5.2.3,5.2.4,5.2.5) we present do not give rise to classical weak solution made of two waves of different families while the last one (Example 5.2.6) produces a non classical shock wave. The first Riemann problem gives rise two rarefactions of the 2-family, the second one leads to three waves (a 2-wave followed by and attached to a 1-wave followed by a 2-wave) and the third one produces a pure phase ($\alpha = 0$) starting from a mixture and contains three shocks. It is interesting to notice that in the third Riemann problem (Example 5.2.5) the value of the velocity of the vanishing phase does not necessarily equal the one of the non vanishing phase. Finally, the last Riemann problem illustrates an admissible solution consisting in two waves of different families whose one is a non classical wave.

Example 5.2.3 *The configuration $\alpha_L = \alpha_R = 0.5$, $\omega_L = -\omega_R = 3$ generates a pure gas intermediate value $U^* = (1, 0)$. The admissible solution consists of two rarefaction waves. See Figure 5.4(a) and Figure 5.4(c).*

Example 5.2.4 *The configuration $\alpha_L = 0$, $\alpha_R > 0$, $\omega_L > 0 > \omega_R$ is an example where the solution is a 2-rarefaction touching the degenerate 1-shock followed by another 2-rarefaction such that $\lambda_2(U^*) = \lambda_2(U^{**}) = 0$ and the speed of degenerate 1-shock is also zero, where $U^* = (0, 0)$, $U^{**} = (1, 0)$ are the intermediate values. See Figure 5.4(b), 5.4(d).*

Example 5.2.5 *The configuration $\alpha_L = \alpha_R = 0.5$, $\omega_L = -\omega_R = -5$ generates a pure liquid and the solution consists in three shocks (a 1-shock connects to 2-shock followed by another 1-shock). See Figure 5.5(a)and 5.5(c).*

Example 5.2.6 *The configuration $\alpha_L = 0.9$, $\alpha_R = 0.3$, $\omega_L = -3$, $\omega_R = 5$ generates a non classical shock and the solution consists in two shocks (a non classical 2-shock connects to a 1-shock). See Figure 5.5(b) and 5.5(d).*

5.2.5 Studying the Cauchy problem

We consider the Cauchy problem of the system (5.4) with the initial data

$$U(x, 0) = \bar{U}(x). \tag{5.28}$$

The well-known approaches to studying the general Cauchy problem for hyperbolic conservation laws are the viscosity method, Glimm method and front tracking method. These methods apply to $n \times n$ system, see the books [GR96], [Ser99], [Bre00], for instance. The global existence to the weak solution of the Cauchy problem in general requires a small total variation of the initial data, i.e almost constant initial data. Considering some particular 2 systems, many authors proved the existence of solution for the large initial data, see [Tem81 ; AM04] for example. In our case, the Riemann problem admits an admissible solution even when the initial data is far apart, this fact motivates us to study the Cauchy problem for the incompressible model by front tracking method. We refer the reader to [Bre00] or [HR00] for the details of the front tracking method. The main idea of such a method lies on compactness property, i.e. a sequence of weak solutions U_ε is constructed such that their total variation is bounded (TVD property), then Helly's theorem implies that there exists a subsequence of U_ε converging to a function U. Moreover, U is a weak solution of the Cauchy problem by a direct method calculation using test function $\mathcal{C}_0^\infty$.

The existence of global weak solutions following the front tracking method is proved step by step solving the Riemann problems. The initial data is firstly approximated by piecewise constant function $U(0, x)$ such that

$$|\bar{U}(x) - U(0, x)| < \varepsilon, \tag{5.29}$$

for some small $\varepsilon > 0$. Then, following the general front tracking method, we consider an *ε-approximate front tracking solution* which is also a piece-wise function approximating the solutions of all Riemann

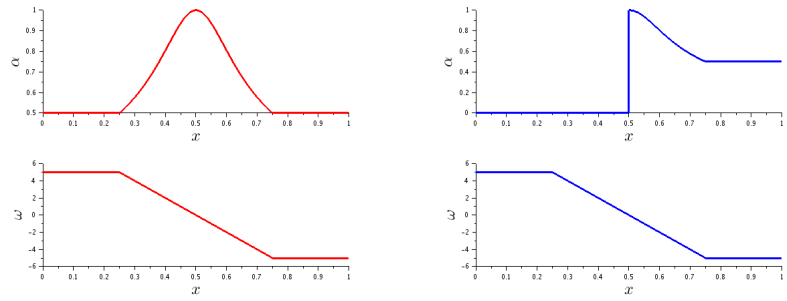

(a) α, ω

(b) α, ω

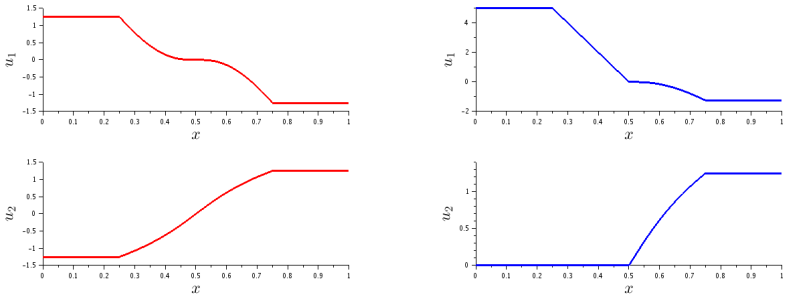

(c) u_1, u_2

(d) u_1, u_2

FIGURE 5.4 – Example 5.2.3 : 2-rarefaction 2-rarefaction, Figure 5.4(a) and 5.4(c). Example 5.2.4 : 2-rarefaction 1-shock 2-rarefaction, Figure 5.4(b) and 5.4(d).

problems. We can consider in our case that two states of ε-approximate front tracking solution are always connected by simple waves (shock or rarefaction waves). To have a full definition of an ε-approximate front tracking solution, one may refer to [Bre00] for details. The main part of our work here is focusing on evaluating outgoing waves of two interacting waves. More precisely, we classify the different cases of the two interacting waves, then compute or predict the total strength of outgoing waves. We note that our system is in fact not strictly hyperbolic and the fields are neither GNL nor LD, finding a suitable condition to have a total variation bounded (TVD) is the key part of our work.
Assuming that the two approaching wave-fronts consist of left, middle, right states labeled by (α_L, ω_L), (α_M, ω_M), (α_R, ω_R). Let us denote σ', σ'' the strength and v', v'' the speed of these two wave-fronts, such that $v' > v''$. If the two approaching wave-fronts are in the same 1-family, i.e. ω is constant, the outgoing wave is either a 1-shock or a 1-rarefaction, hence the total strength of the outgoing wave never increases. This property is also obvious if there is a 1-rarefaction or a 2-rarefaction but not a 2-shock in two approaching wave-fronts, readers can read Appendix 5.5.5 for more details. The cases of two-approaching wave fronts where the total strength of the outgoing waves may increase are as the following

— 1-shock 2-shock when ω is positive (or 2-shock 1-shock when ω is negative).
— there is a 2-shock and ω change sign, i.e $\omega_L < 0 < \omega_R$.

We consider the first case, when the two incoming waves are 1-shock and 2-shock, such that $0 < \omega_L < \omega_R$. For the Riemann problem where the initial data is (α_L, ω_L) and (α_R, ω_R), the outgoing waves are 2-shock followed by a 1-wave. Let us denote σ_2, and σ_1 the strength of these outgoing waves. If the 1-wave is a 1-rarefaction, then it is easy to see that $\sigma_1 + \sigma_2 < \sigma' + \sigma''$. Therefore, our interest focuses on the case where the 1-wave is a 1-shock. In this case, assuming that $U_I = (\alpha_I, \omega_I)$ is the intermediate state of the outgoing waves. The total new strength

$$\begin{aligned} \sigma_2 + \sigma_1 &= |\omega_R - \omega_L| + |\alpha_L - \alpha_I| + |\alpha_R - \alpha_I| \\ &= (\omega_R - \omega_L) + \alpha_L + \alpha_R - 2\alpha_I, \end{aligned}$$

can be compared to the total strength of the incoming waves

$$\begin{aligned} \sigma' + \sigma'' &= |\omega_R - \omega_L| + |\alpha_L - \alpha_M| + |\alpha_R - \alpha_M| \\ &= (\omega_R - \omega_L) - \alpha_L - \alpha_R + 2\alpha_M, \end{aligned}$$

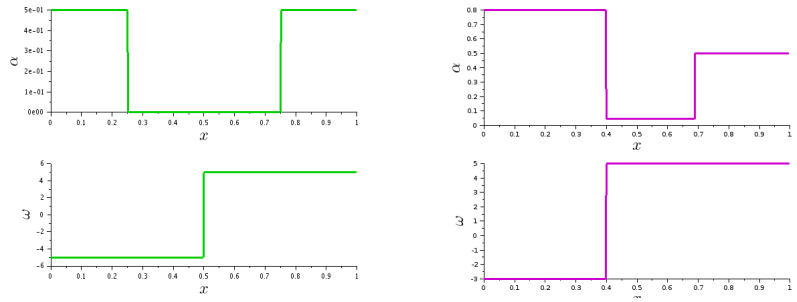

(a) α, ω

(b) α, ω

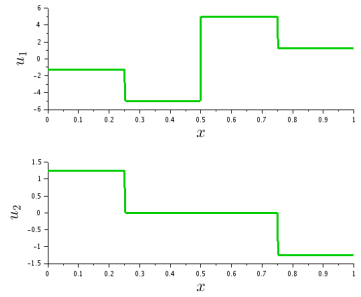

(c) u_1, u_2

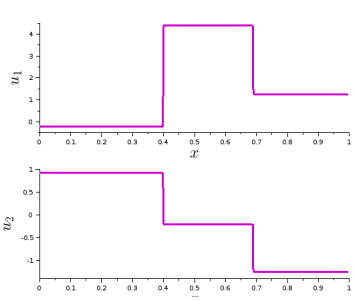

(d) u_1, u_2

FIGURE 5.5 – Example 5.2.5 : 1-shock 2-shock 1-shock, Figure 5.5(a) and 5.5(c) ; Example 5.2.6 : 2-rarefaction 1-shock 2-rarefaction, Figure 5.5(b) and 5.5(d).

The variation of the total strength is

$$\Delta\sigma = (\sigma_1 + \sigma_2) - (\sigma' + \sigma'') = 2(\alpha_R + \alpha_L - \alpha_M - \alpha_I).$$

Because α is in fact bounded, $\Delta\sigma$ can not increase to infinity. However, it is not enough to deduce that the total strength of all Riemann problems are bounded in global time. What we would like is to obtain is that $\Delta\sigma$ is bounded globally. From the equation of 2-shock curve, we get

$$\begin{aligned} \beta_M(\omega_L - \omega_R)\beta_R^2 - \left(\beta_M(\omega_L - \omega_R)(2\rho_1 + 2\rho_2 - \beta_M) - 2\rho_1\rho_2\omega_L\right)\beta_R - 2\rho_1\rho_2\beta_M\omega_R &= 0, \\ \beta_L(\omega_L - \omega_R)\beta_I^2 - \left(\beta_L(\omega_L - \omega_R)(2\rho_1 + 2\rho_2 - \beta_L) - 2\rho_1\rho_2\omega_L\right)\beta_I - 2\rho_1\rho_2\beta_L\omega_R &= 0. \end{aligned}$$

A simple calculation from two equations above gives us

$$\Delta\sigma = \frac{\Delta\omega_{RL}}{\omega_R}\Delta\beta_{RL}, \tag{5.30}$$

where $\Delta\omega_{RL} = \omega_R - \omega_L > 0$ and

$$\Delta\beta_{RL} = \frac{\beta_L\beta_I(\beta_L + \beta_I) - \beta_M\beta_R(\beta_R + \beta_M) + 2(\rho_1 + \rho_2)(\beta_M\beta_R - \beta_L\beta_I) + 2\rho_1\rho_2(\beta_R - \beta_I)}{2\rho_1\rho_2(\rho_2 - \rho_1)}.$$

If we impose that

$$\left\{\frac{1}{|\omega|} : (\alpha, \omega) \in U_0, \alpha \in (0,1)\right\} < \mathcal{C}, \tag{5.31}$$

where $\mathcal{C}$ is some constant then

$$\Delta\sigma = \mathcal{O}(1)\Delta\omega_{RL}\Delta\beta_{RL}, \tag{5.32}$$

where $\mathcal{O}(1)$ denotes some bounded function.The relation actually doesn't depend on time. In fact β_{RL} may be positive (i.e. TVD increases) or negative (i.e. TVD descreases). In general, we have not found a suitable condition for the large initial data so that the TVD property is rigorously obtained. Finding such a condition is a perspective of our works.

Although we can not prove a general result for the Cauchy problem for the incompressible model, we have proved that the total variation of the admissible solution in the next time step do not increase except that the interacting waves are 1-shock 2-shock when ω is positive (or 2-shock 1-shock when ω is negative), 2-shock 2-wave (when ω changes sign) may increase the total variation. These cases may increase the total variation. It implies that if the initial condition does not give rise a 2-shock, then we get TVD, $\omega(t=0)$ satisfying $\omega_L > \omega_R$ is an example.

5.3 Numerical study

We now investigate the numerical simulation of the system (5.4) and show that the basic Roe scheme fails to capture the expected dynamics whereas the Godunov scheme and the Roe scheme with a Harten type correction capture the analytic solution. However in the non classical shock wave (corresponding to a passage through the domain $\mathcal{H}_+$ and $\mathcal{H}_-$), both of these schemes show oscillations. We then extend to the present setting an in-cell discontinuous reconstruction method, see in [Lag04], [DL01], [AC15], [Bou+08], [CMG14], [Agu15] and references therein, which significantly improves the numerical result in this case.
We consider a uniform mesh of the computational domain $[0,1]$ whose N cells are centered at x_i, $i=1,\dots,N$. The space step $\Delta x = x_i - x_{i-1}$ is constant whereas the time step $\Delta t(U^n) > 0$ depends on the discrete field $U^n = (U_i^n)_{i=1,\dots,N}$ which approximates the exact solution $U(x,t)$ at cells i and time $t^n = \sum_{k=0}^{n-1} \Delta t(U^k)$. The time step should satisfy the following CFL condition in order to ensure the stability of the explicit schemes : $\Delta t \leq \frac{\Delta x}{\max_i\{\lambda_1(U_i,U_{i+1}),\lambda_2(U_i,U_{i+1})\}}$, where $\lambda_k(U_i,U_{i+1})$ is the largest value of $|\lambda_k|$ on the path connecting U_i to U_{i+1} using the rarefactions and admissible shock waves computed in Theorem 5 and 6. We point out that $\lambda_k(U_i,U_{i+1})$ may be different from $|\lambda_k(U_i)|$ and $|\lambda_k(U_{i+1})|$ because the characteristic fields are non genuinely nonlinear. Denote U^* intermediate states connecting the left state U_i to the right state U_{i+1} in the problem de Riemann, then

$$\lambda_k(U_i,U_{i+1}) = \max_{U^*}\{|\lambda_k(U_i)|, |\lambda_k(U_{i+1})|, |\lambda_k(U^*)|\}, \quad k=1,2. \tag{5.33}$$

We consider conservative finite volume schemes in the following explicit form :

$$U_i^{n+1} = U_i^n - \frac{\Delta t}{\Delta x}\left(\Phi_{i+1/2}^n - \Phi_{i-1/2}^n\right), \tag{5.34}$$

where $\Phi_{i+1/2}^n$ is the numerical flux function at the interface between cells i and $i+1$, and at time t^n. We compute the numerical flux $\Phi_{i+1/2}^n$ using one of the following strategy.

5.3.1 Godunov scheme

$$\Phi_{i+1/2}^n = \mathbf{F}_{j+1/2}^{\mathrm{God}} = F(U^*(U_i^n, U_{i+1}^n)),$$

where $U^*(U_i^n, U_{i+1}^n))$ is the value taken by the solution of the Riemann problem between the left state U_i^n and the right state U_{i+1}^n at the interface.

5.3.2 Roe scheme with a Harten type correction

$$\Phi_{i+1/2}^n = \mathbf{F}_{j+1/2}^{\mathrm{Har}} = \frac{F(U_i^n) + F(U_{i+1}^n)}{2} \quad - \quad \left(|A^{Roe}(U_i^n, U_{i+1}^n)| + \mathrm{har}_{i,i+1}^n \ \mathrm{Id}\right) \cdot \frac{\Delta U_{i+1/2}}{2},$$

where $\Delta U_{i+1/2} = U_{i+1}^n - U_i^n$, $A^{Roe}(U_i^n, U_{i+1}^n)$ is the Roe matrix, (see the Appendix for its expression), and $\mathrm{har}_{i,i+1}^n = C\max\left(|\lambda_1(U_i^n) - \lambda_1(U_{i+1}^n)|, |\lambda_2(U_i^n) - \lambda_2(U_{i+1}^n)|\right)$. If $C=0$ we recover the standard Roe scheme. However it is well-known that the Roe scheme may capture non admissible solutions (see [Har83]). Hence we used a constant value $C = \frac{1}{5}$ to include a Harten type entropic correction in the Roe scheme.

5.3.3 Reconstruction scheme

In [Lag04] and [DL01], Després and Lagoutière proposed a non-dissipative scheme which bases on an in-cell discontinuous reconstruction of the solution for scalar equations. We also refer the reader to [Bou+08], [CMG14] for the computation of non-classical shocks with such an approach. For the system case, we refer the reader to [AC15], [Agu15] and references therein for more details. One major advantage of this scheme is to capture precisely classical and non classical shock waves, a challenging point in our model owing to non classical shock waves. We do not intend to mention the details of the reconstruction method. Instead, we present the main ideas of the method and summarize the computation of the numerical flux function. In particular, considering our system, the unknown variables is $U = (\alpha, \omega)$ but only α varies in a 1-shock, whereas the 2-shock corresponds to the case where both α and ω vary at the jump. Numerical methods in general capture well the shock when only one of the two variables varies, and show difficulties in the cases where the two variables vary at the jump, especially in the case of the non classical 2-shock ie when the two states located on different branches of a hyperbola. Therefore, we will develop the reconstruction corresponding to this specific configuration. Let us denote $\mathrm{RP}(U_{j-1}, U_{j+1})$ the Riemann problem associated with the left and right initial states U_{j-1} and U_{j+1}. If the solution of $\mathrm{RP}(U_{j-1}, U_{j+1})$ contains an admissible discontinuity between the left state $U_j^- = \left(\alpha_j^-\left(U_{j-1}, U_{j+1}\right), \omega_j^-\left(U_{j-1}, U_{j+1}\right)\right)$ and right state $U_j^+ = \left(\alpha_j^+\left(U_{j-1}, U_{j+1}\right), \omega_j^+\left(U_{j-1}, U_{j+1}\right)\right)$ such that $\alpha_j^- \neq \alpha_j^+$ and $\omega_j^- \neq \omega_j^+$, we propose a discontinuous in-cell reconstruction between U_j^- and U_j^+ in cell j as shown on Figure 5.6. Otherwise, $U_j^- = U_j^+ = U_j$. It is important to note that the discontinuity is not necessarily located at the same place for both variables α and ω. We thus define the coefficient θ_j^α (resp. θ_j^ω) such that the distance from $x_{j-1/2}$ to the discontinuity of the variable α (resp. variable ω) is $\theta_j^\alpha \Delta x$ (resp. $\theta_j^\omega \Delta x$), see Figure 5.6.

— We would first like to locate the discontinuities of α and ω in a way that yields a conservative scheme. θ_j^α and θ_j^ω must satisfy

$$\begin{cases} \theta_j^\alpha \alpha_j^- + \left(1-\theta_j^\alpha\right)\alpha_j^+ = \alpha_j^n, \\ \theta_j^\omega \omega_j^- + \left(1-\theta_j^\omega\right)\omega_j^+ = \omega_j^n. \end{cases}$$

— If $\theta_j^\alpha \notin [0,1]$: No reconstruction for α i.e.

$$\alpha_j^+ = \alpha_j^- = \alpha_j^n.$$

— If $\theta_j^\omega \notin [0.1]$: No reconstruction for ω i.e.

$$\omega_j^+ = \omega_j^- = \omega_j^n.$$

— If $\theta_j^\alpha \in [0,1]$ (and/or $\theta_j^\omega \in [0,1]$), reconstructing for α (and/or ω).

— Let us denote σ_j the exact value of the speed of propagation of the discontinuity $\left(U_j^-, U_j^+\right)$. We then compute the numerical flux function between t^n and $t^n + \Delta t$ by using the reconstructed discontinuities rather than the average values. More precisely, if $\sigma_j > 0$ (resp. $\sigma_j < 0$), we are going to calculate the flux at interface $j+1/2$ (resp. $j-1/2$) by considering that the numerical flux equals the exact flux evaluated on the right value U_j^+, until the corresponding discontinuity reaches the interface $j+1/2$ (resp. $j-1/2$), and the exact flux evaluated on the left value U_j^- afterwards. Therefore, such a flux function will be computed relying on the speed of shock propagation σ_j of the reconstructed discontinuity and on the times $\Delta t_{j+1/2}^\alpha, \Delta t_{j+1/2}^\omega$ needed by this discontinuity to reach the interface $j \pm 1/2$ depending on the sign of σ_j.
More explicitely :

— If $\sigma_j > 0$. Denote $\Delta t_{j+1/2}^\omega = \frac{(1-\theta_j^\omega)\Delta x}{\sigma_j}$, $\Delta t_{j+1/2}^\alpha = \frac{\left(1-\theta_j^\alpha\right)\Delta x}{\sigma_j}$. The numerical flux function $\mathbf{F}_{j+1/2}^{\mathrm{Rec}}$ is computed by using U_j^- and U_j^+.

— If $\theta_j^\alpha \leq \theta_j^\omega$, then

$$\begin{aligned} \Delta t \mathbf{F}_{j+/2}^{\mathrm{Rec}} &= \min\left(\Delta t_{j+1/2}^\omega, \Delta t\right) F(U_j^+) + \max\left(\Delta t - \Delta t_{j+1/2}^\alpha, 0\right) F(U_j^-) \\ &+ \max\left(\min\left(\Delta t_{j+1/2}^\alpha, \Delta t\right) - \Delta t_{j+1/2}^\omega, 0\right) F\left((\alpha_j^+, \omega_j^-)\right). \end{aligned}$$

— If $\theta_j^\alpha > \theta_j^\omega$, then

$$\begin{aligned} \Delta t \mathbf{F}_{j+/2}^{\mathrm{Rec}} &= \min\left(\Delta t_{j+1/2}^\alpha, \Delta t\right) F(U_j^+) + \max\left(\Delta t - \Delta t_{j+1/2}^\omega, 0\right) F(U_j^-) \\ &+ \max\left(\min\left(\Delta t_{j+1/2}^\omega, \Delta t\right) - \Delta t_{j+1/2}^\alpha, 0\right) F\left((\alpha_j^-, \omega_j^+)\right). \end{aligned}$$

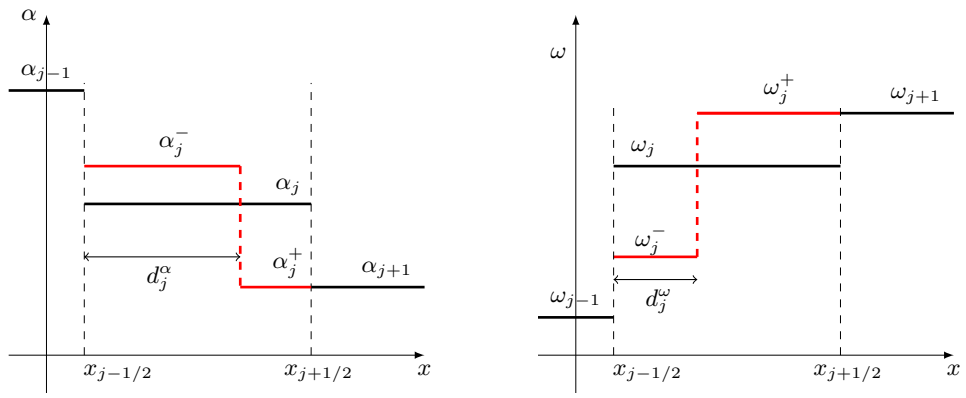

FIGURE 5.6 – Reconstruct U_j by $U_j^- = (\alpha_j^-, \omega_j^-)$, $U_j^+ = (\alpha_j^+, \omega_j^+)$ and $d_j^\alpha = \theta_j^\alpha \Delta x$, $d_j^\omega = \theta_j^\omega \Delta x$.

— If $\sigma_j < 0$. Denote $\Delta t_{j-1/2}^\omega = \frac{\theta_j^\omega \Delta x}{-\sigma_j}$, $\quad \Delta t_{j-1/2}^\alpha = \frac{\theta_j^\alpha \Delta x}{-\sigma_j}$.
The numerical flux function $\mathbf{F}_{j-1/2}^{\text{Rec}}$ is computed by using U_j^- and U_j^+.
— If $\theta_j^\alpha \le \theta_j^\omega$, then

$$\begin{aligned}\Delta t \mathbf{F}_{j-1/2}^{\text{Rec}} &= \min\left(\Delta t_{j-1/2}^\alpha, \Delta t\right) F(U_j^-) + \max\left(\Delta t - \Delta t_{j-1/2}^\omega, 0\right) F(U_j^+) \\ &+ \max\left(\min\left(\Delta t_{j-1/2}^\omega, \Delta t\right) - \Delta t_{j-1/2}^\alpha, 0\right) F\left((\alpha_j^+, \omega_j^-)\right).\end{aligned}$$

— If $\theta_j^\alpha > \theta_j^\omega$, then

$$\begin{aligned}\Delta t \mathbf{F}_{j-1/2}^{\text{Rec}} &= \min\left(\Delta t_{j-1/2}^\omega, \Delta t\right) F(U_j^-) + \max\left(\Delta t - \Delta t_{j-1/2}^\alpha, 0\right) F(U_j^+) \\ &+ \max\left(\min\left(\Delta t_{j-1/2}^\alpha, \Delta t\right) - \Delta t_{j-1/2}^\omega, 0\right) F\left((\alpha_j^-, \omega_j^+)\right).\end{aligned}$$

5.4 Numerical results

We present some numerical results obtained with the constant densities $\rho_1 = 1$, $\rho_2 = 3$, which give a good overview of the wave structure. Moreover, the simulation is implemented on a spacial domain $[0, 1]$, uniform mesh with space step Δx and CFL number is less than or equal to 1. The time step is defined by

$$\Delta t = \text{CFL} \times \frac{\Delta x}{\max_i\{\lambda_1(U_i, U_{i+1}), \lambda_2(U_i, U_{i+1})\}} \tag{5.35}$$

where $\lambda_k(U_i, U_{i+1})$, $k = 1, 2$ are defined by (5.33). We first show in subsection 5.4.1 that the Godunov scheme and the Roe scheme with Harten type correction are able to capture the non classical wave structure joining two states in different domains $\mathcal{H}_-$ and $\mathcal{H}_+$ in the Riemann problem involving a pure phase intermediate state (Examples 5.2.3 and 5.2.5). These schemes however show strong oscillation in capturing the non classical 2-shock wave in Example 5.2.6, see this configuration in Figure 5.3(a), whereas the reconstructing method show very good results, Figure 5.9.
Then in subsection 5.4.2 we simulate the classical problem of phase separation under gravity.

5.4.1 The Riemann problem

The Riemann problem consists in solving the system (5.4) with $K = 0$, $S = 0$ and the initial data

$$U(x, 0) = \begin{cases} (\beta_L, \omega_L) & \text{if} \quad x \le 0, \\ (\beta_R, \omega_R) & \text{if} \quad x > 0. \end{cases} \tag{5.36}$$

From Theorem 7, this problem admits a unique admissible solution satisfying Liu's criterion with $\alpha_1, \alpha_2 \in [0, 1]$. In the special case where $\omega_L = -\omega_R$, the solution involves a pure phase : the lighter if $\omega_L > 0$, and the heavier if $\omega_L < 0$. It consists of two transonic rarefactions in the former case and

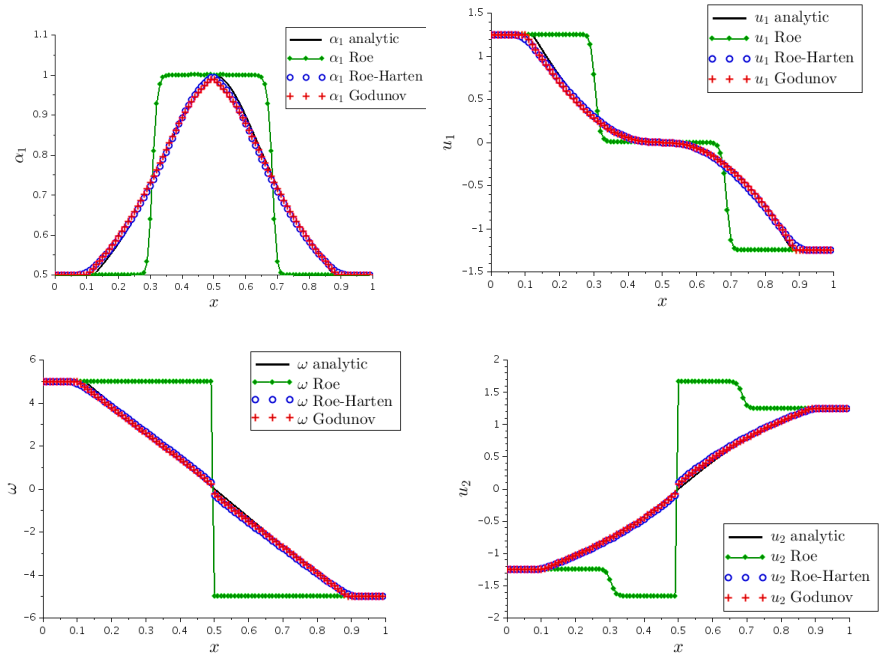

FIGURE 5.7 – Solution of the Riemann problem at time $t = 0.15$ for the initial data $\alpha_1 = \alpha_2 = 0.5$ and $\omega_L = -\omega_R = 5$; 100 cells and CFL $= 0.9$.

three shocks waves in the latter. We present in Figure 5.7 and 5.8, the numerical results obtained using the Godunov scheme, the Roe scheme, and the Roe scheme with the Harten type entropy fix presented at Section 5.3. In the first case $\omega_L > 0$, Figure 5.7, the original Roe scheme is unable to capture the admissible solution and captures instead an inadmissible shock, i.e. does not satisfy the Liu criterion. We remark that the velocity of the liquid in the pure gas region is smooth. In the second case $\omega_L < 0$, Figure 5.8, the original Roe scheme and others schemes capture well the pure liquid state. In this case, the gas velocity in the pure liquid region includes of three shocks and is bounded. The velocity of the vanishing phase in both of cases is not necessarily equal to the one of the pure phase.
The third numerical simulation of the Riemann problem is the non classical 2-shock wave as in Figure 5.3(a). We recall that this 2-shock goes through the domain $\mathcal{H}_-$ and $\mathcal{H}_+$, connects the left state U_L to the intermediate state U_{int} such that each component of U_L and U_{int} is different and the speed propagation of the 2-shock is not equal to zero. These challenges lead to oscillations given by both the Godunov scheme and the Roe scheme with Harten entropy fix while the Roe scheme without entropy fix yields strong oscillations. The admissible solution is well captured only by the reconstruction method, see Figure 5.9 (a uniform mesh with 100 cells), Figure 5.11 (a uniform mesh with 500 cells) and Figure 5.10 for the convergence of these schemes.

5.4.2 The phase separation under gravity

This is a classical test case in the assessment of numerical methods in the modelling of counter-current two phase flows with steep transition (see [Jeo+08]). We consider the model (5.1) with $g = -10m/s^2$, $K = 0$ and $x \in [0, 1]$ with the initial data $u_1(x, 0) = 0, u_2(x, 0) = 0, \alpha_1(x, 0) = 0.5, \alpha_2(x, 0) = 0.5$ and boundary date $u_1(0, t) = u_2(0, t) = u_1(1, t) = u_2(1, t) = 0$. The numerical simulation uses the uniform mesh with 200 cells and CFL $= 0.95$. The transient result in Figure 5.12 (left) shows that the Roe scheme captures an inadmissible shock departing from $x = 1$. This is consistent with the results shown in the previous section since the Riemann problems at the walls yield pure phases intermediate states and a transonic rarefaction fan for the lighter phase. However, the Roe scheme with Harten entropic correction gives a similar result to the Godunov scheme, both of them being consistent with the analysis of the Riemann problem.
Both the physical and mathematical analysis agree that the expected stationary state for the volume fraction and velocities should satisfy $\alpha_1 = 0$ on $[0, 0.5]$ and $\alpha_1 = 1$ on $[0.5, 1]$ velocity $u_2 = 0$ on $[0, 0.5]$ and $u_1 = 0$ on $[0.5, 1]$. However there is a debate as to what should be the value of u_2 (resp. u_1)

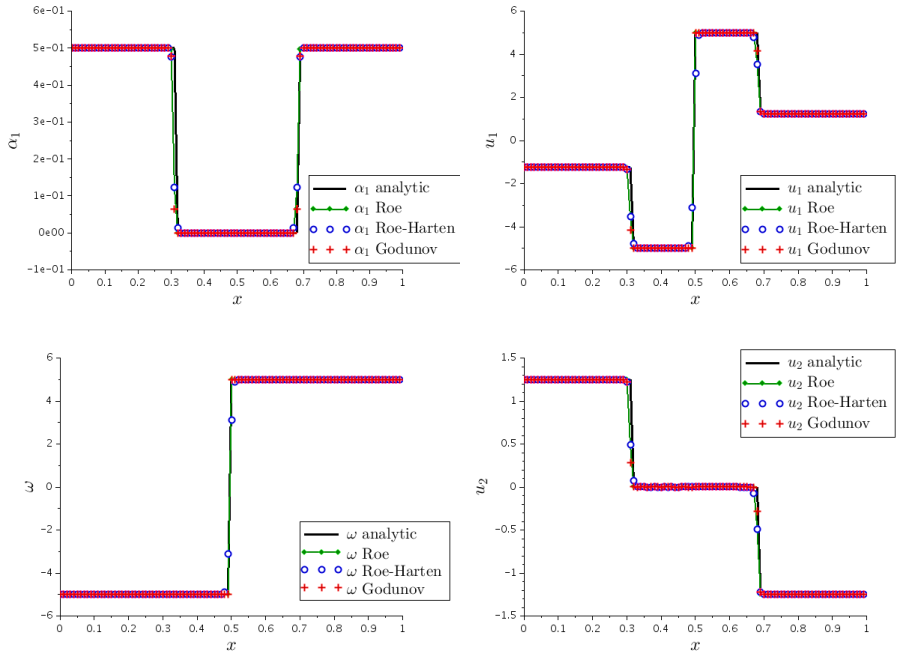

FIGURE 5.8 – Solution of the Riemann problem at time $t = 0.15$ for the initial data $\alpha_1 = \alpha_2 = 0.5$ and $\omega_L = -\omega_R = -5$; 100 cells and CFL $= 0.9$.

on $[0.5, 1]$ (resp. $[0, 0.5]$) since in that region the liquid (resp. the gas) is absent). In our model we can compute the stationary velocity of the liquid which is not zero hence there is no mechanical equilibrium. However there does not exist a stationary value for the gas velocity on the whole of domain, we refer the reader to Appendix 5.5.2 for details. During the numerical simulation, all schemes except the original Roe scheme captured well the vanishing velocity of liquid in the pure gas domain as well as the (non stationary) vanishing velocity of gas in the pure liquid domain.

5.4.3 The boiling channel problem

The boiling channel test case is a simplified description of a nuclear vessel thermalhydraulics in incidental conditions. The inlet water is assumed at saturation and remains liquid in the lower part of the vessel. Due to the heating source term in the core the liquid undergoes phase change and may be purely gaseous in the upper part of the vessel (see for example [CDK14]).
We consider the model (5.4) with $g = 0$ and the piecewise constant phase change function $\Gamma_1(x) = -\Gamma_2(x) = \Gamma_0 1_{[\frac{1}{3}, \frac{2}{3}]}(x)$, for $x \in [0, 1]$. This is a simple 1D description of a nuclear core dewatering, where we do not detail the energy transfers involved in the phase change but only consider a non zero mass source term $\Gamma_k \neq 0$.
In this case, the function $K(x, t)$ is no longer considered to be zero but a function of Γ_1 and the boundary condition. More precisely, see the Appendix 5.5.1.
In the following numerical test, we choose $\Gamma_0 = 3\rho_2$ with the following initial and boundary conditions

Initial data : $\alpha_1(x, 0) = 0,\ u_1(x, 0) = 1,\ u_2(x, 0) = 1,\ \forall x \in [0, 1]$.

Boundary conditions : inlet at $x = 0$ with $u_1(0, t) = u_2(0, t) = 1$, $\alpha_1(0, t) = 0$ and outlet at $x = 1$ with Neumann condition.

The numerical simulation uses the uniform mesh with 200 cells and CFL $= 0.9$. The numerical results at the stationary state using the Roe scheme, and Roe with Harten-type entropy fix compared to the analytical solution (see Appendix 5.5.3) are found in Figure 5.15.

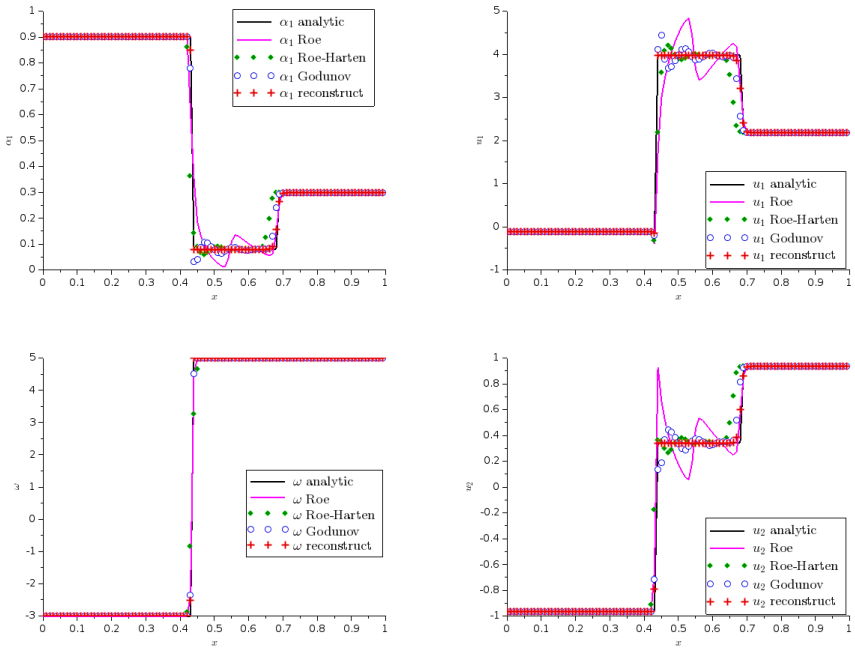

FIGURE 5.9 – Solution of the Riemann problem at time $t = 0.12$ for the initial data $\alpha_L = 0.9, \alpha_R = 0.3$ and $\omega_L = -3, \omega_R = 5$; 100 cells and CFL $= 0.5$.

5.5 Appendix

5.5.1 Appendix : Model derivation

We recall the two-fluid model equations for an isentropic two phase flows in one space dimension :

$$\begin{aligned}
\partial_t \alpha_1\rho_1 + \partial_x(\alpha_1\rho_1 u_1) &= \Gamma_1, && (5.37a)\\
\partial_t \alpha_2\rho_2 + \partial_x(\alpha_2\rho_2 u_2) &= \Gamma_2, && (5.37b)\\
\partial_t(\alpha_1\rho_1 u_1) + \partial_x(\alpha_1\rho_1 u_1^2) + \alpha_1\partial_x P_1 &= \alpha_1\rho_1 g + \Gamma_1 u^i, && (5.37c)\\
\partial_t(\alpha_2\rho_2 u_2) + \partial_x(\alpha_2\rho_2 u_2^2) + \alpha_2\partial_x P_2 &= \alpha_2\rho_2 g + \Gamma_2 u^i. && (5.37d)
\end{aligned}$$

We assume that the two phases are incompressible (ρ_1 and ρ_2 are constant) and recall the closure laws, $\alpha_1 + \alpha_2 = 1$ and $P_1 - P_2 = \frac{\rho_1\rho_2}{2(\rho_1-\rho_2)}(u_1 - u_2)^2$. Therefore the four equation system (5.37a-5.37d) should be solved for the four unknowns (α_1, u_1, u_2, and P_1).
Applying the same method as in [KSS03], we derive a system of two equations, which allows for the study of the void waves and avoids singularities when one phase disappears.
From the equations of mass, (5.37a) and (5.37b), we obtain

$$\partial_x(\alpha_1 u_1 + \alpha_2 u_2) = \frac{\Gamma_1}{\rho_1} + \frac{\Gamma_2}{\rho_2}. \tag{5.38}$$

Therefore the quantity

$$K(x,t) = \alpha_1 u_1 + \alpha_2 u_2 \tag{5.39}$$

implies that

$$K(x,t) = \int_0^x (\frac{1}{\rho_1} - \frac{1}{\rho_2})\Gamma_1(x,t) + \alpha_{10}u_{10} + \alpha_{20}u_{20} \tag{5.40}$$

Assuming that the boundary condition and Γ_1 is independent of time, i.e. $\alpha_{10}, u_{10}, u20$, and Γ_1 are constant in time, then $K = K(x)$. The interfacial velocity u^i considered is $u^i = \alpha_1 u_2 + \alpha_2 u_1$.

From the equation of momentum conservation (5.37c) and (5.37d), we derive

$$\begin{aligned}
u_1\rho_1(\partial_t\alpha_1 + \partial_x\alpha_1 u_1) + \alpha_1\rho_1(\partial_t u_1 + u_1\partial_x u_1) + \alpha_1\partial_x P_1 &= \alpha_1\rho_1 g + \Gamma_1 u^i, && (5.41a)\\
u_2\rho_2(\partial_t\alpha_2 + \partial_x\alpha_2 u_2) + \alpha_2\rho_2(\partial_t u_2 + u_2\partial_x u_2) + \alpha_2\partial_x P_2 &= \alpha_2\rho_2 g + \Gamma_2 u^i. && (5.41b)
\end{aligned}$$

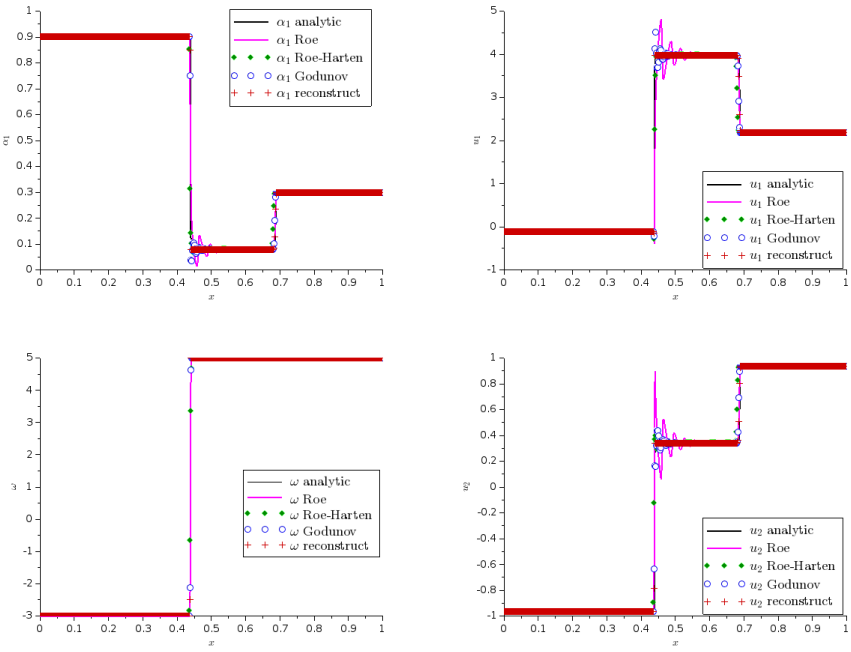

FIGURE 5.10 – Solution of the Riemann problem at time $t = 0.12$ for the initial data $\alpha_L = 0.9, \alpha_R = 0.3$ and $\omega_L = -3, \omega_R = 5$; 500 cells and CFL $= 0.5$.

Thank to (5.37a), (5.37b) and $u^i = \alpha_1 u_2 + \alpha_2 u_1$, these equations can be simplified :

$$\alpha_1 \left(\partial_t(\rho_1 u_1) + \partial_x \frac{\rho_1 u_1^2}{2} \right) + \alpha_1 \partial_x P_1 = \alpha_1 \rho_1 g, \tag{5.42a}$$

$$\alpha_2 \left(\partial_t(\rho_2 u_2) + \partial_x \frac{\rho_2 u_2^2}{2} \right) + \alpha_2 \partial_x P_2 = \alpha_2 \rho_2 g. \tag{5.42b}$$

Assuming that initially $\alpha_1 \alpha_2 \neq 0$, we can simplify by α_1 in (5.42a) and by α_2 in (5.42b), then subtracting the two equations yields

$$\partial_t(\rho_1 u_1 - \rho_2 u_2) + \partial_x \left(\frac{1}{2}(\rho_1 u_1^2 - \rho_2 u_2^2) + P_1 - P_2 \right) = (\rho_1 - \rho_2) g. \tag{5.43}$$

The space differential in (5.43) can be simplified thanks to

$$\begin{aligned} \frac{1}{2}(\rho_1 u_1^2 - \rho_2 u_2^2) + P_1 - P_2 &= \frac{1}{2}(\rho_1 u_1^2 - \rho_2 u_2^2) + \frac{\rho_1 \rho_2}{2(\rho_1 - \rho_2)}(u_1 - u_2)^2 \\ &= \frac{1}{2(\rho_1 - \rho_2)} (\rho_1 u_1 - \rho_2 u_2)^2 . \end{aligned} \tag{5.44}$$

We set the new unknowns (α, ω) as

$$\begin{aligned} \alpha &= \alpha_1, \\ \omega &= \rho_1 u_1 - \rho_2 u_2. \end{aligned} \tag{5.45}$$

The original unknowns u_1 and u_2 can be recovered from (5.39) and (5.45) :

$$u_1 = \frac{(1-\alpha)\omega}{\alpha(\rho_2 - \rho_1) + \rho_1} + \frac{K\rho_2}{\alpha(\rho_2 - \rho_1) + \rho_1}, \quad u_2 = \frac{-\alpha\omega}{\alpha(\rho_2 - \rho_1) + \rho_1} + \frac{K\rho_1}{\alpha(\rho_2 - \rho_1) + \rho_1}.$$

Finally, from (5.37a), (5.43) and (5.44) we obtain the 2×2 system

$$\begin{cases} \partial_t \alpha + \partial_x \alpha u_1 = \dfrac{\Gamma_1}{\rho_1}, \\ \partial_t \omega + \partial_x \left(\frac{\omega}{2(\rho_1 - \rho_2)} \right) = (\rho_1 - \rho_2) g, \end{cases}$$

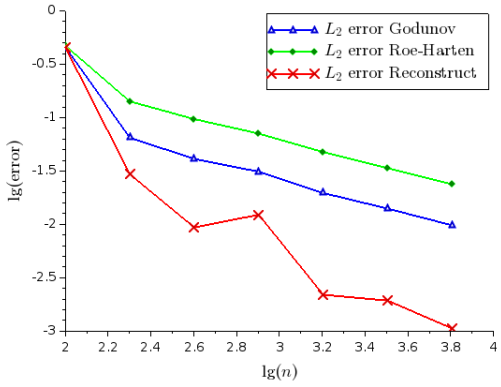

FIGURE 5.11 – Convergence curves (mesh refinement for the Riemann problem with initial data $\alpha_L = 0.9, \alpha_R = 0.3$ and $\omega_L = -3, \omega_R = 5$; CFL $= 0.5$).

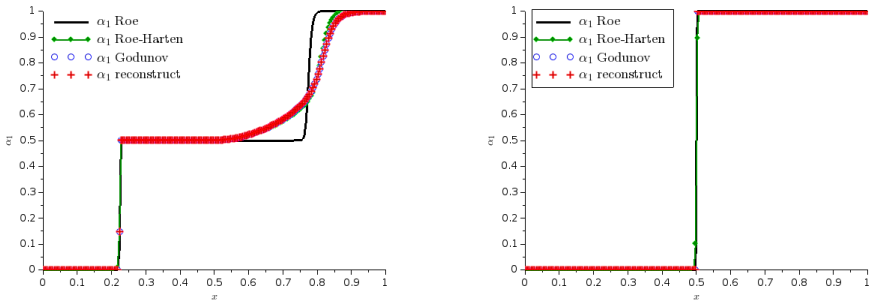

(a) Transient (b) Stationary

FIGURE 5.12 – Volume fraction α_1 for the sedimentation problem, 200 cells, CFL $= 0.95$.

and the incompressible two-fluid model can be written in closed form as

$$\begin{cases} \partial_t \alpha + \partial_x \left(\frac{\alpha(1-\alpha)\omega}{\alpha(\rho_2-\rho_1)+\rho_1} + \frac{K\rho_1\rho_2}{(\rho_1-\rho_2)(\alpha(\rho_2-\rho_1)+\rho_1)} \right) = 0, \\ \partial_t \omega + \partial_x \left(\frac{\omega^2}{2(\rho_1-\rho_2)} \right) = (\rho_1-\rho_2)g, \end{cases} \tag{5.46}$$

since K is constant in space and time.

5.5.2 Appendix : Vanishing velocity of the sedimentation problem

We consider the stationary state of the 2×2 system (5.46) assuming that $g < 0$ and $\rho_1 < \rho_2$. The first equation in (5.46) at stationary state and the boundary condition together with (5.39) yield

$$\begin{aligned} \alpha_1 u_1 &= 0, \\ \alpha_2 u_2 &= 0. \end{aligned}$$

We seek a solution consisting of two zones. A bottom zone with pure phase 2 : $\alpha_2 = 1$ and constant velocity $u_2 = 0$ in the region $x \in [0, 0.5]$ and a top zone with pure phase 1 : $\alpha_1 = 1$ and constant velocity $u_1 = 0$ in the region $x \in [0.5, 1]$. We are going to use the second equation of the system (5.46) to determine the vanishing velocity of phase 2 in the region $x \in [0.5, 1]$.
The second equation of the system (5.46), using the physical variables u_1 and u_2 (or equivalently equation 5.43) is

$$\partial_x \left(\rho_1 \frac{u_1^2}{2} - \rho_2 \frac{u_2^2}{2} + \frac{\rho_1\rho_2}{2(\rho_1-\rho_2)}(u_1-u_2)^2 \right) = (\rho_1-\rho_2)g. \tag{5.47}$$

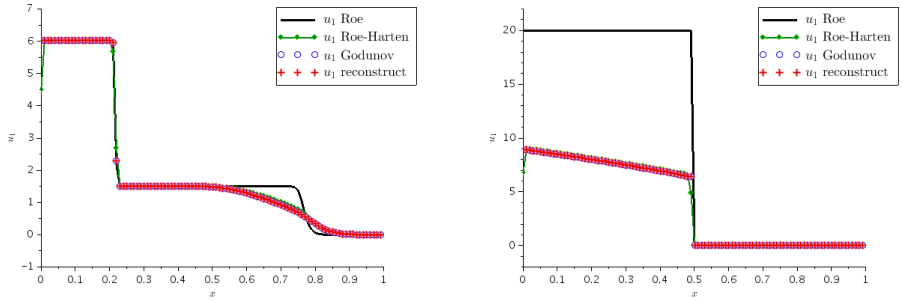

(a) Transient (b) Stationary

FIGURE 5.13 – The velocity u_1 for the sedimentation problem.

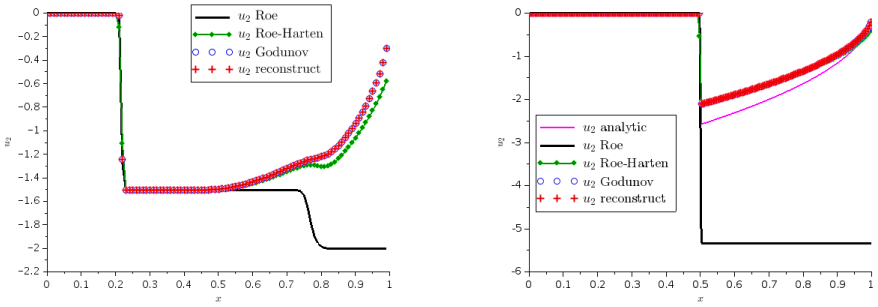

(a) Transient (b) Stationary

FIGURE 5.14 – The velocity u_2 for the sedimentation problem.

Integrating (5.47) we obtain the **two phase Bernoulli's principle** :

$$\rho_1 \frac{u_1^2}{2} - \rho_2 \frac{u_2^2}{2} + \frac{\rho_1 \rho_2}{2(\rho_1 - \rho_2)}(u_1 - u_2)^2 - (\rho_1 - \rho_2) g x = \text{constant}. \tag{5.48}$$

In order to compute the vanishing phase velocity of phase 2, we remark that the velocities at the walls $x = 1$ are $u_1 = u_2 = 0$. Hence the constant in (5.48) equals $-(\rho_1 - \rho_2)g$, and since $u_1 = 0$ for $x \in [0.5, 1]$ the two phase bernoulli's principle becomes

$$\frac{\rho_2^2}{\rho_1 - \rho_2} \frac{u_2^2(x)}{2} = (\rho_1 - \rho_2) g (x - 1) \qquad \text{for} \quad x \in [0.5, 1].$$

Hence

$$u_2(x) = -\sqrt{2\left(1 - \frac{\rho_1}{\rho_2}\right) g (x - 1)} \quad \text{for } x \in [0.5, 1]. \tag{5.49}$$

The velocity profile is therefore not constant and furthermore shows a discontinuity at the interface $x = 0.5$.

We remark that we cannot determine a vanishing velocities for phase 1 in the region $x \in [0, 0.5]$. Indeed since $u_2 = 0$ for $x \in [0, 0.5]$, the two-phase Bernoulli's principle takes the form

$$\frac{\rho_1^2}{\rho_1 - \rho_2} \frac{u_1^2(x)}{2} = (\rho_1 - \rho_2) g x \qquad \text{for} \quad x \in [0, 0.5]. \tag{5.50}$$

Since $g = -10m/s < 0$, the equation (5.50) has no solution as it yields $u_1^2 < 0$.

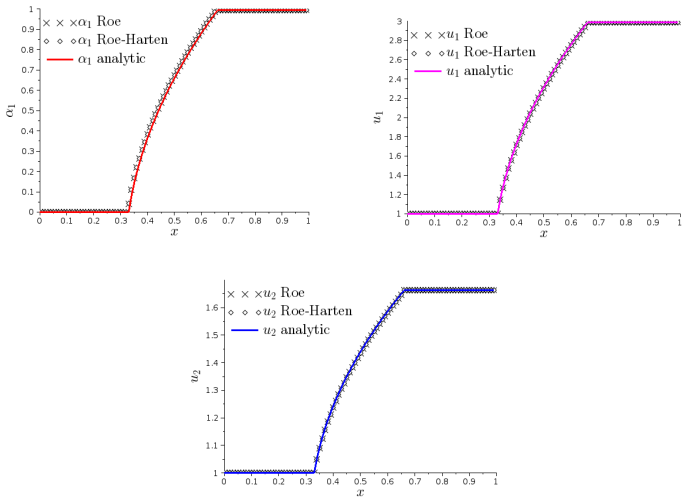

FIGURE 5.15 – The stationary state for the boiling channel problem on a uniform mesh with 100 cells and CFL = 0.9.

5.5.3 Appendix : Analytical solution of the boiling channel for the incompressible model at the stationary state

We seek a stationary solution to the following system

$$\begin{cases} \partial_x(\alpha_1\rho_1u_1) = \Gamma_1 \\ \partial_x(\alpha_2\rho_2u_2) = \Gamma_2 \\ \partial_x(\rho_1u_1^2 - \rho_2u_2^2 + \frac{\rho_1\rho_2}{\rho_1-\rho_2}(u_1-u_2)^2) = 0 \end{cases}.$$

Hence

$$\alpha_1\rho_1u_1 = \int_0^x \Gamma_1 + \alpha_{10}\rho_1u_{10} \tag{5.51}$$

$$\alpha_2\rho_2u_2 = \int_0^x \Gamma_2 + \alpha_{20}\rho_2u_{20} \tag{5.52}$$

$$\rho_1u_1 - \rho_2u_2 = \rho_1u_{10} - \rho_2u_{20} \tag{5.53}$$

Eliminating u_1 and u_2 in equation (5.53) yields

$$u_1 = \frac{\int_0^x \Gamma_1 + \alpha_{10}\rho_1u_{10}}{\alpha_1\rho_1} \tag{5.54}$$

$$u_2 = \frac{\int_0^x \Gamma_2 + \alpha_{20}\rho_2u_{20}}{\alpha_2\rho_2} \tag{5.55}$$

$$\frac{\int_0^x \Gamma_1 + \alpha_{10}\rho_1u_{10}}{\alpha_1} - \frac{\int_0^x \Gamma_2 + \alpha_{20}\rho_2u_{20}}{\alpha_2} = \rho_1u_{10} - \rho_2u_{20}$$

We need to find α_1 in

$$(1-\alpha_1)\left(\int_0^x \Gamma_1 + \alpha_{10}\rho_1u_{10}\right) - \alpha_1\left(\int_0^x \Gamma_2 + \alpha_{20}\rho_2u_{20}\right) = \alpha_1(1-\alpha_1)(\rho_1u_{10} - \rho_2u_{20}),$$

which is equivalent to

$$\alpha_1^2(\rho_1u_{10} - \rho_2u_{20}) - \alpha_1((\alpha_{10}+1)\rho_1u_{10} - \alpha_{10}\rho_2u_{20}) + \int_0^x \Gamma_1 + \alpha_{10}\rho_1u_{10} = 0. \tag{5.56}$$

We first look for a stationary solution such that $\alpha_1(x) < 1$ for $x \in [0, \frac{2L}{3}[$, and $\alpha(x) = 1$ for $x \in [\frac{2L}{3}, L]$ (pure gas at the outlet and mixture in the middle). We therefore have $\int_0^{\frac{2L}{3}} \Gamma_1 = \frac{L}{3}\Gamma_0$ and taking $x = \frac{2L}{3}$ in the equation (5.56) yields

$$\Gamma_c = \frac{3}{L}\alpha_{20}\rho_2 u_{20}.$$

If we solve a model with $\Gamma_0 < \Gamma_c$ then there will still be some water in the core in the stationary regime and no dry vapour at the outlet. The maximum value of α_1 is reached at $x = \frac{2L}{3}$, and (5.56) yields

$$\alpha_{1max}^2(\rho_1 u_{10} - \rho_2 u_{20}) - \alpha_{1max}((\alpha_{10}+1)\rho_1 u_{10} - \alpha_{10}\rho_2 u_{20}) + \frac{L}{3}\Gamma_0 + \alpha_{10}\rho_1 u_{10} = 0.$$

If instead $\Gamma_0 > \Gamma_c$ then we will have dewatering of the core and dry vapour at the outlet : $\exists x_{dryout} \in [\frac{L}{3}, \frac{2L}{3}]$, such that $\alpha_1(x) < 1$ for $x \in [0, x_{dryout}[$, and $\alpha(x) = 1$ for $x \in [x_{dryout}, L]$. We can find the position of the pure vapour steam by taking $x = \frac{2L}{3}$ in the equation (5.56) : $\int_0^L \Gamma_1 = (x_{dryout} - \frac{L}{3})\Gamma_0$

$$x_{dryout} = \frac{\alpha_{20}\rho_2 u_{20}}{\Gamma_0} + \frac{L}{3} \in \left[\frac{L}{3}, \frac{2L}{3}\right].$$

As the final state displays regions with pure phases, a natural question to ask is whether it is possible to assign a value to the velocity field of the missing phase. In [JE08] the authors considered that the phase velocities should be equal : $u_1 = u_2$, but that hypothesis is not consistent with the mass flow equations (5.51) and (5.52). The theoretical values of the velocities u_1 and u_2 can be obtained from (5.54) and (5.55).

5.5.4 Appendix : The Roe matrix

A Roe matrix $A(U_L, U_R)$ for the system (5.4) and two states $U_L, U_R \in \mathcal{H}$ is a diagonalisable matrix such that

$$\begin{aligned} F(U_L) - F(U_R) &= A(U_L, U_R)(U_L - U_R) \\ A(U, U) &= \nabla F(U) \end{aligned}$$

After some calculations, we obtained and used the following Roe matrix $A^{Roe}(U_R, U_L) = \begin{pmatrix} a & b \\ c & d \end{pmatrix}$, where

$$\begin{cases} a &= \dfrac{w_L + w_R}{2(\rho_1 - \rho_2)}\left(1 - \dfrac{\rho_1\rho_2}{\beta_L\beta_R}\right), \\ b &= \dfrac{1}{2(\rho_1 - \rho_2)}\left[\dfrac{(\beta_L - \rho_1)(\beta_L - \rho_2)}{\beta_L} + \dfrac{(\beta_R - \rho_1)(\beta_R - \rho_2)}{\beta_R}\right], \\ c &= 0, \\ d &= \dfrac{\omega_L + \omega_R}{2(\rho_1 - \rho_2)}. \end{cases}$$

5.5.5 Appendix : Wave interacting potential for the incompressible model

Classifying a couple of approaching wave-fronts, whose left, middle, right states are (α_L, ω_L), (α_M, ω_M), (α_R, ω_R), as in the following :

1. **In a same 1-family.** Assuming that two 1-wave-fronts have strength σ_1' and σ_1'', whose speeds are v_1' and v_1'', correspondingly, such that $v_1' > v_1''$. Because two interacting wave-fronts are in the same 1-family, ω is constant. Therefore,

$$\sigma_1' = |\alpha_L - \alpha_M| \text{ and } \sigma_1'' = |\alpha_R - \alpha_M|.$$

   (a) **1-shock 1-shock**. We have

$$v_1' = \frac{\omega}{\rho_1 - \rho_2}\left(1 - \frac{1}{\beta_L\beta_M}\right) \text{ and } v_1'' = \frac{\omega}{\rho_1 - \rho_2}\left(1 - \frac{1}{\beta_R\beta_M}\right).$$

   $v_1' > v_1''$ implies that

— If $\omega > 0$, then $\alpha_L < \alpha_R$. It is satisfied because $\alpha_L < \alpha_M$ and $\alpha_M < \alpha_R$. Consequently, the outgoing front-wave is a 1-shock.
— If $\omega < 0$, then $\alpha_L > \alpha_R$. It is satisfied because $\alpha_L > \alpha_M$ and $\alpha_M > \alpha_R$. Consequently, the outgoing front-wave is a 1-shock.
In both cases, we have the outgoing wave is a 1-shock whose strength is

$$\sigma_1 = \sigma_1' + \sigma_1''.$$

(b) **1-shock 1-rare**. We have

$$\upsilon_1' = \frac{\omega}{\rho_1 - \rho_2}\left(1 - \frac{1}{\beta_L \beta_M}\right) \text{ and } \upsilon_1'' = \frac{\omega}{\rho_1 - \rho_2}\left(1 - \frac{1}{(\beta_M)^2}\right).$$

$\upsilon_1' > \upsilon_1''$ implies that
— If $\omega > 0$, then $\alpha_L < \alpha_M$. 1-rarefaction implies that $\alpha_M > \alpha_R$. The outgoing wave is of 1-family, 1-shock or 1-rarefaction.
— If $\omega < 0$, then $\alpha_L > \alpha_M$. 1-rarefaction implies that $\alpha_M < \alpha_R$. The outgoing wave is of 1-family, 1-shock or 1-rarefaction.
In both cases, we have the outgoing wave is a 1-shock or 1-rarefaction whose strength is

$$\sigma_1 < \sigma_1' + \sigma_1''.$$

(c) **1-rare 1-shock**. We have

$$\upsilon_1' = \frac{\omega}{\rho_1 - \rho_2}\left(1 - \frac{1}{(\beta_M)^2}\right) \text{ and } \upsilon_1'' = \frac{\omega}{\rho_1 - \rho_2}\left(1 - \frac{1}{\beta_R \beta_M}\right).$$

$\upsilon_1' > \upsilon_1''$ implies that
— If $\omega > 0$, then $\alpha_M < \alpha_R$. 1-rarefaction implies that $\alpha_L > \alpha_M$. The outgoing wave is of 1-family, 1-shock or 1-rarefaction.
— If $\omega < 0$, then $\alpha_M > \alpha_R$. 1-rarefaction implies that $\alpha_L < \alpha_M$. The outgoing wave is of 1-family, 1-shock or 1-rarefaction.
In both cases, we have the outgoing wave is a 1-shock or 1-rarefaction whose strength is

$$\sigma_1 < \sigma_1' + \sigma_1''.$$

(d) **1-rare 1-rare** : this two wave-fronts cannot interact.

2. **In a same 2-family.** Assuming that two 2-wave-fronts have strength σ_2' and σ_2'', whose speed are υ_2' and υ_2'', correspondingly, such that $\upsilon_2' > \upsilon_2''$. Explicitely, the strength of two incoming waves are

$$\sigma_2' = |\alpha_L - \alpha_M| + |\omega_L - \omega_M| \text{ and } \sigma_2'' = |\alpha_R - \alpha_M| + |\omega_R - \omega_M|.$$

(a) **2-shock 2-shock**. We have

$$\upsilon_2' = \frac{\omega_L + \omega_M}{2(\rho_1 - \rho_2)} \text{ and } \upsilon_2'' = \frac{\omega_R + \omega_M}{2(\rho_1 - \rho_2)}.$$

Moreover, two 2-shocks imply $\omega_L < \omega_M < \omega_R$. Therefore, the condition $\upsilon_2' > \upsilon_2''$ is satisfied. Because $\omega_L < \omega_R$, there is a 2-shock wave in outgoing waves. We come back with the Riemann problem where $U_L = (\alpha_L, \omega_L)$ and $U_R = (\alpha_R, \omega_R)$. The outgoing waves might consist of 2-shock and almost two 1-shocks or a 1-rarefaction. The strength of outgoing waves are $\sum \sigma_1$ and σ_2 such that
— If $\omega_L < \omega_R < 0$ or $0 < \omega_L < \omega_R$,

$$\sigma_1 + \sigma_2 = \sigma_2' + \sigma_2''. \tag{5.57}$$

The equality (5.57) is obtained from the properties of the shock curves. See Figure of the shock curves in the article CMS.
— If $\omega_L < 0 < \omega_R$, then it might have $\Sigma\sigma_1 + \sigma_2 > \sigma_2' + \sigma_2''$.

(b) **2-shock 2-rarefaction**. We have

$$v_2' = \frac{\omega_L + \omega_M}{2(\rho_1 - \rho_2)} \text{ and } v_2'' = \frac{\omega_M}{\rho_1 - \rho_2}.$$

The condition of the 2-shock and the 2-rarefaction implies $\omega_L < \omega_M$ and $\omega_M > \omega_R$. Therefore, the condition $v_2' > v_2''$ is satisfied. We come back the Riemann problem where $U_L = (\alpha_L, \omega_L)$ and $U_R = (\alpha_R, \omega_R)$. The outgoing waves might consist of a 2-shock or a 2-rarefaction and almost two 1-shocks or a 1-rarefaction.
— If $\omega_L < 0 < \omega_R$, it might have $\Sigma\sigma_1 + \sigma_2 > \sigma_2' + \sigma_2''$.
— If $\omega_L < \omega_R < 0$ or $0 < \omega_L < \omega_R$, we have $\sigma_1 + \sigma_2 < \sigma_2' + \sigma_2''$.

3. **In two different families**. Assuming that two wave-fronts have strength σ_1' and σ_2', whose speed are v_1' and v_2', correspondingly. Assume that ω is positive.
   (a) **1-shock 2-shock**. It might have $\sigma_1 + \sigma_2 > \sigma_1' + \sigma_2'$.
   (b) **1-shock 2-rarefaction**. We have $\sigma_1 + \sigma_2 \leq \sigma_1' + \sigma_2'$.
   (c) **1-rarefaction 2-shock**. We have $\sigma_1 + \sigma_2 \leq \sigma_1' + \sigma_2'$.
   (d) **1-rarefaction 2-rarefaction**. We have $\sigma_1 + \sigma_2 \leq \sigma_1' + \sigma_2'$.

5.5.6 Appendix : The incompressible drift model

In this part, we are interested in particular case of the drift model : incompressible models, which are simpler than the original compressible models and allow us to study mathematical properties profoundly. In the incompressible models, the partial densities are assumed to be constant, the number of equations is therefore fewer. We will present in this part a derivation of the incompressible model obtained from the drift flux model and then analyze its properties. This strategy is again applied for the two-fluid model in the following chapter. We however can not study the incompressible slip model since the void fraction α is a function of enthalpy h.

Incompressible drift models : non convex scalar equations

Considering the one dimensional incompressible two-phase flow of the drift flux model (4.10a-4.10d), the mass equations yield

$$\partial_x(\alpha_1 u_1 + \alpha_2 u_2) = 0 \Rightarrow \alpha_1 u_1 + \alpha_2 u_2 = K(t),$$

where K is a function of time determined by the boundary conditions. We can obtain the phasic velocities from f and K using the formulas

$$u_1 = K + \alpha_2 \phi(\alpha),$$
$$u_2 = K - \alpha_1 \phi(\alpha),$$

where $\phi(\alpha) := u_1 - u_2 = (\alpha - 1)^{k-1} v_\infty$. The conservation equation of the balance of vapor neglecting the phase change function can be rewritten in form of a scalar equation for α_1 ;

$$\partial_t \alpha_1 + \partial_x(\alpha_1 K + \alpha_1 \alpha_2 \phi(\alpha_1)) = 0.$$

Mathematical properties

For simplicity, we assume that $K = 0$, the resulting scalar flux function is then

$$f(\alpha) = \alpha_1 \alpha_2 \phi(\alpha_1) = v_\infty \alpha (1 - \alpha)^k, \tag{5.58}$$

with some constants v_∞ and $k \geq 0$. The first derivative f' and the second derivative f'' of the flux f in (5.58) are

$$f'(\alpha) = v_\infty (1 - \alpha)^{k-1} \left(1 - (1 + k)\alpha\right), \tag{5.59}$$
$$f''(\alpha) = v_\infty k (1 - \alpha)^{k-2} \left((k + 1)\alpha - 2\right). \tag{5.60}$$

The value of k then effects strongly the characteristic property of the flux function.
— If $0 \leq k \leq 1$, f is then concave, see Figure 5.16(a).
— If $k > 1$, f is then no longer concave, see Figure 5.16(b). Riemann problems may therefore admit composite waves, see example in Section 3.3.2.

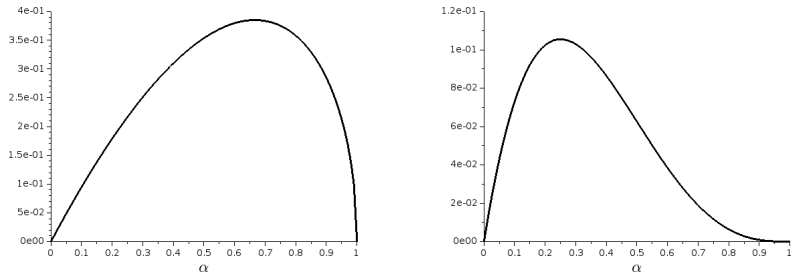

(a) (b)

FIGURE 5.16 – Flux function $f(\alpha)$ in (5.58) with $v_\infty = 1$ and different value of k, Figure 5.16(a) $k = 0.5$ and Figure 5.16(b) $k = 3$.

Phase separation examples

The phase separation is a classical test of two-phase flow models to validate mathematical models and numerical methods due to the existence of trivial stationary state. Furthermore, this test in general leads to a counter-current flow which has complicated dynamics and therefore the two-fluid models are usually chosen. However in this particular drift flux model, the phase separation test is carried out by using suitable boundary conditions.
Using the assumption $K = 0$ as previously mentioned, we then apply phase separation tests to illustrate the properties of the one dimensional incompressible drift flux model.
Considering a uniform mesh on the spacial domain $[0, 1]$, all test cases share the same initial condition $\alpha = 0.5$ as well as the boundary condition $\alpha_{(x=0)} = 0$, $\alpha_{(x=1)} = 1$. In our incompressible model, it is clear that only these boundary conditions can produce a phase separation at the stationary state in the sense that the Riemann problems using such conditions can generate pure liquid $\alpha = 0$ and pure gas $\alpha = 1$. In fact, the same boundary conditions applied for the phase separation test for the compressible drift flux model are found in [Tou87] whereas one usually uses *wall boundary conditions* in this simulation for a more general two-fluid models, see Section 6.2.2.
Due to the effect of k to the characteristic property of the flux function, the variation of k is then applied for example $k = 1$, $k = 2$, $k = 4$. Following the convex-hull construction presented in Section 1.1.6, it is possible to derive the structure of the admissible solutions to the Riemann problems. In details,

- if $k = 1$, the wave connecting the left state $\alpha = 0$ to the right state $\alpha = 0.5$ and the wave connecting the left state $\alpha = 0.5$ to the right state $\alpha = 1$ are shock waves ;
- if $1 < k < 3$, the wave connecting the left state $\alpha = 0$ to the right state $\alpha = 0.5$ is a shock while the wave connecting the left state $\alpha = 0.5$ to the right state $\alpha = 1$ is a composite wave (a shock followed by a rarefaction) ;
- if $k \geq 3$, the wave connecting the left state $\alpha = 0$ to the right state $\alpha = 0.5$ is a shock while the wave connecting the left state $\alpha = 0.5$ to the right state $\alpha = 1$ is a rarefaction.

In order to illustrate the tests, we apply the classical Godunov scheme, see Figure 5.17(a), 5.17(b), 5.17(c) for transient state with different values of k while for the stationary state, all of them give rise the phase separation, i.e. $\alpha = 0$ for $x \in [0, 0.5]$ and $\alpha = 1$ for $x \in [0.5, 1]$, Figure 5.17(d). It can be deduced that the wave connecting a homogeneous state to a pure liquid state is always a shock wave, the wave connecting a homogeneous state to a pure gas state is not a shock wave except $k = 1$. The structure of the transient phase separation is in general not symmetrical as one sometimes thinks, [PCC03 ; EF03 ; CP06 ; MEF09 ; SH13]. This property is consistent to the numerical results of the incompressible two-fluid model, see Chapter 5, and the compressible two-fluid models, see Section 6.2.2.

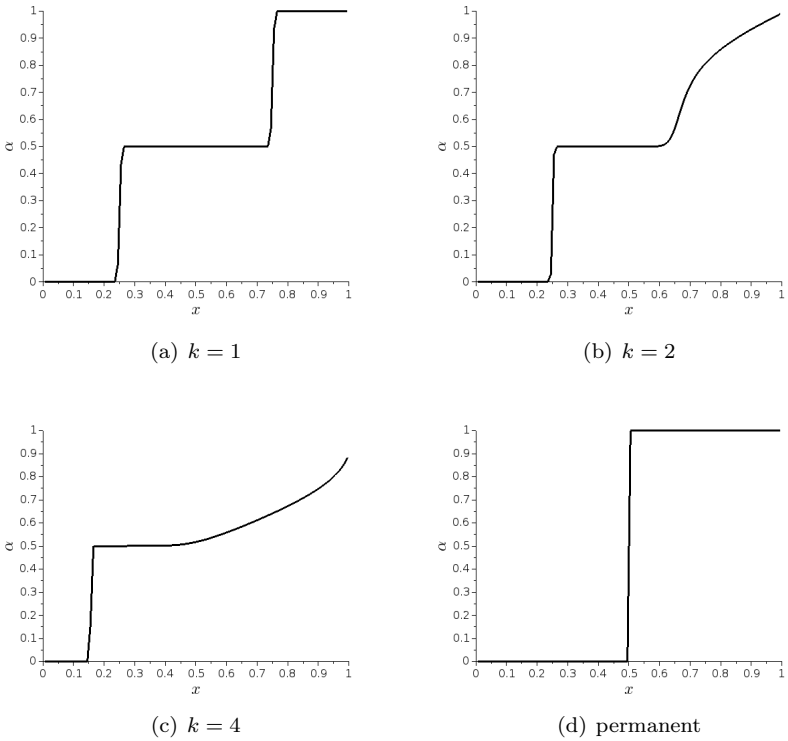

(a) $k = 1$ (b) $k = 2$

(c) $k = 4$ (d) permanent

FIGURE 5.17 – Transient state with different values of k : Figure 5.17(a), 5.17(b), 5.17(c). Permanent state : Figure 5.17(d).

Chapitre 6

Numerical simulation of the five equations two-fluid model

This chapter is set out to study the common temperature *five-equation two-fluid model*. The quasilinear form is presented. Since we can not explicitly compute the spectrum of the Jacobian matrix, the approximate eigenvalues of the isentropic two-fluid model is instead supposed to be a reference. For the numerical part in this chapter, we present in details the computation of the Roe matrix $\tilde{\mathbf{A}}(U_L, U_R)$ for the five-equation model. In order to apply the Roe-type scheme, an algorithm for the computation of the absolute matrix $|\tilde{\mathbf{A}}|$ and its sign $\text{sgn}(\tilde{\mathbf{A}})$ in [Ndj07a] is recalled. In addition, the Harten-type entropy fix is suggested to associate with the classical Roe scheme. As for the preservation of the correct stationary state, the source upwinding method is studied and proved efficient. We then apply the five-equation two-fluid model to simulate some classical but challenging test cases. The stiffened gas law is used as equation of state for simplicity. The first test case is the water faucet problem, which is a classical one used to validate the numerical methods in two-phase flows. This test is difficult due to the presence of the discontinuous transient state. The center-type schemes are usually not able to simulate this problem whereas the Roe-type schemes or the one using the full eigenvalues shows good results, following [PCC03], [SH13], [EF05], [Ndj07b]. The second test case is a sedimentation problem, i.e. a phase separation by gravity. This test is challenging due firstly to the presence of counter-current flows where the two partial velocities go in different directions, which yields many sonic points ; and secondly to the existence of a nontrivial stationary state displaying vanishing phases and with a discontinuous void fraction profile. This test is classically used to verify numerical methods developed for two-phase flow models, see [Coq+97 ; MEF09 ; SH13] for one pressure two-fluid model, and [ACR12] for the two pressures two-fluid model. In order to obtain a physically relevant solution to the sedimentation test case it is important to use a two-fluid approach since the two phasic velocities are not correlated. The last numerical test is the boiling channel, which is an important test for the nuclear reactor thermal hydraulics. Numerical results show that the source upwinding is important in capturing the correct stationary state.
Among the two-phase flow models in Chapter 4, the five-equation model is the simplest one that can implement all the above test cases due to the fact that it is necessary to have two momentum equations for the sedimentation test and at least one energy equation for the boiling channel. Moreover, the more general six-equation model yields numerous difficulties concerning the two partial energy equations such as the treatment of $p\partial_t\alpha_k$, $k = g, l$ (mathematical difficulty) and the distribution heat $\Phi = \Phi_g + \Phi_l$ for the description of the overheat vapour (very complicated physics). Therefore, we use the five-equation model in all the numerical simulations in this chapter. The numerical analysis and results presented here will be submitted in an article [NNC15a] which is in preparation.

6.1 Numerical methods

We will discuss in detail numerical methods and some special treatments used for the simulation of the two-fluid models in this document. We concentrate on the Roe solver and therefore full details of the computation of the Roe matrix will be presented.

6.1.1 Introduction to the computation of the Roe matrix

Given the two constant state U_L and U_R, following [Roe81] the Roe matrix $\tilde{\mathbf{A}}(U_L, U_R)$ corresponding to the flux function $F(U)$ of the conservation laws $\partial_t U + \partial_x F(U) = 0$ must satisfy the following properties

(1) $\tilde{\mathbf{A}}(U,U) = \mathbf{A}(U) = \nabla F(U)$ (consistency property).

(2) $F(U_R) - F(U_L) = \tilde{\mathbf{A}}(U_L, U_R)(U_R - U_L)$ (conservativity property).

(3) $\tilde{\mathbf{A}}(U_R, U_L)$ diagonalizable (hyperbolicity property).

Although the mean value theorem confirms the existence of the Roe matrix satisfying the (2) property (conservativity property), the computation of the Roe matrix is in general complicated. We do not intend to recall the construction of the Roe matrix for general conservative systems, we instead only focus on the equations of fluid dynamics. For instance, the well-known result of P. Roe in 1981 for the Euler system of gas dynamics, see [Roe81], in which the author introduced a simple construction of the Roe matrix satisfying all properties (1)-(3) by using a special change of variable. The main idea is to build a so-called *parameter vector* $\mathbf{Q}$. The resulting Roe matrix of Euler system for ideal gas can be presented by the Jacobian matrix. More precisely, the Roe matrix can be written as in the following form

$$\tilde{\mathbf{A}}(U_R, U_L) = \mathbf{A}(\mathbf{Q}), \tag{6.1}$$

where

$$\mathbf{Q} = \begin{pmatrix} \tilde{\rho} \\ \tilde{\rho}\tilde{u} \\ \tilde{\rho}\tilde{H} \end{pmatrix} \tag{6.2}$$

and

$$\tilde{\rho} = \sqrt{\rho_L} + \sqrt{\rho_R}, \quad \tilde{u} = \frac{\sqrt{\rho_L}u_L + \sqrt{\rho_R}u_R}{\sqrt{\rho_L} + \sqrt{\rho_R}}, \quad \tilde{H} = \frac{\sqrt{\rho_L}H_L + \sqrt{\rho_R}H_R}{\sqrt{\rho_L} + \sqrt{\rho_R}}. \tag{6.3}$$

Many extension of the approach of P. Roe have been made. In the case of the Euler system of gas dynamics we refer to [MVZ97] and numerous references therein. For two-phase flow systems, P. Roe's approach has been employed by Toumi et al in [Tou+00] for the drift flux model and in [TK96] for the two-fluid model. In the case of the drift flux model ([Tou+00]), the Roe matrix is constructed using the assumption of mechanical equilibrium which allows the definition of a parameter-vector for the mixture similar to the one in the Euler system. On the other hand, for the two-fluid model in [TK96], the parameter-vector includes the ones of each phase. These appoaches in general give an approximate Roe matrix in the sense that the conservative property (2) is only approximately satisfied.

Our objective is to find a Roe matrix for the five-equation model which includes two conservation laws of mass, two conservation laws of momentum for each phase and one conservation laws of the mixture energy. We can apply neither the approach of [Tou+00] due to the mechanical nonequilibrium nor the one of [TK96] due to one commom energy equation. We therefore follow the approach in [MFM10], where the authors separate the flux function into the convective part and pressure part, then apply Roe average conditions for each part. More details of the averaging, let us first denote $[\centerdot] = (\centerdot)_R - (\centerdot)_L$ as the jump of a parameter $\centerdot$. To express the jump of the flux function F as a combination of the jumps of the conservative variables, we first consider the following identities

$$[p+q] = [p] + [q], \tag{6.4a}$$

$$[pq] = \bar{p}[q] + \bar{q}[p], \tag{6.4b}$$

$$\left[\frac{1}{q}\right] = -\frac{[q]}{\ddot{q}^2}, \tag{6.4c}$$

where $\bar{\centerdot}$ denotes an arithmetic and $\ddot{\centerdot}$ a geometric mean value. If the flux function $F = (F_1, \ldots, F_d)$ is an algebraic fraction of the unknown vector U, $\vec{n}$ is normal vector in $\mathbb{R}^d$, then we get

$$[F \cdot \vec{n}] = F(U_R) \cdot \vec{n} - F(U_L) \cdot \vec{n} = \sum_i a_{ij}[U_j], \quad i,j = 1, \ldots, p, \tag{6.5}$$

where a_{ij} depends on U_L and U_R. The matrix obtained from a_{ij} satisfies the first and third condition of the Roe matrix due to the identities in (6.4a-6.4c) although it is not sure that this matrix is diagonalizable. In practice, it is in general diagonalizable if the difference between left and right states is not too large.
Following this approach, we compute the Roe matrix for the five-equation model in the next section and for the drift flux model, the reader can find in Appendix 6.2.6.

6.1.2 Roe matrix for five-equation model

The unknown conservative vector of the five-equation model is

$$U = (\alpha_g\rho_g, \alpha_l\rho_l, \alpha_g\rho_g u_g, \alpha_l\rho_l u_l, \alpha_g\rho_g E_g + \alpha_l\rho_l E_l). \tag{6.6}$$

The Roe matrix for the five-equation model was first computed in [Fer10] by using the formula (6.5). Following this approach we present in details the computation of the one dimensional Roe matrix in the case where we suppose that the equations of state yield $\mathrm{d}e_k = c_{v,k}\mathrm{d}T$, $k = g, l$. Such a Roe matrix is however easily extended in multidimensional case. We will apply (6.5) to compute the matrix $A = (a_{ij})$. In the system of two-fluid models, the main difficulty lies in the decomposition of the pressure $[p]$ on the base of the unknown variables $[U]$. To do that, we first consider a general equation of state in thermodynamics

$$\rho_k = \frac{\partial\rho_k}{\partial p}dp + \frac{\partial\rho_k}{\partial e_k}de_k, \tag{6.7}$$

where subscript k denotes g or l corresponding to gas or liquid. To simplify the notation, we introduce

$$\frac{1}{a_k^2} = \frac{\partial\rho_k}{\partial p}, \quad b_k = \frac{\partial\rho_k}{\partial e_k}. \tag{6.8}$$

In order to compute the Roe approximation for the energy equation, we assume that the jump of ρ_k can be performed as

$$[\rho_k] = \frac{1}{\hat{a}_k^2}[p] + \hat{b}_k[e_k], \tag{6.9}$$

where $\hat{a}_k \approx a_k$, $\hat{b}_k \approx b_k$ such that (6.9) is satisfied. Using the relation $[(\alpha_g + \alpha_l)] = 0$, we will compute $[p]$ as a function of $[U], [e_g], [e_l]$. Firstly, considering

$$[m_g] = \bar{\alpha_g}[\rho_g] + \bar{\rho}_g[\alpha_g], \tag{6.10}$$
$$[m_l] = \bar{\alpha_l}[\rho_l] + \bar{\rho}_l[\alpha_l], \tag{6.11}$$

where $m_k = \alpha_k\rho_k$.
Multiplying the equation (6.10) by $\bar{\rho}_l$ and the equation (6.11) by $\bar{\rho}_g$, then adding the two equations, we get

$$\bar{\rho}_l[m_g] + \bar{\rho}_g[m_l] = \bar{\alpha_g}\bar{\rho}_l[\rho_g] + \bar{\alpha_l}\bar{\rho}_g[\rho_l]. \tag{6.12}$$

From (6.9) and (6.12),

$$\begin{aligned}\bar{\rho}_l[m_g] + \bar{\rho}_g[m_l] &= \bar{\alpha_g}\bar{\rho}_l\left(\frac{1}{\hat{a}_g^2}[p] + \hat{b}_g[e_g]\right) + \bar{\alpha_l}\bar{\rho}_g\left(\frac{1}{\hat{a}_l^2}[p] + \hat{b}_l[e_l]\right)\\ &= \left(\frac{\bar{\alpha_g}\bar{\rho}_l}{\hat{a}_g^2} + \frac{\bar{\alpha_l}\bar{\rho}_g}{\hat{a}_l^2}\right)[p] + \bar{\alpha_g}\bar{\rho}_l\hat{b}_g[e_g] + \bar{\alpha_l}\bar{\rho}_g\hat{b}_l[e_l].\end{aligned} \tag{6.13}$$

Thus,

$$\frac{[p]}{\hat{\varrho}^2} = \bar{\rho}_l[m_g] + \bar{\rho}_g[m_l] - \bar{\alpha_g}\bar{\rho}_l\hat{b}_g[e_g] - \bar{\alpha_l}\bar{\rho}_g\hat{b}_l[e_l], \tag{6.14}$$

where $\hat{\varrho}^2 = \left(\frac{\bar{\alpha_g}\bar{\rho}_l}{\hat{a}_g^2} + \frac{\bar{\alpha_l}\bar{\rho}_g}{\hat{a}_l^2}\right)^{-1} = \frac{\hat{a}_g^2\hat{a}_l^2}{\bar{\alpha_g}\bar{\rho}_l\hat{a}_l^2 + \bar{\alpha_l}\bar{\rho}_g\hat{a}_g^2} = \frac{1}{\frac{\bar{\alpha_g}\bar{\rho}_l}{\hat{a}_g^2} + \frac{\bar{\alpha_l}\bar{\rho}_g}{\hat{a}_l^2}}$. Then, we also get

$$[\rho_g] = \frac{\hat{\varrho}^2}{\hat{a}_g^2}\left(\bar{\rho}_l[m_g] + \bar{\rho}_g[m_l] - \bar{\alpha_g}\bar{\rho}_l\hat{b}_g[e_g] - \bar{\alpha_l}\bar{\rho}_g\hat{b}_l[e_l]\right) + \hat{b}_g[e_g], \tag{6.15}$$

$$[\rho_l] = \frac{\hat{\varrho}^2}{\hat{a}_l^2}\left(\bar{\rho}_g[m_l] + \bar{\rho}_l[m_g] - \bar{\alpha_l}\bar{\rho}_g\hat{b}_l[e_l] - \bar{\alpha_g}\bar{\rho}_l\hat{b}_g[e_g]\right) + \hat{b}_l[e_l]. \tag{6.16}$$

It is also necessary to compute $[\alpha]$. From (6.10), (6.11), (6.15), (6.16), we get

$$\begin{aligned}
[\alpha_g] &= \frac{1}{\bar\rho_g}\left([m_g]-\bar\alpha_g[\rho_g]\right)\\
&= \frac{1}{\bar\rho_g}\left([m_g]-\bar\alpha_g\left(\frac{\hat\varrho^2}{\hat a_g^2}\left(\bar\rho_l[m_g]+\bar\rho_g[m_l]-\bar\alpha_g\bar\rho_l\hat b_g[e_g]-\bar\alpha_l\bar\rho_g\hat b_l[e_l]\right)+\hat b_g[e_g]\right)\right)\\
&= \bar\alpha_l\frac{\hat\varrho^2}{\hat a_l^2}[m_g]-\bar\alpha_g\frac{\hat\varrho^2}{\hat a_g^2}[m_l]+\frac{\bar\alpha_g\hat b_g}{\bar\rho_g}\left(\frac{\hat\varrho^2}{\hat a_g^2}\bar\alpha_g\bar\rho_l-1\right)[e_g]+\bar\alpha_l\hat b_l\frac{\hat\varrho^2}{\hat a_g^2}[e_l]\\
&= \bar\alpha_l\frac{\hat\varrho^2}{\hat a_l^2}[m_g]-\bar\alpha_g\frac{\hat\varrho^2}{\hat a_g^2}[m_l]-\bar\alpha_g\bar\alpha_l\hat b_g\frac{\hat\varrho^2}{\hat a_l^2}[e_g]+\bar\alpha_g\bar\alpha_l\hat b_l\frac{\hat\varrho^2}{\hat a_g^2}[e_l]\\
&= \hat\varrho^2\left(\frac{\bar\alpha_l}{\hat a_l^2}[m_g]-\frac{\bar\alpha_g}{\hat a_g^2}[m_l]-\frac{\bar\alpha_g\bar\alpha_l\hat b_g}{\hat a_l^2}[e_g]+\frac{\bar\alpha_g\bar\alpha_l\hat b_l}{\hat a_g^2}[e_l]\right).
\end{aligned}\tag{6.17}$$

Since $[p]$ and $[\alpha]$ are expressed as functions of $[m_g]$, $[m_l]$, $[e_g]$, $[e_l]$. It remains to compute $[e_g]$ and $[e_l]$. Following the identities (6.4a-6.4c), in one dimension, we obtain

$$\begin{aligned}
[\alpha\rho ue] &= \bar e[q]+\bar q[e],\\
\left[\alpha\rho u^3\right] &= \overline{u^3}[m]+\overline{m}[u^3]=\overline{u^3}[m]+\overline{m}(2\bar u^2+\overline{u^2})[u]=\overline{u^3}[m]+(2\bar u^2+\overline{u^2})([q]-\bar u[m])\\
&= -2\bar u\ddot u^2[m]+(2\bar u^2+\overline{u^2})[q],\\
[p\alpha u] &= \overline{\alpha u}[p]+\overline{p}[(\alpha u)=\overline{\alpha u}[p]+\frac{\overline{p}}{\overline{\rho}}\left([q]-\overline{\alpha u}[\rho]\right)=\frac{\overline{p}}{\overline{\rho}}[q]+\overline{\alpha u}\left([p]-\frac{\overline{p}}{\overline{\rho}}[\rho]\right),\\
\left[\alpha\rho u^2\right] &= \overline{u^2}[m]+2\overline{m}\bar u[u]=\overline{u^2}[m]+2\bar u([q]-\bar u[m])\\
&= \left(\overline{u^2}-2\bar u^2\right)[m]+2\bar u[q]=-\ddot u^2[m]+2\bar u[q],
\end{aligned}$$

where we neglected the subscript $_g$ or $_l$. Let us denote $u_{kn}=u(k)n(k)$, $k=i,j$ where $1\le i,j\le d$ and $\vec n$ is the outward normal vector. The computation of the Roe matrix is completely similar in general d-dimensional case with some remarks

$$[\alpha\rho u_iu_j]=\left(\overline{u_iu_j}-2\bar u_i\bar u_j\right)[m]+\bar u_i[q_j]+\bar u_j[q_i],\tag{6.18}$$

$$\sum_j[\alpha\rho u_iu_jn_j]=\sum_j\left(\left(\overline{u_iu_{jn}}-2\bar u_i\bar u_{jn}\right)[m]+\bar u_{in}[q_j]+\bar u_{jn}[q_i]\right),\tag{6.19}$$

$$\left[\alpha\rho u_iu_j^2\right]=\left(\overline{u_iu_j^2}-2\bar u_i\bar u_j^2-\bar u_i\overline{u_j^2}\right)[m]+2\bar u_i\bar u_j[q_j]+\overline{u_j^2}[q_i],\tag{6.20}$$

$$\begin{aligned}
\frac12\sum_{i,j}\left[\alpha\rho u_{in}u_j^2\right] &= \frac12\sum_{i,j}\left(\overline{u_{in}u_j^2}-2\bar u_{in}\bar u_j^2-\bar u_{in}\overline{u_j^2}\right)[m]+\sum_{i,j}\bar u_{in}\bar u_j[q_j]+\frac12\sum_{i,j}\overline{u_j^2}n(i)[q_i]\\
&= \frac12\sum_{i,j}\left(\overline{u_{in}u_j^2}-2\bar u_{in}\bar u_j^2-\bar u_{in}\overline{u_j^2}\right)[m]+\sum_{i,j}\bar u_{jn}\bar u_i[q_i]+\frac12\sum_{i,j}\overline{u_j^2}n(i)[q_i],
\end{aligned}$$

The common energy flux function (4.23e) is

$$F^E=\alpha_g\rho_gE_gu_g+\alpha_l\rho_lE_lu_l+P(\alpha_gu_g+\alpha_lu_l)\quad\text{where } E_k=e_k+\frac12v_k^2.\tag{6.21}$$

We compute $\left[F^E\right]$ by decomposing its components as follows

$$F^E = \alpha_g\rho_gu_ge_g+\alpha_l\rho_lu_le_l+\frac12\alpha_g\rho_gu_g^3+\frac12\alpha_l\rho_lu_l^3+P\alpha_gu_g+P\alpha_lu_l$$

Similarly, the volumic density of the total energy denoted by E

$$E=\alpha_g\rho_g\left(e_g+\frac12u_g^2\right)+\alpha_l\rho_l\left(e_l+\frac12u_l^2\right),\tag{6.22}$$

has its jump

$$\begin{aligned}
[E] &= [\alpha_g\rho_g e_g] + [\alpha_l\rho_l e_l] + \frac{1}{2}\left[\alpha_g\rho_g u_g^2\right] + \frac{1}{2}\left[\alpha_l\rho_l u_l^2\right] \\
&= \bar{e}_g[m_g] + \bar{e}_l[m_l] + \overline{m}_g[e_g] + \overline{m}_l[e_l] - \frac{\ddot{u}_g^2}{2}[m_g] + \bar{u}_g[q_g] - \frac{\ddot{u}_l^2}{2}[m_l] + \bar{u}_l[q_l] \\
&= \left(\bar{e}_g - \frac{\ddot{u}_g^2}{2}\right)[m_g] + \left(\bar{e}_l - \frac{\ddot{u}_l^2}{2}\right)[m_l] + \bar{u}_g[q_g] + \bar{u}_l[q_l] + \overline{m}_g[e_g] + \overline{m}_l[e_l],
\end{aligned}$$

or equivalently

$$\overline{m}_g[e_g] + \overline{m}_l[e_l] = [E] - \left(\bar{e}_g - \frac{\ddot{u}_g^2}{2}\right)[m_g] - \left(\bar{e}_l - \frac{\ddot{u}_l^2}{2}\right)[m_l] - \bar{u}_g[q_g] - \bar{u}_l[q_l]. \tag{6.23}$$

Assume that $e_k = e_k(T)$, and

$$de_k = \frac{\partial e_k}{\partial T} dT. \tag{6.24}$$

We denote $c_{v,k} = \frac{\partial e_k}{\partial T}$ and $\hat{c}_{v,k} \approx c_{v,k}$ such that

$$[e_k] = \hat{c}_{v,k}[T]. \tag{6.25}$$

From (6.23), we can compute $[T]$ as below

$$\left(\hat{c}_g\overline{m}_g + \hat{c}_l\overline{m}_l\right)[T] = [E] - \left(\bar{e}_g - \frac{\ddot{u}_g^2}{2}\right)[m_g] - \left(\bar{e}_l - \frac{\ddot{u}_l^2}{2}\right)[m_l] - \bar{u}_g[q_g] - \bar{u}_l[q_l] \tag{6.26}$$

$$[T] = \frac{1}{\hat{c}_g\overline{m}_g + \hat{c}_l\overline{m}_l}\left([U_5] - \left(\bar{e}_g - \frac{\ddot{u}_g^2}{2}\right)[U_1] - \left(\bar{e}_l - \frac{\ddot{u}_l^2}{2}\right)[U_2] - \bar{u}_g[U_3] - \bar{u}_l[U_4]\right).$$

From (6.9) and (6.14),

$$\begin{aligned}
[p] - \frac{\overline{p}}{\bar{\rho}_k}[\rho_k] &= [p] - \frac{\overline{p}}{\bar{\rho}_k}\left(\frac{1}{\hat{a}_k^2}[p] + \hat{b}_k[e_k]\right) \\
&= \left(1 - \frac{\overline{p}}{\hat{a}_k^2\bar{\rho}_k}\right)[p] - \frac{\overline{p}\hat{b}_k}{\bar{\rho}_k}[e_k].
\end{aligned} \tag{6.27}$$

$$\begin{aligned}
\left[F^E\right] &= \bar{e}_g[q_g] + \bar{e}_l[q_l] + \bar{q}_g[e_g] + \bar{q}_l[e_l] \\
&+ (\bar{u}_g^2 + \frac{1}{2}\overline{u_g^2})[q_g] + (\bar{u}_l^2 + \frac{1}{2}\overline{u_l^2})[q_l] - \bar{u}_g\ddot{u}_g^2[m_g] - \bar{u}_l\ddot{u}_l^2[m_l] \\
&+ \left(\frac{\overline{p}}{\bar{\rho}_g}[q_g] + \frac{\overline{p}}{\bar{\rho}_l}[q_l]\right) + \overline{\alpha_g u_g}([p] - \frac{\overline{p}}{\bar{\rho}_g}[\rho_g]) + \overline{\alpha_l u_l}([p] - \frac{\overline{p}}{\bar{\rho}_l}[\rho_l]),
\end{aligned}$$

or equivalently,

$$\begin{aligned}
\left[F^E\right] &= \left(\eta\hat{\varrho}^2\bar{\rho}_l - \bar{u}_g\ddot{u}_g^2\right)[U_1] + \left(\eta\hat{\varrho}^2\bar{\rho}_g - \bar{u}_l\ddot{u}_l^2\right)[U_2] \\
&+ \left(\bar{e}_g + \bar{u}_g^2 + \frac{1}{2}\overline{u_g^2} + \frac{\overline{p}}{\bar{\rho}_g}\right)[U_3] + \left(\bar{e}_l + \bar{u}_l^2 + \frac{1}{2}\overline{u_l^2} + \frac{\overline{p}}{\bar{\rho}_l}\right)[U_4] \\
&+ \left(\overline{q}_g - \frac{\overline{\alpha_g u_g}\,\overline{p}\hat{b}_g}{\bar{\rho}_g} - \eta\hat{\varrho}^2\bar{\alpha}_g\bar{\rho}_l\hat{b}_g\right)[e_g] \\
&+ \left(\overline{q}_l - \frac{\overline{\alpha_l u_l}\,\overline{p}\hat{b}_l}{\bar{\rho}_l} - \eta\hat{\varrho}^2\bar{\alpha}_l\bar{\rho}_g\hat{b}_l\right)[e_l],
\end{aligned} \tag{6.28}$$

where

$$[e_k] = \frac{\hat{c}_k}{\hat{c}_g\overline{m}_g + \hat{c}_l\overline{m}_l}\left([U_5] - \left(\bar{e}_g - \frac{\ddot{u}_g^2}{2}\right)[U_1] - \left(\bar{e}_l - \frac{\ddot{u}_l^2}{2}\right)[U_2] - \bar{u}_g[U_3] - \bar{u}_l[U_4]\right), \tag{6.29}$$

and

$$\eta = \left(\overline{\alpha_g u_g}\left(1 - \frac{\overline{p}}{\hat{a}_g^2\bar{\rho}_g}\right) + \overline{\alpha_l u_l}\left(1 - \frac{\overline{p}}{\hat{a}_l^2\bar{\rho}_l}\right)\right). \tag{6.30}$$

Finally, the Roe matrix for the five-equation two-fluid model in one dimensional space derived is

$$\tilde{\mathbf{A}} = \tilde{\mathbf{A}}_1 + \tilde{\mathbf{A}}_2, \tag{6.31}$$

where

$$\tilde{\mathbf{A}}_1 = \begin{bmatrix} 0 & 0 & 1 & 0 & 0 \\ 0 & 0 & 0 & 1 & 0 \\ -2\ddot{u}_g^2 & 0 & 2\bar{u}_g & 0 & 0 \\ 0 & -2\ddot{u}_l^2 & 0 & 2\bar{u}_l & 0 \\ \left[F^E\right]_1 & \left[F^E\right]_2 & \left[F^E\right]_3 & \left[F^E\right]_4 & \left[F^E\right]_5 \end{bmatrix},$$

$$\tilde{\mathbf{A}}_2 = \begin{bmatrix} 0 & 0 & 0 & 0 & 0 \\ 0 & 0 & 0 & 0 & 0 \\ \tilde{\alpha}_g[p]_1 + \Delta p[\alpha_g]_1 & \tilde{\alpha}_g[p]_2 + \Delta p[\alpha_g]_2 & \tilde{\alpha}_g[p]_3 + \Delta p[\alpha_g]_3 & \tilde{\alpha}_g[p]_4 + \Delta p[\alpha_g]_4 & \tilde{\alpha}_g[p]_5 + \Delta p[\alpha_g]_5 \\ \tilde{\alpha}_l[p]_1 + \Delta p[\alpha_l]_1 & \tilde{\alpha}_l[p]_2 + \Delta p[\alpha_l]_2 & \tilde{\alpha}_l[p]_3 + \Delta p[\alpha_l]_3 & \tilde{\alpha}_l[p]_4 + \Delta p[\alpha_l]_4 & \tilde{\alpha}_l[p]_5 + \Delta p[\alpha_l]_5 \\ 0 & 0 & 0 & 0 & 0 \end{bmatrix},$$

the jumps $[p]$, $[\alpha]$, $\left[F^E\right]$ are computed by (6.14), and (6.17), (6.28) respectively.

Roe matrix in the case of stiffened gas

We consider one particular equation of state, stiffened gas law

$$p_k = (\gamma_k - 1)\rho_k e_k - \gamma_k p_{k\infty}, \quad k = g, l, \tag{6.32}$$

see details in Section 6.1.7. Then, $\hat{a}_k$ and $\hat{b}_k$ in this case are

$$\frac{1}{\hat{a}_k^2} = \frac{\bar{e}_k}{(\gamma_k - 1)\ddot{e}_k^2}, \tag{6.33}$$

$$\hat{b}_k = \frac{P_{k\infty} - \overline{p}}{(\gamma_k - 1)\ddot{e}_k^2}. \tag{6.34}$$

We assume that the internal energy has takes the following linearized form

$$e_k = e_k^0 + c_{v,k}^0(T - T_0). \tag{6.35}$$

Then, it is clear that

$$\hat{c}_{v,k} = c_{v,k}^0, \tag{6.36}$$

see (6.25). The jump $\left[F^E\right]$, equation (6.28), in this case can be computed explicitly by using (6.33), (6.34), (6.36) and

$$\eta\hat{\varrho}^2 = \left(\overline{\alpha_g u_g}\left(1 - \frac{\overline{p}}{\hat{a}_g^2\bar{\rho}_g}\right) + \overline{\alpha_l u_l}\left(1 - \frac{\overline{p}}{\hat{a}_l^2\bar{\rho}_l}\right)\right)\frac{1}{\frac{\bar{\alpha}_g\bar{\rho}_l}{\hat{a}_g^2} + \frac{\bar{\alpha}_l\bar{\rho}_g}{\hat{a}_l^2}}. \tag{6.37}$$

6.1.3 Computation of the sign $\mathbf{sgn}(A)$ and the absolute value $|A|$ of a matrix A

The scalar sign function is defined for $x \in \mathbb{C}\backslash i\mathbb{R}^*$ by

$$\mathrm{sgn}(x) = \begin{cases} 1 & \text{if } \mathrm{Re}(x) > 0, \\ 0 & \text{if } x = 0, \\ -1 & \text{if } \mathrm{Re}(x) < 0. \end{cases} \tag{6.38}$$

Let us consider a real $n \times n$ diagonalizable matrix A with the eigenvalues $\lambda_1, \ldots, \lambda_n \in \mathbb{C}\backslash i\mathbb{R}^*$, left eigenvectors $\mathbf{l}_1, \ldots, \mathbf{l}_n$, right eigenvectors $\mathbf{r}_1, \ldots, \mathbf{r}_n$ such that $\mathbf{l}_i \cdot \mathbf{r}_i = 1$, $i = 1, \ldots, n$. Then, the sign and absolute value functions of the matrix A are defined by

$$\mathrm{sgn}(A) = \sum_{i=1}^{n} \mathrm{sgn}(\lambda_i) \mathbf{l}_i \otimes \mathbf{r}_i, \quad |A| = \sum_{i=1}^{n} |\lambda_i| \mathbf{l}_i \otimes \mathbf{r}_i. \tag{6.39}$$

In general, the computation of the left eigenvectors and right eigenvectors is expensive, especially when two eigenvalues are not far apart, see [GL13]. Therefore, different algorithms relying on iteration methods or interpolation are developed to compute the matrix sign and absolute value. For more details we refer the reader to [Sol+14 ; Ndj08] and references therein. We would like here to introduce an algorithm presented in [Ndj08] that we will use for the numerical simulation in this document.
Considering an interpolation polynomial $P_{\mathrm{int}} \in \mathbb{R}[X]$. Thanks to the property

$$P_{\mathrm{int}}(A) = |A| \iff P_{\mathrm{int}}(\lambda_i) = |\lambda_i|, \forall i = 1, \ldots, n, \tag{6.40}$$

$$P_{\mathrm{int}}(A) = \mathrm{sgn}(A) \iff P_{\mathrm{int}}(\lambda_i) = \mathrm{sgn}(\lambda_i), \forall i = 1, \ldots, n, \tag{6.41}$$

they can compute the polynomial $P_{\mathrm{int}} \in \mathbb{R}_{n_d-1}[X]$, where n_d is the number of distinct eigenvalues of matrix A. Denote

$$P_+(X) = \prod_{\mathrm{Re}(\lambda_i) \geq 0} (X - \lambda_i), \quad P_-(X) = \prod_{\mathrm{Re}(\lambda_i) < 0} (X - \lambda_i). \tag{6.42}$$

Follow [Ndj08],

$$P_{\mathrm{int}}(X) = X + P_+(X)Q_+(X), \text{ or } P_{\mathrm{int}}(X) = 1 + P_+(X)Q_+(X), \tag{6.43}$$

where

$$Q_+(\lambda_i) = \frac{-2\lambda_i}{P_+(\lambda_i)}, \text{ or } Q_+(\lambda_i) = \frac{-2}{P_+(\lambda_i)}, \forall \lambda_i : \mathrm{Re}(\lambda_i) < 0. \tag{6.44}$$

We therefore need to compute Q_+ which is simpler than P_{int}. Due to the formula of Q_+ in (6.44), it would be good if the number of λ_i such that $\mathrm{Re}(\lambda_i) < 0$ is less than the number of λ_i such that $\mathrm{Re}(\lambda_i) \geq 0$, otherwise applying the computation on $-A$. The rest of algorithm remains calculating the interpolation polynomial $Q_+(X)$.
A highlight advantage of this algorithm is fastness and robustness in comparison with other algorithm, [Ndj08] and it allows to compute generally $|A|$ and $\mathrm{sgn}(A)$. However a disadvantage of such an algorithm is that it requires all exact eigenvalues of the matrix A. In the computational simulation, we will use the package LAPACK [1] to compute the eigenvalues.

6.1.4 Treatment of the non conservative product

We refer to the Section 4.3.4 for an introduction to different considerations of non conservative products in the two-fluid model. In the numerical analysis of this section, we do not consider the temporal non-conservative product by using the five-equation two-fluid model (4.23a-4.23e) and consider the linearization of the void fraction by $\tilde{\alpha}_g$ in equation (4.160).

6.1.5 Treatment of the source term

Some specific considerations about the source terms have been introduced in Section 2.3. Among those, because of the non smoothness of $S(U)$, we chose the source term upwinding approach suggested by Bermudez and Vazquez in [BV94]. The resulting source terms at the cell C_j are considered in the explicit numerical method as the following equation

$$U_j^{n+1} = U_j^n - \frac{\Delta t}{\mathrm{Vol}_j} \sum_{j_k \in \mathrm{neighbor}(j)} s_{jj_k} \left(\mathbf{F}_{\mathrm{i}}(U_j^n, U_{j_k}^n) \right) + \Delta t S_j^{\mathrm{up}}, \tag{6.45}$$

1. A Linear Algebra PACKage : www.netlib.org/lapack

where

$$S_j^{\text{up}} = \frac{1}{\text{Vol}_j} \sum_{j_k \in \text{neighbor}(j)} \text{Vol}_{jj_k} \left(\frac{\mathbb{I}\text{d} - \text{sgn}\left(A^{\text{Roe}}_{j,j_k}\right)}{2} \tilde{S}_{j,j_k} \right), \tag{6.46}$$

such that

$$\sum_{j_k \in \text{neighbor}(j)} \text{Vol}_{jj_k} = \text{Vol}_j \quad \text{and} \tag{6.47}$$

$\tilde{S}_{j,j_k}$ is some approximation of the source term S on the interface (j, j_k), which is usually taken as $\tilde{S}_{j,j_k} = \dfrac{S_j + S_{j_k}}{2}$ where $S_j = S(U_j^n, x_j)$.
We observed a significant improvement of the quality of our simulations using the source upwinding approach (the oscillations disappeared) and propose here an analysis justifying the connection between the source upwinding and the preservation of the stationary state in the case of 1D linear systems.

1D analysis of the consistency with the stationary state for stiff linear systems

Considering a one dimensional hyperbolic system $\partial_t U + \partial_x F(U) = S(U, x)$, a numerical solution U_j is supposed to be well captured at the stationary state if it satisfies

$$F(U_{j+1}) - F(U_j) = \Delta x \tilde{S}_{j+1/2}, \tag{6.48}$$

where

$$\tilde{S}_{j+1/2} = \tilde{S}(U_j, U_{j+1}, x_j, x_{j+1}) = \frac{1}{\Delta x} \int_{x_j}^{x_{j+1}} S(U, x) \mathrm{d}x, \tag{6.49}$$

Without specific mention, we always consider a simple approximation of (6.49), which is

$$\tilde{S}_{j+1/2} = \frac{S_j + S_{j+1}}{2}, \tag{6.50}$$

where $S_j = S(U_j, x_j)$.

We consider here the upwind scheme applied to the linear flux $F(U) = AU$ where A is a real diagonalizable matrix. The interfacial numerical flux of the upwind scheme can be expressed as

$$\mathbf{F}_{j+1/2} = \frac{F_j + F_{j+1}}{2} - |A_{j,j+1}| \frac{U_{j+1} - U_j}{2}, \tag{6.51}$$

$$\mathbf{F}_{j-1/2} = \frac{F_j + F_{j-1}}{2} - |A_{j-1,j}| \frac{U_j - U_{j-1}}{2}. \tag{6.52}$$

Following the work in [BV94], the upwinding of the source term S_j in (6.45) is defined as

$$S_j^{\text{up}} = \frac{\mathbb{I}\text{d} - \text{sgn}\left(A^{\text{Roe}}_{j,j+1}\right)}{2} \tilde{S}_{j+1/2} + \frac{\mathbb{I}\text{d} + \text{sgn}\left(A^{\text{Roe}}_{j-1,j}\right)}{2} \tilde{S}_{j-1/2}. \tag{6.53}$$

The overall upwind scheme with upwinding source can be rewritten as

$$U_j^{n+1} = U_j^n - \frac{\Delta t}{\Delta x} \left(\mathbf{F}_{j+1/2} - \mathbf{F}_{j-1/2} - \Delta x S_j^{\text{up}} \right). \tag{6.54}$$

The numerical result reaches a stationary state when

$$\mathbf{F}_{j+1/2} - \mathbf{F}_{j-1/2} = \Delta x S_j^{\text{up}}. \tag{6.55}$$

According to [BV94], the numerical results of the steady state are improved when applying source upwinding through the formula (6.53). Although this method can not ensure the preservation of the stationary state for a general system of nonlinear balance laws described by (6.48), it can do in the case of linear systems. Let us see the following lemma, i.e.

Lemma 2 *Considering the following linear system of balance laws in one dimension*

$$\frac{\partial U}{\partial t} + \frac{\partial \mathbf{A}U}{\partial x} = S(U,x), \quad x \in \mathbb{R}, \tag{6.56}$$

where the unknown vector $U \in \mathbb{R}^p$, $\mathbf{A}$ is a diagonalizable constant matrix in $\mathbb{R}^{p\times p}$ with non zero eigenvalues, and $S \in L^1_{loc}(\mathbb{R}^p \times \mathbb{R}$ is possibly discontinuous in U and x. Then the upwinding source terms (6.53) implies that the discrete stationary state satisfies (6.48) with $F = \mathbf{A}U$ and $\tilde{S}_{j+1/2} = \dfrac{S(U_j,x_j) + S(U_{j+1},x_{j+1})}{2}$.

Proof : The proof of this lemma is proposed by Mr Ndjinga as follows.
In the linear system, the equation (6.51) and (6.52) can be rewritten as

$$\mathbf{F}_{j+1/2} = \frac{\mathbf{A}U_j + \mathbf{A}U_{j+1}}{2} - \mathrm{sgn}(\mathbf{A})\frac{\mathbf{A}U_{j+1} - \mathbf{A}U_j}{2}, \tag{6.57}$$

$$\mathbf{F}_{j-1/2} = \frac{\mathbf{A}U_{j-1} + \mathbf{A}U_j}{2} - \mathrm{sgn}(\mathbf{A})\frac{\mathbf{A}U_j - \mathbf{A}U_{j-1}}{2}. \tag{6.58}$$

The numerical stationary state (6.55) yields

$$\begin{aligned}\frac{\mathbb{I}\mathrm{d} - \mathrm{sgn}(\mathbf{A})}{2}\frac{\mathbf{A}U_{j+1} - \mathbf{A}U_j}{\Delta x} + \frac{\mathbb{I}\mathrm{d} + \mathrm{sgn}(\mathbf{A})}{2}\frac{\mathbf{A}U_j - \mathbf{A}U_{j-1}}{\Delta x}\\ = \frac{\mathbb{I}\mathrm{d} - \mathrm{sgn}(\mathbf{A})}{2}\frac{S_j + S_{j+1}}{2} + \frac{\mathbb{I}\mathrm{d} + \mathrm{sgn}(\mathbf{A})}{2}\frac{S_{j-1} + S_j}{2}.\end{aligned} \tag{6.59}$$

Multiplying (6.59) by $\dfrac{\mathbb{I}\mathrm{d} - \mathrm{sgn}(\mathbf{A})}{2}$, we obtain

$$\frac{\mathbb{I}\mathrm{d} - \mathrm{sgn}(\mathbf{A})}{2}\frac{\mathbf{A}U_{j+1} - \mathbf{A}U_j}{\Delta x} = \frac{\mathbb{I}\mathrm{d} - \mathrm{sgn}(\mathbf{A})}{2}\frac{S_j + S_{j+1}}{2}. \tag{6.60}$$

Multiplying (6.59) by $\dfrac{\mathbb{I}\mathrm{d} + \mathrm{sgn}(\mathbf{A})}{2}$, we obtain

$$\frac{\mathbb{I}\mathrm{d} + \mathrm{sgn}(\mathbf{A})}{2}\frac{\mathbf{A}U_{j+1} - \mathbf{A}U_j}{\Delta x} = \frac{\mathbb{I}\mathrm{d} + \mathrm{sgn}(\mathbf{A})}{2}\frac{S_j + S_{j+1}}{2}. \tag{6.61}$$

Adding equations (6.60) and (6.61) yields the conclusion of the lemma.

$$\frac{\mathbf{A}U_{j+1} - \mathbf{A}U_j}{\Delta x} = \frac{S_j + S_{j+1}}{2}. \tag{6.62}$$

□

6.1.6 Entropy fix

General Harten-type entropy fixes have been introduced in Section 2.2.2. Among those, we here apply a simple entropy fix, the so-called Harten-type entropy fix, by first defining

$$\bar{\delta} = \max_l\{|\lambda_k(U_L) - \lambda_k(U_R)|\} \text{ and } l \in \{1,..,p\}\backslash\{\text{acoustic waves}\}, \tag{6.63}$$

we then add an amount of numerical viscosity for all characteristic fields by the same function $\bar{\delta}$, which takes into account the velocity difference of all waves except the acoustic waves. The numerical flux function with the entropy fix Harten-type is rewritten

$$\mathbf{F}^{\mathrm{H}}(U_L,U_R) = \frac{1}{2}\left(F(U_L) + F(U_R)\right) - \frac{1}{2}(|A(U_L,U_R)| + \bar{\delta}\mathbb{I}\mathrm{d})(U_R - U_L). \tag{6.64}$$

The advantage of this Harten-type entropy fix is that it is simple and easy to implement in any complicated code using Roe-type schemes. It requires only a computation the eigenvalues of the left state and right state supplementary in addition.

6.1.7 Stiffened gas equation of state

As mentioned in Section 4.1.5, it is necessary to take into account the equation of state to close a system of two-phase flow. Such an equation in thermodynamics defines a relation between pressure, density and temperature and is in general formulated by the mathematical equation (4.27). In industrial applications, one usually considers an accurate equation of state obtained by experimental measurement. However, we here focus on the mathematical aspect in an open source environment. The equation of state is therefore chosen as simple as possible. Without specific mention, the numerical tests in this chapter will use the following stiffened equation of state

$$p_k = (\gamma_k - 1)\rho_k e_k - \gamma_k p_{\infty k}, \tag{6.65}$$

associated to a linearized internal energy law

$$e_k = e_k^0 + c_{v,k}^0 (T - T_0). \tag{6.66}$$

where k represents either liquid (l) or gas (g), p_k the pressure, ρ_k the density and e_k internal energy.

Computing γ_k and $p_{\infty k}$

We recall that the sound speed of a fluid described by a stiffened gas law is given by the formula

$$c_{sk}^2 = \frac{\gamma_k (p + p_{\infty k})}{\rho_k}. \tag{6.67}$$

γ_k and $p_{\infty k}$ are constant that are chosen so that the stiffened gas law reproduces water and steam behaviour the best. We chose to determine these constants from the knowledge at some boiling point $(p_0, T_0 = T^{sat}(p_0))$ of the internal energy e_{0k}, density ρ_{0k} and sound speed c_{0sk}. More precisely, the following data are taken from the NIST website, [ST].

$$\begin{array}{lll} p_0 = 155 \text{ bars}, & T_0 = 345\,^\circ C, & \\ \rho_v^0 = 100\, kg/m^3, & e_v^0 = 2500\, kJ/kg, & h_v^0 = 2655\, kJ/kg, \\ \rho_l^0 = 600\, kg/m^3, & e_l^0 = 1600\, kJ/kg, & h_l^0 = 1626\, kJ/kg, \\ c_{s,l} = 620 m/s, & c_{s,v} = 430 m/s. & \end{array} \tag{6.68}$$

Then, we obtain

$$\gamma_v = 1 + \frac{430^2}{2.6\,10^6} = 1.07, \tag{6.69}$$

$$\gamma_l = 1 + \frac{620^2}{1.6\,10^6} = 1.24, \tag{6.70}$$

$$p_{\infty v} = \frac{\frac{430^2}{2.6\,10^6} 100 \times 2.5\,10^6 - 155\,10^5}{1 + \frac{430^2}{2.6\,10^6}} = 1.87\,10^6, \tag{6.71}$$

$$p_{\infty l} = \frac{\frac{620^2}{1.6\,10^6} 600 \times 1.6\,10^6 - 155\,10^5}{1 + \frac{620^2}{1.6\,10^6}} = 1.73\,10^8. \tag{6.72}$$

6.1.8 Computing the primitive variable from the conservative variables in the five-equation model

During the simulation it is essential to transfer the value of conservative variables (6.6) derived by the system PDEs to the primitive variables, which are

$$(\alpha, p, u_g, u_l, T), \tag{6.73}$$

in the five-equation model.
The two velocities u_g, u_l are computed by

$$u_g = \frac{\alpha_g \rho_g u_g}{\alpha_g \rho_g}, \quad u_l = \frac{\alpha_l \rho_l u_l}{\alpha_l \rho_l}. \tag{6.74}$$

Computation of the temperature

The common temperature (T) is computed thanks to the mixture total energy variable

$$\alpha_g\rho_g E_g + \alpha_l\rho_l E_l = \alpha_g\rho_g e_g + \alpha_l\rho_l e_l + \frac{1}{2}\alpha_g\rho_g u_g^2 + \frac{1}{2}\alpha_l\rho_l u_l^2, \tag{6.75}$$

and the closure laws $e_k = c_{v,k}T$, $k = g, l$ which yield

$$T = \frac{(\alpha_g\rho_g E_g + \alpha_l\rho_l E_l) - \frac{1}{2}\alpha_g\rho_g u_g^2 - \frac{1}{2}\alpha_l\rho_l u_l^2}{\alpha_g\rho_g c_{v,g} + \alpha_l\rho_l c_{v,l}}. \tag{6.76}$$

Computation of the pressure

In order to compute the common pressure p in the two-fluid model, one use the following equation

$$\frac{m_g}{\rho_g} + \frac{m_l}{\rho_l} = 1, \tag{6.77}$$

which is rewritten by the closure law (4.25) using partial mass $m_g = \alpha_g\rho_g$, $m_l = \alpha_l\rho_l$, and the equations of state $\rho_g = \rho_g(p, e_g)$, $\rho_l = \rho_l(p, e_l)$. The pressure is computed by solving (6.77). With the general equations of state, it requires an iterative method to find the pressure. In the stiffened equation of state, the computation is much simplified. More precisely, the stiffened equation of state (6.65) implies

$$\rho_g = \frac{p + \gamma_g p_{\infty,g}}{(\gamma_g - 1)e_g(T)}, \tag{6.78}$$

$$\rho_l = \frac{p + \gamma_l p_{\infty,l}}{(\gamma_l - 1)e_l(T)}. \tag{6.79}$$

Equation (6.77) then leads to a second order polynomial in the pressure as follows

$$ap^2 + bp + c = 0, \tag{6.80}$$

where

$$a = 1, \tag{6.81}$$

$$b = (\gamma_g p_{\infty,g} + \gamma_l p_{\infty,l} - m_g(\gamma_g - 1)e_g - m_l(\gamma_l - 1)e_l), \tag{6.82}$$

$$c = \gamma_g\gamma_l p_{\infty,g} p_{\infty,l} - p_{\infty,g}\gamma_g m_l(\gamma_l - 1)e_l - p_{\infty,l}\gamma_l m_g(\gamma_g - 1)e_g. \tag{6.83}$$

Rewrite c as

$$c = \gamma_g\gamma_l p_{\infty,g} p_{\infty,l} - p_{\infty,g}\gamma_g\alpha_l(\bar{p}_l + \gamma_l p_{\infty,l}) - p_{\infty,l}\gamma_l\alpha_g(\bar{p}_g + \gamma_g p_{\infty,g}) \tag{6.84}$$

$$= -(p_{\infty,g}\gamma_g\alpha_l\bar{p}_l + p_{\infty,l}\gamma_l\alpha_g\bar{p}_g), \tag{6.85}$$

where $\bar{p}_l = (\gamma_l - 1)\rho_l e_l - \gamma_l p_{\infty,l}$, and $\bar{p}_g = (\gamma_g - 1)\rho_g e_g - \gamma_g p_{\infty,g}$.
If $\bar{p}_l > 0$ and $\bar{p}_g > 0$, then $c < 0$ and the equation (6.80) leads to a unique positive pressure.
The densities ρ_k, $k = g, l$ are derived directly by the equation of state $\rho_k = \rho_k(p, e_k)$. The void fraction $\alpha = \frac{\alpha_g\rho_g}{\rho_g}$ is therefore achieved.

6.2 Numerical results

This section will illustrate the potentialities by using the numerical methods associated with some special treatments, specific algorithms ... which are explained in Section 6.1. We present here some test cases, which are either classical but challenging or specifically interesting for the power plant systems using the five-equation two-fluid model (4.23a-4.23e).
The first test case is the water faucet problem, which is a classical one usually used to validate the numerical methods in two-phase flow. This test is difficult due to a presence of the discontinuous transient state. The center-type schemes are usually not able to simulate this problem whereas the Roe-type schemes or the one using the full eigenvalues shows good results, following [PCC03], [SH13], [EF05], [Ndj07b].

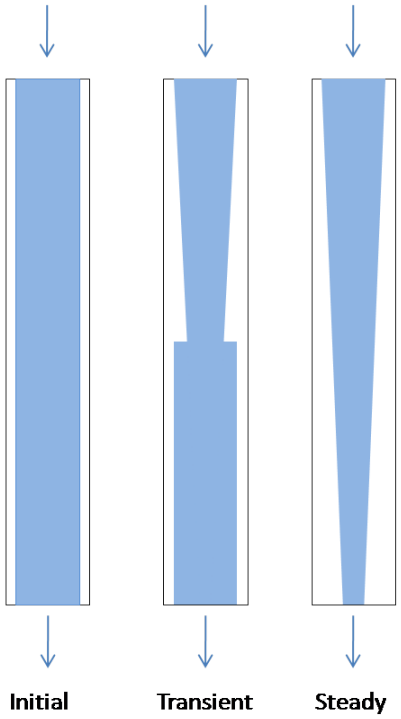

FIGURE 6.1 – A sketch of the water faucet test.

The second test case is a sedimentation problem, i.e. a phase separation by gravity. This test is challenging due to the presence of counter-current flows, of which two partial velocities go in different directions. This test is classically used to verify numerical methods developed for two-phase flow models, see [Coq+97 ; MEF09 ; SH13] for one pressure two-fluid model, and [ACR12] for the two pressures two-fluid model, due to the existence of a nontrivial stationary state whose the void fraction is discontinuous. Moreover, the sedimentation is interesting since it illustrates a phase disappearance, i.e. a vanishing phase. To implement the sedimentation test, it is necessary to take into account the two-fluid models. We perform this test using the five-equation two-fluid model although the variation of temperature is negligible.
The last numerical test is the boiling channel, which is an important test for the nuclear reactor thermal hydraulics. In this case, it is essential to consider the energy equation. In order to reduce the difficulties of the complete six equation model, we will use the five-equation model in this test. The computation of the Roe matrix presented in Section 6.1.2 will be used here.

6.2.1 Water faucet problem

The water faucet problem was proposed by Ransom in [Ran87], it is then studied by many authors to validate the numerical methods for two-phase flows, see [PCC03], [SH13], [EF05] and references therein. One interesting point of the faucet problem is that the void fraction of the reference solution admits a discontinuous transient state, see Figure 6.1. Therefore, diffusively numerical schemes may well be observed in this test case. Numerous different numerical methods are applied to the water faucet problem in the literature. The Roe-type schemes are the ones well simulating this problem, see [Ndj07b], [Mun07] for example. We are interested in comparison between the Roe schemes, with or without Harten-type entropy fix in this test case, so that numerical diffusion can be observed.
To implement the water faucet simulation, we consider the uniform initial data of the void fraction $\alpha = 0.2$, pressure $p = 10^5 Pa$, vapor velocity $u_g = 0$, liquid velocity $u_l = 10m/s$, and $T = 293K$. The inlet boundary condition is fixed by the the same initial data while the pressure at the outlet is fixed $p = 10^5 Pa$. The gravity $g = 10m/s^2$ is the unique source term considered in this test.

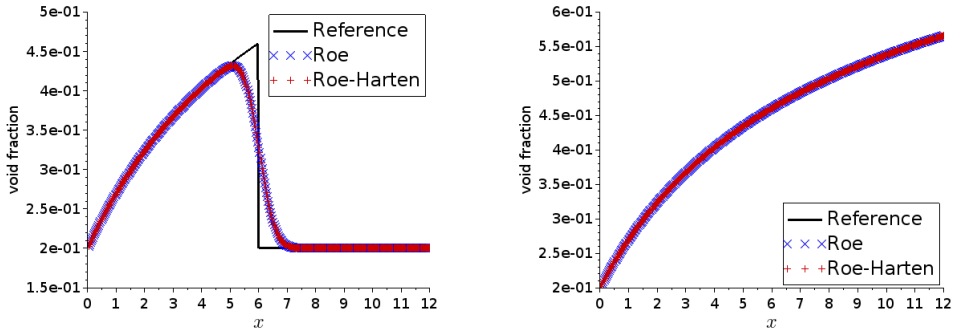

(a) (b)

FIGURE 6.2 – Void fraction of water faucet at the transient state (Figure 6.2(a)) and at the stationary state (Figure (6.2(b)) in a tube $12\,m$ in length, structure mesh with 400 cells and CFL $= 0.95$.

Reference solution

In [Coq+97], the authors provide the following analytical solution of the void fraction

$$\alpha_g(x,t) = \begin{cases} 1 - \dfrac{\alpha_{l,0} u_{l,0}}{\sqrt{u_{l,0}^2 + 2gx}} & \text{if } x < u_{l,0}t + \frac{1}{2}gt^2, \\ 1 - \alpha_{l,0} & \text{otherwise,} \end{cases} \tag{6.86}$$

and the liquid velocity is presented in [EF03] as follows

$$u_l(x,t) = \begin{cases} \sqrt{u_{l,0}^2 + 2gx} & \text{if } x < u_{l,0}t + \frac{1}{2}gt^2, \\ u_{l,0} + gt & \text{otherwise.} \end{cases} \tag{6.87}$$

The formula (6.86) and (6.87) are obtained by using an incompressible liquid assumption and neglecting the variation of the pressure in space. More details of the proof can be found in [Mun05].

Equations of state

Due to the fact that we perform this test at the pressure condition $p = 10^5\,Pa$, the equations of state we use is the stiffened law

$$p_k = (\gamma_k - 1)\rho_k e_k - \gamma_k p_{k\infty}, \quad k = g, l,$$

with the following parameters

$$\gamma_g = 1.34, \quad \gamma_l = 6.66728, \quad p_{g\infty} = 0, \quad p_{l\infty} = 3.41997\,10^8.$$

Numerical simulation

The numerical simulation considers the Roe scheme and the Roe scheme with Harten-type entropy fix on the spacial domain $[0, 12]$ with 400 cells in uniform mesh, CFL $= 0.95$. The void fraction of the transient state of both schemes displayed in Figure 6.2(a) shows that the entropy fix does not give rise considerable diffusion in this test case. For the void fraction of the stationary state, we refer the reader to Figure 6.2(b). In addition, Figure 6.2.1 shows the numrical results of the water faucet in two-dimensional space.

6.2.2 Sedimentation

The sedimentation, i.e. phase separation by gravity, is a classical but challenging test to validate the numerical methods applied for the two-phase flow models in fluid mechanics. Although Toumi could present the sedimentation test in a vertical tube using the drift-flux model in [Tou87] by imposing zero volume fraction of gas and liquid at boundary, i.e. not the usual wall conditions, such a test is

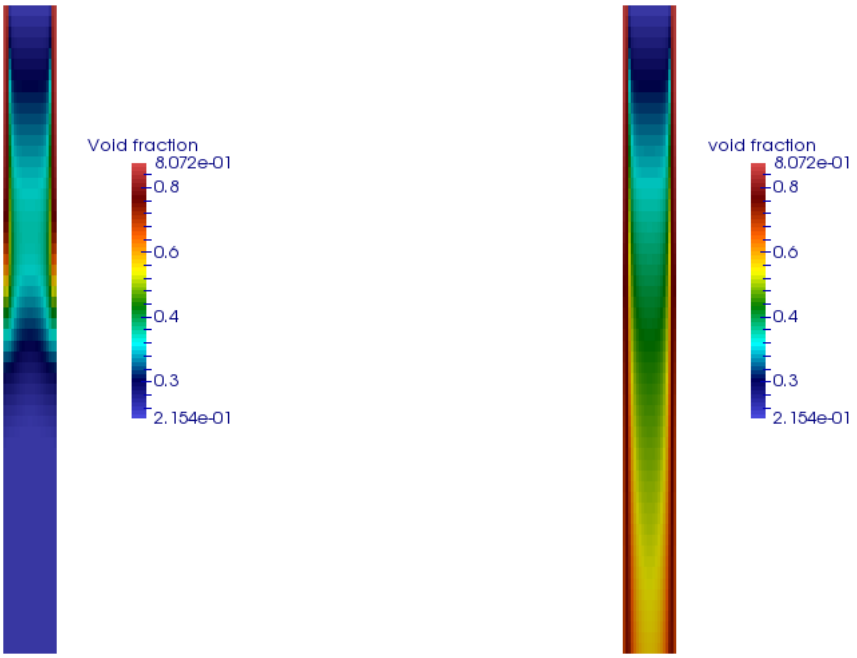

FIGURE 6.3 – The 2D numerical results of the water faucet problem in a vertical tube (12 m in length and 1 m in diameter) using the Roe scheme : void fraction at transient state (left) and stationary state (right). The inlet are chosen such that $\alpha = 0.2$ in the middle and $\alpha = 0.8$ near the wall of the tube.

usually simulated by using two-phase flow models having two conservation equation of momentum of each phase. It arises from the fact that the counter-current flow in the sedimentation leads to extremely different dynamics of each phase, any relation between two velocities in the mixture model is therefore not sufficiently satisfactory. Examples of the sedimentation test using two-fluid model can be found for example in [PCC03 ; EF03 ; CP06 ; MEF09 ; SH13].
Let us introduce the configuration of the sedimentation. Such a test considers a homogeneous mixture of gas and liquid in the initial data, i.e. $\alpha_{g(t=0)} = \alpha_{l(t=0)} = 0.5$, associates with zero velocity for each phase $u_{g(t=0)} = u_{l(t=0)} = 0$. The common pressure is initially assumed to be constant and be equal to 155×10^5 Pa, high pressure in the PWR. The wall boundary condition is considered by assuming the velocities of each phase is zero at the wall $u_g^{\text{wall}} = u_l^{\text{wall}} = 0$. The phase separation is first studied in a vertical tube. All the source terms on the right hand side of the two-fluid models are neglected except the gravity, which is taken to be $\vec{g} = -10\, m/s^2$. The equations of state used are the stiffened law with parameters presented in Section 6.1.7. The expecting numerical results at the stationary state is that pure liquid occupies the lower part of the tube whereas the upper one is filled by pure gas. About the transient results, we recall Chapter 5, in which we present in details the theoretical and numerical results for the incompressible two-fluid model. Such results show that the structure of the void fraction at the transient state is not symmetrical. The void fraction wave connecting the pure liquid to the mixture is a shock wave while the one connecting the pure gas to the mixture is a rarefaction. This result is again observed in the numerical simulation of the compressible two-fluid model, see Figure 6.6. In the literature, one usually assumes a symmetrical structure of the void fraction during the transient state to be a reference or analytical solution, although the numerical results obtained by different numerical methods show that it is not the case, see for example Fig. 9 in [EF03], Fig.12 in [PCC03], Fig.10(a) in [MEF09], Fig.12 in [CP06], Fig.18(a) in [SH13] for the volume fraction at the transient state. These numerical results are consistent with the analysis of the Riemann problem and sedimentation given in Chapter 5.
We implement the numerical simulation using the five-equation model. As we know that the classical Roe scheme is not suitable to simulate the sedimentation, it gives rise unbounded gas velocity and violate the positivity after 29500 time step, see the resulting Roe scheme in Figure 6.5. The key point of our method is using Roe scheme associated with Harten-type entropy fix which is presented in Section 6.1.6. The numerical result of the sedimentation at the steady state in one-dimensional space is shown in Figure 6.7.

Moreover, in two-dimensional space with the Cartesian mesh whose the space step $\Delta x = 0.05$ on the

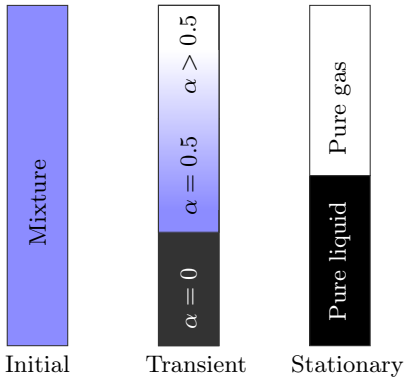

FIGURE 6.4 – A sketch of the void fraction (α) of the sedimentation.

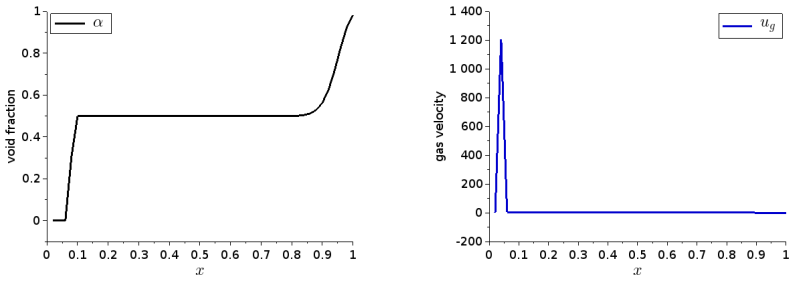

(a) (b)

FIGURE 6.5 – The classical Roe scheme fails to simulate the sedimentation, the numerical results at the time step $n = 29500$, CFL $= 0.5$.

domain $[0, 1] \times [1, 2]$, the gravity $\vec{g} = (7, -7)$, the numerical result of the sedimentation using the Roe scheme with Harten-type entropy fix is shown in Figure 6.8.

6.2.3 Boiling channel

The boiling channel is a classical benchmark problem in the simulation of the two-phase flows, especially in power plant application. The challenging point of the boiling channel is that the phase (vapor) appearance may happen due to a slow liquid velocity at the entrance of the channel, i.e. the void fraction $\alpha = 0$ becomes positive. It therefore exists a configuration where the void fraction is zero on one side, i.e. a vanishing phase, and positive on the other side. Moreover, an important challenge is that the non trivial stationary regime of this test may be not well preserved due to the approximate error in the numerical methods.

Initial data and boundary conditions

The initial data are chosen such that the void fraction $\alpha_{t=0} = 0$, i.e. pure liquid, slow liquid velocity $u_{l(t=0)} = 1\, m/s$, high pressure $p_{t=0} = 155 \times 10^5 Pa$, subcooled liquid temperature $T_{t=0} = 565K$. The boiling channel is simulated in a tube with length $L = 4.2\, m$, the inlet is fed by the subcooled pure liquid at temperature $T_{\text{inlet}} = 565\, K$ and velocity $u_{l(\text{inlet})} = 1\, m/s$. The fixed pressure at the outlet is assumed to be $p_{\text{outlet}} = 155 \times 10^5 Pa$.

Physical parameters

Considering the stiffened equation of state in Section 6.1.7, in order to compute the coefficients γ_k and $p_{\infty k}$, we use the law fitted around the boiling point $p_0 = 155 \times 10^5\, Pa, T_0 = T^{sat}(p) = 345°C$. For more details, see Section 6.1.7.

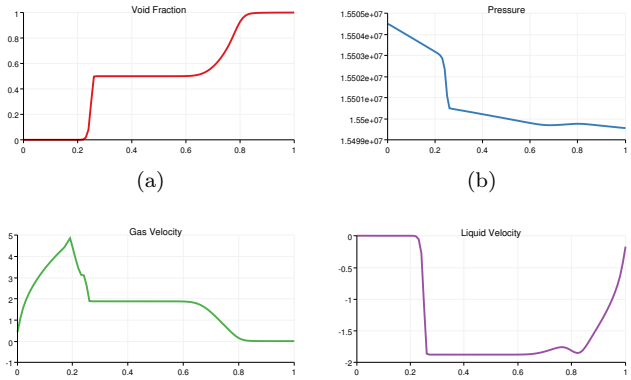

(a) (b) (c) (d)

FIGURE 6.6 – Numerical results of the sedimentation at transient state, on a tube $1\,m$ in length, structure mesh with 200 cells and CFL $= 0.5$.

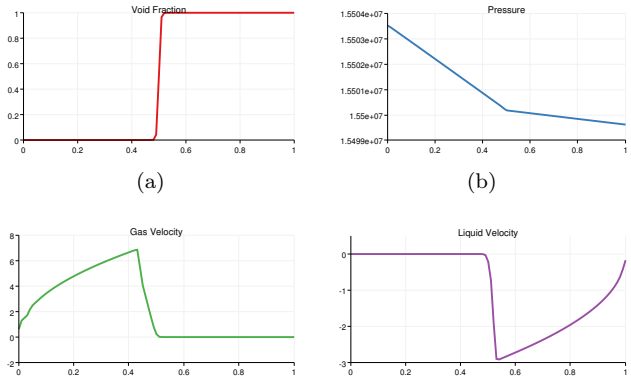

(a) (b) (c) (d)

FIGURE 6.7 – Numerical results of the sedimentation at steady state, on a tube $1\,m$ in length, structure mesh with 200 cells and CFL $= 0.5$.

Source terms

Considering the five-equation two-fluid model in Section 4.1.4, the source terms on the right hand side in the boiling channel simulation is supposed to be

$$S = \begin{bmatrix} \Gamma_g \\ \Gamma_l \\ \Gamma_g \vec{u}^i \\ \Gamma_l \vec{u}^i \\ \Phi \end{bmatrix} \tag{6.88}$$

where Φ is heat source function, u^i is the interfacial velocity which we impose $\vec{u}^i = \alpha_g \vec{u}_l + \alpha_l \vec{u}_g$, Γ_g and Γ_l are the phase transfer functions such that $\Gamma_g + \Gamma_l = 0$. These transfer functions in the numerical test in this document are supposed to be functions of enthalpy and heat source, i.e. $\Gamma_g = \Gamma_g(h, \Phi)$, by the following formula

$$\Gamma_g = \begin{cases} \dfrac{\Phi}{\mathcal{L}} & \text{if} \quad h_l^{\text{sat}} < h < h_g^{\text{sat}}, \\ 0 & \text{otherwise}, \end{cases} \tag{6.89}$$

where h_k^{sat} is the saturation enthalpy of the phase k, $\mathcal{L}$ is latent heat. In the numerical simulation, $\mathcal{L}$, h_k^{sat} and Φ are supposed to be constants determined from the database [ST]. More precisely, we choose $\Phi = 10^8\, W/m^3$ and $\mathcal{L} = 10^6\, J/kg$, the phase change function Γ_g is then really discontinue.
The phase change function given by (6.89) leads to a discontinuous source term. Although the conservation laws system associated with the stiff source are largely studied in the literature, the well-posed

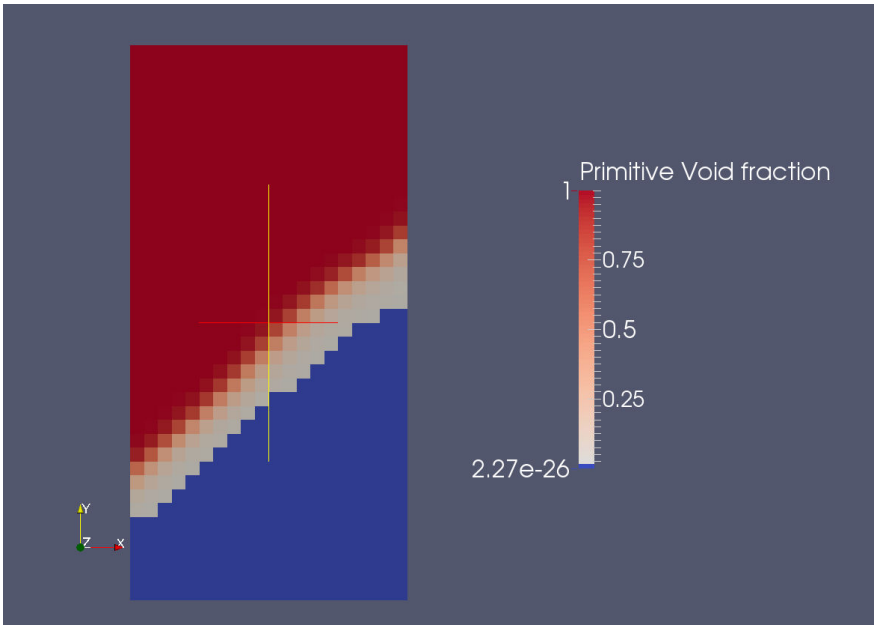

FIGURE 6.8 – The numerical result of the void fraction at the stationary state in the sedimentation test with $\vec{g} = (7, -7)$, CFL $= 0.25$.

of these general systems is still open. We however address the reader to [Bre88], where the author proves the existence of a unique solution to ordinary differential equations $\dot{x}(t) = f(t, x(t))$ where $x(t_0) = x_0 \in \mathbb{R}^d$ and f may be discontinuous with respect to both variables x, t. Moreover, in this test case, it is not easy to analyse the stationary state by generally considering the five-equation model. We however present the analytical steady state in the case of mechanical equilibrium, see Appendix 6.2.5.

In order to reduce the difficulty of the vanishing phase we use the Harten-type entropy fix presented in Section 6.1.6. The numerical results show that the centered treatment of the source term gives rise spurious oscillations of the void fraction wave and can not reach the stationary state. Figure 6.9 shows the numerical result using the Roe scheme with Harten-type entropy fix and the centering source terms at the time step $n = 10^5$, the simulation in fact can not continue due to the violation the positivity of the void fraction.
The upwinding source terms, see Section 6.1.5, is therefore applied. Numerical results show that such a the source terms treatment improves the preservation of the stationary state, see Figure 6.10. The forms of all the curves in Figure 6.10 have a similar structure of the numerical results obtained by the drift flux model, see Figure 6.11 in Appendix 6.2.4 although the mechanical equilibrium assumption in the drift flux test case can not give the two partial velocities.

6.2.4 Appendix : Numerical simulation of the boiling channel in the case of the drift flux model

Considering a mechanical equilibrium of the drift flux model (4.10a :4.10d) and neglecting the gravity and all the source terms corresponding to the wall friction force, the resulting model in one dimension has the following form

$$\partial_t \rho_m + \partial_x(\rho_m u) = 0, \tag{6.90a}$$
$$\partial_t(\alpha_g \rho_g) + \partial_x(\alpha_g \rho_g u) = \Gamma_g, \tag{6.90b}$$
$$\partial_t(\rho_m u) + \partial_x(\rho_m u^2 + p) = 0, \tag{6.90c}$$
$$\partial_t(\rho_m E_m) + \partial_x(\rho_m E_m u + pu) = \Phi, \tag{6.90d}$$

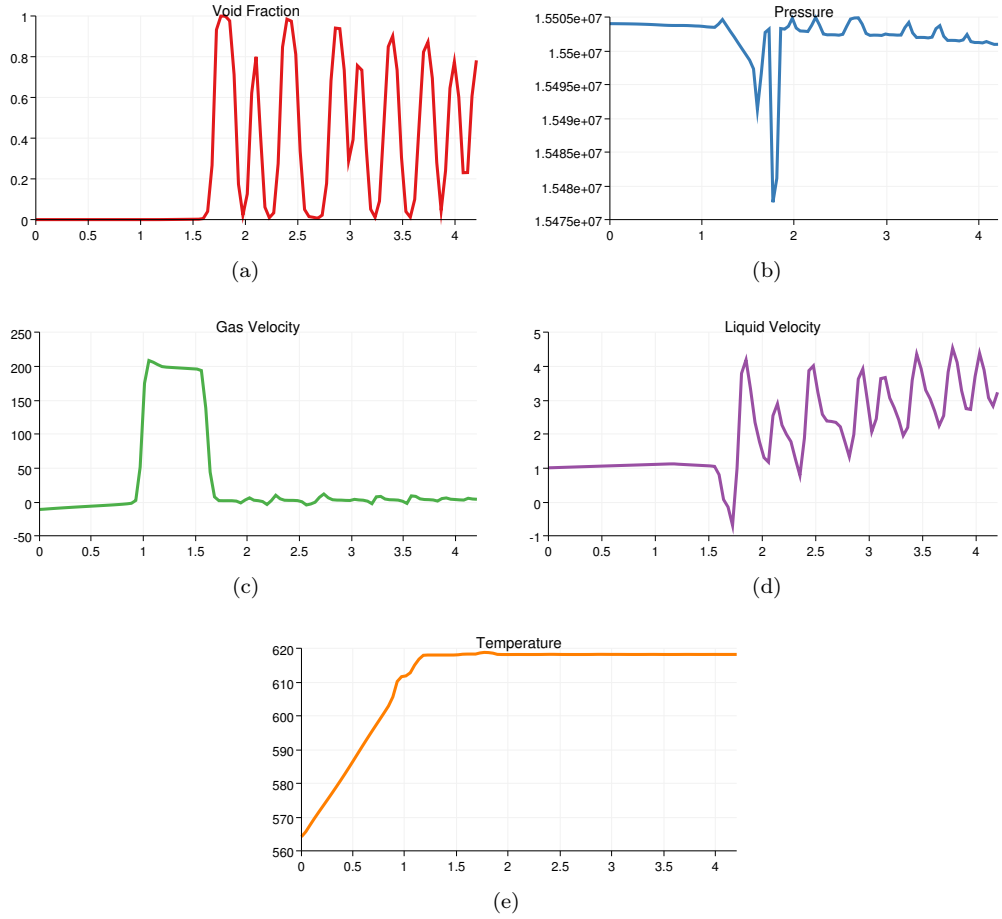

FIGURE 6.9 – Numerical results using the Roe scheme with Harten-type entropy fix without upwinding source term on a heated tube $4.2\,m$ in length, structure mesh with 200 cells, CFL $= 0.5$, at the time step $n = 10^5$. This simulation can not reach the stationary state.

where $u = u_g = u_l$ is the velocity, Φ is the heat source and the phase change function defined bases on the saturation enthalpies $(h_l^{\text{sat}}, h_g^{\text{sat}})$ as follows

$$\Gamma_g = \begin{cases} \dfrac{\Phi}{\mathcal{L}} & \text{if} \quad h_l^{\text{sat}} < h < h_g^{\text{sat}}, \\ 0 & \text{otherwise}, \end{cases} \tag{6.91}$$

We then perform the numerical results of the model (6.90a-6.90d) using the same physical parameters as well as boundary and initial data in the Section 6.2.3 at the stationary state in Figure 6.11.

6.2.5 Appendix : Stationary regime of the boiling channel

The following analysis considers the mechanical equilibrium condition, i.e. we assume that the two velocities u_g and u_l are equal to u. It is therefore necessary to take into account only one mixture momentum equation. In this case, the stationary of the five-equation model (4.23a-4.23e) with the source term S defined by (6.88) yields

$$\partial_x q = 0, \tag{6.92a}$$
$$\partial_x (q c_v) = \Gamma_v, \tag{6.92b}$$
$$\partial_x \frac{q^2}{\rho} + \partial_x p = 0, \tag{6.92c}$$
$$\partial_x \left[q \left(h + \frac{1}{2} \frac{q^2}{\rho^2} \right) \right] = \Phi, \tag{6.92d}$$

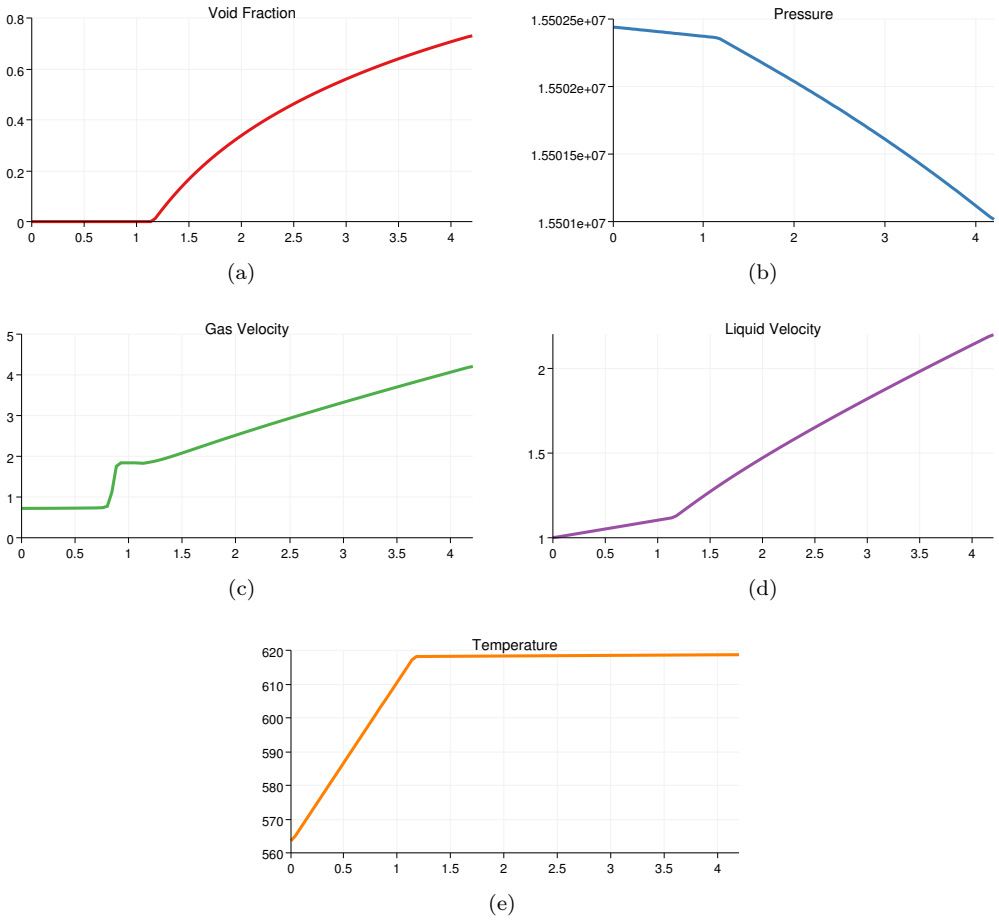

FIGURE 6.10 – Stationary state of the boiling channel.
Numerical results using the Roe scheme with Harten-type entropy fix with upwinding source term on a heated tube 4.2 m in length, structure mesh with 200 cells, CFL = 0.5, at the stationary state.

where we denoted

$$\begin{aligned} \rho &= \alpha_g\rho_g + \alpha_l\rho_l, \\ q &= \rho u, \\ h &= \frac{\alpha_g\rho_g e_g + \alpha_l\rho_l e_l}{\rho} + \frac{p}{\rho}. \end{aligned}$$

Integrating the first two equations (6.92a), (6.92b), we obtain

$$\begin{aligned} q(x) &= q_e, \\ \partial_x c_v &= \frac{\Gamma_v}{q_e}, \\ -\frac{q_e^2}{\rho^2}\partial_x\rho + \partial_x p &= 0, \\ \partial_x h - \frac{q_e^2}{\rho^3}\partial_x\rho &= \frac{\Phi}{q_e}. \end{aligned}$$

Due to the fact that ρ is the function of p, h and the void concentration c_g by the relation

$$\rho = \frac{1}{\dfrac{c_v}{\rho_v} + \dfrac{1-c_v}{\rho_l}}, \tag{6.93}$$

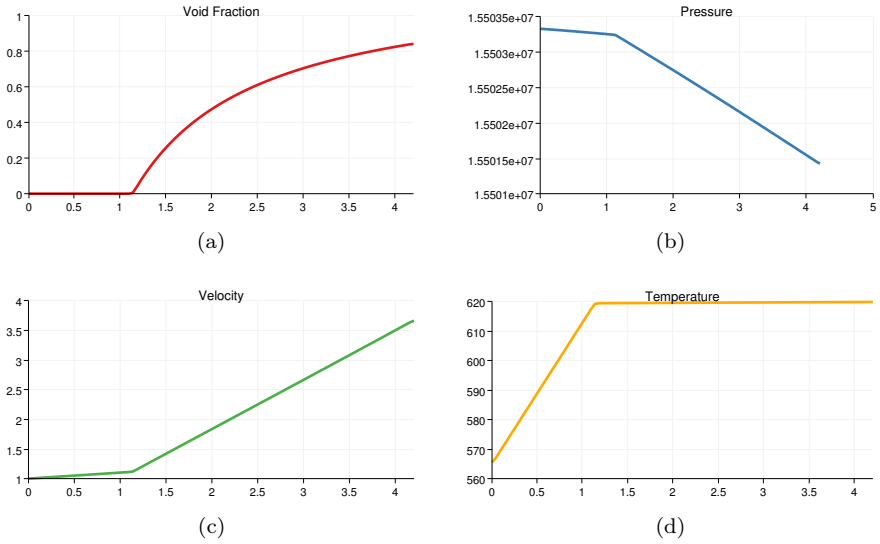

FIGURE 6.11 – Numerical stationary state of the boiling channel using the **drift flux model** on a heated tube $4.2\,m$ in length, structure mesh with 200 cells, CFL $= 0.5$.

we then replacing the derivation of ρ, $\partial_x \rho = \dfrac{\partial \rho}{\partial p}\partial_x p + \dfrac{\partial \rho}{\partial h}\partial_x h + \dfrac{\partial \rho}{\partial c_v}\partial_x c_v$, into the system (6.92a)-(6.92d) and obtain

$$\begin{aligned}
q(x) &= q_e, \\
\partial_x c_v &= \frac{\Gamma_v}{q_e}, \\
\left(1 - \frac{q_e^2}{\rho^2}\frac{\partial \rho}{\partial p}\right)\partial_x p - \frac{q_e^2}{\rho^2}\frac{\partial \rho}{\partial h}\partial_x h - \frac{q_e^2}{\rho^2}\frac{\partial \rho}{\partial c_v}\partial_x c_v &= 0 \qquad (6.94) \\
\left(1 - \frac{q_e^2}{\rho^3}\frac{\partial \rho}{\partial h}\right)\partial_x h - \frac{q_e^2}{\rho^3}\frac{\partial \rho}{\partial p}\partial_x p - \frac{q_e^2}{\rho^3}\frac{\partial \rho}{\partial c_v}\partial_x c_v &= \frac{\Phi}{q_e}. \qquad (6.95)
\end{aligned}$$

Calculating $\left(\left(1 - \dfrac{q_e^2}{\rho^3}\dfrac{\partial \rho}{\partial h}\right)(6.94) + \dfrac{q_e^2}{\rho^2}\dfrac{\partial \rho}{\partial h}(6.95)\right)$ et $\left(\dfrac{q_e^2}{\rho^3}\dfrac{\partial \rho}{\partial p}(6.94) + \left(1 - \dfrac{q_e^2}{\rho^2}\dfrac{\partial \rho}{\partial p}\right)(6.95)\right)$, we finally obtain

$$\left[\left(1 - \frac{q_e^2}{\rho^3}\frac{\partial \rho}{\partial h}\right)\left(1 - \frac{q_e^2}{\rho^2}\frac{\partial \rho}{\partial p}\right) - \frac{q_e^2}{\rho^2}\frac{\partial \rho}{\partial h}\frac{q_e^2}{\rho^3}\frac{\partial \rho}{\partial p}\right]\partial_x p - \left(\left(1 - \frac{q_e^2}{\rho^3}\frac{\partial \rho}{\partial h}\right)\frac{q_e^2}{\rho^2} + \frac{q_e^2}{\rho^2}\frac{\partial \rho}{\partial h}\frac{q_e^2}{\rho^3}\right)\frac{\partial \rho}{\partial c_v}\partial_x c_v$$

$$= \frac{q_e^2}{\rho^2}\frac{\partial \rho}{\partial h}\frac{\Phi}{q_e},$$

$$\left[\left(1 - \frac{q_e^2}{\rho^2}\frac{\partial \rho}{\partial p}\right)\left(1 - \frac{q_e^2}{\rho^3}\frac{\partial \rho}{\partial h}\right) - \frac{q_e^2}{\rho^2}\frac{\partial \rho}{\partial h}\frac{q_e^2}{\rho^3}\frac{\partial \rho}{\partial p}\right]\partial_x h - \left(\frac{q_e^2}{\rho^3}\frac{\partial \rho}{\partial p}\frac{q_e^2}{\rho^2} + \left(1 - \frac{q_e^2}{\rho^2}\frac{\partial \rho}{\partial p}\right)\frac{q_e^2}{\rho^3}\right)\frac{\partial \rho}{\partial c_v}\partial_x c_v$$

$$= \left(1 - \frac{q_e^2}{\rho^2}\frac{\partial \rho}{\partial p}\right)\frac{\Phi}{q_e},$$

which are simplied in the following form

$$\begin{aligned}
q(x) &= q_e, \\
\partial_x c_v &= \frac{\Gamma_v}{q_e}, \\
\left(1 - \frac{q_e^2}{\rho^2 c^2}\right)\partial_x p &= \frac{q_e}{\rho^2}\frac{\partial \rho}{\partial h}\Phi + \frac{q_e^2}{\rho^2}\frac{\partial \rho}{\partial c_v}\partial_x c_v = \frac{q_e}{\rho^2}\frac{\partial \rho}{\partial h}\Phi - q_e\left(\frac{1}{\rho_v} - \frac{1}{\rho_l}\right)\Gamma_v, \\
\left(1 - \frac{q_e^2}{\rho^2 c^2}\right)\partial_x h &= \left(1 - \frac{q_e^2}{\rho^2}\frac{\partial \rho}{\partial p}\right)\frac{\Phi}{q_e} + \frac{q_e^2}{\rho^3}\frac{\partial \rho}{\partial c_v}\partial_x c_v = \left(1 - \frac{q_e^2}{\rho^2}\frac{\partial \rho}{\partial p}\right)\frac{\Phi}{q_e} + \frac{q_e}{\rho}\left(\frac{1}{\rho_v} - \frac{1}{\rho_l}\right)\Gamma_v.
\end{aligned}$$

where c is the mixture sound speed.
It is therefore deduced that if $0 < q_e < \rho c$ then $\partial_x p < 0$ and $\partial_x h > 0$.

6.2.6 Appendix : Computing the Roe matrix for the drift flux model

Considering the drift-flux model

$$\begin{aligned}
\frac{\partial \alpha_g\rho_g + \alpha_l\rho_l}{\partial t} &+ \nabla\cdot(\rho_m\vec{u}_m) = 0, && \text{(6.96a)}\\
\frac{\partial \alpha_g\rho_g}{\partial t} &+ \nabla\cdot(\alpha_g\rho_g\vec{u}_g) = \Gamma_g, && \text{(6.96b)}\\
\frac{\partial(\rho_m\vec{u}_m)}{\partial t} &+ \nabla\cdot(\rho_m\vec{u}_m\otimes\vec{u}_m + \rho_m c_g(1-c_g)\vec{u}_r\otimes\vec{u}_r + p\cdot \mathrm{Id})\\
&= \rho_m\vec{g} + \vec{F}^{\mathrm{w}}, && \text{(6.96c)}\\
\frac{\partial}{\partial t}(\rho_m E_m) &+ \nabla\cdot\left(\alpha_g\rho_g H_g{}^t\vec{u}_g + \alpha_l\rho_l H_l{}^t\vec{u}_l\right)\\
&= \rho_m\vec{g}\cdot\vec{u}_m + \vec{F}^{\mathrm{w}}\cdot\vec{u}_m + Q^{\mathrm{w}}. && \text{(6.96d)}
\end{aligned}$$

We first neglect the relative velocity, i.e. $u_g = u_l$. For simplification of notation, we consider the model (6.96a-6.96d) in one dimension.
The conservative variables are

$$U = {}^t(\rho, m_g, q, \rho E_m), \tag{6.97}$$

and the flux function

$$F = {}^t(q, m_g u, \rho u^2 + p, \rho u e_m + \frac{1}{2}\rho u^3 + pu), \tag{6.98}$$

where $\rho = (\alpha_g\rho_g + \alpha_l\rho_l)$, $m_g = \alpha_g\rho_g$, $q = \rho u$, $E_m = \dfrac{\alpha_g\rho_g E_g + \alpha_l\rho_l E_l}{\rho}$, $e_m = \dfrac{\alpha_g\rho_g e_g + \alpha_l\rho_l e_l}{\rho}$.

Our objective is to decompose the jump $[F]$ on the jump of the conservative variables $[U]$. Firstly, we compute some jumps which are trivial and independent to the equation of state. Let us denote $[.] = (.)_R - (.)_L$ a jump, $\bar{.}$ an arithmetic, and $\ddot{.}$ a geometric mean value of the left state and the right one. Using the jump of the velocity

$$[u] = \frac{[q] - \bar{u}[\rho]}{\overline{\rho}}, \tag{6.99}$$

we derive

$$\begin{aligned}
\left[\rho u^2\right] &= -\ddot{u}^2[\rho] + 2\bar{u}[q],\\
[m_g u] &= \overline{m}_g[u] + \bar{u}[m_g]\\
&= \frac{\overline{m}_g}{\overline{\rho}}([q] - \bar{u}[\rho]) + \bar{u}[m_g],\\
\left[\rho u^3\right] &= -2\bar{u}\ddot{u}^2[\rho] + (2\bar{u}^2 + \overline{u^2})[q],\\
[\rho u e_m] &= \frac{\overline{\rho e}_m}{\bar{\rho}}([q] - \bar{u}[\rho]) + \bar{u}\left[\rho e_m\right],\\
[\rho e_m] &= [\rho E_m] + \frac{1}{2}\ddot{u}^2[\rho] - \bar{u}[q],\\
\bar{m}_g[e_g] + \bar{m}_l[e_l] &= [\rho E_m] + \frac{1}{2}\ddot{u}^2[\rho] - \bar{e}_g[m_g] - \bar{e}_l([\rho] - [m_g]) - \bar{u}[q]. && \text{(6.100)}
\end{aligned}$$

Due to the fact that the temperature T is approximately linear to the internal energy, we then assume that $[e_g] = c_{v,g}[T]$, $[e_l] = c_{v,l}[T]$. These assumptions associated with (6.100) yield

$$[T] = \hat{\varrho}\left([\rho E_m] + \frac{1}{2}\ddot{u}^2[\rho] - \bar{e}_g[m_g] - \bar{e}_l([\rho] - [m_g]) - \bar{u}[q]\right), \tag{6.101}$$

where $\hat{\varrho} = \dfrac{1}{\overline{m}_g c_{v,g} + \overline{m}_l c_{v,l}}$. We then can compute $[p]$ by using the following assumption obtained by the thermodynamics laws. More precisely, we assume that

$$[p] = \hat{a}_{1,g}\,[\rho_g] + \hat{a}_{2,g}[e_g], \tag{6.102a}$$
$$[p] = \hat{a}_{1,l}\,[\rho_l] + \hat{a}_{2,l}[e_l]. \tag{6.102b}$$

Using the relation $[\alpha_g + \alpha_r] = 0$, we will compute $[p]$ as a function of $[U], [e_g], [e_l]$. Firstly, considering

$$[m_g] = \bar{\alpha}_g[\rho_g] + \bar{\rho}_g[\alpha_g], \tag{6.103}$$
$$[m_l] = \bar{\alpha}_l[\rho_l] + \bar{\rho}_l[\alpha_l], \tag{6.104}$$

where $m_k = \alpha_k \rho_k$.
Multiplying the equation (6.103) by $\bar{\rho}_l$ and the equation (6.104) by $\bar{\rho}_g$, then adding the two equations, we get

$$\bar{\rho}_l[m_g] + \bar{\rho}_g[m_l] = \bar{\alpha}_g\bar{\rho}_l[\rho_g] + \bar{\alpha}_l\bar{\rho}_g[\rho_l]. \tag{6.105}$$

From (6.102) and (6.105),

$$\begin{aligned}\bar{\rho}_l[m_g] + \bar{\rho}_g[m_l] &= \bar{\alpha}_g\bar{\rho}_l\left(\hat{a}_{1,g}[p] + \hat{b}_g[e_g]\right) + \bar{\alpha}_l\bar{\rho}_g\left(\hat{a}_{1,l}[p] + \hat{b}_l[e_l]\right)\\ &= \left(\bar{\alpha}_g\bar{\rho}_l\hat{a}_{1,g} + \bar{\alpha}_l\bar{\rho}_g\hat{a}_{1,l}\right)[p] + \bar{\alpha}_g\bar{\rho}_l\hat{a}_{2,g}[e_g] + \bar{\alpha}_l\bar{\rho}_g\hat{a}_{2,l}[e_l].\end{aligned} \tag{6.106}$$

Then we derive

$$[p] = \hat{\kappa}\left(\bar{\rho}_l[m_g] + \bar{\rho}_g[m_l] + \hat{\nu}[T]\right),$$

where we applied

$$\hat{\kappa} = \left(\bar{\alpha}_g\bar{\rho}_l\hat{a}_{1,g} + \bar{\alpha}_l\bar{\rho}_g\hat{a}_{1,l}\right)^{-1}, \tag{6.107}$$
$$[e_g] = c_{v,g}[T],$$
$$[e_l] = c_{v,l}[T],$$
$$\hat{\nu} = \bar{\alpha}_g\bar{\rho}_l\hat{a}_{2,g}c_{v,g} + \bar{\alpha}_l\bar{\rho}_g\hat{a}_{2,l}c_{v,l}. \tag{6.108}$$

Finally, we can write the jump of the flux in a form $[F] = \tilde{\mathbf{A}}[U]$, where

$$\tilde{\mathbf{A}} = \begin{bmatrix} 0 & 0 & 1 & 0\\ -\dfrac{\overline{m}_g\bar{u}}{\bar{\rho}} & \bar{u} & \dfrac{\overline{m}_g}{\bar{\rho}} & 0\\ -\ddot{u}^2 + p_1 & p_2 & 2\bar{u} + p_3 & p_4\\ -\left(\bar{p} + \overline{\rho E}_m\right)\dfrac{\bar{u}}{\bar{\rho}} + \bar{u}p_1 & \bar{u}p_2 & \dfrac{\bar{p} + \overline{\rho E}_m}{\bar{\rho}} + \bar{u}p_3 & \bar{u} + \bar{u}p_4 \end{bmatrix}, \tag{6.109}$$

and

$${}^t p_{i,i=1,\dots,4} = \hat{\kappa}\begin{bmatrix} \bar{\rho}_g + \hat{\rho}\hat{\nu}\left(\dfrac{1}{2}\ddot{u}^2 - \bar{e}_l\right)\\ \bar{\rho}_l - \bar{\rho}_g + \hat{\rho}\hat{\nu}\left(\bar{e}_l - \bar{e}_g\right)\\ -\hat{\rho}\hat{\nu}\bar{u}\\ \hat{\rho}\hat{\nu}\end{bmatrix}, \tag{6.110}$$

we recall that $\hat{a}_{1,k}, \hat{a}_{2,k}$, $k = g, l$ are defined by (6.102) and

$$\hat{\kappa} = \left(\bar{\alpha}_g\bar{\rho}_l\hat{a}_{1,g} + \bar{\alpha}_l\bar{\rho}_g\hat{a}_{1,l}\right)^{-1},$$
$$\hat{\varrho}\hat{\nu} = \frac{\bar{\alpha}_g\bar{\rho}_l\hat{a}_{2,g}c_{v,g} + \bar{\alpha}_l\bar{\rho}_g\hat{a}_{2,l}c_{v,l}}{\overline{m}_g c_{v,g} + \overline{m}_l c_{v,l}}.$$

Remark : if the stiffened gas equations are chosen, i.e. $p = (\gamma_k - 1)\rho_k e_k - \gamma p_{k\infty}$, $k = g, l$, then the corresponding $\hat{a}_{1,k}, \hat{a}_{2,k}$ are defined by

$$\hat{a}_{1,k} = \frac{\bar{e}_k}{(\gamma_k - 1)\ddot{e}_k^2}, \tag{6.111}$$
$$\hat{a}_{2,k} = \frac{p_{k\infty} - \bar{p}}{(\gamma_k - 1)\ddot{e}_k^2}. \tag{6.112}$$

Similarly, take into account the normal vector direction $\vec{n}$ in multidimensional case, we obtain the jump of the flux function $[F_n] = \tilde{\mathbf{A}}_n[U]$, where

$$\tilde{\mathbf{A}}_n = \begin{bmatrix} 0 & 0 & {}^t\vec{n} & 0 \\ -\dfrac{\overline{m}_g \bar{\vec{u}} \cdot \vec{n}}{\bar{\rho}} & \bar{\vec{u}} \cdot \vec{n} & \dfrac{\overline{m}_g}{\bar{\rho}}({}^t\vec{n}) & 0 \\ \overline{\vec{u}(\vec{u} \cdot \vec{n})} - 2\bar{\vec{u}}(\bar{\vec{u}} \cdot \vec{n}) + p_1\vec{n} & p_2\vec{n} & (\bar{\vec{u}} \cdot \vec{n})\mathbb{I}\mathrm{d} + \bar{\vec{u}} \otimes \vec{n} + p_{3,..2+d} \otimes \vec{n} & p_{3+d}\vec{n} \\ -\left(\bar{p} + \overline{\rho E}_m\right)\dfrac{\bar{\vec{u}} \cdot \vec{n}}{\bar{\rho}} + (\bar{\vec{u}} \cdot \vec{n})p_1 & (\bar{\vec{u}} \cdot \vec{n})p_2 & \dfrac{\bar{p} + \overline{\rho E}_m}{\bar{\rho}}{}^t\vec{n} + (\bar{\vec{u}} \cdot \vec{n})p_{3,..2+d} & \bar{\vec{u}} \cdot \vec{n} + (\bar{\vec{u}} \cdot \vec{n})p_{3+d} \end{bmatrix},$$

and

$${}^t p_{i,i=1,\ldots,3+d} = \hat{\kappa} \begin{bmatrix} \bar{\rho}_g + \hat{\rho}\hat{\nu}\left(\dfrac{1}{2}\|\ddot{u}\|^2 - \bar{e}_l\right) \\ \bar{\rho}_l - \bar{\rho}_g + \hat{\rho}\hat{\nu}\left(\bar{e}_l - \bar{e}_g\right) \\ -\hat{\rho}\hat{\nu}\bar{\vec{u}} \\ \hat{\rho}\hat{\nu} \end{bmatrix}.$$

6.3 Conclusion

Using the five-equation two-fluid model, we have simulated some numerical tests.
The resulting simulation by the Roe schemes with and without the Harten-type entropy fix in the water faucet test case shows that such an entropy fix does not give rise considerably additional diffusion at the transient state. The two methods give almost the same results, i.e. the precision of the classical Roe scheme does not much change when the Harten-type entropy fix is added.

Unlike the water faucet test case, the separation by gravity is successfully implemented only in the case the Harten-type entropy fix is applied due to the presence of the vanishing phase. Numerical results show the two bounded velocities of vapor and liquid on the whole domain of simulation, i.e. even for the absent phases.

Different from the first two tests, the difficulty of the boiling channel lies in the stiff source terms, of which the normal treatment, i.e. centred source, can not capture the correct stationary state. Applying the upwinding source method, the Roe scheme with the Harten-entropy correction much improves the simulation and well preserves the stationary state.

Chapitre 7

Package CoreFlows

This chapter is intended to introduce the programming environment used to simulate the compressible two-phase flow model in this document. We used the open source package named *CoreFlows* which is developed in C++ by PhD students and interns at CEA Saclay under the supervision of Michael Ndjinga. This package was firstly developed by T.-H Dao (2009-2013) and B. Lieuray (2009), in a parallel context for a PhD on domain decomposition methods. The two initial models where a gas dynamics system and an isentropic two-fluid model. My contribution has consisted in transferring the whole package to a sequential structure and using CDMATH toolbox generate and manage meshes and fields. Now it is easy to generate general meshes (structured and unstructured meshes) and fields in multidimensional space. The five-equation two-fluid model (4.23) was then added using a new method to compute the Roe matrix, see Section 6.1.2. The source upwinding stratey was then added and allowed the treatment of discontinuous source terms (phase change function and heat source field).
Wee present here important libraries required to use CoreFlows as well as its framework.

7.1 Libraries used in CoreFlows

The CoreFlows package is developed using the following libraries.

— Library **PETSc** [1] which stands for Portable, Extensible Toolkit for Scientific Computation is a prerequisite for the compilation of CoreFlows. It is a rich open library supporting data structure and routines for numerical computation of partial differential equations. It is the standard tool for managing large size vectors and sparse matrix and solve linear systems with various methods and preconditionners.

— Library **CDMATH** [2] which is a toolbox for the easy generation and management of meshes and fields in dimensions one, two and three. It is a prerequisite of CoreFlows that is based on the library medcoupling of the project Salome-platform [3]. It is used for the mesh and field definitions and the saving the results of the computation in a VTU or MED file. CDMATH offers a user friendly programming environment in C++ and Python and the user can merely focus on the objects (Mesh, Field, Vector, Matrix, LinearSolver) needed for his models and numerical methods.

— **Paraview** [4] is necessary to visualize the meshes and fields generated by CoreFlows. Paraview is a powerfull tool allowing the visualization of large size fields, generating streamlines, isovalue surfaces, or animations in a user firendly interface that is either graphical or Python based.

Moreover, an external library joined in PETSc also used in the code is LAPACK [5], which is applied to compute the eigenvalues of the Roe matrix mainly in five-equation model.

1. http ://www.mcs.anl.gov/petsc/
2. https ://github.com/PROJECT-CDMATH/CDMATH
3. http ://www.salome-platform.org/
4. http ://www.paraview.org/
5. http ://www.netlib.org/lapack/

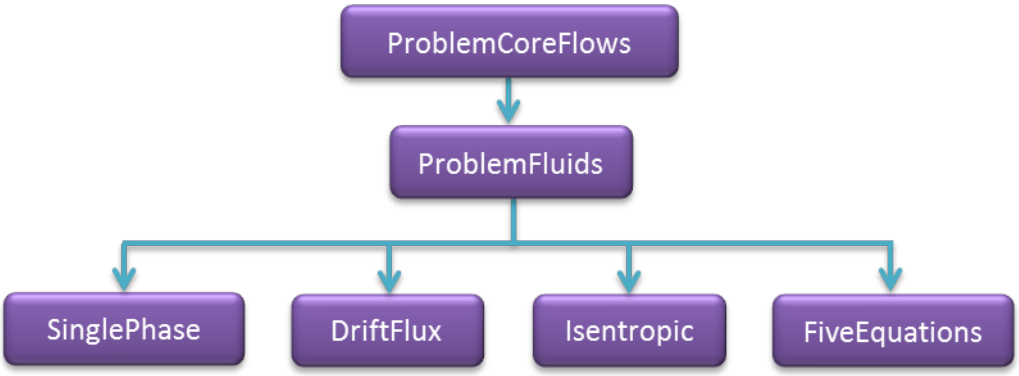

FIGURE 7.1 – Classes in CoreFlows package.

7.2 Framework of CoreFlows

The CoreFlows package structure follows the CEA convention **ICoCo** which stands for **Interface for Code Coupling**. In general, this convention defines a list of step to solve the partial differential equations. The numerical result in the next time step is then evolved by the following functions namely

- computeTimeStep,
- initTimeStep,
- solveTimeStep,
- validateTimeStep,
- abortTimeStep,
- iterateTimeStep,
- isStationary.

Among those, computeTimeStep is the most important function, it characterizes the numerical methods. The details of these functions can be found in [DP12].
In addition, the CoreFlows package now includes the drift model and the python interface thanks to the developments by T. SID ABDELKADER during her internship at CEA. This package therefore becomes more friendly with the users, who would like to study the dynamics of the single-phase and two-phase flows including different models.
The organization of the package including classes is showed in Figure 7.2. Moreover, in order to treat the equation of state, we construct a class namely *fluid* which presently contains only the stiffened gas laws. For more information about the CoreFlows package concerning the structure, models, numerical methods, physical consideration as well as the requiring libraries and installation, we refer the reader to the documentation of the CoreFlows.

7.3 Visualization of the CoreFlows

The numerical data obtained from CoreFlows are written in files VTU which can be visualized by different post-processing utilities. We prefer to use ParaView which is an open-source package supporting to analyze extremely large datasets. Thanks to the flexible and intuitive user interface, the post-processing facilitates the user. For example, interface Python is an advantage of ParaView, that allows to visualize numerical results quickly. There are many options to create a Python file in ParaView. For one is not familiar to Python, ParaView supports a technique to create a Python script through manual actions, i.e. "start trace" and "stop trace". Moreover the script Python can be saved as a macro in ParvaView, which permits the user to execute the script only one click. For more information about installation and guides of ParaView, we refer the reader to their website.

7.4 Example of test case code

We include here an example of the main script files "main.cpp" and "main.py" in the CoreFlows package. The test case is the boiling channel test solved with the five equation two-fluid model (see section 6.2.3).

7.4.1 An example of C++ script

Listing 7.1 – CoreFlows C++ script file for the boiling channel

```
#include "FiveEqsTwoFluid.hxx"
#include <iostream>

using namespace std;

int main()
{
    int spaceDim=1;

    double inletVoidFraction=0;
    vector<double>inletVelocityX(2,2);
    double inletTemperature=563;
    double outletPressure=155e5;

    // physical constants
    double heatPower=1e8;
    int nbPhase=2;

    FiveEqsTwoFluid  myProblem(around155bars600K,spaceDim);
    int nVar = myProblem.getNumberOfVariables();

    double xinf=0.0;
    double xsup=4.2;
    int nx=50;

    // Prepare for the initial condition
    vector<double> VV_Constant(nVar);
    // constant vector
    VV_Constant[0] = inletVoidFraction;
    VV_Constant[1] = outletPressure;
    VV_Constant[2] = inletVelocityX[0];
    VV_Constant[3] = inletVelocityX[1];
    VV_Constant[2+spaceDim*nbPhase] = inletTemperature;

    cout << "Construction de la condition initiale ... " << endl;

    // generate initial condition
    myProblem.setInitialFieldConstant(spaceDim,VV_Constant,xinf,
                                      xsup,nx,"inlet","outlet");

    //set the boundary conditions
    myProblem.setInletBoundaryCondition("inlet",inletVoidFraction,
                                        inletTemperature,inletVelocityX);
    myProblem.setOutletBoundaryCondition("outlet", outletPressure);

    // physical parameters
    myProblem.setHeatSource(heatPower);

    // set the numerical method
    myProblem.setNumericalMethod(upwind, Explicit);
    myProblem.setWellBalancedCorrection(true);
    myProblem.setEntropicCorrection(true);

    // name file save
    string fileName = "1DBoilingChannel";
```

```
56
57      // parameters calculation
58      unsigned MaxNbOfTimeStep =10000;
59      int freqSave = 10;
60      double cfl = 0.5;
61      double maxTime = 5;
62      double precision = 1e-5;
63
64      myProblem.setCFL(cfl);
65      myProblem.setPrecision(precision);
66      myProblem.setMaxNbOfTimeStep(MaxNbOfTimeStep);
67      myProblem.setTimeMax(maxTime);
68      myProblem.setFreqSave(freqSave);
69      myProblem.setFileName(fileName);
70
71      // evolution
72      myProblem.initialize();
73      cout<<"Running "+fileName <<endl;
74
75      bool ok = myProblem.run();
76      if (ok)
77          cout << "Simulation "<<fileName<<" is successful !" << endl;
78      else
79          cout << "Simulation "<<fileName<<"  failed ! " << endl;
80
81      cout << "------------ End of calculation ------------" << endl;
82      myProblem.terminate();
83
84      return ok;
85  }
```

7.4.2 An example of python script

Listing 7.2 – CoreFlows C++ script file for the boiling channel

```
1  #!/usr/bin/env python
2  # -*-coding:utf-8 -*
3
4  import CoreFlows as cf
5
6  def FiveEqsTwoFluid_1DBoilingChannel():
7
8      spaceDim = 1;
9      # Prepare for the mesh
10     xinf = 0 ;
11     xsup=4.2;
12     nx=50;
13
14     # set the limit field for each boundary
15
16     inletVoidFraction=0;
17     inletVelocityX=[2]*2;
18     inletTemperature=563;
19     outletPressure=155e5;
20
21     # physical constants
22     heatPower=1e8;
23
```

```
24      myProblem = cf.FiveEqsTwoFluid(cf.around155bars600K,spaceDim);
25      nVar =  myProblem.getNumberOfVariables();
26
27      # Prepare for the initial condition
28      VV_Constant =[0]*nVar;
29
30      # constant vector
31      VV_Constant[0] = inletVoidFraction;
32      VV_Constant[1] = outletPressure ;
33      VV_Constant[2] = inletVelocityX[0];
34      VV_Constant[3] = inletVelocityX[1];
35      VV_Constant[4] = inletTemperature ;
36
37
38      #Initial field creation
39      print("Building initial data " );
40      myProblem.setInitialFieldConstant(spaceDim,VV_Constant,xinf,
41                                        xsup,nx,"inlet","outlet");
42
43      # set the boundary conditions
44      myProblem.setInletBoundaryCondition("inlet",inletVoidFraction,
45                                          inletTemperature,inletVelocityX)
46      myProblem.setOutletBoundaryCondition("outlet", outletPressure);
47
48      # set physical parameters
49      myProblem.setHeatSource(heatPower);
50
51      # set the numerical method
52      myProblem.setNumericalMethod(cf.upwind, cf.Explicit);
53      myProblem.setLinearSolver(cf.GMRES,cf.ILU,True);
54      myProblem.setEntropicCorrection(True);
55      myProblem.setWellBalancedCorrection(True);
56
57      # name of result file
58      fileName = "1DBoilingChannel";
59
60      # simulation parameters
61      MaxNbOfTimeStep = 3 ;
62      freqSave = 1;
63      cfl = 0.95;
64      maxTime = 5;
65      precision = 1e-6;
66
67      myProblem.setCFL(cfl);
68      myProblem.setPrecision(precision);
69      myProblem.setMaxNbOfTimeStep(MaxNbOfTimeStep);
70      myProblem.setTimeMax(maxTime);
71      myProblem.setFreqSave(freqSave);
72      myProblem.setFileName(fileName);
73      myProblem.setNewtonSolver(precision,20);
74      myProblem.saveConservativeField(True);
75      if(spaceDim>1):
76          myProblem.saveVelocity();
77          pass
78
79      # evolution
80      myProblem.initialize();
81      print("Running python "+ fileName );
```

```
82
83      ok = myProblem.run();
84      if (ok):
85          print( "Simulation python " + fileName + " is successful !" );
86          pass
87      else:
88          print( "Simulation python " + fileName + "  failed ! " );
89          pass
90
91      print( "------------ End of calculation !!! ----------" );
92
93      myProblem.terminate();
94      return ok
```

General conclusions and perspectives

The thesis was set out to explore the mathematical analysis and the numerical simulation of boiling flow models in nuclear power plants thermal hydraulics. The relevant models considered to study were the slip, drift and two-fluid models. Our study concentrates on the question of whether the general mathematical properties of the two-phase flow models are similar to the ones of the single phase flow. The study has also sought to know if there exists a positive solution ($\alpha \in [0, 1]$) with bounded velocities that are not necessarily equal when one phase disappears in the two-fluid models.

Our study on the incompressible limit of the drift and two-fluid models in Chater 5 shows that the characteristic fields of these system differs from the single phase one due to the fact that they are neither GNL nor LD. The solution of the Riemann problem displays composite waves and the number of simple waves can be greater than the number of equations of the PDEs system.

Although the study of the compressible models can not give the full eigenstructure of the Jacobian matrices, some particular cases have been explored in Section 4.2. The resulting achievement again affirms that the characteristic are more complicated whenever a mechanical disequilibrium is taken into account. All models display two acoustic waves with a mixture sound speed that is smaller that each phasic sound speed and that are genuinely nonlinear for small relative velocities. Moreover, the approximate eigenvalues of the two-fluid models shows that the sonic points appears in normal flow conditions, and that is completely different from the single phase flow.

Due to the existence of sonic points in the two-fluid models, we propose to apply the Roe scheme with a Harten-type entropy fix in some classical tests. Neglecting the detection of sonic points, a Harten-type entropy fix is used on the whole interesting domain. The results of the sedimentation test case in Section 6.2.2 shows the existence of two bounded velocities even for the absent phases without any additional friction nor code tuning.

An important part of the thesis is the study of the boiling channel problem. This test case is challenging not only owing to the phase appearance but also the irregular source terms, see Section 6.2.3. In order to preserve the correct stationary state, it is essential to consider a special discretization of these source terms, i.e. not centered ones. The upwinding of source terms is therefore employed along the classical Roe scheme with the Harten-type entropy fix. The resulting stationary state is finally well captured and has the structure similar to the one of the drift model, of which we can derive the formula of the analytical solutions at the stationary state.

A limitation of our study is that the numerical results where obtained using explicit schemes, i.e. using very small time steps and the capture of the stationary state costs much computational time, especially in 2D and 3D simulations. The next challenge will be to use implicit scheme in order to improve the calculating time and provide more results in 2D and 3D.

The source terms arising in the thermal hydraulics depend on the unknown vector and usually are irregular. Studying the existence and uniqueness of the PDEs in this discontinuous source case where the Cauchy-Lipschitz theorem does not apply will be a perspective of this thesis.

Regarding the physical model, including the viscous and thermal conductive terms would lead interesting challenges on complex geometries with unstructured or non conformal meshes. Also taking into account the thermal disequilibrium in the mathematical analysis of the models is a demand from the thermal hydraulics community.

Bibliography

[AC15] N. Aguillon et C.Chalons. « Nondiffusive conservative schemes based on approximate Riemann solvers for Lagrangian gas dynamics ». In : *submitted* (2015).

[ACJ14] J. Aragonaa, J.F. Colombeau et S.O. Juriaans. « Non linear generalized functions and jump conditions for a standard one pressure liquid-gas model ». In : *Journal of Mathematical Analysis and Applications* 418 (2014), p. 964–977.

[ACR12] A. Ambroso, C. Chalons et P.A. Raviart. « A Godunov-type method for the seven-equation model of compressible two-phase flow ». In : *Computers & Fluids* 54 (2012), p. 67–91.

[Agu15] N. Aguillon. « Problèmes d'interfaces et couplages singuliers dans les systèmes hyperboliques : analyse et analyse numérique ». Université Paris XI, 2015.

[AK10] R. Abgrall et S. Karni. « A comment on the computation of non-conservative products ». In : *Journal of Computation Physics* 229 (2010), p. 2759–2763.

[AM04] Fabio Ancona et Adrea Marson. « Well-posedness for General 2×2 Systems of Conservation Laws ». In : *Memoirs of the American Mathematical Society* 69 (2004).

[Ami97] K. El Amine. « Modélisation et analyse numérique des écoulements diphasiques en déséquilibre ». PhD Thesis. Université Paris 6, 1997.

[Bes00] D. Bestion. « The appearance and disappearance in the CATHARE code ». In : *Trends in Numerical and Physical Modeling for Industrial Multiphase Flows, Cargese, FRANCE 27th* (2000).

[Bes90] D. Bestion. « The physical closure laws in the CATHARE code ». In : *Nuclear Engineering and Design* 124 (1990), p. 229–245.

[BGH00] T. Buffard, T. Gallouet et J.-M. Hérard. « A sequel to a rough Godunov scheme : application to real gases ». In : *Computers & Fluids* 29 (2000).

[Bou+08] B. Boutin et al. « Convergent and conservative schemes for non-classical solutions based on kinetic relations ». In : *Interfaces and Free Boundaries* 10 (2008).

[Bou00] F. Bouchut. *Nonlinear stability of finite volume methods for hyperbolic conservation laws and well-balances scheme for sources*. Frontiers in Mathematics, 2000.

[Bre00] A. Bressan. *Hyperbolic Systems of Conservation Laws : The One-dimentional Cauchy Problem*. Oxford Lecture Series in Mathematics et Its Applications, 2000.

[Bre88] A. Bressan. « Unique solutions for a class of discontinuous differential equations ». In : *Proceedings of the AMS* 104 (1988).

[BV94] A. Bermudez et M. E. Vazquez. « Upwind method for hyperbolic conservation laws with source terms ». In : *Computers Fluids* 23.8 (1994), p. 1049–1071.

[CDK14] Floraine Cordier, Pierre Degond et Anela Kumbaro. « Phase Appearance or Disappearance in Two-Phase Flows ». In : *J. Sci. Compu.* 58 (2014).

[Cha81] S. Chandrasekhar. *Hydrodynamic and Hydromagnetic Stability*. Dover Publication - New York, 1981.

[CMG14] C. Chalons, M.-L Delle Monache et P. Goatin. « A numerical scheme for moving bottlenecks in traffic flow ». In : *submitted to the Proceedings of HYP2014 international conference* (2014).

[Coq+02] F. Coquel et al. « Closure laws for a two-fluid two-pressure model ». In : *Comptes Rendus Mathematique* 334 (2002), p. 927–932.

[Coq+97] F. Coquel et al. « A numerical method using upwind schemes for the resolution of two-phase flows ». In : *Journal Computational Physics* 136 (1997), p. 272–288.

[CP06] J.R. Garcìa Cascales et H. Paillère. « Application of AUSM schemes to multi-dimensional compressible two-phase flow problems ». In : *Nuclear Engineering and Design* 236 (2006), p. 1225–1239.

[Daf10] C.M. Dafermos. *Hyperbolic conservation laws in continuum physics*. T. 325. Grundlehren der mathematischen Wissenschaften, 2010.

[DD05] B. Després et F. Dubois. *Système hyperboliques de lois de conservation*. Les Éditions de École Polytechnique, 2005.

[DL01] B. Després et F. Lagoutière. « Contact discontinuity capturing schemes for linear advection and compressible gas dynamics ». In : *Journal of Scientific Computing* 16.4 (2001).

[DM96] F. Dubois et G. Mehlman. « A non-parameterized entropy correction for Roe's approximate Riemann solver ». In : *Numer. Math.* 73 (1996), p. 169–208.

[DP12] Estelle DEVILLE et Fabien PERDU. *Documentation of the Interface for Code Coupling : ICoCo*. Référence DEN/DANS/DM2S/STMF/LMES. 2012.

[DP99] D. A. Drew et S. L. Passman. *Theory of Multicomponents Fluids*. Springer-Verlag-New York, 1999.

[DT11] M. Dumbser et E-F. Toro. « A Simple Extension of the Osher Riemann Solver to Non-conservative Hyperbolic Systems ». In : *J Sci Comput* 48 (2011), p. 70–88.

[EF03] S. Evje et T. Flatten. « Hybrid flux-splitting schemes for a common two-fluid model ». In : *Journal of Computational Physics* 192 (2003), p. 175–210.

[EF05] S. Evje et T. Flatten. « Hybrid central-upwind schemes for numerical resolution ». In : *M2AN ESAIM* 39 (2005), p. 253–273.

[EF07] S. Evje et T. Flatten. « On the wave struecture of two-phase flow models ». In : *SIAM J. APPL. MATH.* 67 (2007).

[Fer10] P.-J.-M Ferrer. « Numerical and mathematical analysis of a five-equation model for two-phase flow ». Master's Thesis. SINTEF Energy Research, 2010.

[GL13] Gene H. Golub et Charles F. Van Loan. *Matrix computations, 4th*. The Johns Hopkins University Press, 2013.

[GR96] E. Godlewski et P.-A Raviart. *Numerical Approximation of Hyperbolic Systems of Conservation Laws*. T. 118. Appllied Mathematical Sciences - Springer, 1996.

[Har83] A. Harten. « High resolution schemes for hyperbolic conservation laws ». In : *Journal Computational Physics* 49 (1983), p. 357–393.

[HH83] A. Harten et J. M. Hyman. « Self adjusting grid methods for one-dimensional hyperbolic conservation laws ». In : *Journal Computational Physics* 50 (1983), p. 253–269.

[HR00] H. Holden et N.H. Risebro. *Front tracking for hyperbolic conservation laws*. Springer - Applied mathematical sciences volume 152, 2000.

[IH11] M. Ishii et T. Hibiki. *Thermo-Fluid Dynamics of Two-Phase Flow*. Springer, 2011.

[Ish75] M. Ishii. *Thermo-fluid dynamic theory of two-phase flow*. Paris : Eyrolles, 1975.

[JE08] D. Jamet et P. Emonot. *Rapport d'avancement 2007. Diphasique à 6 équations et une pression*. Rapp. tech. CEA, 2008.

[Jeo+08] J. J. Jeong et al. « A semi-implicit numerical scheme for transient two-phase flows on unstructured grids ». In : *Nuclear Engineering and Design* 238 (2008).

[Jin01] Shi Jin. « A STEADY-STATE CAPTURING METHOD FOR HYPERBOLIC SYSTEMS WITH GEOMETRICAL SOURCE TERMS ». In : *Mathematical Modelling and Numerical Analysis* 35.4 (2001), p. 631–645.

[KI83] S. Kakac et M. Ishii, éds. *Advances in Two-Phase Flow and Heat Transfer Fundamentals and Applications*. T. 1. Martinus Nijhoff Publishers, 1983.

[KPS04] Th. Katsaounis, B. Perthame et C. Simeoni. « Upwinding sources at interfaces in conservation laws ». In : *Mathematical Modelling and Numerical Analysis* 17.3 (2004), p. 309–316.

[KSS03] B. L. Keyfitz, R. Sanders et M. Sever. « Lack of Hyperbolicity in the Two-Fluid Model for Two-Phase Incompressible Flow ». In : *Discrete and Continuous Dynamical Systems-Series B* 3/4 (2003), p. 541–563.

[Lag04] F. Lagoutière. « A non-dissipative entropic scheme for convex scalar equations via discontinuous cell-reconstruction ». In : *C. R. Acad. Sci. Paris, Ser. I 338* (2004).

[LeF02] P.G. LeFloch. *Hyperbolic Systems of Conservation Laws, the Theory of Classical and Nonclassical Shock Waves*. Birkhauser, 2002.

[LeV04] R.J. LeVeque. *Finite Volume Methods for Hyperbolic Problems*. Cambridge University Press, 2004.

[LeV92] R.J. LeVeque. *Numerical Methods for Conservation Laws*. Birkhäuser, 1992.

[LPS96] Pierre-Louis Lions, Benoît Perthame et Panagiotis E. Souganidis. « Existence and stability of entropy solutions for the hyperbolic systems of isentropic gas dynamics in Eulerian and Lagrangian coordinates ». In : *Communications on Pure and Applied Mathematics* 49.6 (1996), p. 599–638.

[LS80] T.-P. Liu et J. A. Smolle. « On the Vacuum State for the Isentropic Gas Dynamics Equations ». In : *ADVANCES IN APPLIED MATHEMATICS* 1 (1980), p. 345–359.

[MEF09] S.T. Munkejord, S. Evje et T. Fltten. « A MUSTA Scheme for a Nonconservative Two-Fluid Model ». In : *SIAM J. Sci. Comput.* 31 (2009), p. 2587–2622.

[MFM10] Alexandre Morin, Tore Fltten et Svend Tollak Munkejord. « A Roe Scheme for a Compressible Six-Equation Two-Fluid Model ». In : *Int. J. Numer. Meth. Fluids* (2010), p. 1–28.

[MLM95] G. Dal Maso, P. LeFloch et F. Murat. « Definition and weak stability on non conservative products ». In : *Journal of Math Pures Application* 74 (1995), p. 483–548.

[Mun05] S.T Munkejord. « Analysis of the two-fluid model and the drift-flux model for numerical calculation of two-phase flow ». PhD thesis. Norwegian University of Science et Technology, 2005.

[Mun07] S.T Munkejord. « Comparison of Roe-type methods for solving the two-fluid model with and without pressure relaxation ». In : *Computers & Fluids* 36 (2007).

[MVZ97] L. Mottura, L. Vigevano et M. Zaccanti. « An evaluation of Roe's scheme generalization for equilibrium real gas flows ». In : *Journal of computation physics* 138 (1997).

[Ndj+08] M. Ndjinga et al. « Numerical simulation of hyperbolic two-phase flow models using a Roe-type solver ». In : *Nuclear Eng. and Design* 238/8 (2008).

[Ndj07a] M. Ndjinga. « Influence of interfacial pressure on the hyperbolicity of the two-fluid model ». In : *Comptes Rendus Mathematique* 344 (2007), p. 407–412.

[Ndj07b] M. Ndjinga. « Quelques aspects de modélisation et d'analyse des systèmes issus des écoulements diphasiques ». Ecole Centrale de Paris, 2007.

[Ndj08] M. Ndjinga. « Computing the matrix sign and absolute value functions ». In : *C. R. Acad. Sci. Paris* 346 (2008), p. 119–124.

[NNC14] T.-P.-K Nguyen, M. Ndjinga et C. Chalons. « Numerical simulation of an incompressible two-fluid model ». In : *Finite Volumes for Complex Applications VII-Methods and Theoretical Aspects*. Sous la dir. de J. Fuhrmann, M. Ohlberger et C. Rohde. 2014.

[NNC15a] M. Ndjinga, T.-P.-K Nguyen et C. Chalons. « Mathematical analysis an numerical simulation of the two-fluid model with counter current phase dynamics ». In : *In preparation* (2015).

[NNC15b] T.-P.-K Nguyen, M. Ndjinga et C. Chalons. « A 2 2 HYPERBOLIC SYSTEM MODELLING INCOMPRESSIBLE TWO PHASE FLOWS - THEORY AND NUMERICS ». In : *submited* (2015).

[PCC03] H. Paillère, C. Corre et J.R. Garcìa Cascales. « On the extension of the AUSM+ scheme to compressible two-fluid models ». In : *Computers & Fluids* 32 (2003), p. 891–916.

[Ran87] V.H Ransom. « Numerical bencmark tests ». In : *Multiphase Sci. Tech.* 3 (1987).

[RH84] V.H Ransom et D.L Hicks. « Hyperbolic two-pressure models for two-phase flow ». In : *Journal of Computational Physics* 53 (1984), p. 124–151.

[Roe81] P.L. Roe. « Approximate Riemann Solvers, Parameter Vectors, and Difference Schemes ». In : *Journal of Computational Physics* 43 (1981), p. 357–372.

[Rom98] J.E. Romate. « An approximate Riemann solver for a two-phase flow model with numerically given slip relation ». In : *Computers & Fluids* 27 (1998).

[Sal12] K. Saleh. « Analyse et Simulation Numérique par Relaxation dÉcoulements Diphasiques Compressibles ». Université Paris VI, 2012.

[SBA07] S. Sahmim, F. Benkhaldoun et F. Alcrudo. « A sign matrix based scheme for non-homogeneous PDE's with an analysis of the convergence stagnation phenomenon ». In : *Journal of Computational Physics* 226 (2007), p. 1753–1783.

[Ser99] Denis Serre. *System of Conservation Laws 1 : Hyperbolicity, Entropies, Shock Waves*. Cambridge University Press, 1999.

[SH13] Y. Shekari et E. Hajidavalloo. « Application of Osher and PRICE-C schemes to solve compressible isothermal two-fluid models of two-phase flow ». In : *Computers & Fluids* 86 (2013), p. 363–379.

[Sol+14] F. Soleymani et al. « Some Matrix Iterations for Computing Matrix Sign Function ». In : *Journal of Applied Mathematics* 2014 (2014), p. 000–000.

[ST] National Institute of Standards et Technology. *Thermophysical properties of fluid systems*. `http://webbook.nist.gov/chemistry/fluid/`. Accessed : 2015-10-30.

[Stu77] J. H. Stuhmiller. « The Influence of Interfacial Pressure Forces on the Character of Two-Phase Flow Model Equations ». In : *int. J. Multiphase Flow* 3 (1977).

[SW84] H. B. Stewart et B. Wendroff. « Two-phase flow : Models and methods ». In : *J. of Comp. Physics* 56.3 (1984).

[Tem81] J.B. Temple. « Solutions in the Large for the Nonlinear Hyperbolic Conservation Laws of Gas Dynamics ». In : *Journal of differential equations* 41 (1981), p. 96–161.

[TK96] I. Toumi et A. Kumbaro. « An Approximate Linearized Riemann Solver for a Two-Fluid Model ». In : *Journal of Computational Physics* 124 (1996), p. 286–300.

[TKP99] I. Toumi, A. Kumbaro et H. Paillere. « Approximate Riemann solvers and flux vector splitting schemes for two-phase flow ». In : *30th Computational Fluid Dynamics* (1999).

[Tou+00] I. Toumi et al. « FLICA-4 : a three-dimensional two-phase flow computer code with advanced numerical methods for nuclear applications ». In : *Nuclear Engineering and Design* 200 (2000).

[Tou87] I. Toumi. « Etude du problème de Riemann et construction de schéma numériques type Godunov multidimensionnels des modèles d'écoulements diphasiques ». Université Paris VI, 1987.

[Ver06] A. Vernier. *Validation de Modèles Multichamps dans le Logiciel OVAP*. Rapp. tech. École Nationale Supérieure des Mines de Paris, 2006.

[Yan06] T. Yang. « Singular behavior of vacuum states for compressible fluids ». In : *Journal of Computational and Applied Mathematics* 190 (2006), p. 211–231.